SPCA & REGUCALCIN: EXPRESSION, ACTIVITY & REGULATION IN MAMMALIAN Ca^{2+} HOMEOSTASIS

by

PEI FONG LAI

A thesis submitted to
The University of Birmingham
for the degree of
DOCTOR OF PHILOSOPHY

School of Biosciences
College of Life & Environmental Sciences
The University of Birmingham
September 2010

Abstract

The secretory pathway Ca^{2+}-ATPase (SPCA) provides the Golgi apparatus with a luminal Ca^{2+} store, which is used to modulate the activity of Ca^{2+}-dependent enzymes involved in controlling the secretory pathway and post-translational modification of proteins. This Ca^{2+} store controlled by SPCA is also believed to be agonist-releasable. Regucalcin (RGN), (also known as senescence marker protein 30 (SMP30)) is believed to be a Ca^{2+}-binding protein expressed in an age-dependent manner, whereby its protein levels decrease in a number of organs as aging progresses. It has been suggested to be able to affect the activities of the sarco/endo-plasmic reticulum Ca^{2+}-ATPase (SERCA), as well as other Ca^{2+}-dependent enzymes. On the other hand, RGN's ability to bind Ca^{2+} has been argued against and this protein has been shown to modulate the activities of enzymes not involved in Ca^{2+} homeostasis, as well as have intrinsic enzymatic activity in itself as a gluconolactonase.

It was of interest in the present studies to examine how SPCA can be regulated and how RGN can contribute to the regulation of Ca^{2+} homeostasis within intact cells. As a result, the following novel attributes of SPCA and RGN were shown: (1) SPCA expression and activity are sensitive to glucose homeostasis in rat vascular smooth muscle cells (VSMCs); (2) hSPCA1d activity can be inhibited without altering hSERCA2b activity by using bis-phenol and 2-APB; (3) TFP and TBBPA affect both hSPCA1d and hSERCA2b activities to the same degrees, while cADPR and NAADP have no effect on hSPCA1d (and possibly hSERCA2b in the case of cADPR) activity; (4) RGN mRNA expression can be found in some specialised cell types of the male rat reproductive system; and (5) human RGN over-expression can influence Ca^{2+} mobilisation stimulated by 1μM thapsigargin and 10μM histamine, possibly via alteration of SERCA expression. The present study has also made available a custom-made recombinant form of rat RGN and anti-RGN polyclonal antibodies.

It can be strongly suggested that SPCA plays a role in diabetes because of its sensitivity to glucose concentrations, coupled with its involvement in the secretory pathway and ability to influence vasopressin response in VSMCs. Bis-phenol has now been quantitatively shown to be a potent and specific inhibitor of SPCA, giving it great potential to be used as a pharmacological tool for future research on this Ca^{2+}-ATPase. For RGN, it appears promising that this cytosolic protein has a role to play in male fertility, while its role in Ca^{2+} homeostasis is likely to involve modulating ER Ca^{2+} storage capacity and strength of Ca^{2+}-mediated hormone response.

ACKNOWLEDGEMENT

I am very thankful to my supervisor, Dr Frank Michelangeli, for all the encouragement, guidance and patience he has given me during my time in research as both an undergraduate and PhD student. I want to thank the Biotechnology & Biological Sciences Research Council and the Biochemical Society for providing me with the valuable financial support I needed for my research, as well as the opportunities I have taken to network with other researchers and present my work at conferences in Belgium, Italy and the UK. I thank all researchers I have named in this thesis, who have so kindly given me plasmids, antibodies and cell-lines that I needed to do my research. I endlessly give my appreciation to my family, especially my mum, and friends outside of the university for giving me the time and space to allow me to pursue the ambition of doing a PhD over the last four years, and for always doing their best to support me. I am immensely grateful to everyone I have worked with and around in the School of Biosciences, especially those on the third and seventh floor in Biosciences Tower. Special thanks to Prof Baz Jackson, Dr Scott White and Nick Cotton for the advice and support they have given me. Special thanks to Lucinda Huxley, Fawaz Al-Mousa, Miriam Obiozo, Simon Whitehead, Tabish Ahmed, Sara Alfasi, Rachel Kendrick and Richard Logan, who did their PhDs with me, along with many others over the years, and shared their experiences along the way.

CONTENTS

LIST OF FIGURES

LIST OF TABLES

LIST OF ABBREVIATIONS

16HBE14o: human bronchial epithelial cells

2-APB: 2-aminoethoxydephenyl-borate

A7r5: rat embryonic thoracic aortic smooth muscle cells

AM: acetoxymethyl ester

ATP: adenosine 5'-triphosphate

ATP2A2: human sarco/endo-plasmic reticulum calcium ATPase, isoform 2 (gene)

ATP2C1: human secretory pathway calcium ATPase, isoform 1 (gene)

AVP: arginine vasopressin

Bis-phenol: bis(2-hydroxy-3-tert-butyl-5-methyl-phenyl)methane

Bisphenol-A: 4,4'-dihydroxy-2,2-diphenylpropane

BLAST: Basic Local Alignment Search Tool (National Institute of Health, USA)

BSA: bovine serum albumin

C-terminal: carboxyl-terminal

Ca^{2+}: calcium ion

$[Ca^{2+}]$: concentration of calcium ions

$CaCl_2$: calcium chloride

cADPR: cyclic adenosine diphosphate ribose

CaM: calmodulin

CaR: calcium-sensing receptor

CD: circular dichroism

cDNA: complementary deoxyribonucleic acid

Cl^-: chloride ions

COS-1: African green monkey kidney cells

COS-7: African green monkey kidney cells

CPA: cyclopiazonic acid

dcAMP: dubutyryl cyclic adenosine monophosphate

DD: Darier's disease

DEPC: diethylpyrocarbonate

dH_2O: deionised water

DMEM: Dulbecco's Modified Eagle Media

DMSO: dimethyl sulfoxide

DNA: deoxyribonucleic acid

dNTP: deoxynucleotide triphosphates

DPBS: Dulbecco's phosphate buffered saline

DTT: dithiothreitol

ECL: enhanced chemiluminescence

EDTA: ethylenediaminetetraacetic acid

EF hand: calcium ion-binding motif

EGFP: enhanced green fluorescent protein

EGTA: ethylene glycol tetraacetic acid

ER: endoplasmic reticulum

ERAD: endoplasmic reticulum-associated degradation

FBS: foetal bovine serum

F/F_o: fluorescence intensity (measured/basal) ratio

FITC: fluorescein isothiocyanate

fMLP: N-formyl-methionyl-leucyl-phenylalanine

FRT: rat thyroid epithelial cells

FT-ICR: Fourier-transform ion cyclotron resonance

GAPDH: glyceraldehyde 3-phosphate dehydrogenase

H^+: proton ions

H4-II-E: rat kidney hepatoma cells

HBSS: Hank's Buffered Saline Solution

HCE: proton/calcium ion exchanger

HCl: hydrochloric acid

HCX: proton/calcium ion exchanger

HeLa: human cervix adenocarcinoma cells

HEK 293: human embryonic kidney 293 cells

HEPES: 4-(2-hydroxyethyl)-1-piperazineethanesulfonic acid

HG: high glucose, hyperglycaemic

HHD: Hailey-Hailey disease

Hisx6: hexa-histidine

HRP: horseradish peroxidase

hSPCA1: human secretory pathway calcium ATPase, isoform 1 (protein)

hSPCA2: human secretory pathway calcium ATPase, isoform 2 (protein)

IC_{50}: inhibitory concentration producing half-maximal response

IL8: interleukin-8

INS1: rat pancreatic islet β-cells

IP_3: inositol-1,4,5-triphosphate

IP_3R: inositol-1,4,5-triphosphate receptor

IP_4: inositol-1,3,4,5-tetrakisphosphate

IPTG: isopropyl β-D-1-thiogalactopyranoside

K^+: potassium ion

$KC_2H_3O_2$: potassium acetate

kDa: kilodaltons

KH_2PO_4: potassium di-hydrogen phosphate

K_d: dissociation constant for a binding interaction

K_i: dissociation constant for an inhibitor of an enzyme-catalysed reaction

K_m: dissociation constant for a substrate of an enzyme-catalysed reaction

KOH: potassium hydroxide

LB: Luria-Bertani

MC3T3-E1: mouse osteoblastic cells

MCU: mitochondrial calcium uniporter

Mg^{2+}: magnesium ion

$MgCl_2$: magnesium chloride

$MgSO_4$: magnesium sulphate

MIN6: mouse pancreatic islet β-cells

Mn^{2+}: manganese ion

$[Mn^{2+}]$: concentration of manganese ions

$MnCl_2$: manganese chloride

MOPS: 3-morpholinopropane-1-sulfonic acid

mRNA: messenger ribonucleic acid

N-glycans: amino-glycans

N-terminal: amino-terminal

NAADP: nicotinic acid adenine dinucleotide phosphate

NAADPR: nicotinic acid adenine dinucleotide phosphate receptor

NaCl: sodium chloride

NaH_2PO_4: sodium di-hydrogen phosphate

$NaHCO_3$: sodium hydrogen carbonate

NaN_3: sodium azide

NCA: nuclear calcium ATPase

NCE: sodium/calcium ion exchanger

NCX: sodium/calcium ion exchanger

NEM: N-ethylmaleimide

NF1: nuclear factor 1

NG: normal glucose, euglycaemic

NH_4: ammonium

Ni^{2+}: nickel ion

NOS: nitric oxide synthase

NRK52E: rat kidney epithelial cells

O.D: optical density

P19: mouse embryonic carcinoma cells

PAGE: polyacrylamide gel electrophoresis

PBS: phosphate buffered saline

PCR: polymerase chain reaction

PDB: Protein Data Bank

PI3K: phosphatidylinositol 3-kinase

PMCA: plasma membrane calcium ATPase

pmr1: plasma membrane related calcium ATPase 1 (yeast gene)

PMR1: plasma membrane related calcium ATPase 1 (yeast protein)

PMSF: phenylmethylsulfonyl fluoride

PTH: parathyroid hormone

PTP: permeability transition pore

$RbCl_2$: rubidium chloride

RGPR-p117: regucalcin gene promoter region-related protein 117

RGN: regucalcin

ROC: receptor-operated calcium channels

ROS: reactive oxygen species

RPL19: ribosomal protein L19

RyR: ryanodine receptor

S.E.M: standard error of the mean

SDS: sodium dodecyl sulphate

SERCA: sarco/endo-plasmic reticulum calcium ATPase

SERCA1a: sarco/endo-plasmic reticulum calcium ATPase, variant 1a

SERCA2a: sarco/endo-plasmic reticulum calcium ATPase, variant 2a

SH-SY5Y: human brain neuroblastoma cells

siRNA: silencing ribonucleic acid

SMOC: second messenger-operated calcium channels

SMP30: senescence marker protein 30

SOC: store-operated calcium channels

SOD: superoxide dismutase

SPCA: secretory pathway calcium ATPase

SPCA1: secretory pathway calcium ATPase, isoform 1

SR: sarcoplasmic reticulum

T_3: thyroid hormone

T_m: melting/annealing temperature

TBBPA: tetrabromobisphenol-A

TCA: trichloroacetic acid

TEMED: tetramethylethylenediamine

TFP: trifluoroperazine

TG: thapsigargin

TM4: mouse testicular Sertoli cells

TMR: tetramethylrhodamine

TPC: two-pore channel

Tris: tris(hydroxymethyl)aminomethane

TTBS: Tween-20 Tris buffered saline

Tween-20: polyoxyethylene (20) sorbitan monolaurate

UPR: unfolded protein response

VOC: voltage-operated calcium channels

VSMC: vascular smooth muscle cells

WGA: wheat germ agglutinin

CHAPTER 1.

INTRODUCTION

CHAPTER 1.
INTRODUCTION

1.1. Ca^{2+} in Cells (An Overview)

1.1.1. The Importance of Cellular Ca^{2+}

Ca^{2+} homeostasis is an essential part of maintaining normal function of a eukaryotic cell by contributing to a diverse number of processes that span its entire life cycle. It has two general biochemical functions, which are to act as either a structural stabiliser or cofactor upon binding to a protein (Williams, 2006). The processes in which Ca^{2+} is important can be both specialised to a specific cell type or exist for housekeeping purposes in all cells. Examples of such processes include initiating skeletal muscle contraction upon Ca^{2+} binding to troponin C (Cohen et al., 1980) and activation of a multitude of kinases by the Ca^{2+}-calmodulin complex (CaM) (Swulius and Waxham, 2008).

There are two aspects of Ca^{2+} homeostasis that make it possible for this cation to be able to contribute to a vast number of different processes. Firstly, it is controlled by a large number of different proteins, which are found in the form of transporters, enzymes and modulators, and altogether give a "toolkit" for intracellular Ca^{2+} handling (Berridge et al., 2003). The second is that Ca^{2+} is distributed into discrete pools within a cell with the use of membrane-bound organelles as specialised storage compartments (Michelangeli et al., 2005). The maintenance of different Ca^{2+} concentrations ($[Ca^{2+}]$) by components of the aforementioned toolkit at these different pools create ionic gradients, which can be used to re-distribute Ca^{2+} around different parts of a cell rapidly when required. This results in significantly large changes in $[Ca^{2+}]$ between the organelles, extracellular space and cytoplasm. Along with Ca^{2+}, all cells have Ca^{2+}-dependent proteins, which are also segregated into discrete intracellular environments, and those with non-complementary organelle- or process-specific functions are kept apart from each other. Changes in the distribution of Ca^{2+} act as switches, which either turn on or off the activity of different sets of Ca^{2+}-dependent proteins to give a change in the number and type of Ca^{2+}-dependent processes that take place in a cell within a given time.

1.1.2. Ca^{2+} Distribution Within a Cell

The movement of Ca^{2+} in a cell to the right place and at the right time is key. For instance, too little Ca^{2+} in the cytoplasm of spermatozoa could prevent the acrosome reaction from taking place (Yanagimachi and Usui, 1974, Breitbart, 2002). On the other hand, too much Ca^{2+} in the cytoplasm of hippocampal neurons can cause cell death instead of mediating the normal signalling pathways associated with glutamate stimulation (Randall and Thayer, 1992). Thus Ca^{2+} movement needs to be tightly controlled. The use of a large number of Ca^{2+} channels, exchangers and pumps, as well as discrete Ca^{2+} stores, (figure 1.1.2.1) give this control (Michelangeli et al., 2005).

There are two main routes of Ca^{2+} transit in a cell, which are that between the cytoplasm and organelles, and between the cytoplasm and extracellular space. Both of these routes run bi-directionally. The movement of Ca^{2+} into the cytoplasm leads to the initiation and propagation of major signalling pathways, whereas the movement of Ca^{2+} out of the cytoplasm results in their termination. Caspase-dependent apoptosis is an example of a process that requires the flow of Ca^{2+} into the cytoplasm to take place (Orrenius et al., 2003). Ca^{2+} movement between the cytoplasm and organelles is required for processes specific to the latter, whereby an example would be the requirement of Ca^{2+} by dehydrogenases in the citric acid cycle that takes place in the mitochondria (Traaseth et al., 2004).

1.1.3. Ca^{2+} Channels, Pumps & Exchangers

Many of the Ca^{2+} transporters known to exist in cells are shown in figure 1.1.2.1. The movement of Ca^{2+} from the extracellular space into the cytoplasm is controlled by three main types of channel proteins, namely voltage-operated Ca^{2+} channels (VOCs), receptor-operated Ca^{2+} channels (ROCs), and store-operated Ca^{2+} channels (SOCs) (Bootman et al., 2001). Members of these three types of Ca^{2+} transporters are all located at the plasma membrane. Two other proteins, which are the Na^{+}/Ca^{2+} exchanger (NCX, also known as NCE) and the plasma membrane Ca^{2+}-ATPase (PMCA), promote Ca^{2+} movement in the opposite direction and are also located at the plasma membrane (Michelangeli et al., 2005). These proteins work together to maintain a $[Ca^{2+}]$ of >1mM at the extracellular space and approximately 0.1μM in the cytoplasm, giving a 10,000-fold difference on either side of the plasma membrane and thus a very steep Ca^{2+} gradient in a resting cell (Rizzuto and Pozzan, 2006).

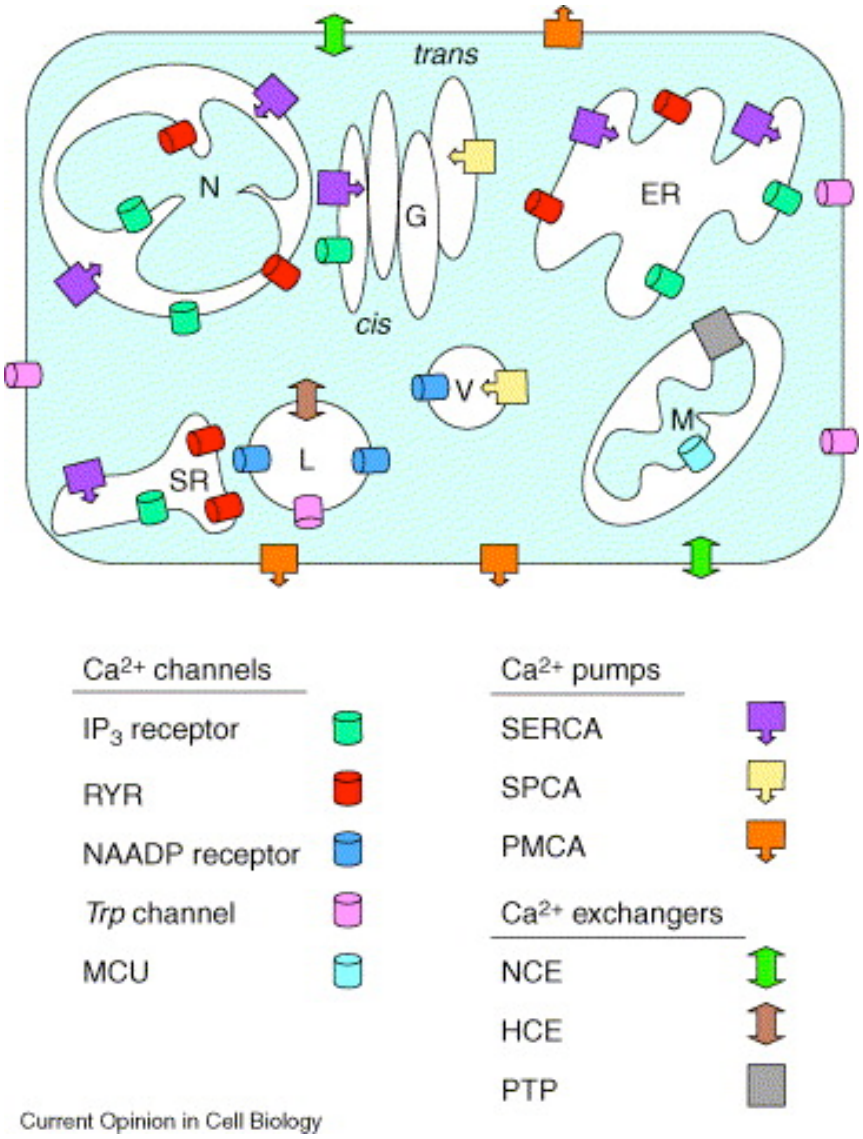

Figure 1.1.2.1. Ca^{2+} Channels, Exchangers & Pumps in a Cell

The diagram shows the organelles (N – nucleus, G – Golgi apparatus, ER – endoplasmic reticulum, M – mitochondria, V – vacuoles, L – lysosomes, SR – sarcoplasmic reticulum) that can act as Ca^{2+} stores within a cell and their associated Ca^{2+} transporters (Michelangeli et al., 2005).

The proteins required for the transit of Ca^{2+} from the inside of their storage organelles into the cytoplasm are the second messenger-operated Ca^{2+} channels (SMOCs), which include the inositol-1,4,5-triphosphate receptor (IP_3R), ryanodine receptor (RyR) and potentially the nicotinic acid adenine dinucleotide phosphate receptor (NAADPR) (the latter of which has been recently identified as a two-pore channel (TPC) (Calcraft et al., 2009)). The opposite movement along this route is directed by a different set of transporters, which include the H^+/ Ca^{2+} exchanger (HCX, also known as HCE), the mitochondrial Ca^{2+} uniporter (MCU), and the sarcoplasmic/endoplasmic reticulum (SR/ER) Ca^{2+}-ATPase (SERCA) (Michelangeli et al., 2005). The magnitude of difference in $[Ca^{2+}]$ between the cytoplasm and lumens of different organelles vary. In a resting cell, cytosolic $[Ca^{2+}]$ is approximately 0.1μM (Badminton et al., 1996), while the approximate luminal $[Ca^{2+}]$ in the nucleus, ER, Golgi apparatus, and mitochondria are 0.1μM (Badminton et al., 1996), 0.5mM (Pinton et al., 1998), 0.3mM (Pinton et al., 1998) and 0.1μM (Vay et al., 2009), respectively. These values were determined using Ca^{2+}-sensitive aequorin proteins, which were expressed specifically at the organelles measured for their luminal $[Ca^{2+}]$ in human cervix carcinoma (HeLa) cells.

1.1.4. Patterns & Rhythms of Ca^{2+} Signalling

The co-operation of all the transporters mentioned above is required to adjust and balance Ca^{2+} gradients in a cell. Typically, when a cell is in its resting state, a high $[Ca^{2+}]$ is located at the extracellular space and within organelles, and this is balanced with a low $[Ca^{2+}]$ in the cytoplasm. A dynamic redistribution of Ca^{2+} occurs between these three compartments when a cell is stimulated (e.g. by a hormone or neurotransmitter).

Segregation of Ca^{2+} inside a cell is not just from the use of different organelles as their stores. Ca^{2+} microdomains also exist, which are local build-ups of Ca^{2+} at the points of its entry into and out of the cytoplasm. These can vary in their location, size and number within a cell. They come in the form of sparklets, sparks, blinks, syntillas and puffs, but can sometimes be referred to more generally as Ca^{2+} spikes (Berridge, 2006). Ca^{2+} microdomains are formed by SMOCs and via Ca^{2+} influx across the plasma membrane. The RyRs are responsible for sparks, blinks and syntillas, and the IP_3Rs give puffs. One type of microdomain, the sparklet, is formed by VOCs. The key

purpose of forming Ca^{2+} microdomains, like multiple membrane-bound Ca^{2+} stores, is to keep different Ca^{2+}-controlled processes isolated to specific regions of a cell. For example, syntillas have been observed to form at nerve terminals and are used for stimulating neurotransmitter release, which is a process that can only occur at this part of hypothalamic neuronal cells (De Crescenzo et al., 2004). All types of Ca^{2+} microdomains are transient events (except when large numbers of Ca^{2+} puffs are formed to create global (i.e. whole cell) Ca^{2+} changes), which presumably help to keep different processes spatially and temporally separated by reducing the chance of different sets of Ca^{2+} changes merging together. A disruption of time and space confinement of different sets of Ca^{2+} microdomains can lead to disease, such as alcoholic pancreatitis (Petersen et al., 2006).

1.1.5. Ca^{2+} Stores in Organelles

Organelles that act as intracellular Ca^{2+} stores include the nucleus, mitochondria and SR/ER. One of the first observations that led to the recognition of the nucleus as a Ca^{2+} store was from experiments with nuclei isolated from calf thymus (Naora et al., 1961). Since then, nuclear Ca^{2+} stores have been suggested to have a number of uses, ranging from regulation of gene expression to activation of kinases (Gomes et al., 2006). Early observations of mitochondria being able to internalise Ca^{2+} included that from experiments with rat kidney (Deluca and Engstrom, 1961), and subsequently the purpose of mitochondrial Ca^{2+} storage has been linked to apoptotic cell death as well as other processes (Duchen et al., 2008). The observation of SR's ability to contribute to muscle contraction by utilising its internal source of Ca^{2+} (Weber et al., 1963) was one of the first to support SR/ER's role as an intracellular Ca^{2+} store. Now it is well established that Ca^{2+} in the ER is required for various functions, including the folding and secretion of proteins (Burdakov et al., 2005).

1.2. The Golgi Apparatus (An Intracellular Ca^{2+} Store)

1.2.1. Structure & Function of the Golgi Apparatus

The Golgi apparatus (as shown in figure 1.2.1.1) was an entity discovered by (and subsequently named after) Camillo Golgi from his work done on Purkinje cells (Droscher, 1998). It is an intracellular structure composed of stacks of membranous disks, which are individually called cisterna and each have a lumen containing various structural and enzymatic proteins. The cisternae are organised into three parts, which

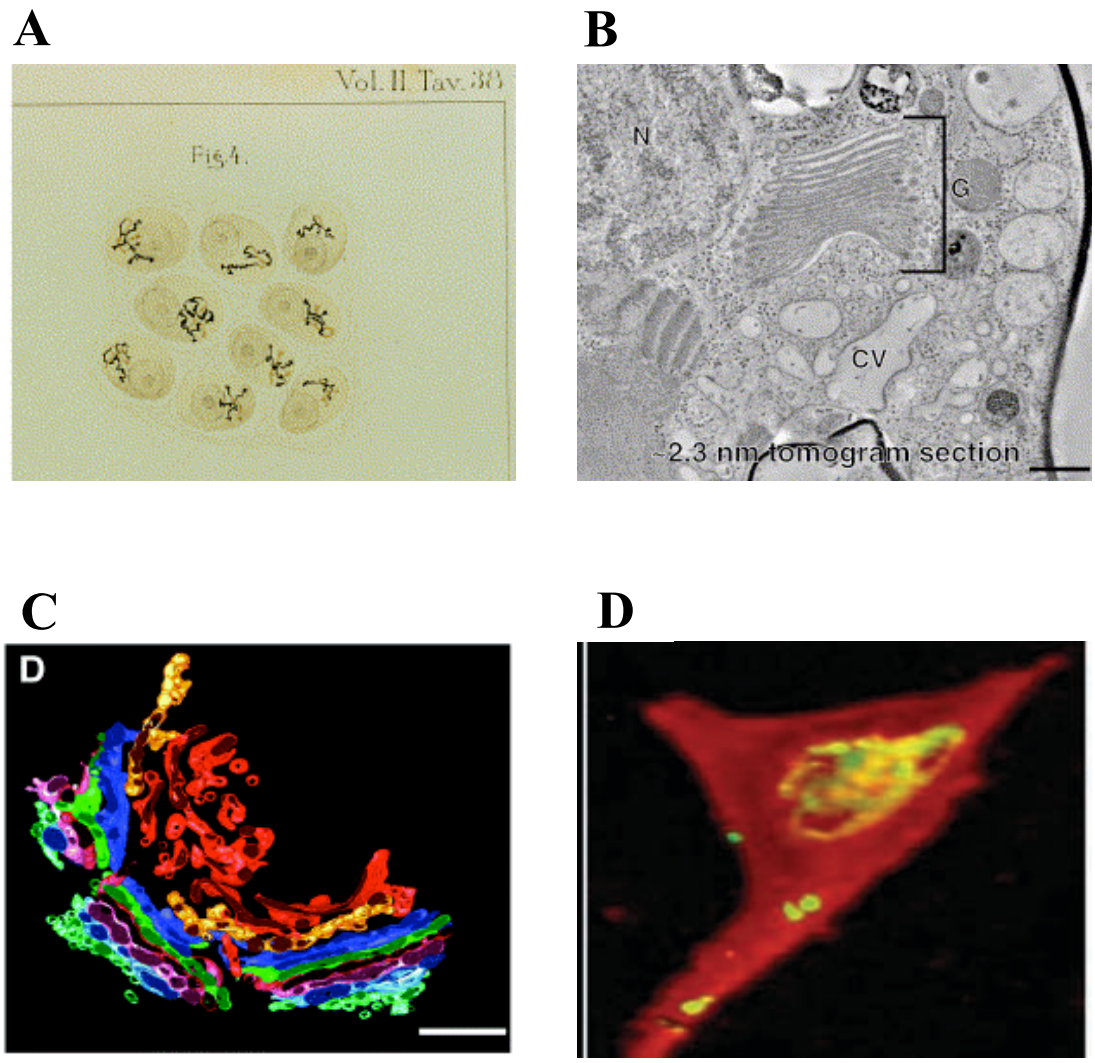

Figure 1.2.1.1. Images of the Golgi Apparatus

The Golgi apparatus is depicted here in the form of (**A**) an original drawing by Camillo Golgi as a structure next to the nucleus in each of nine cells (Bentivoglio, 1998), (**B**) an electron microscopy photograph as the structure labelled "G" (Donohoe et al., 2006), (**C**) a three-dimensional model with its different compartments represented in different colours (Mogelsvang et al., 2004), and (D) fluorescence microscopy photographs of a vascular smooth muscle cell as the yellow structure labelled by immunohistochemistry (Michelangeli et al., 2005).

are known as the cis-, medial- and trans- Golgi. The cis- and trans- parts make up the ends of the Golgi apparatus whilst the medial- part is positioned between them (Marsh and Howell, 2002). The Golgi apparatus is best known for its role in the post-translational modification and transport of newly synthesised proteins. It is also capable of synthesising lipids and distributing them around the cell (Slomiany et al., 1993). This organelle is now also believed to contribute to cell signalling, with reasons for this including the finding of pro-apoptotic factors at its membrane (Hicks and Machamer, 2005), the contents of phosphoinositide-modifying enzymes (used for lipid signalling) in its lumen (De Matteis et al., 2005) and its ability to act as a Ca^{2+} store (Dolman and Tepikin, 2006).

1.2.2. The Golgi Apparatus & Ca^{2+} Homeostasis

One of the first links made between the Golgi apparatus and Ca^{2+} homeostasis came from experiments that showed the structural integrity of the former within rat parathyroid glands is dependent on the $[Ca^{2+}]$ in their surrounding medium (Roth and Raisz, 1964). Another study showed microsomes derived from rat parotid and submaxillary glands are capable of transporting Ca^{2+} and required ATP to do so. Most of the Ca^{2+} uptake observed from these membranes was suggested to have come from the Golgi apparatus and, from this, it was hypothesised that Ca^{2+} in this organelle could play a role in protein secretion (Selinger et al., 1970). Previous research had already shown Ca^{2+} is required for agonist-stimulated secretion of enzymes (Hokin, 1966). Following this, Ca^{2+}-activated ATPase activity in the Golgi apparatus was found to exist in hamster chromaffin cells and it was noted to be distinct from ATPase activities detected at the plasma membrane and mitochondria (Benedecz et al., 1972).

1.2.3. Ca^{2+} Storage in the Golgi Apparatus: Secretory Cells

One of the earliest direct demonstrations of ATP-dependent Ca^{2+} uptake at the Golgi apparatus was done using bovine mammary glands, from which the kinetics and ATP dependence of this activity were observed to be similar to that found at the SR of skeletal muscle (Baumrucker and Keenan, 1975). The same observation was later made in murine mammary tissue (Watters and Neville, 1981). Other tissue types that have been used in early studies to show the Golgi apparatus is a functional Ca^{2+} store include mice pituitary gland (Klein et al., 1972) and rat intestines (Freedman et al., 1977). However, it should be noted that these studies used early (and thus not very

well-defined) techniques of cell fractionation to isolate Golgi apparatus membranes, which may have contained contaminating ER.

1.2.4. Ca^{2+} Transport at the Golgi Apparatus

Ca^{2+} transport in Golgi apparatus-derived membrane vesicles from lactating rat mammary glands requires an activating phosphate group (e.g. the liberated phosphate group from hydrolysed ATP) and a Ca^{2+} gradient. Both sulphydryl and uncoupling reagents can inhibit Ca^{2+} transport in these vesicles, which suggests sulhydryl groups and H^+ movement across their membranes are required for Ca^{2+} movement. Golgi apparatus-derived vesicles are also capable of accumulating enough Ca^{2+} to build a concentration gradient of 470:1, with the lowest [Ca^{2+}] at the extravesicular side (West, 1981). Movement of Ca^{2+} through the membranes of such vesicles requires ATP and is dependent on the presence of Mg^{2+}. The effect of Mn^{2+} has also been tested and its replacement of Mg^{2+} can result in a "deleterious" effect on Ca^{2+} uptake (West, 1981).

Using murine mammary glands, the K_m for Mg^{2+}-ATP and Ca^{2+} have been calculated to be 2μM and 0.8μM, respectively, in Golgi apparatus-derived membranes. The same organ has also been used to demonstrate exogenous CaM is unlikely to affect ATPase activity of the Golgi apparatus, which is in contrast to its notable effects on PMCA (Watters, 1984). Sensitivity to quercetin (an inhibitor of Ca^{2+}-stimulated ATPase activity) has been found to differ between the ATPase activities of Golgi apparatus membranes, erythrocyte plasma membranes and SR membranes. The K_i for this inhibitor is approximately 5μM for both erythrocyte plasma membranes and SR membranes, but has no significant inhibitory effect on Golgi apparatus membranes (Watters, 1984). Note that the values stated above came from experiments that were done with the use of non-physiological [Ca^{2+}]. In contrast, Ca^{2+}-activated ATPase activity measured from the Golgi apparatus-derived vesicles from rat mammary gland using assay medium [Ca^{2+}] closer to that found under normal physiological conditions (2.3μM) (Virk et al., 1985) (c.f. 5μM (West, 1981) and 0.5mM (Baumrucker and Keenan, 1975)) has shown the K_m for Ca^{2+} at this organelle and associated with its ATPase activity is 0.14μM, with a V_{max} of 3.1nmol Ca^{2+}/min/mg protein. The stoichometry between ATP-dependent Ca^{2+} transport in these vesicles and their Ca^{2+}-stimulated ATPase activity was also determined to be

within the range of 0.3-0.7, which is similar to values calculated for the more established "membrane-bound Ca^{2+}-stimulated ATPases" (i.e. SERCA and PMCA).

1.3. Ca^{2+}-ATPases (An Overview)

1.3.1. The Basic Function of a P-Type ATPase

An ATPase is an enzyme that hydrolyses ATP in order to use both (1) the energy released from breaking a high-energy phosphate-phosphate bond (located between the β and γ phosphate groups of ATP) and (2) the negatively-charged phosphate group liberated from such a reaction to promote a change in its structural conformation. This change leads to its transportation of ions from one side of a membrane to the other in the case of P-type ATPases, such as the Na^{+}-K^{+}-ATPase and SERCA (Moller et al., 1996). The conformational change of a P-type ATPase is promoted by the liberated γ-phosphate group of hydrolysed ATP electrostatically binding to a catalytic aspartate residue, which subsequently causes a rearrangement of amino acid side chains at close proximity to the bound phosphate group. This results in a significant macromolecular change in structure of the ATPase.

1.3.2. The Ca^{2+}-ATPases - SERCA, PMCA & NCA

The link between Ca^{2+} and P-type ATPases was first suggested from observations of Ca^{2+} being able to strongly activate ATPase activity found in myosin extracts from rabbit leg muscle (Bailey, 1942). Later on, it was hypothesised the SR can act as a mobilisable Ca^{2+} store for the purpose of muscle contraction (Ebashi, 1961). Since then, a 2.6Å resolution crystal structure of SERCA has been published (Toyoshima et al., 2000) and this revealed more about the mechanisms involved in the transport of Ca^{2+} by the ATPase that was originally identified in myosin. Two other Ca^{2+}-ATPases are also known to exist, which are PMCA (Brini, 2009) and the nuclear Ca^{2+}-ATPase (NCA) (Nicotera et al., 1989). However, NCA is now believed to be identical to SERCA (Lanini et al., 1992).

1.4. The Structure & Function of a Ca^{2+}-ATPase (The SERCA Model)

1.4.1. Ca^{2+}-ATPases: Members of the P-type ATPase Family

Four classes of transport ATPases are known to date, which are the P, V, F and ABC ATPases. SERCA and PMCA are both classed as the P-type ATPases. Both of these Ca^{2+}-ATPases have the same basic structure of a membrane protein consisting of ten transmembrane α-helices (M1-M10), or eleven in the case of SERCA2b (Dhitavat et al., 2003), and four domains, the latter of which are the transmembrane (M), actuator (A), phosphorylation (P) and nucleotide-binding (N) domains. All discussion about Ca^{2+}-ATPase structure from hereon in this section will refer to SERCA because it is the only Ca^{2+}-ATPase that has had its structure thoroughly studied (Toyoshima, 2008). The crystal structures of SERCA are shown in figure 1.4.1.1.

1.4.2. M: The Transmembrane Domain

The M (trans**m**embrane) domain is a membrane-embedded yet still notably dynamic part of the protein. Amino acid residues in helices M4-M8 form the Ca^{2+}-binding sites at the centre of the protein, which are known as site I and site II in SERCA. Site I is formed mainly by the M5 and M6 helices, while site II is formed by the M4 and M6 helices. Amino acid residues that contribute to the Ca^{2+}-binding sites do so by using their oxygen atoms to co-ordinate with their nearest Ca^{2+} at a distance of 2.2-2.6Å. The two sites can be distinguished from each other based on which oxygen atoms their Ca^{2+}-coordinating amino acids use to bind Ca^{2+}. Amino acids at site I all use oxygen atoms located at their side chains, whereas those at site II (with the exception of N796) use oxygen atoms of the carbonyl groups located at their main-chain. PMCA has been calculated to have a 1:1 stoichiometric ratio for the number of Ca^{2+} transported for every one ATP molecule it hydrolyses and this suggests it only has one functional Ca^{2+}-binding site, which was identified to be equivalent to site I (Schatzma.Hj, 1973).

In addition to the Ca^{2+}-binding sites, there are two other important parts of the M domain that contribute to the binding of Ca^{2+} by SERCA and its related ATPases. The first is the N-terminal region of the M3 helix, which has been shown to be where thapsigargin (a potent SERCA pump inhibitor) binds to Ca^{2+}-ATPase close to its F256 residue (Yu et al., 1998, Wootton and Michelangeli, 2006). Mutagenesis experiments have suggested this region of the SERCA pump is involved in forming

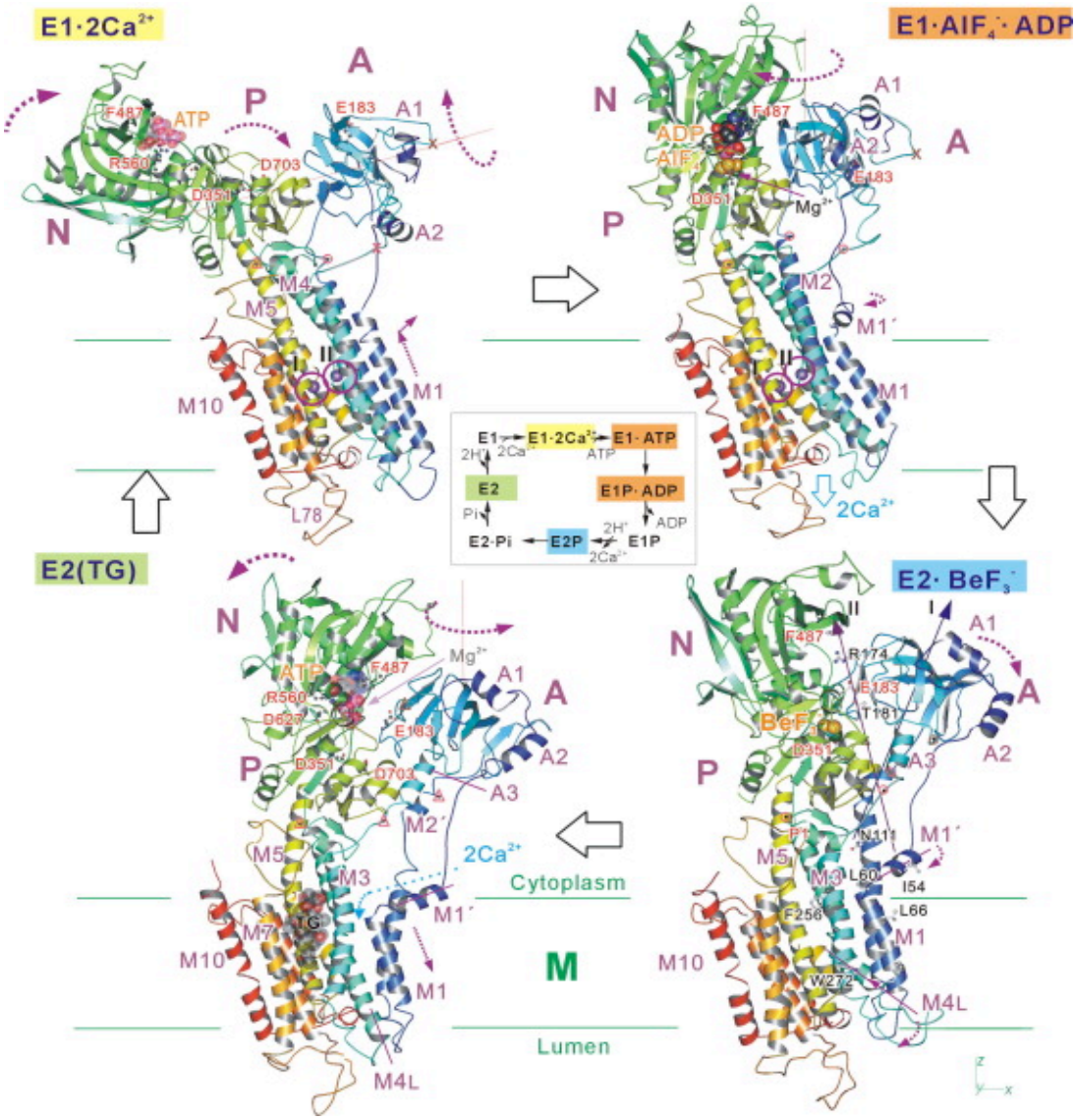

Figure 1.4.1.1. Crystal Structures & Reaction Cycle of SERCA

Crystal structures for the four reaction states of SERCA that form during the process of Ca^{2+} transport, along with SERCA's reaction cycle (middle inset), are shown. The letters M (transmembrane), P (phosphorylation), N (nucleotide) and A (actuator) next to the structures indicate the positions of the four structural domains of SERCA (Toyoshima, 2008).

the "gateway" to site I and site II (Andersen et al., 2001). The second region of importance at the M domain is known as the L67 loop, which is a part of the amino acid sequence that forms a loop connecting the M6 and M7 helices. Mutational studies have shown this 25 amino acid-long loop is important in maintaining the structural integrity of the whole protein, contributes to the susceptibility of the pump being phosphorylated following ATP hydrolysis and defines its affinity for Ca^{2+} (Zhang et al., 2001).

1.4.3. P: The Phosphorylation Domain

The P domain is where the catalytic aspartate residue required for the binding of a liberated γ-phosphate group after ATP hydrolysis is located (the 'P' in the name stands for '**p**hosphorylation'). The catalytic aspartic residue of SERCA is D351 (Carafoli, 2002) and that for PMCA is D475 (Verma et al., 1988). This domain is formed by two parts of the SERCA amino acid sequence, which sit in a central position of the folded pump whilst completely protruding into the cytoplasm. One of the two parts of this domain is linked to the M4 helix, while the other is linked to the M5 helix, and both are connected to the N domain (to be discussed of later on) at opposite ends. A key residue found in the P domain is K684, which uses its positively-charged side chain to stabilise the negative charge of the "transition state complex" that results from the electrostatic interaction between the catalytic aspartate residue and the liberated γ-phosphate group of hydrolysed ATP. It is this residue, along with a number of catalytically important short sequences (e.g. the $DKTGT^{355}$ sequence) and the Rossman fold of this domain, which makes SERCA a member of the haloacid dehalogenase superfamily of proteins (Wuytack et al., 2002).

1.4.4. N: The Nucleotide-Binding Domain

The N (**n**ucleotide-binding) domain is where ATP binds. This takes place near the vicinity of amino acid residues F487, R489 and K492, which have been shown to be required for ATP binding in SERCA (McIntosh et al., 1996). This domain protrudes into the cytoplasm and is the largest of the three domains that is positioned in this way. It is likely that the N domain is highly mobile because SERCA's crystal structure shows it is more than 25Å away from the P domain's catalytic aspartate residue when both bound to Ca^{2+} and in the absence of ATP. Thus it would have to

move in order to transfer the liberated γ-phosphate group of hydrolysed ATP between these two domains. This mobility of the N domain is likely to be possible due to the flexibility of the amino acid sequence that links the N domain to the P domain, suggesting it can act as a hinge between these two domains (Stokes and Green, 2003).

1.4.5. A: The Actuator Domain

The A (**a**ctuator) domain is the remaining one of the three domains that has been found to protrude into the cytoplasmic side of the membrane in which SERCA is embedded. It is the smallest of all four domains of the protein and consists of the 110 amino acids located between the M2 and M3 helices, along with 40 amino acids at the N-terminus of the pump. This domain's sensitivity to protease digestion suggests it is highly mobile and its position relative to the N and P domains make it very likely to be involved in the movements of these two domains that are necessary for the transfer of a phosphate group between them (Toyoshima et al., 2000).

1.4.6. The Reaction Cycle of Ca^{2+}-ATPases

The mechanism of action to be discussed here for the SERCA Ca^{2+}-ATPase is believed to be the same as that for all other P-type ATPases. It is sometimes referred to as a Post-Albers-type reaction cycle (Apell, 2004). The Ca^{2+}-ATPase is believed to exist in two main conformations, which are the E1 state (where the protein has a high affinity for Ca^{2+}) and the E2 state (when the protein has a low affinity for Ca^{2+}). There are three main processes involved in the cycle, which are ion/ATP binding, ATP hydrolysis, and conformational change (Moller et al., 2005). The existence of the reaction steps to be discussed was first suggested from measurements made of the kinetic parameters associated with Ca^{2+}-dependent ATPase activity found in SR vesicles from rabbit skeletal muscle, such as Ca^{2+} affinity and rate of ATP hydrolysis (Takakuwa and Kanazawa, 1981a, Takakuwa and Kanazawa, 1981b). The regions at which these steps take place in the SERCA structure was not elucidated until its first high resolution crystal structure was made available (Toyoshima et al., 2000).

The first step of the SERCA reaction cycle (middle inset in figure 1.4.1.1) is the binding of two cytosolic Ca^{2+} to the pump at the M domain and thus the formation of the E1 state (Ca_2E1). The second step is the formation of a high-energy intermediate ($Ca_2E1{\sim}P$) following ATP-binding at the N domain and subsequent phosphorylation of the catalytic aspartate residue in the P domain of the ATPase. This

is followed by the third step of the mechanism, which is a transition from the high-energy intermediate state to the low-energy intermediate state (E2P), via a major conformational change of the ATPase, which puts the opening of its ion-binding site into a position that faces the other side the membrane in which the ATPase is embedded. This results in the release of the bound Ca^{2+} from the pump and into the lumen of the organelle or the extracellular space, with their subsequent replacement by two or three H^+ at the ion-binding site. The forth and final step to give a complete cycle is the hydrolytic release of the bound phosphate group with another conformational change, but this time moving the opening of the ion binding site to face the cytoplasmic side of the membrane (i.e. its original position at the start of the cycle) to form the E1 state again. The bound H^+ are removed when this cycle is re-started by the binding of two new Ca^{2+} (Wuytack et al., 2002).

1.5. The Golgi Apparatus Ca^{2+}-ATPase: PMR1 in Yeast

1.5.1. The Genetics of PMR1

It was in yeast *Sacchromyces cerevisiae* (*S.cerevisiae*) where a gene that encodes a Golgi apparatus Ca^{2+}-ATPase was first isolated. The gene was named pmr1 and was identified based on its homology to the gene known to encode a plasma membrane-located ATPase in the same organism, named pma1 (Serrano et al., 1986). From this, it was suggested that pmr1 is likely to encode a Ca^{2+}-ATPase-type ion pump homologous to P-type ion pumps, and which resembled SERCA and PMCA (Rudolph et al., 1989). At the same time, another gene, named bsd1, was found to protect yeast deficient in superoxide dismutase (SOD) expression from oxidative stress when mutated to give a recessive phenotype. Furthermore, the position of this gene was found to match that mapped for the pmr1 gene and thus the two were identical (Lapinskas et al., 1995).

1.5.2. Activity & Role of PMR1

The identification of PMR1's "significant sequence similarity" with mammalian SERCA and PMCA (at their N-terminus and region between transmembrane helices 5-6) was what first suggested PMR1 to be a Ca^{2+}-ATPase (Rudolph et al., 1989). BLAST sequence analysis shows PMR1 shares 34% amino acid sequence identity with human SERCA (all three isoforms). It is at least partially located at the Golgi apparatus in yeast, but not at all in the ER or plasma membrane when endogenously

expressed. PMR1's possible role in the secretory pathway was demonstrated from experiments where pmr1 mutant strains of yeast were monitored for their ability to glycosylate invertase and proteolytically process α factor. These processes require the activity of GDPase (an enzyme involved in Golgi apparatus-localised glycosylation) and KEX2 (an endoprotease), respectively. The absence of pmr1 expression was shown to cause defects in both processes, which however could be partially (glycosylation) or fully (proteolytic processing) recovered by increasing [Ca^{2+}] in the external medium (Antebi and Fink, 1992). Other processes that involve the Golgi apparatus, such as vacuolar sorting of carboxypeptidase Y (CpY) and unfolded protein response (UPR) pathway (the detection and removal of misfolded proteins in the ER), have also been shown to be defective in mutant yeast unable express pmr1. Though control of UPR can be recovered following heterologous expression of SERCA1a (note that yeast do not express SERCA), which originally suggested endogenous PMR1 supplies the ER with Ca^{2+} as well as the Golgi apparatus in yeast (Durr et al., 1998).

The initial rates of Ca^{2+} uptake in *S.cerevisiae*-derived membranes rich in PMR1 protein have been calculated to be within the range of 1-2 nmol/min/mg protein, which agrees well with rates determined from rat mammary gland Golgi membranes (Virk et al., 1985). PMR1 is distinct from mammalian SERCA and PMCA due to their difference in sensitivity to certain inhibitors. Vanadate inhibits SERCA and PMCA with K_i values of 50-300μM and 0.6μM, respectively, whereas PMR1 has a K_i value of 130μM, which would make it appear to relate more to SERCA. However, it has also been demonstrated that PMR1 cannot be inhibited by thapsigargin, at least at concentrations of up to 5μM, and Ca^{2+} transport activity measurements have shown PMR1 resembles PMCA by having only one Ca^{2+} binding site (Sorin et al., 1997).

Recently, PMR1 expression in yeast has been shown to be able to influence viral recombination, using the *Tomato bushy stunt virus* (TBSV) (a virus that normally infects tomato plants). Loss of PMR1 expression increased the TBSV's rate of RNA recombinant formation, which is a factor of the viral life cycle that promotes resistance to viral infections by increasing their genetic diversity. This effect was attributed to PMR1 keeping cytosolic Mn^{2+} concentration low, which hinders the process of viral RNA recombination (Jaag et al., 2010).

1.5.3. Important Amino Acid Residues in PMR1

Some of the residues identified to be of significance to PMR1 function include Q783 in the M6 helix, which has been suggested to play a role in Mn^{2+}-selective binding. E329 in the M4 helix and A749 in the M5 helix are likely to play a role in Ca^{2+}-selective binding. Residues that have been noted to be important for correct folding and Golgi apparatus localisation of the PMR1 pump are N774, D778, T817 and D856, which are within the region between the M6-M8 helices (Wei et al., 2000). Phenotype screening experiments confirmed Q783 is involved in Mn^{2+} transport and showed D778 is required for cation binding. V335 and F738 have also been identified as two residues that are likely to contribute to PMR1's ability to transport Mn^{2+}, which is due to their likely interaction with Q783 and the location of all three residues at the membrane interface of the pump. The exact positions of the Q783 and V335 side chains have been noted to be important because swapping the position of these amino acids causes loss of PMR1 activity (Mandal et al., 2000).

Mutant yeast lacking in PMR1 expression have an increased level of sensitivity to high [Ca^{2+}]. Such yeast accumulate more Ca^{2+} than wildtype, are less responsive to changes in extracellular [Ca^{2+}] and are also more sensitive to Mg^{2+}. The latter suggests the transport of Ca^{2+} and Mg^{2+} competitively influenced each other. The wildtype phenotype can, however, be recovered in these mutants after they are made to express hSPCA1 (the human PMR1 homolog (to be discussed in detail later) (Hu et al., 2000, Sudbrak et al., 2000)), which suggested the Ca^{2+} transport properties of PMR1 and its human homolog are very similar (Szigeti et al., 2005).

1.5.4. Control of PMR1 Expression

Tcn1p (also known as Crz1p) is a transcription factor in yeast that is likely to control pmr1 expression in response to changes in cytosolic [Ca^{2+}] via its regulation by calcineurin (a Ca^{2+}-activated phosphatase) (Matheos et al., 1997). PMR1's expression is also linked with that of another Ca^{2+}-ATPase, named PMC1, which is localised in the vacuoles of yeast. Simultaneous low or no expression of both pmc1 and pmr1 genes in yeast can cause an increase in cytosolic [Ca^{2+}] and subsequently growth arrest. However, loss of PMR1 alone does not affect yeast growth significantly and growth arrest from loss of both PMC1 and PMR1 expression only occurs when calcineurin is activated (Cunningham and Fink, 1994, Cunningham and Fink, 1996).

1.6. The Golgi Apparatus Ca^{2+}-ATPase: SPCA in Other Eukaryotes

Note that any PMR1 homolog from hereon are those expressed in higher eukaryotes and will be referred to as a secretory pathway Ca^{2+}-ATPase (SPCA).

1.6.1. C.elegans

Caenorhabditis elegans (*C.elegans*) express two mRNA transcripts that encode for SPCA, which differ at their 5'-untranslated sequence and can be trans-spliced to give additional transcripts. Their predicted amino acid sequences share around 50% identity with yeast PMR1 and 37% identity with rat SERCA2a. However, this organism does not appear to express multiple isoforms of SPCA at the protein level. Further sequence analysis has shown it only has one Ca^{2+}-binding site, which makes it resemble PMCA as shown in studies with PMR1 (Sorin et al., 1997). However, this site shares high sequence similarity with the site II Ca^{2+}-binding site found in SERCA, rather than site I unlike PMCA. SPCA has been directly observed to be localised at the Golgi apparatus in *C.elegans* (Van Baelen et al., 2001).

1.6.2. Sea urchin

Sea urchin sperm express SPCA and it is unusual compared to its homologs in other species because it is localised to the mitochondrion rather than the Golgi apparatus of each cell. This is one of a very few cell types that has been shown to have an atypical location for SPCA function (Gunaratne and Vacquier, 2006). Thapsigargin and cyclopiazonic acid (CPA; a mycotoxin) have very little influence on intracellular $[Ca^{2+}]$ in sea urchin sperm cells, which suggests SPCA is the main Ca^{2+}-ATPase in these cells because of this protein's insensitivity to these inhibitors of Ca^{2+} transport as suggested from previous studies (Sorin et al., 1997). Furthermore, SPCA is likely to be important in the acrosome reaction in sea urchin sperm because bis-phenol (an inhibitor of all Ca^{2+}-ATPases (Brown et al., 1994)) can inhibit this process (Gunaratne and Vacquier, 2006).

1.6.3. Drosophila

Drosophila melanogaster (*D.melanogaster*) is another eukaryote that expresses SPCA, which was initially named SPoCK for this organism and comes in the form of three different isoforms. These isoforms are located at different organelles, which are

the Golgi apparatus (SPoCK-A), ER (SPoCK-B), and peroxisome (SPoCK-C). Like the Golgi apparatus and ER, the peroxisome is a Ca^{2+} store (Raychaudhury et al., 2006). Again, like sea urchin sperm cells, *D.melanogaster* demonstrates an atypical location of SPCA function in the form of this latter organelle. The SPoCK gene product has a predicted 50% identity match with yeast PMR1. SPoCK-A and SPoCK-B have been shown to contribute to Ca^{2+} signalling in embryonic S2 cells and adult renal tubule principal cells from *D.melanogaster*, respectively. Whereas SPoCK-C plays a role in bulk Ca^{2+}transport in peroxisome-derived spherites commonly found in the renal anterior tubule of *D.melanogaster*. Thus, whereas SPoCK-C is only associated with Ca^{2+} transport and storage, the SPoCK-A and –B isoforms can contribute to Ca^{2+} homeostasis and/or Ca^{2+} signalling (Southall et al., 2006).

1.7. The Golgi Apparatus Ca^{2+}-ATPase: SPCA in Mammalian Cells

1.7.1. Rat SPCA

Mammalian SPCA was originally identified using DNA probes of the *S.cerevisiae* pmr1 gene to screen for a homolog in rat cDNA libraries derived from brain, kidney, testes and stomach tissue. From this, two mRNA sequences of two different lengths, 3.9kb and 5kb, were isolated. Their predicted translated amino acid sequences exhibited all the conserved domains known to be associated with P-type ATPases, and shared a high level of sequence similarity with PMCA, SERCA and PMR1 (Gunteski-Hamblin et al., 1992). BLAST analysis shows rat SPCA (Pubmed protein databank entry number NP_571982.2) shares 33% sequence identity with human SERCA (all three isoforms) at their amino acid sequences. The abundance of mRNA for both sequences is notably high in brain, lung and stomach. Though most rat tissues are able to express some SPCA and so it is likely to play a general housekeeping role in most cell types. A third mRNA transcript size, 3.7kb, is expressed in rat testes, and a forth transcript size, 6kb, has also been isolated. The 3.7kb and 3.9kb mRNA sequences only differ at their C-terminus and thus the 3.7kb transcript is likely to be an alternatively spliced variant of the 3.9kb transcript (Gunteski-Hamblin et al., 1992).

1.7.2. Argument Against the Existence Of Mammalian SPCA

It was once argued that Ca^{2+}-activated ATPase activity previously measured may have been from newly synthesised SERCA and/or PMCA in transit through the Golgi apparatus rather than from one specifically located at the Golgi apparatus. Using

Golgi apparatus membrane fractions isolated from rats that were treated with a protein synthesis inhibitor, cycloheximide (to ensure the lumen of this organelle carried little or no proteins in transit to other organelles), Taylor et al. showed the ATPase activity that had been located in the Golgi apparatus previously was most likely have been a detection of both SERCA and PMCA (Taylor et al., 1997). Although there has been one recent study that supports the localisation of SPCA at the plasma membrane of cells in rat liver (Dmitriev et al., 2003), a greater number of others have given substantial evidence in support of the existence of mammalian SPCA at the Golgi apparatus following Taylor et al.'s work (Missiaen et al., 2001, Van Baelen et al., 2001, Wootton et al., 2004, Sepulveda et al., 2007, Sepulveda et al., 2009), including a demonstration of SPCA's localisation at the Golgi apparatus using immunohistochemistry (figure 1.7.2.1).

1.8. The Role of SPCA in Eukaryotic Cells

1.8.1. SPCA in Oxidative Stress

C.elegans has previously been used to demonstrate the role of SPCA in the oxidative stress response pathway, which is a process also found in mammalian cells (Cho et al., 2005). From this, it has been observed that this organism's sensitivity to Ca^{2+} and Mn^{2+} depletion is abnormal when endogenous SPCA expression is artificially depleted (using RNA silencing methods). Furthermore, SPCA-depletion in *C.elegans* mutants deficient in superoxide dismutase 1 (SOD1) expression (and thus are highly susceptible to oxidative stress) result in the mutants being less oxygen-sensitive compared to control cells, which resembles previous findings in yeast (Lapinskas et al., 1995). Resistance to oxidative stress in the double mutant has been attributed to SPCA's role in Mn^{2+} homeostasis (rather than its Ca^{2+} handling function) due to the requirement for Mn^{2+} by antioxidant enzymes and the ability of this ion to act as a radical oxygen species (ROS) scavenger (Cho et al., 2005).

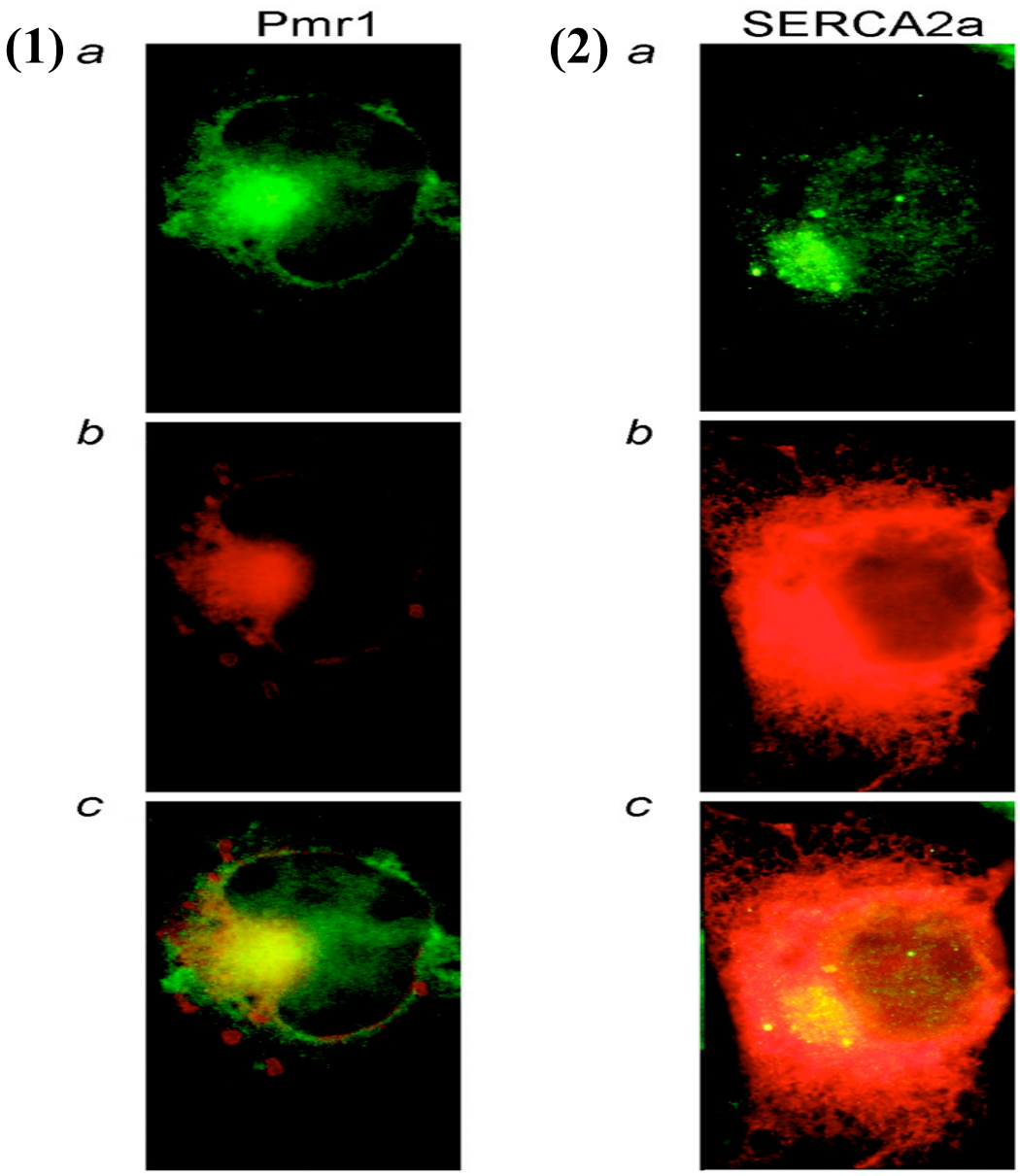

Figure 1.7.2.1. Immunolocalisation of Over-Expressed SPCA & SERCA in COS-1 Cells

Over-expressed *C.elegans* SPCA protein (green staining in (1a) and (1c)) is shown to co-localise with the Golgi apparatus marker, 58K protein (red staining in 1b) and (1c)), in COS-1 cells. Whereas over-expressed rabbit SERCA2a protein (green staining in (2a) and (2c)) does not co-localise as tightly with 58K protein (red staining in (2b) and (2c)) and is more diffusely distributed in COS-1 cells than SPCA (Missiaen et al., 2001).

1.8.2. SPCA in Protein Synthesis & ER Stress

SPCA's role in protein folding and post-translational modification of newly synthesised proteins in the ER and Golgi apparatus was suggested from siRNA knockdown experiments with cell lines. Depletion of SPCA expression by this method in rat thyroid cells (FRT) and human embryonic kidney 293 cells (HEK 293) can prevent mutant *cog* thyroglobulin, which cannot be correctly glycosylated, from being removed via ER-associated degradation (ERAD). However, the same result has not been observed with all proteins, such as mutant insulin that also cannot be correctly glycosylated. From this, it has been suggested that a protein's dependence on SPCA activity for its glycosylation depends on the amount of N-glycans they require. Loss of SPCA expression is unlikely to reduce ERAD directly because knockdown of SPCA expression in HEK 293 cells does not change the expression levels of BiP (an ER chaperone), which normally increases when the unfolded protein response (UPR) pathway is activated by ERAD defects. At the same time, FRT cells are more susceptible to tunicamycin-induced ER stress, which occurs as a result of a defective ERAD system, when SPCA expression is knocked down. Thus it has been suggested that SPCA assists ERAD by affecting its activity downstream of its activation, possibly by providing Ca^{2+} required by ER chaperones (e.g. BiP) (Ramos-Castaneda et al., 2005).

1.8.3. SPCA in Lactation

SPCA expression has been shown to increase in mammary tissue during the progression of pregnancy in rats. SPCA turnover in mammary tissue can be rapid enough to result in mRNA expression becoming seven to eight times higher in lactating mammary glands than in brain. At the same time, SPCA protein levels can be two to three times higher in mammary glands than in brain. SPCA protein expressed is also 2kDa bigger in mammary glands than that expressed in rat brain and testes. This latter observation was attributed to either alternative splicing or post-translational modification, but it has yet to be established which one is correct (Reinhardt et al., 2000). The importance of SPCA expression in the process of lactation has also been emphasised by a more recent study, which has shown SPCA protein levels are reduced by 80-95% within 24 hours of this process being stopped artificially, leading to the start of involution by causing mitochondrial overload and subsequent cell death to stop milk production (Reinhardt and Lippolis, 2009).

1.8.4. Influence of SPCA on Other Ca^{2+} Homeostasis Proteins

The abundance of SPCA can influence the expression levels of a number of other proteins involved in Ca^{2+} homeostasis (at least when over-expressed). By over-expressing rat SPCA in the African green monkey kidney cell line, COS-7, the abundance of SERCA, PMCA and calreticulin (an ER-localised Ca^{2+}-binding protein) have been shown to decrease. On the other hand, expression levels of CALNUC (a Golgi apparatus-localised Ca^{2+}-binding protein) increases following over-expression of rat SPCA in these cells (Reinhardt et al., 2004).

1.8.5. SPCA in Insulin Secretion

RNA silencing of SPCA expression in both the pancreatic islet β-cell-lines from rat, INS1, and mice, MIN6, results in a higher than normal influx of Ca^{2+} following SOC activation, which is reduced to control levels when cells are treated with nimodipine (a voltage-gated Ca^{2+} channel inhibitor). However, voltage-gated Ca^{2+} channel expression and activity do not differ between SPCA-depleted and control cells. Furthermore, glucose-stimulated insulin secretion is increased but basal insulin secretion remains the same as control levels in SPCA-depleted cells. Glucose-stimulated Ca^{2+} oscillations have also been noted to be different in their duration and frequency between SPCA-depleted and control cells. Thus it has been suggested that SPCA's role is not solely to store Ca^{2+} into the Golgi apparatus and secretory vesicles, but also (at least in rat pancreatic β-cells) to modulate Ca^{2+} signalling, which can affect the activity of plasma membrane-located voltage-gated Ca^{2+} channels (Mitchell et al., 2004).

1.8.6. SPCA in Brain Development & Function

SPCA1 (one of two SPCA isoforms expressed in mammalian cells) knockout mice have shown this Ca^{2+}-ATPase is required for closure of the neural tube during embryonic development. This is in contrast to its apparent lack of contribution to development of the cardiovascular system, which was observed to be normal in homozygous null mutants that all died by gestation day 11.5. Death of these null mutants was attributed to higher than normal apoptotic activity and "Golgi-specific stress", both of which are likely to have been due to deficient handling of Ca^{2+} and

Mn^{2+} by the Golgi apparatus (Okunade et al., 2007). SPCA1 expression and activity have also been shown to increase in the brain (specifically noted in the cortex, hippocampus and cerebellum) during the early stages of postnatal development in mice. In addition to this, intracellular localisation of SPCA1 can change over time with progression of development. Its associated pattern of change in localisation made authors suggest that this Ca^{2+}-ATPase may play a role in neuronal migration and morphogenesis (Sepulveda et al., 2008). Furthermore, SPCA has also been associated with neuronal differentiation after experiments with a mouse neuroblastoma cell line, N2a, showed SPCA1 knockdown in expression hinders neurite formation and Golgi apparatus-localised protein trafficking (Sepulveda et al., 2009).

Experiments that focused on SPCA1 expression in pig cerebellum has shown its activity can be detected in both synaptosomes and microsomes in this part of the brain, and have a restricted intracellular localisation pattern that corresponds to "major compartments" of the Golgi apparatus found in the soma of Purkinje cells and interneurons. Furthermore, the ability of Mn^{2+} to inhibit Ca^{2+} transport by SPCA1 in cerebellar neurons suggests it is involved in neurodegenerative diseases that are promoted by Mn^{2+} toxicity (Sepulveda et al., 2007). Levels of SPCA expression and activity have also been shown to be sensitive to oxidative stress in ischemic rat brain (Pavlikova et al., 2009).

1.9. SPCA & Ca^{2+} Signalling in Mammalian Cells

1.9.1. C.elegans SPCA in COS-1 cells

COS-1 (an African green monkey SV40 transformed kidney cell line) cells made to express *C.elegans* SPCA by transfection can produce one of either two different responses to 0.1mM ATP stimulation after pre-treatment with thapsigargin, which are either (1) a "steady" rise and gradual fall in $[Ca^{2+}]$, or (2) oscillatory "baseline Ca^{2+} spiking". Both of these responses have been observed to be near-equally common in transfected COS-1 cells (Missiaen et al., 2001). Such cells pre-treated with thapsigargin (in order to remove the effects of SERCA) and stimulated with ATP have also been used to demonstrate the effects of a number Ca^{2+} signalling effectors on SPCA.

From this, it has been shown that the ER is 55% more sensitive to IP_3 stimulation in control cells than those made to over-express *C.elegans* SPCA. Treatment with caffeine (an inhibitor of IP_3Rs (Brown et al., 1992), as well as

activator of RyRs (Tovey et al., 1998)) can produce a latent period between capacitative Ca^{2+} entry (CCE) and subsequent ATP-stimulated Ca^{2+} release in *C.elegans* SPCA-over-expressing COS-1 cells, which is not observed in control and SERCA1-over-expressing cells. This latent period is followed by a rapid cytosolic [Ca^{2+}] rise rather than a more gradual one seen in control and SERCA1-over-expressing cells. It has been suggested that the difference in IP_3R sensitivity between control and SPCA-over-expressing COS-1 cells, as demonstrated with caffeine, is responsible for the latent period observed between CCE and ATP-stimulated Ca^{2+} release in *C.elegans* SPCA-over-expressing cells.

Another finding from the same experimental COS-1 cell model is that ATP stimulation results in Ca^{2+} oscillations (mostly of the steady baseline-type) in over 50% of thapsigargin pre-treated SPCA-over-expressing cells, which was in contrast to the classic Ca^{2+} response profile of a sustained Ca^{2+} rise followed by a gradual fall back to basal levels observed in 90% of control and SERCA1-over-expressing cells. Furthermore, ilimaquinone (a Golgi-apparatus-disrupting agent) can have a diverse number of effects on the Ca^{2+} oscillations observed in ATP-stimulated SPCA-over-expressing cells, ranging from the modification of their frequency or amplitude to their complete inhibition. From this, it has been suggested that these Ca^{2+} oscillations observed in both cell types may be influenced by protein kinase D activity because ilimaquinone disrupts the Golgi apparatus by activating its vesiculation via this enzyme. Note that the vesiculation process itself is unlikely to be responsible for ilimaquinone's effects because brefeldin A (another compound that promotes Golgi apparatus vesiculation) has no effect on the Ca^{2+} oscillations observed in SPCA-over-expressing cells (Missiaen et al., 2001).

1.9.2. SPCA & Ca^{2+} Signalling In Other Mammalian Cell Types

The rat aortic smooth muscle cell line, A7r5, and human bronchial epithelial cell line, 16HBE14o, have been shown to contain thapsigargin-insensitive Ca^{2+} uptake activity that contributes to 8% and 11%, respectively, of the total activity. Treatment of these cells with sodium azide, oligomycin and antimycin A demonstrate these uptake systems are not associated with the mitochondria. Thapsigargin-insensitive Ca^{2+} stores in A7r5 cells are releasable upon IP_3 stimulation (Missiaen et al., 2001), and such Ca^{2+} stores in both cell lines are not mobilisable following treatment with high concentrations (0.1-20mM) of inositol-1,3,4,5-tetrakisphosphate (IP_4), cyclic ADP-

ribose (cADPR), caffeine or nicotinic acid adenine dinucleotide phosphate (NAADP). Furthermore, thapsigargin-insensitive Ca^{2+} stores in A7r5 cells can contribute to cell signalling following hormone stimulation, which has been demonstrated using arginine vasopressin (AVP) (Missiaen et al., 2002).

Other cell types, such as the human epithelial cell line, HeLa, human foreskin-derived keratinocytes and COS-1 (the latter made to over-express C.elegans SPCA due to low endogenous SPCA levels), as well as 16HBE14o and A7r5 cells, were later used to further demonstrate the sensitivity of thapsigargin-insensitive Ca^{2+} stores to agonist stimulation. Their associated agonists were histamine (HeLa), ATP (keratinocytes, 16HBE14o and COS-1) and AVP (A7r5). These agonists were chosen because their associated signalling pathways are mediated by IP_3 and thus the focus was on the relationship between IP_3R activity and thapsigargin-insensitive Ca^{2+} stores. From the use of this range of cell types, it was shown that thapsigargin-insensitive Ca^{2+} stores are not responsible for agonist-stimulated Ca^{2+} release in all except SPCA-over-expressing COS-1 cells, which suggested their endogenous SPCA does not contribute to Ca^{2+}-mediated responses following IP_3 stimulation and its role is to only supply Ca^{2+} to the Golgi apparatus-localised Ca^{2+}-dependent enzymes (Vanoevelen et al., 2004).

This would conflict with previous findings from A7r5 cells (Missiaen et al., 2002) and later experiments with human neutrophil granulocytes (Baron et al., 2009). However, the authors of the latter suggested this discrepancy was likely to have been due to a difference in the thapsigargin concentration used to inhibit SERCA activity between the studies and noted 10μM thapsigargin, which was used on the five cell lines in the previous study, can inhibit SPCA activity (Dode et al., 2006). Thus a lower thapsigargin concentration (0.1μM) and shorter treatment time were used to inhibit SERCA activity more specifically (after comparison with 10μM thapsigargin also showed complete loss of Ca^{2+}-mediated agonist response) in studies with human neutrophils, which showed thapsigargin-insensitive Ca^{2+} stores are releasable by treatment with agonists (N-formyl-methionyl-leucyl-phenylalanine (fMLP) and interleukin-8 (IL8)) that promote the Ca^{2+}-dependent process of chemokinesis (Baron et al., 2009) (figure 1.9.2.1).

The trans-Golgi compartment of the Golgi apparatus is where SPCA is expressed in mammalian cells and contains a free luminal Ca^{2+} concentration of 130μM according to a recent study with HeLa cells (Lissandron et al., 2010). The

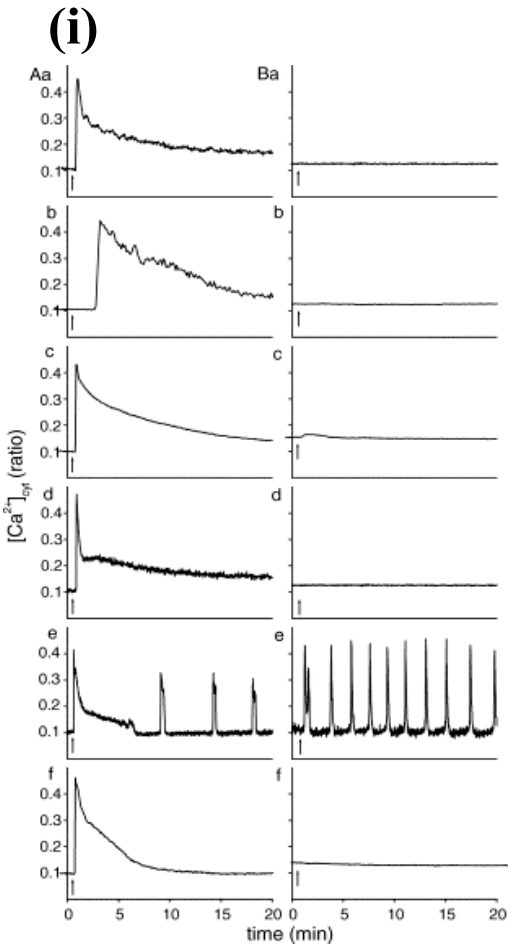

Figure 1.9.2.1. Thapsigargin-Insensitive Ca^{2+}-Mediated Responses to Agonists in Various Mammalian Cell Lines & Thapsigargin Sensitivity of SPCA

(**i**) Responses to agonist-induced changes in $[Ca^{2+}]$ at the cytosol in the absence (A) and presence (B) of 10μM thapsigargin pre-treatment from (a) HeLa cells, (b) keratinocytes, (c) 16HBE14o cells, (d) normal COS-1 cells, (e) COS-1 cells over-expressing *C.elegans* SPCA and (f) A7r5 cells (Vanoevelen et al., 2004). (**ii**) Sensitivity of human SPCA activity to thapsigargin inhibition, whereby the dotted line represents the same measurements made for SERCA1a (Dode et al., 2006). (**iii**) Studies on human neutrophils using 0.1μM and 10μM thapsigargin pre-treatment in an attempt to detect for SPCA activity in agonist (e.g. fMLP) response (Baron et al., 2009).

same study also showed SPCA-controlled Ca^{2+} stores contribute to ~30% of all agonist-releasable Ca^{2+} stores and ~60% of such stores that are not derived from the ER. Furthermore, it demonstrated that RyR, and not IP_3R, controls the release of Ca^{2+} from SPCA-controlled stores, at least in rat cardiac ventricular myocytes.

1.10. SPCA in Humans

1.10.1. Identification of hSPCA1 & its Splice Variants

Human SPCA1 (hSPCA1) was originally discovered in two studies that focused on the genetic cause of Hailey-Hailey disease (HHD) (to be discussed later) (Hu et al., 2000, Sudbrak et al., 2000). Its gene, named ATP2C1, is located at chromosome 3 in humans at position 3q21 and is the loci for mutations associated with HHD (Ikeda et al., 1994). The ATP2C1 gene sequence matches considerably well with those that encode the P-type Ca^{2+}-ATPases rat SPCA (97%) and yeast PMR1 (49%) (Sudbrak et al., 2000). Four open reading frames can be found between exon 26 and 28 of its gene sequence (Hu et al., 2000, Sudbrak et al., 2000). Only two alternatively spliced mRNA sequences from ATP2C1 were initially found, which were named ATP2C1a and ATP2C1b (Hu et al., 2000, Sudbrak et al., 2000). This was followed later on by the isolation of two more splice variants, which were named ATP2C1c and ATP2C1d (Fairclough et al., 2003).

So far, four hSPCA1 protein splice variants have been identified and are named hSPCA1 -a, -b, -c and -d. It has been possible to express all except the hSPCA1c splice variant in HEK 293 cells. Sequence analysis of hSPCA1c shows this variant does not have a part of its amino acid sequence that corresponds to a complete transmembrane helix M10 structure, which is found in the other three splice variants. Furthermore, attempts to measure Ca^{2+}-stimulated thapsigargin-insensitive phospho-enzyme formation and Ca^{2+} transport activity from this variant have been unsuccessful, unlike the other three variants (Dode et al., 2005). Taken together, it has been suggested that hSPCA1c is non-functional.

Kinetic parameters associated with Ca^{2+}-ATPase activity of the remaining three hSPCA1 splice variants have been measured and compared to SERCA1a, following their over-expression in COS-1 cells. From this, hSPCA1 functional splice variants have been demonstrated to have lower maximum ATP-binding affinities, slower ATP turnover rates (attributed to their slower rates of dephosphorylation) and higher Ca^{2+}-binding affinities than SERCA1a. The latter would apparently conflict

with rates of Ca^{2+} dissociation from these Ca^{2+}-ATPases being faster than SERCA1a. However, this was explained by the idea that the apparent higher Ca^{2+}-binding affinities of hSPCA1 -a, -b and -d are not due to stronger binding of Ca^{2+} but is instead caused by slow processing of the Ca^{2+}-bound phosphoenzyme intermediate. ATP turnover rates of the three functional hSPCA1 isoforms are not affected by pH or K^+ concentration, unlike SERCA1a (Dode et al., 2005).

1.10.2. hSPCA2

The isoform of hSPCA1, named hSPCA2, shares 64% amino acid identity with hSPCA1 (Xiang et al., 2005). Unlike hSPCA1, hSPCA2 has a more limited tissue distribution for its expression, whereby the tissue types that have been shown to express the most hSPCA2 are the testes and brain in one study (Xiang et al., 2005), and stomach and rectal tissue in another study (Vanoevelen et al., 2005a). As shown in figure 1.10.2.1, the latter study involved a more extensive search into the tissue distribution pattern of hSPCA2 by using mRNA samples from 83 different tissue types, compared to protein samples from 9 references in the former study, which did not test stomach and rectal tissue. The trans-Golgi network is where hSPCA2 has been observed to localise (at least in rat hippocampus-derived neuronal cells), along with its vesicular derivatives, with a "perinuclear" and "punctate" pattern of distribution. This is the same as hSPCA1 according to previous observations (Behne et al., 2003), but in contrast to PMR1's localisation in the medial-Golgi apparatus compartment in yeast (Durr et al., 1998). Sub-cellular localisation of hSPCA2 in human colon tissue also showed it is located primarily at the Golgi apparatus, whilst having a "juxtanuclear" distribution pattern at this organelle with hSPCA1 (Vanoevelen et al., 2005b).

A study using a mutant yeast strain, which failed to express PMR1 but was transformed to express hSPCA2, showed the Mn^{2+} handling efficiency of hSPCA2 is the same as hSPCA1. However, hSPCA2 does not transport Ca^{2+} as efficiently as hSPCA1. The lower Ca^{2+} transport efficiency of hSPCA2 is explained by its lower binding affinity for Ca^{2+} compared to hSPCA1, which is evident from their K_m values of 1.35μM and 0.25μM, respectively. Furthermore, the lower Ca^{2+} affinity of hSPCA2 could be due to its EF hand-like motif (a motif commonly associated with Ca^{2+}-binding) being less well conserved compared to hSPCA1. Yeast cells made to express hSPCA2 in the absence of PMR1 are less efficient in handling unfolded

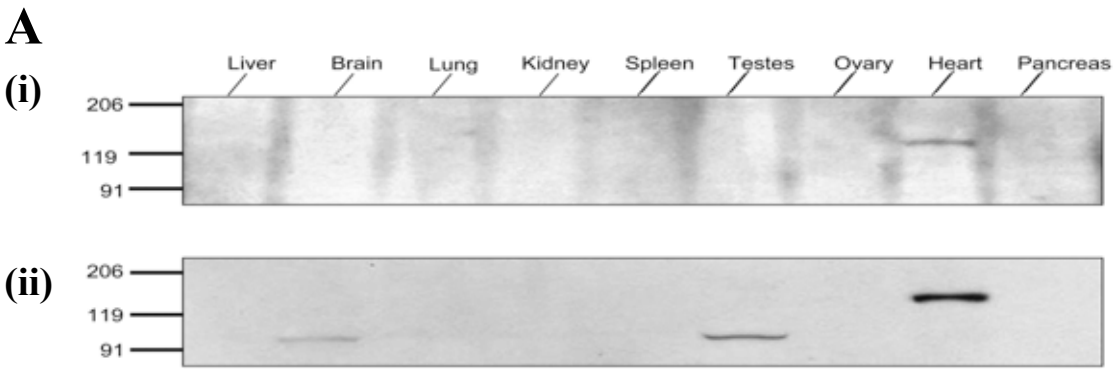

B

(i)

	1	2	3	4	5	6	7	8	9	10	11	12
A												
B												
C												
D												
E												
F												
G												
H												

(ii)

	1	2	3	4	5	6	7	8	9	10	11	12
A												
B												
C												
D												
E												
F												
G												
H												

(iii)

	1	2	3	4	5	6	7	8	9	10	11	12
A	whole brain	cere-bellum left	substantia nigra	heart	esohagus	colon, transverse	kidney	lung	liver	leukemia HL-60	fetal brain	yeast total RNA
B	cerebral cortex	cere-bellum right	accum-bens nucleus	aorta	stomach	colon, descen-ding	skeletal muscle	placenta	pancreas	HeLa S3	fetal heart	yeast tRNA
C	frontal lobe	corpus callosum	thalamus	atrium left	duodenum	rectum	spleen	bladder	adrenal gland	leukemia K-562	fetal kidney	*E. coli* rRNA
D	parietal lobe	amygdala	pituitary gland	atrium right	jejenum		thymus	uterus	thyroid gland	leukemia MOLT-4	fetal liver	*E. coli* DNA
E	occipetal lobe	caudate nucleus	spinal cord	ventricle left	ileum		peripheral blood leukocyte	prostate	salivary gland	Burkitt's lymphoma Raji	fetal spleen	poly r(A)
F	temporal lobe	hippo-campus		ventricle right	ilocecum		lymph node	testis	mammary gland	Burkitt's lymphoma Daudi	fetal thymus	human Cot-1 DNA
G	cortex postcentr gyrus	medulla oblongata		inter-ventricular septum	appendix			ovary		colorectal carcinoma SW480	fetal lung	human DNA 100 ng
H	pons	putamen		apex of the heart	colon, ascending		trachea			lung carcinoma A549		human DNA 500 ng

Figure 1.10.2.1. Tissue Distribution of hSPCA1 & hSPCA2 Expression

(**A**) Western blots showing the detection of hSPCA2 protein (~100kDa; molecular masses noted on the left) in only brain and testes out of 9 different tissue types (**ii**). The protein band detected in heart tissue at blot D was present on the control blot, thus not hSPCA2 protein (**i**). Lung, kidney and spleen tissues had produced ~100kDa hSPCA2 protein bands in other Western blots (Xiang et al., 2005). (**B**) mRNA hybridisation dot blots for hSPCA2 (**i**) and hSPCA1 (**ii**) at 83 different tissue types (**iii**) (Vanoevelen et al., 2005b).

proteins compared to wildtype PMR1-expressing cells. Taken together, hSPCA2 expression in the brain and its conserved Mn^{2+} transport efficiency (with loss of Ca^{2+} transport ability) have been linked to Mn^{2+} neurotoxicity-related disease, such as Parkinson's disease, whereby hSPCA2 could contribute to the brain's ability to deal with Mn^{2+} toxicity (Xiang et al., 2005).

Over-expression of hSPCA2 in mammalian COS-1 cells has been shown to not affect their endogenous protein levels of hSPCA1 nor SERCA2b. With regards to ion-transporting efficiency, hSPCA2 is more efficient in Mn^{2+} transport than hSPCA1 and has a K_m for Mn^{2+} binding of 0.27μM when over-expressed in COS-1 cells. This K_m value differs from that determined using yeast cells made to express hSPCA2, which may be due to differing Golgi apparatus structure and lipid composition (Vanoevelen et al., 2005a, Xiang et al., 2005).

1.10.3. The Kinetics of hSPCA2 Activity

One study has compared the functional kinetics of hSPCA2 with that of one of the four hSPCA1 splice variants, hSPCA1d (Dode et al., 2006). From this, hSPCA2 has been shown to have a weaker apparent affinity for Ca^{2+} but slower rate of Ca^{2+} dissociation than hSPCA1d. The conflict between these two findings is explained by the E_1-P(Ca^{2+}) to E_2-P transition being faster for hSPCA2 than hSPCA1d. Another difference between the two hSPCA isoforms is that hSPCA2 is more prone to thapsigargin inhibition, which is shown by K_m values of 28μM for hSPCA1d and 2μM for hSPCA2. This difference in sensitivity to thapsigargin has been attributed to a higher dephosphorylation rate and slower rate of E2 to E1 transition, producing a greater amount of hSPCA2 protein found in the E2 state (which thapsigargin binds to) at any given time compared to hSPCA1. The hSPCA2 isoform also has a higher ATP turnover rate than hSPCA1d, though it was still lower than that for SERCA1a. Furthermore, hSPCA2 has a lower affinity for phosphate binding and consequently a faster dephosphorylation rate compared to both hSPCA1d and SERCA1a, which may be the cause of a faster ATP turnover rate observed for the former Ca^{2+}-ATPase.

The two hSPCA isoforms resemble each other with regard to their lack of sensitivity to pH and K^+ concentration. The lack of sensitivity to pH changes, which was recognised by the authors to be characteristic of the hSPCA pumps, has been attributed to these pumps being embedded in Golgi apparatus membranes (Dode et al., 2005). Such membranes have a higher content of sterols and sphingolipids than

ER membranes and this property of the former make them ideal for stabilising the E2 state of a Ca^{2+}-ATPase, which is unstable following the release of its bound Ca^{2+} because of the exposure of multiple negative charges at the Ca^{2+}-binding site. The E2 state of SERCA is instead stabilised by the binding of protons and filling of the Ca^{2+}-binding site with water molecules, which makes this Ca^{2+}-ATPase sensitive to pH (Michelangeli et al., 1990). The lack of K^+ sensitivity by both hSPCA isoforms has been suggested to be due to the absence of an acidic residue corresponding to E732 in SERCA, which has been found to be involved in K^+-binding in the latter Ca^{2+}-ATPase (Shigekawa et al., 1978). A neutral (N704 in hSPCA2) or shorter (D674 in hSPCA1d) residue at the equivalent position in the amino acid sequence of hSPCA is found instead.

1.10.4. hSPCA1 & Human Spermatozoa

An example of a cell type that uses hSPCA1 for a specialised role is human spermatozoa. This cell type has been shown to express hSPCA1, which is likely to contribute to progesterone-stimulated Ca^{2+} oscillations because it is a process that involves the mobilisation of Ca^{2+} from intracellular stores not controlled by SERCA pumps (shown by their insensitivity to both thapsigargin and CPA inhibition) (Harper et al., 2005). The association of hSPCA1 with such Ca^{2+} oscillations in human sperm cells make it unlikely to be involved in the acrosome reaction, which contrasts observations made previously in sea urchin spermatozoa (Gunaratne and Vacquier, 2006). Like yeast, mature human spermatozoa are unlikely to express SERCA-type pumps, which makes hSPCA1 the main intracellular Ca^{2+}-ATPase in this cell type. In human sperm, hSPCA1 is located in the region between the anterior midpiece and the rear of the sperm head (a region known as the redundant nuclear envelope) (Harper et al., 2005), unlike SPCA's mitochondrial localisation in sea urchin sperm (Gunaratne and Vacquier, 2006).

1.11. Hailey-Hailey Disease (HHD): The Clinical Significance of hSPCA1

1.11.1. HHD – The Pathology

Hailey-Hailey disease (HHD; also known as familial benign chronic pemphigus) is an inheritable disease of autosomal dominance, which manifests itself primarily in keratinocytes at the skin in the form of blisters, redness and erosions. Age of onset varies but is most commonly within the range of 30-40 years (Dobson-Stone et al.,

2002). A key histological observation of HHD is loss of cell-cell adhesion between keratinocytes, a condition known as acantholysis, which has been described to give the skin's epidermis a "dilapidated brick wall" appearance (Sudbrak et al., 2000).

1.11.2. hSPCA1 Mutations in HHD

Genetic profiles of 64 HHD patients in one study (Dobson-Stone et al., 2002) were used to organise their ATP2C1 mutations into three groups, which were those likely to cause (1) "non-sense-mediated mRNA decay", (2) fault in mRNA splicing, and (3) non-conservative amino acid substitutions. Even within these three groups, no pattern was found between type and/or location of the mutations and the phenotype produced by them with regards to features such as, for example, age of onset and severity of lesions. Thus there is no single cause of HHD at the gene level and any one of a number of faults to hSPCA1, be it its absence or incorrect protein folding, can result in the HHD phenotype.

1.11.3. hSPCA1 & Ca^{2+} Homeostasis in HHD Keratinocytes

HHD is caused by deregulation of Ca^{2+} homeostasis. This was originally suggested from its similarities to Darier's disease (DD), which is caused by mutations in the gene that encodes the SERCA2 pump (ATP2A2) (Sakuntabhai et al., 1999). Under conditions of normal and high extracellular [Ca^{2+}], HHD keratinocytes have a higher resting intracellular [Ca^{2+}] and weaker ability to respond to changes in [Ca^{2+}] in the external environment when compared to normal keratinocytes. This observation, together with the idea that hSPCA1 is a Ca^{2+} pump, suggests a decrease in hSPCA1 activity would disrupt post-translational modification of proteins involved in cell-cell adhesion, which takes place in the Golgi apparatus and requires Ca^{2+} most likely to be supplied by hSPCA1 (Hu et al., 2000). Another way abnormal hSPCA1 activity could cause HHD is by disrupting Ca^{2+}-mediated cell signalling in keratinocytes (Sudbrak et al., 2000).

It has been confirmed that hSPCA1 (like most of its homologs) is localised to the Golgi apparatus in human keratinocytes, more specifically at the trans-Golgi membranes (Durr et al., 1998). Its protein levels are often observed to be lower than normal both in differentiated and undifferented keratinocytes of HHD patients. Ca^{2+} uptake is also deficient at the Golgi apparatus in HHD keratinocytes, when compared to normal keratinocytes, in the same two differentiation states. The severity of this

Ca^{2+} transport deficiency varies, corresponding well with the variable phenotypes of HHD patients. Total intracellular [Ca^{2+}] is lower than normal in HHD differentiated cells but normal in undifferentiated cells, which suggests hSPCA1 plays an important role in Ca^{2+} handling in the former type of keratinocytes (Behne et al., 2003).

The Ca^{2+} handling properties of normal human keratinocytes resembles that of COS-1 cells made to over-express the *C.elegans* SPCA gene. The Golgi apparatus is also the major location of Ca^{2+} uptake in human keratinocytes, unlike other cell types (e.g. rat liver cells) that use the ER for most of their Ca^{2+} uptake. Ca^{2+}-mediated responses to ATP stimulation in normal and SPCA-over-expressing COS-1 cells, as well as normal human keratinocytes, have been observed to differ. Whilst the response profile of a single rise and subsequent fall in cytosolic [Ca^{2+}] is seen in all three cell types, the onset of a Ca^{2+} rise following ATP stimulation is immediate in normal COS-1 cells but is distanced from the time point of ATP addition by a long latency period in the other two cell types (Callewaert et al., 2003). Note that this latter response profile has been observed previously in the same two types of COS-1 cells (Missiaen et al., 2001). A long latency period between stimulation and response was also observed in SPCA-over-expressing COS-1 cells and human keratinocytes, but not in normal COS-1 cells, when CCE was induced (Callewaert et al., 2003). It has been suggested that this response profile, characteristic of hSPCA1, is caused by extracellular Ca^{2+} entering the Golgi apparatus and being kept away from the cytoplasm for a longer period of time by hSPCA1 activity compared to normal COS-1 cells.

1.11.4. hSPCA1 Splice Variants

The Ca^{2+} and Mn^{2+} transport efficiencies of hSPCA1d has been measured in COS-1 cells made to express the ATP2C1d-encoded splice variant only (Fairclough et al., 2003). This splice variant was chosen for study because it has the longest predicted amino acid sequence and thus is more likely to manifest all the phenotypic defects associated with the mutations tested. From this, hSPCA1d's K_m for Ca^{2+} has been measured to be 0.2μM, which is similar to the values obtained for the hSPCA1a variant (0.26μM) (Ton et al., 2002) and *C.elegans* SPCA (0.25μM) (Van Baelen et al., 2001). In addition to this, hSPCA1d's affinity for Mn^{2+} has been suggested to be very similar to that for Ca^{2+} because the [Mn^{2+}] required to inhibit half of the pump's

total Ca^{2+} transport capacity is the same as the K_m value for Ca^{2+} affinity (Fairclough et al., 2003).

1.12. Control of hSPCA1 Expression

Two transcription factors, Sp1 and YY1, have been observed to interact with the 5'-untranslated region of the ATP2C1 gene in keratinocytes. The region of transcriptional regulation is between the region of -347 and +76 nucleotides from the transcriptional start site. This region contains both the promotor binding site and cis-enhancing elements, the latter of which are involved in altering the expression levels of their associated gene. Sp1, but not YY1, expression levels have been found to increase in normal keratinocytes when their extracellular [Ca^{2+}] is increased, which is likely to also increase total hSPCA1 expression activity in these cells. This may explain why the skin of some HHD patients only manifests their defects in the presence of environmental stress (i.e. when extracellular Ca^{2+} levels change significantly). Thus some cases of HHD may be caused by mutation in a part of ATP2C1's promoter region that is Sp1's binding site, which would allow normal hSPCA1 expression at resting [Ca^{2+}] but result in lack of ability to adapt to stress-induced changes in environmental [Ca^{2+}] (Kawada et al., 2005). In other HHD phenotypes, the transcription stage of ATP2C1's gene expression is normal but hSPCA1's protein levels or function is defective (Fairclough et al., 2003), which would make the affected keratinocytes unlikely to cope well with both resting conditions and stress-associated changes in external [Ca^{2+}].

1.13. An Overview of Regucalcin (RGN)

1.13.1. RGN: A Ca^{2+}-Binding Protein

Regucalcin (RGN) was first identified as a cytosolic Ca^{2+}-binding protein in rat liver (Yamaguchi and Yamamoto, 1978). It is unusual due to the absence of an EF hand motif in its structure, which is a structural motif that was once seen as an essential feature for a protein to able to bind Ca^{2+}. Later on, it was demonstrated that this protein is capable of contributing to Ca^{2+} signalling, just like proteins such as CaM and calcineurin, despite its apparent major structural deficit. To date, it has been shown to be involved in calcium homeostasis in various organs, most notably the liver and kidneys (Yamaguchi, 2000a). This protein is also sometimes referred to as the

senescent marker protein 30 (SMP30) because its expression levels in a number of tissues appear to be age-dependent (Fujita, 1999).

1.13.2. The RGN Gene

RGN consists of 299 amino acids, has a molecular weight of approximately 33kDa, and the gene which encodes it has been located on the X-chromosome in rats (region Xq11.1-12) and humans (region Xp11.3-q11.2) (Fujita et al., 1995). The RGN gene has been found to exist in the genomes of a number of other mammalian organisms, including dogs and chickens, but has notably not been found in yeast (Shimokawa et al., 1995). Comparisons made between gene sequences from seven different vertebrate species have shown the coding regions of the RGN gene have been highly conserved during evolution. At the protein level, the amino acid sequences corresponding to these genes also demonstrate a high degree of conservation, with 69.9-91.3% similarity between all RGN proteins from the same seven different sources (Misawa and Yamaguchi, 2000a).

The RGN gene is made up of seven exons and six introns. Its 5'-flanking region is where transcription factors bind to alter RGN expression levels in response to changes in the concentration of certain factors, such as oral calcium administration (Murata and Yamaguchi, 1998). Important sequences within the 5'-flanking region for basal and regulated gene expression have been elucidated (Murata and Yamaguchi, 1999). The promoter region of the RGN gene has been suggested to contain 28 transcription factor binding sites, and those that repress its expression (e.g. Sp1, C/EBP-β and SRY) are believed to bind within the region of -513 to -352 nucleotides from the transcriptional start site (Rath et al., 2008). In humans, it has been noted that the RGN gene can be transcribed to produce two transcripts of different lengths. Detailed analysis showed that only their 5'-untranslated regions differ, which may contribute to the synthesis of different transcripts at different times or stresses (Misawa and Yamaguchi, 2000b). Not all factors that affect RGN gene transcription influence Ca^{2+} homeostasis. A key example of this is the effect of dexamethasone (a corticosteroid), which has been demonstrated to increase RGN mRNA levels significantly in rat kidney cortex but, at the same time, has no effect on the calcium content within this organ (Kurota and Yamaguchi, 1996).

1.13.3. Transcriptional Control of RGN Expression

Nuclear transcription factors that are most likely to influence RGN expression levels include NFI-A1 and AP-1 (Yamaguchi, 2005), as well as the regucalcin gene promoter region-related protein (RGPR-p117) (Misawa and Yamaguchi, 2001). RGPR-p117 is expressed in a number of higher organisms (including humans, rats, dogs, cows and fish) and has a well conserved gene sequence (Misawa and Yamaguchi, 2002). This transcription factor, when phosphorylated, is believed to bind the TTGGC sequence of the nuclear factor (NF1)-like motif in the regucalcin gene promoter sequence, and possibly promoter regions of other genes that also have this motif (Yamaguchi, 2009).

RGPR-p117 proteins in mammals consist of 1045-1060 amino acids and all have a conserved DNA-binding leucine zipper motif (Sawada and Yamaguchi, 2005). One RGPR-p117 splice variant of 625 amino acids has been found in humans and suggested to be involved in the formation of placental carcinomas (Yamaguchi, 2009). Post-translational modification of RGPR-p117 is likely to be essential for its function as a transcription factor because recombinant RGPR-p117 protein has been shown to be unable to bind the RGN gene promoter (Yamaguchi et al., 2003a) and analysis of its amino acid sequence has suggested it contains a number of sites for phosphorylation, N-glycosylation and amidation (Yamaguchi, 2009)

Unlike RGN, RGPR-p117 expression is unaffected by the aging process (Yamaguchi et al., 2003a), but it has been shown in rats to be sensitive to Ca^{2+} administration when expressed in the liver (Misawa and Yamaguchi, 2002). Over-expression studies in the rat kidney epithelial cell-line, NRK52E, have suggested RGPR-p117 is involved in the regulation of RGN expression when the latter is required for inhibiting DNA and protein synthesis (Tomono et al., 2007), and also in preventing apoptotic cell death by altering the mRNA expression levels of caspase proteins (Yamaguchi et al., 2007). Related experiments have shown RGPR-p117 over-expression alone cannot significantly alter RGN mRNA levels and that hormonal control is also required (Yamaguchi, 2009).

1.13.4. Hormonal Regulation of RGN Expression

Insulin treatment of food-deprived rats has been demonstrated to increase RGN mRNA levels in rat liver (Yamaguchi et al., 1995). Furthermore, it has also been shown that RGN over-expression can cause insulin resistance in the rat hepatoma cell

line, H4-II-E, by repressing the expression of proteins involved in insulin signalling (e.g. insulin receptor and phosphatidylinositol 3-kinase (PI3K)) (Nakashima and Yamaguchi, 2007). Parathyroid hormone (PTH) can also increase RGN mRNA expression levels, which has been demonstrated in the mouse osteoblastic cell line, MC3T3-E1 (Yamaguchi et al., 2008a). This effect of PTH on RGN could be related to its stimulatory effect on RGPR-p117 mRNA expression levels, which has been observed in NRK52E cells (Yamaguchi, 2009). As mentioned above, RGN mRNA levels have also been observed to be affected by dexamethasone (a glucocorticoid) in the kidney cortex of rats (Kurota and Yamaguchi, 1996).

Studies on different rat tissues have suggested 17-β-estradiol (an estrogen) can either increase (e.g. liver) (Yamaguchi and Oishi, 1995) or decrease (e.g. mammary gland and prostate) RGN mRNA levels (Maia et al., 2008). Thyroid hormone (T_3) can have varied effects that is time-dependent, whereby treatment of rats with T_3 to induce hyperthyroidism can initially result in higher than normal RGN mRNA levels in liver but this effect decreases with prolonged (5.5 days) treatment before eventually leading to the opposite effect (Sar et al., 2007).

1.13.5. RGN Distribution in Mammalian Cells

RGN mRNA is not expressed widely among all tissues in organisms that have the gene, though the findings that can be found in the literature so far often conflict with each other as to which tissues do express RGN. In rat, RGN protein has been detected in samples of liver and kidney at abundant levels, both with the use of ELISA and Western blotting (Yamaguchi et al., 1991, Yamaguchi and Isogai, 1993, Yamaguchi et al., 2002b). On the other hand, there has been a conflict between data from these two methods of analysis, as well as from immunohistochemistry experiments, for samples from spleen, testis, skeletal muscle, lung, duodenum, colon and heart of rat (Yamaguchi et al., 1991, Yamaguchi and Isogai, 1993, Yamaguchi et al., 2002b). RGN expression in rat brain has in some studies been shown to not exist at the protein level (Yamaguchi et al., 2002b) and in other studies has been detected successfully (Yamaguchi et al., 1991, Yamaguchi et al., 1999). Mice have been shown to endogenously express detectable levels of RGN mRNA in liver, kidney, lung and cerebrum (Mori et al., 2004). This same study on mice also showed mice express RGN mRNA in testis and lung, which conflicts with the findings from Western blotting and immunohistochemistry experiments stated above for rats. Sex-dependent

differences in RGN expression have also been observed in rat stomach tissue for endogenous expression, as well as in a number of other tissues when transgenically expressed (Yamaguchi et al., 2002b).

RGN has been suggested to play a role in bone resorption/loss from experiments with transgenic mice (Yamaguchi et al., 2002a, Uchiyama and Yamaguchi, 2004, Yamaguchi et al., 2004b, Yamaguchi et al., 2005). Lower than normal RGN protein levels have been suggested to be associated with X-linked muscular dystrophy from experiments with mice diaphragm, and the same study has also demonstrated RGN expression in mice heart and limb muscle (Doran et al., 2006). However, the expression of RGN in rat heart is questionable due to conflicting outcomes of attempts to detect it, whereby some have shown it cannot be detected (Yamaguchi et al., 1991, Yamaguchi and Isogai, 1993, Yamaguchi et al., 2002b) and some have shown it can be detected (Yamaguchi and Nakajima, 2002). Discrepancy in RGN expression in rat heart may or may not be due to differences in age of the animals used for study (Akhter et al., 2007, Lim et al., 2009). Mammary glands and prostates in rats have been identified as other tissues where RGN is expressed (Maia et al., 2008, Maia et al., 2009).

1.13.6. The Protein Structure of RGN

RGN from mouse has been shown to share 60-66% amino acid sequence similarity with yeast (residues 136-186) and bacterial (residues 142-192) RNA polymerases, but it shares little homology with mammalian RNA polymerase (Ishigami et al., 2003). Circular dichroism experiments (Yamaguchi, 1988) have shown rat liver RGN has an α-helical content of 34% in the absence of Ca^{2+}, but this percentage decreases when Ca^{2+} is present in its surrounding medium and this suggests RGN binds Ca^{2+} by loosening its structure. The same study also calculated that one RGN protein is capable of binding up to seven Ca^{2+}, however, a later study disputed this finding by suggesting RGN has no Ca^{2+}-binding activity (Kondo et al., 2004). The isoelectric point of rat RGN is 5.20 (Yamaguchi, 1988, Yamaguchi, 2005). Two attempts have been made to obtain a crystal structure of human RGN, with the most recent one successfully demonstrating the ability of this protein to bind one Ca^{2+} (Warizaya et al., 2004) (Chakraborti and Bahnson, 2010). Figure 1.13.6.1 shows early predictions of secondary structure features within the rat RGN amino acid sequence, alongside the completed crystal structure of human RGN published in 2010. The main contrast

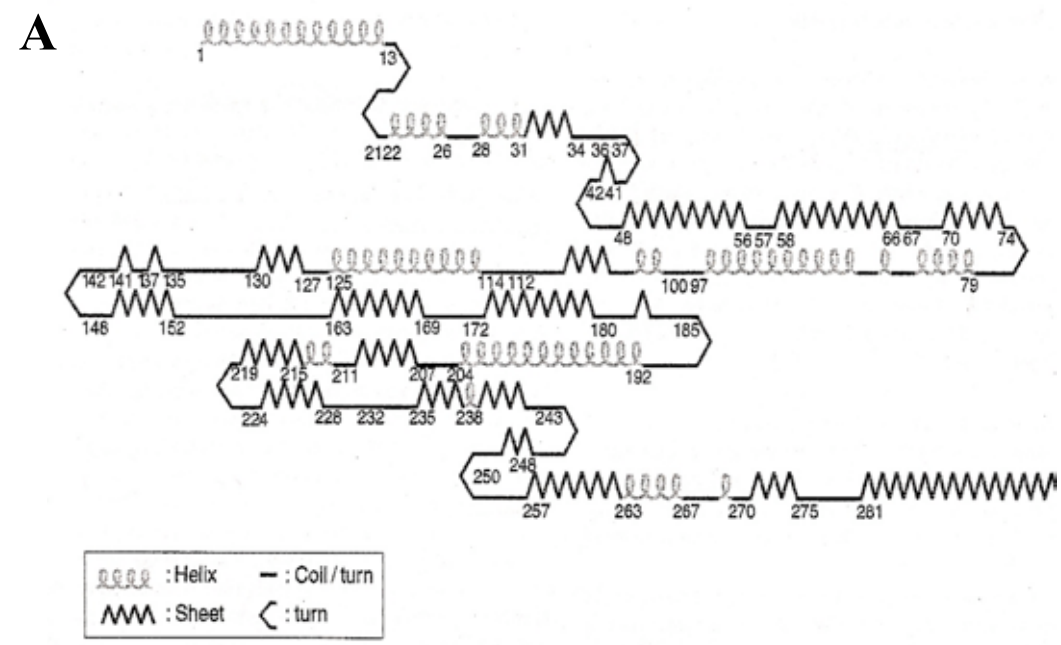

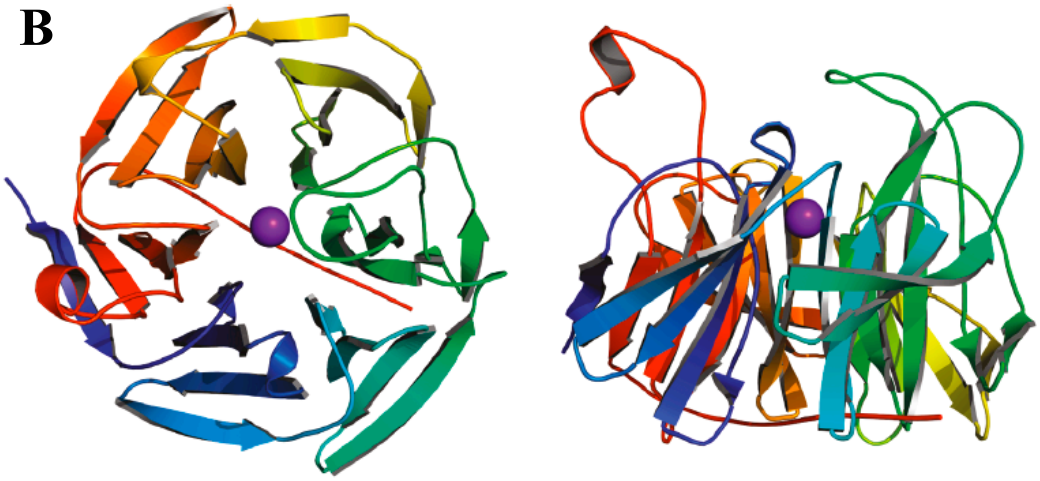

Figure 1.13.6.1. The Predicted & Solved Structures of RGN Protein

(A) Predicted secondary structure features of the rat RGN amino acid sequence, which contains 299 amino acids and the numbers indicate the positions of these residues from the N-terminus (left) to the C-terminus (right) (Yamaguchi, 2005). (B) The solved crystal structure of human RGN, shown to bind to a single Ca^{2+} in the centre of its six-β-propeller barrel fold (Chakraborti and Bahnson, 2010)

between these two structures, along with data from circular dichroism experiments, is the crystal structure shows far less α-helical content in the RGN protein structure.

1.14. RGN & Ca^{2+}-ATPases

1.14.1. First Observations for Regulation of Ca^{2+}-ATPases by RGN

RGN's role in regulating Ca^{2+}-ATPase activity was first suggested from experiments with rat liver plasma membranes (Yamaguchi et al., 1988) and microsomes (Yamaguchi and Mori, 1989). More detail on RGN's ability to alter Ca^{2+}-ATPase activity was obtained from studies with microsomes from rat kidney cortex (Kurota and Yamaguchi, 1997). Later on, brain microsomes (Yamaguchi et al., 1999), liver microsomes (Takahashi and Yamaguchi, 1999), liver mitochondria (Takahashi and Yamaguchi, 2000), liver nuclei (Tsurusaki and Yamaguchi, 2000a), and heart muscle microsomes (Yamaguchi and Nakajima, 2002) were all used to investigate the effect of RGN on their Ca^{2+}-ATPase activities. From this, the way in which RGN influences Ca^{2+}-ATPase activities has been shown to depend on where the Ca^{2+}-ATPase in question is located, with regards to the cell type and organelle.

1.14.2. RGN Effects on Microsomal Ca^{2+}-ATPases

In rats, the way and extent to which RGN modulates Ca^{2+}-ATPase activity in microsomes depends on the latter's organ of origin. The brain (Yamaguchi et al., 1999) has been identified as an organ in which RGN reduces such activity, whereas the opposite action has been observed in heart (Yamaguchi and Nakajima, 2002), kidney cortex (Kurota and Yamaguchi, 1997) and liver (Yamaguchi and Mori, 1989). For example, the concentration of RGN shown to give maximal increase of Ca^{2+}-ATPase activity, which was determined by measuring amount of phosphate liberated from reactions (and thus the activity was ATPase-specific), has been calculated to be 10^{-5}M in kidney cortex and 10^{-8}M in heart muscle. Furthermore, the effects of dibutyryl cyclic AMP (dcAMP), IP_3, digitonin (a solubilizer of membrane lipids) and CaM on microsomal Ca^{2+}-ATPase activity have also been demonstrated to differ, both in the presence and absence of RGN, between the same four organs (Yamaguchi and Mori, 1989, Kurota and Yamaguchi, 1997, Yamaguchi et al., 1999, Yamaguchi and Nakajima, 2002).

Nevertheless, there are also similarities between microsomal membranes from rat brain, heart, kidney and liver with regards to the effects of RGN on their Ca^{2+}-

ATPase activities. These include its inability to overcome the inhibitory effect of vanadate, thapsigargin and N-ethylmaleimide (NEM; a thiol reactive compound), as well as its lack of influence on the enhancing effect of dithiothreitol (DTT; a reducing agent) (Yamaguchi and Mori, 1989, Kurota and Yamaguchi, 1997, Yamaguchi et al., 1999, Yamaguchi and Nakajima, 2002). RGN also has little to no influence on Mg^{2+}-ATPase activity in all four organs. Observations from experiments with NEM and DTT suggest SH-groups in Ca^{2+}-ATPases (most likely those in their active sites) are involved in the regulation of these ion pumps by RGN (Takahashi and Yamaguchi, 1994).

1.14.3. Effects of RGN on Mitochondrial & Nuclear Ca^{2+}-ATPases

Rat liver has been used in the past to demonstrate the effects of RGN on Ca^{2+}-ATPase activities in the mitochondria (Takahashi and Yamaguchi, 2000) and nucleus (Tsurusaki and Yamaguchi, 2000a), whereby it has been shown to increase and decrease such activity, respectively. In the presence of CaM, RGN's activatory effect in rat liver mitochondria was unaffected, whereas the removal of RGN's inhibitory effect in rat liver nuclei can result in CaM enhancing their Ca^{2+}-ATPase activity. It has been suggested that RGN can translocate from the cytosol into the nucleus (Omura and Yamaguchi, 1999), and RGN protein has also been detected in the mitochondria (Yamaguchi et al., 2008b).

Similarities that the mitochondria and nucleus share are the same as that found between microsomal Ca^{2+}-ATPase activities from liver, kidney cortex, brain and heart muscle, with regards to RGN's effects in the presence of vanadate, NEM and DTT. Other treatments have also been tested on these two organelles to identify which types of Ca^{2+}-ATPases are acted on by RGN. In the nucleus, 1μM thapsigargin has been shown to inhibit the same Ca^{2+}-ATPase activity that RGN also hinders, thus demonstrating that RGN acts on SERCA (Tsurusaki and Yamaguchi, 2000a). The same effect of thapsigargin has also been shown in experiments with liver (Yamaguchi and Mori, 1989) and heart (Yamaguchi and Nakajima, 2002) microsomes. Experiments on mitochondria have shown ruthenium red and lanthanum chloride (Ca^{2+}-uniporter inhibitors) can completely block the activatory effect of RGN on this organelle's Ca^{2+}-ATPase activity, which suggests RGN can also influence the activity of Ca^{2+}-uniporters (Takahashi and Yamaguchi, 2000).

1.14.4. RGN at the Plasma Membrane Ca^{2+}-ATPase

RGN is likely to be able to affect the activity of PMCA as well as SERCA. Over-expression of human RGN in the hepatic cell line, HepG2 (Fujita et al., 1998), and the mouse carcinoma cell line, P19 (Son et al., 2008), have both demonstrated this. In HepG2 cells, higher than normal RGN protein levels was linked to an increase in both ATP-stimulated Ca^{2+} efflux activity and resistance to A23187 ionophore-induced cell death. The latter effect was also observed in P19 cells that over-expressed RGN. However, such P19 cells showed no difference compared to control cells with regards to their Ca^{2+}-mediated responses to thapsigargin in the absence of external Ca^{2+}, which suggests RGN does not influence SERCA activity (at least when over-expressed). Rat RGN over-expression in a rat kidney proximal tubular epithelial cell-line, NRK52E, has also been shown to repress the expression of L-type Ca^{2+} channels and Ca^{2+}-sensing receptor (CaR) (Nakagawa and Yamaguchi, 2006).

1.15. Other Targets of RGN in Ca^{2+} Signalling

1.15.1. An Overview of Other RGN Targets

In rat liver, RGN has been suggested to affect the activities of proteins other than Ca^{2+}-ATPases, such as plasma membrane-localised GTPases (Takahashi and Yamaguchi, 2001), glucose-6-phosphatase (Ca^{2+}-activated, not basal, activity) (Yamaguchi et al., 1989), protein kinase C (Yamaguchi and Mori, 1990), as well as calpain and possibly other cysteinyl proteases (Yamaguchi and Nishina, 1995). In rat brain, the activities of Ca^{2+}-dependent protein kinases (Hamano and Yamaguchi, 2001) can be altered by RGN. The same has also been noted for nitric oxide synthase (NOS) and nuclear protein tyrosine phosphatase in the brains of RGN transgenic rats (Tobisawa and Yamaguchi, 2003). Superoxide dismutase (SOD) (Ichikawa and Yamaguchi, 2004) and protein phosphatase (Ichikawa et al., 2004) are two other proteins, along with NOS (Ma and Yamaguchi, 2002), that can have its activity affected by RGN in rat hearts. Another organ where NOS has been shown to be prone to RGN's influence on its activity is the liver, as shown in transgenic rats (Yamaguchi et al., 2003b).

1.15.2. More RGN Effects in the Nucleus

RGN's ability to translocate into the nucleus, which is promoted by protein kinase C activation according to observations made in NRK52E cells (Nakagawa and

Yamaguchi, 2008), has been linked to a possible role for RGN in cancer because it can directly bind to DNA and nuclear proteins to regulate the expression of genes involved in promoting tumour formation (e.g. p53 and c-src) (Tsurusaki and Yamaguchi, 2004). RGN has also been shown to inhibit both nuclear protein kinases (Katsumata and Yamaguchi, 1998) and phosphatases (Omura and Yamaguchi, 1999). It has been suggested that Ca^{2+}-activated DNA fragmentation in isolated nuclei from rat liver can be prevented by RGN's ability to inhibit the activity of Ca^{2+}-activated endonucleases (Yamaguchi and Sakurai, 1991). Ca^{2+}/CaM-dependent cAMP phosphodiesterase (Yamaguchi and Tai, 1991) is another enzyme that can have its activity suppressed by RGN. For both of the latter enzymes, it has been hypothesised that RGN inhibits their activities by binding and thus sequestering activatory Ca^{2+} away from them. On the other hand, RGN has been shown to be able to bind to CaM (Omura and Yamaguchi, 1998) and this interaction may explain the effect the former has on Ca^{2+}/CaM-dependent cAMP phosphodiesterase, as well as other similar enzymes that are regulated by CaM. Other targets of RGN at the nucleus are shown in figure 1.15.2.1.

1.16. Roles of RGN in Mammalian Cells

1.16.1. RGN & Aging

In terms of the role of RGN, it has been most notably linked with the process of aging. In rats, the abundance of RGN mRNA has been observed to increase from non-detectable to maximal levels in the liver of an 18-day old embryo developing up to the stage of a 35-day old adult. Following this, the trend then reverses to give a decline in RGN mRNA levels as aging progressed to the onset of senescence in liver and kidney cells. This latter event coincides with an increase in c-fos and c-jun expression levels (Fujita, 1999), which are proteins that make up the AP-1 factor and have been shown to be able to bind onto the RGN gene in liver cells (Yamaguchi, 2005). Despite the RGN gene being located in the X chromosome, its role in aging is not sex-dependent, at least in rats (Fujita, 1999). Though RGN expression levels do differ in liver between the sexes in rats regardless of age, whereby male rats have been shown to express more RGN mRNA than female rats (Ueoka and Yamaguchi, 1998).

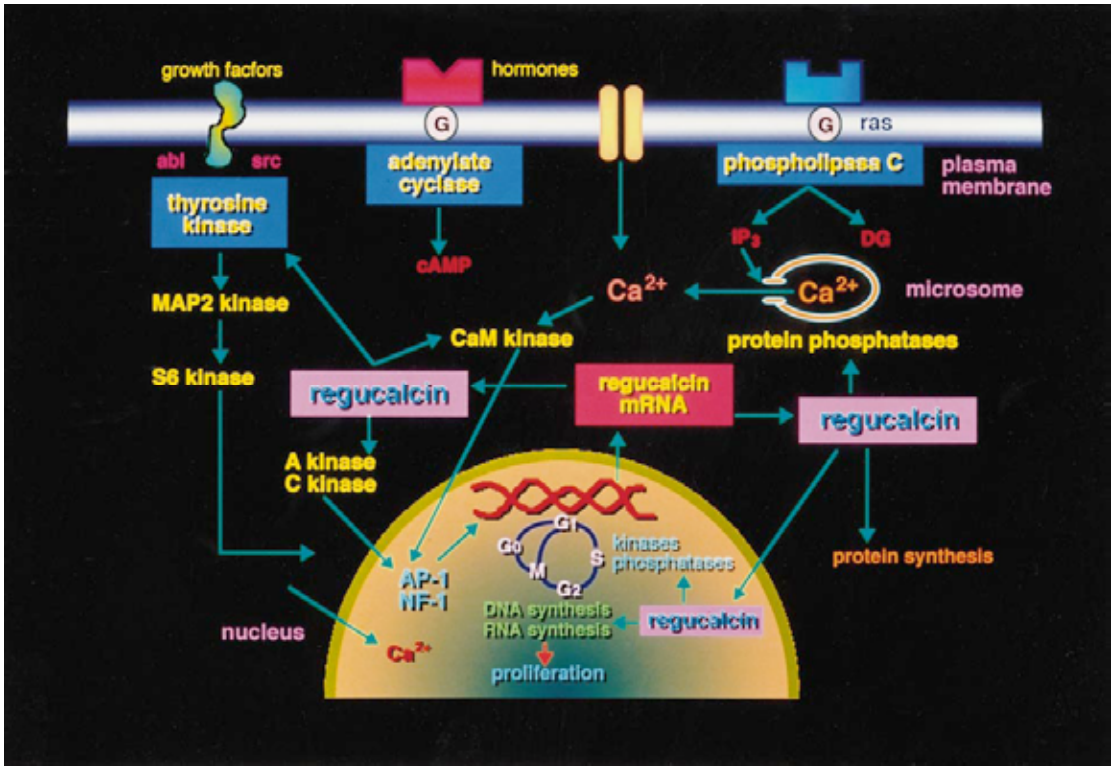

Figure 1.15.2.1. The Targets of RGN at the Nucleus

The diagram shows the signalling pathways that RGN are believed to be able to affect the activities of by interacting with some other associated proteins. These targets of RGN, which are located at the nucleus, are important in rat liver regeneration (Yamaguchi, 2000b)

Later, experiments with HepG2 cells showed RGN over-expression is capable of preventing cell death caused by Ca^{2+} ionophore treatment, which was explained by RGN's ability to enhance PMCA Ca^{2+} transport activity (Fujita et al., 1998). In addition to this, PMCA's responsiveness to this modulation of its activity by RGN in rat brain is lost as aging progresses (Hanahisa and Yamaguchi, 2001). Smad3-knockout mice are resistant to radiation-induced liver damage and it has been suggested that their higher than normal expression levels of RGN could explain their resistance to apoptosis (Jeong et al., 2008). This latter observation further supports the idea that RGN plays a protective role in liver cells.

The expression level of RGN in brain has been shown to decrease with increasing age in rats (Fujita et al., 1992, Yamaguchi et al., 1999, Fujita, 1999). Treatment with amyloid β-peptide protein (residues 1-42; well established to be associated with Alzheimer's disease) has been demonstrated to stimulate a decrease in RGN gene expression in primary rat cortical neuronal cells. With this, a compound called EUK4010 was shown to be capable of partially reversing the reduced RGN expression of this treatment (Sun et al., 2006).

1.16.2. RGN & Liver Regeneration

RGN mRNA levels increase in regenerating livers from start to completion of the process, which suggests it has a role in tissue maturation. Partial hepatectomy of a rat's liver can induce an increase in its RGN mRNA abundance, which is most notable 24-hours after surgery and thus suggests enhancement of RGN expression occurs in the S-phase of the cell cycle (Yamaguchi, 2000b). Changes in RGN expression levels have also been shown to directly correlate with the Ca^{2+} content in liver (Yamaguchi and Kanayama, 1995). With regards to function, RGN has been shown to inhibit DNA (Yamaguchi and Kanayama, 1996, Misawa et al., 2001, Morooka and Yamaguchi, 2002) and protein (Tsurusaki and Yamaguchi, 2000b) synthesis (both with and without the presence of Ca^{2+}) in regenerating liver. Thus RGN is likely to play a role in controlling DNA and protein synthesis levels in this process. Diabetes and alcohol consumption, both of which can affect liver health, can both decrease RGN expression levels in rats (Isogai et al., 1997). Transgenic rats, which were treated to exhibit a hyperlipidemic disease state, have shown RGN can decrease leptin mRNA levels in both liver and adipose tissue, as well as also decrease

adiponectin mRNA levels in liver (Yamaguchi et al., 2004a, Yamaguchi and Nakagawa, 2007).

1.16.3. RGN the Anti-Oxidant

RGN is capable of preventing oxidative stress damage in brain tissue by maintaining low levels of both reactive oxygen species (ROS) and NADPH oxidase activity (Son et al., 2006). This may be related to RGN being able to influence SOD activity in rat heart (Ichikawa and Yamaguchi, 2004). Indeed, over-expression of human RGN in HepG2 cells has been linked to reduced SOD protein levels (Handa et al., 2009). Over-expression of human RGN in P19 cells has been shown to be protective against oxidative stress induced by peroxy radicals (Son et al., 2008). RGN protein levels have been shown to increase in the hippocampus of rat brain 4 weeks after being treated with kainate, which induces oxidative stress, and this change in RGN expression is likely to be promoted by activation of the ERK signalling pathway (Son et al., 2009). RGN can act as a liver-specific gluconolactonase and plays an important role in vitamin C metabolism, which has been confirmed with the use of RGN knockout mice (section 1.17).

1.16.4. RGN & Cancer

Over-expression of human RGN in P19 cells has been shown to result in decreased cell proliferation when compared to control transfectants (Son et al., 2008). RGN protein levels have also been noted to be lower in H4-II-E cells when compared to normal rat liver cells (Inagaki and Yamaguchi, 2000). Furthermore, RGN mRNA levels have been shown to correlate with the progressive stages of tumour formation, whereby the former decreases as tumour growth and de-differentiation worsens, in breast and prostate cancers (Maia et al., 2009). These observations support the idea that a decrease in RGN expression could promote or be a consequence of tumorigenesis.

1.17. RGN Knockout Mice

In addition to male and female transgenic rats that have been used to demonstrate the effects of RGN in a number of tissues (section 1.13.5, 1.15.1 and 1.16.2), a RGN knockout mouse model has also been generated. Experiments with RGN knockout mice have shown such mice are highly susceptible to tumour necrosis factor-α-

induced apoptosis in liver (Ishigami et al., 2002). Furthermore, the livers of RGN knockout mice accumulate a higher than normal amount of lipid, which would indicate a deregulation of lipid metabolism (Ishigami et al., 2004). This is likely to be related to the ability of RGN to affect leptin and adiponectin expression levels in liver and adipose tissue (Yamaguchi et al., 2004a, Yamaguchi and Nakagawa, 2007). Poor glucose tolerance, caused by suppressed glucose-stimulated insulin secretion, has been observed of RGN knockout mice (Hasegawa et al., 2010).

The lungs of RGN knockout mice at the ages of 1,3 and 6 months are similar in structure to lungs from older mice, whereby they are characterised by enlarged peripheral airspace in the absence of alveolar destruction (Mori et al., 2004). Furthermore, these knockout mice are more susceptible to age- and smoking-related oxidative stress in their lungs. Thus it has been suggested that RGN could act in a protective role against diseases induced by long-term smoking, such as pulmonary emphysema (Sato et al., 2006). Indeed, the lungs of RGN knockout mice can manifest characteristics of pulmonary emphysema (Koike et al., 2010). Another organ that is in constant contact with atmospheric oxygen, and thus highly susceptible to oxidative stress, is the skin. RGN knockout mice suffer from poor skin development due to lower than normal ability to synthesise hydroxyproline, which is a modified amino acid that is essential for the maintenance of collagen strength in skin and hair, as well as lungs (Arai et al., 2009).

The most well characterised effect of RGN absence in the knockout mouse model is the removal of its ability to contribute to the synthesis of vitamin C, which is recognised as the main function of RGN that gives it its protective role against oxidative stress. RGN acts as a gluconolactonase and has been suggested to play a role in vitamin C synthesis in mice by lactonising L-gulonic acid to form L-gulono-γ-lactone, which is the penultimate reaction step of the ascorbic acid biosynthetic pathway (Kondo et al., 2006). RGN knockout mice are susceptible to developing scurvy and their loss of ability to synthesise vitamin C has been linked to an observation of increased superoxide formation in the brain of these mice following 4 and 8 weeks of vitamin C deprivation in their diet (Kondo et al., 2008). Hearing loss (Kashio et al., 2009) and higher than normal susceptibility to liver fibrosis (Park et al., 2010) have also been observed in RGN knockout mice and attributed to absence of vitamin C production. It should be noted that humans do not synthesise vitamin C but

do express RGN. The function of RGN in humans with regards to its role in dealing with oxidative stress has yet to be fully determined.

1.18. Aims of the Present Research

From examining the literature above, it was clear that information behind the regulation of SPCA activity was missing. The role of SPCA in hormone signalling under physiological conditions and in the context of disease had not been explored fully. SPCA's involvement in diseases other than HHD had not been of much focus in publications already available on this Ca^{2+}-ATPase. A well-recognised specific inhibitor of SPCA activity that could leave SERCA activity unaffected had yet to be available for use in SPCA research. This is all in contrast to the wealth of information that is available for SPCA's closely related microsomal Ca^{2+}-ATPase, SERCA.

For RGN, which was even more novel than SPCA, research had been done on its expression pattern in a relatively small range of tissue types, as well as on its role as a gluconolactonase in the vitamin C biosynthesis in mice. There are certainly other tissues that have yet to be tested for RGN expression in order to further define roles for RGN that are unrelated to vitamin C production. Studies have been done on RGN's ability to influence the activity of Ca^{2+}-dependent enzymes (in cell-free reaction mixtures), and the regulation of RGN expression by hormones and transcription factors has also been explored. However, only two studies have been done in the past on the effects of RGN on Ca^{2+} homeostasis with regards to its influence on Ca^{2+} mobilisation in intact cells.

The research to be discussed from hereon focuses on the aspect of regulation on SPCA and RGN. The main two aims of the study on SPCA were (1) to examine whether SPCA expression and/or activity can be affected by a disease state mimicked in cell culture (diabetes was chosen to fulfil this) and (2) to identify an inhibitor that can inhibit SPCA activity without affecting that of SERCA in isolated microsomes and intact cells. The main three aims of study on RGN were (1) to identify a new cell or tissue type that expresses RGN, (2) to visualise the effects of RGN on ER Ca^{2+} storage and hormone-stimulated Ca^{2+} mobilisation in intact cells, and (3) to produce a recombinant rat RGN that could be used to produce anti-RGN antibody (to help with the other two aims of the RGN study) and be purified for detailed biochemical studies.

CHAPTER 2.

MATERIALS & METHODS

CHAPTER 2.
MATERIALS & METHODS

2.1. Mammalian Cell Culture

2.1.1. General Mammalian Cell Culture Sterile Technique

Mammalian cell culturing was done using a vertical laminar flow hood. Cells were incubated at 37^{o}C and 5% v/v CO_2 using a CO_2 incubator. All materials placed into the flow hood and incubator were sterilised using 70% v/v ethanol. Surfaces of the flow hood were also cleaned with 70% v/v ethanol before and after use. All solutions and cell-handling materials were either purchased in sterile form (e.g. culture flasks and pipettes) or sterilised by autoclaving (at 110-120^{o}C and 15psi for 20 minutes) prior to their use in the flow hood. Waste solutions were discarded into Precept (Johnsons).

2.1.2. A7r5 Cell Culture & Glucose Treatment

Rattus norvegicus (Norwegian rat) embryonic thoracic aortic smooth muscle cell-line, A7r5 (a gift from Prof. C.W. Taylor; University of Cambridge, UK), was cultured in Dulbecco's Modified Eagle Medium (DMEM; Lonza), which was supplemented with 10% v/v foetal bovine serum (FBS; PAA), 4mM L-glutamine (PAA), 1% v/v penicillin-streptomycin (filter-sterilised with a 0.2μm pore filter) (PAA) and 1% v/v non-essential amino acids (PAA). The media also contained 25mM D-glucose for general culture of cells (as recommended by the American Type Culture Collection (ATCC)) and to obtain cells in a hyperglycaemic (HG) state. Media that contained 5.5mM D-glucose instead was used to obtain cells in a physiologically normal glucose (NG)-fed state. The media was replaced with fresh media every 2 and 4 days after sub-culturing. Cells were used for sample collection or experiments 5 days after sub-culturing.

2.1.3. COS-7 Cell Culture & Transfection

Cercopithecus aethiops (African green monkey) kidney cell-line, COS-7 (a gift from Dr. N. Hotchin; University of Birmingham, UK), was cultured in DMEM (Lonza), which was supplemented with 10% v/v FBS (PAA), 2mM L-glutamine (PAA) and 1% v/v penicillin-streptomycin (filter-sterilised) (PAA). The media also contained 5.5mM D-glucose as the only glucose concentration used for culture of COS-7 cells.

Cells were transfected one day after sub-culturing using Genejuice reagent (Novagen) and maxiprep DNA (section 2.3.1). The manufacturer's protocol for the use of the transfection reagent was followed. Cells were seeded (section 2.1.4) at a density of $1x10^5$ cells per well of a 12-well plate, $2x10^5$ cells per well of a 6-well plate, or $1.2x10^6$ cells per 10cm diameter Petri dish. Cells were transfected 24 hours after seeding.

The transfection reagent was mixed with transfection media, which was DMEM media (without phenol red) (PAA) containing 25mM D-glucose and only supplemented with 2mM L-glutamine (PAA) (i.e. no FBS and antibiotics). This first mixture was incubated in the culture hood for 5 minutes. Maxiprep DNA was added to the mixture and incubated in the culture hood for a further 15-20 minutes before being added to the culture media. After applying the transfection mixture, cells were returned to the cell culture incubator for 48 hours before experimental use.

An optimised ratio of 3µg:9µl of plasmid DNA-to-transfection reagent was used per 100µl of transfection media in each well of a 6-well plate for all plasmids used (as advised by Dr. J. Vanoevelen; Katholieke Universiteit Leuven, Belgium). Manufacturer's instructions were followed to re-scale quantities of DNA, transfection reagent and transfection media for plates and Petri dishes of other sizes. From this, 1.5µg:4.5µl and 18µg:54µl ratios of DNA-to-reagent was used for each well of a 12-well plate and each 10cm diameter Petri dish, respectively.

2.1.4. Sub-culturing of Mammalian Cells

Sub-culturing (also known as 'passaging') was done when cells were judged to be approximately 70-80% confluent (i.e. total cell population covered 70-80% of the culture flask surface on which cells had adhered to) by viewing them using a Nikon TMS light microscope at 100x magnification. Media was removed from cells in culture flasks, which were then washed with Dulbecco's phosphate buffered saline (DPBS; Lonza). Trypsin-EDTA (Invitrogen) or trypsin-Versene (Lonza) solution was then applied and incubated with the cells for 2-5 minutes in the CO_2 incubator. After this treatment (known as 'trypsinisation'), the culture flask was agitated by gentle tapping to fully detach its contents of cells, fresh media was added to re-suspend the cells and a small volume of this suspension was transferred into a new culture flask containing fresh media (referred to as 'seeding') to start a new passage of cell culture.

Cells were sub-cultured every 3-4 days for general maintenance. With regards to volumes of solutions typically used for a 75cm^2 culture flask, cells would be grown in 10ml of media, washed with 5ml of DPBS, trypsinised with 2ml of trypsin solution, re-suspended after trypsinisation with 5ml of media and 1-2ml of cell suspension would be used to seed a new 75cm^2 flask. These volumes would be re-scaled for culture flasks of other sizes (e.g. 25cm^2 and 162cm^2).

2.1.5. Cryopreservation & Rejuvenation of Mammalian Cells

Cells were frozen in liquid nitrogen, when not required for cell culture, to maintain a reserve of them for future use. After sub-culturing, the remaining suspension of cells not used to seed a new flask was centrifuged at 900g for 10 minutes at 4^{o}C, the media was removed and the cell pellet was re-suspended in fresh media containing 10% v/v DMSO (sterile, biotechnology grade; Sigma). 5ml of media would be used for cells from a 75cm^2 flask that was 70-80% confluent and had only been sub-cultured to produce one new 75cm^2 flask of cells. This cell suspension was then aliquoted into cryovials and stored in an isopropanol jacket at -80^{o}C for 1-5 days. After this, the frozen vials were moved into and stored long-term in a liquid nitrogen storage tank until required for cell culture.

To use the frozen cells for cell culturing (known as 'rejuvenation'), cryovials were taken out of liquid nitrogen and its contents quickly thawed by repeated agitation of the cryovial in a 37^{o}C water bath. The thawed cells would then be diluted 10-fold with fresh media and centrifuged at 900g for 10 minutes at 4^{o}C. The media was then removed and cell pellet re-suspended in fresh media at the appropriate volume to fill a new culture flask for growth in the cell culture incubator. The media was changed 24 hours later. Frozen vials of *Mus musculus* (mouse) Sertoli cell-line, TM4, and *Homo sapiens* (human) neuroblastoma cell-line, SH-SH5Y (a gift from Dr. M. Grant; University of Birmingham, UK) were thawed and centrifuged in the way as stated above for the preparation of their total cell lysates, but were not seeded into cell culture flasks for growth.

2.1.6. Counting Mammalian Cells using a Haemocytometer

To quantify the population of cells in a suspension, 10µl of the cell suspension was applied onto the counting grid of a haemocytometer, which was sealed with its coverslip and viewed under the light microscope. The counting grid used was as

shown in figure 2.1.6.1. The volume of each of the nine large squares (referred to as the 'corner' or 'middle' square in figure 2.1.6.1) was 0.1µl (1mm width x 1mm length x 0.1mm depth). Three out of the nine large squares were selected randomly for counting their individual content of cells. The three numbers of cells were then averaged and multiplied by 10 to give the number of cells in 1µl of the original cell suspension from which the sample was taken. By dividing the required number of cells (e.g. the seeding density for wells of a 6-well plate) by the concentration of cells in the cell suspension, the volume of cells needed to obtain the former of these two was determined.

2.1.7. Preparation of Acid-Etched Coverslips

1cm diameter glass coverslips were immersed in a minimal volume of concentrated nitric acid and left for 1 hour in a fume cupboard. The acid was then discarded into a copious volume of cold tap water and a running tap of cold water was used to fully dilute the acid still on the coverslips for 5-10 minutes. After excess water was discarded, the coverslips were transferred into a glass Petri dish and rinsed with fresh cold tap water for 30 minutes. Following this, the water in the glass Petri dish was removed as much as possible and coverslips were immersed in a minimal volume of 100% v/v methanol. The Petri dish of acid-etched coverslips was left in a fume cupboard for 24-48 hours to allow the methanol to evaporate off before being autoclaved.

2.1.8. Mammalian Cell Culture on Acid-Etched Coverslips

Each well of a 12-well plate was filled with one acid-etched coverslip, followed by 0.5ml of autoclaved 2% w/v gelatin solution (made by dissolving porcine skin gelatin powder (Sigma) in dH_2O) and incubated in the cell culture incubator for 30 minutes. During this time, the cell suspension needed for seeding the coverslips was obtained by sub-culturing (section 2.1.4) and its population of cells counted (section 2.1.6) to determine the volume of cells required to seed each coverslip. For A7r5 cells, $1x10^4$ cells were used to seed each coverslip for fluorescence Ca^{2+} imaging (section 2.5.1), and $3\text{-}4.5x10^4$ cells were used to seed each coverslip for immunofluorescence and lectin staining (section 2.5.2). For COS-7 cells, $1x10^5$ cells were used to seed each coverslip for both fluorescence Ca^{2+} imaging and immunofluorescence experiments. For each well of the 12-well plate, the gelatin solution was removed, replaced with

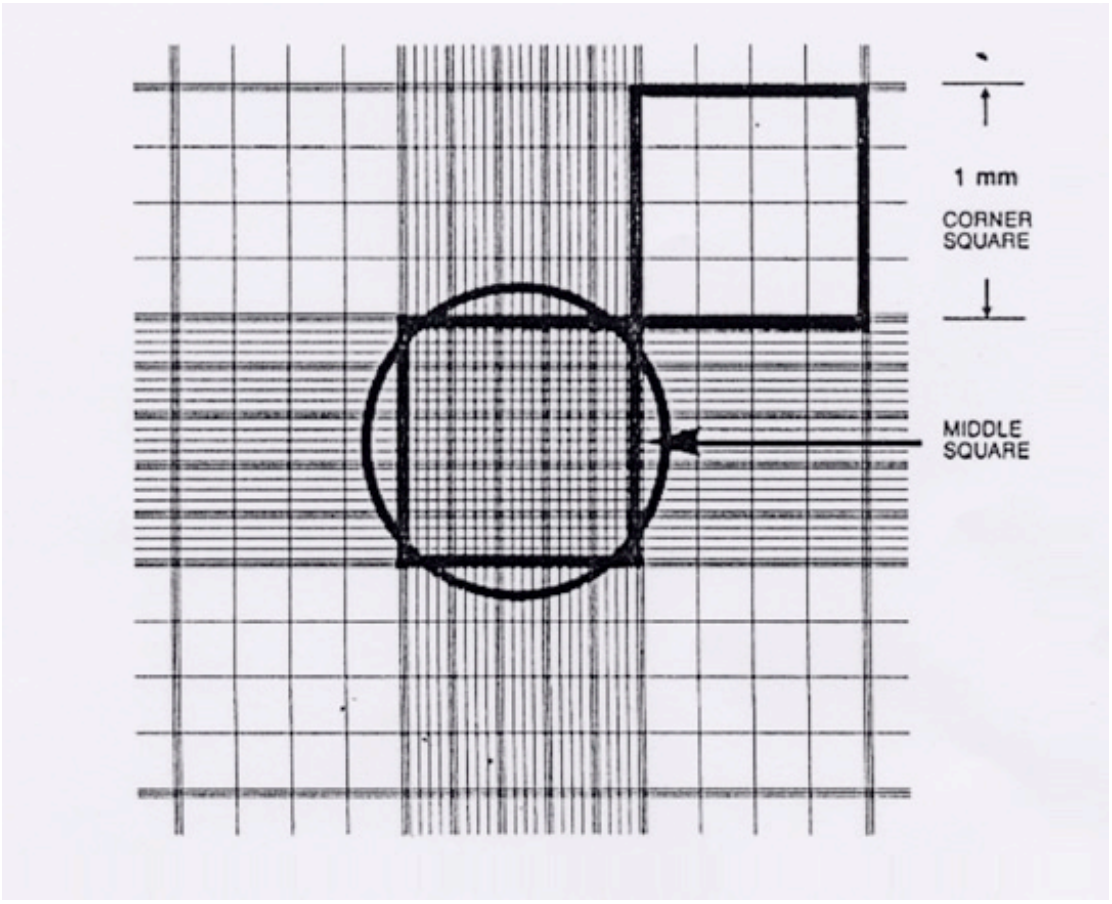

Figure 2.1.6.1. The Counting Grid of a Haemocytometer

(Image source: The Health Protection Agency (UK) website (http://www.hpacultures.org.uk/technical/ccp/cellcounting.jsp))

2ml of fresh media and the cells were seeded onto the coverslips.

2.2. Sample Preparation from Mammalian Cells

2.2.1. cDNA from Cell Culture mRNA Extracts

0.1% v/v diethylpyrocarbonate (DEPC)-treated PBS (DEPC-PBS) was made by adding DEPC (Sigma) to PBS (0.14M NaCl, 2.7mM KCl, 1.5mM KH_2PO_4 and 8.1mM Na_2HPO_4; pH 7.4) and left in a fume cupboard overnight before being autoclaved. DEPC-dH_2O was also made (by treating dH_2O with DEPC in the same way as PBS), which was used to make 70% v/v ethanol for cleaning work surfaces and materials entering the flow hood.

Cells were grown from a seeded density of $6x10^5$ cells per $75cm^2$ culture flask. They were harvested by trypsinisation, centrifuged at 900g for 10 minutes at 4^oC, the media was removed and cell pellet re-suspended in DPBS to have its population counted (section 2.1.6). The latter cell suspension was then centrifuged again at 900g for 10 minutes at 4^oC to allow removal of DPBS and re-suspension of the cell pellet with DEPC-PBS to give a concentration of $1x10^4$ cells/µl. This last suspension of cells was used for extraction of total mRNA content from $2x10^4$ cells and its conversion to cDNA copies using a CellsDirect™ cDNA synthesis kit (Invitrogen), along with a GeneE thermocycler (Techne), and following manufacturer's instructions. Sample preparation was done in the flow hood. All cDNA samples were stored at -80^oC.

2.2.2. Total Cell Lysate from Cell Cultures & Adult Boar Sperm

For A7r5 cells, a proportion of each cell suspension used for cDNA preparation was also used for preparing total cell lysates. $1\text{-}1.25x10^6$ cells were mixed with an equal volume of lysis buffer (50mM Tris-HCl (pH 7.4), 150mM NaCl, 1mM EDTA, 1% v/v Triton X100, 1% w/v sodium deoxycholate, 0.1% w/v SDS and 1mM PMSF) and incubated on ice for 2 hours, before being passed through a 25-guage needle via a syringe 5 times to homogenise the mixture. The cell lysate was then centrifuged at 2,400g for 5 minutes at room temperature, the supernatant was collected and the pellet was discarded. The protein concentration in the samples (the supernatants) was determined using the Bradford assay (section 2.4.3). Samples were stored at -80^oC.

The method used for preparing cell lysates from other cell-lines, as well as adult boar sperm, was the same as that for A7r5 cells, but were lysed whilst still

attached to culture plates (except for boar sperm cells, which were cleared from ejaculate fluid by centrifugation at 900g for 10 minutes at 4°C before lysis buffer was added to the cell pellet). Media was removed from the cells, which were washed with DPBS before lysis buffer was added to them. Cells were incubated with the lysis buffer for 10 minutes at room temperature (or 1 hour on ice for boar sperm) with gentle agitation, before the cell lysate was homogenised, centrifuged and supernatant collected as described for A7r5 cells.

2.2.3. Microsomal Membranes from Cell Cultures

The method was modified from that described previously (Wootton et al, 2004). A7r5 cells were seeded and grown at equal densities on 10cm diameter Petri dishes. COS-7 cells were transfected and grown on 10cm diameter Petri dishes (section 2.1.3). A7r5 cells were harvested by trypsinisation, centrifuged at 900g for 10 minutes at 4°C to allow removal of the media, and the cell pellet was re-suspended in DPBS. COS-7 cells were washed with DPBS after removal of media, detached from Petri dishes using a cell scraper and collected into fresh DPBS.

In both cases, the cells were then centrifuged at 900g for 10 minutes at 4°C, the DPBS was removed and the cells were re-suspended in microsomal membrane preparation buffer (5mM HEPES-KOH (pH 7.2), 0.32M sucrose, 0.2mM benzamidine HCl, 10µM leupeptin HCl and 0.2mM PMSF). This cell suspension was homogenised on ice using a Polytron homogeniser (with regular pauses to prevent over-heating of the sample), followed by 30 strokes of a Potter homogeniser. The homogenate was centrifuged at 20,000g for 15 minutes at 4°C and the supernatant collected. The pellet was re-suspended in fresh buffer to be homogenised and centrifuged again. Both supernatants were combined and centrifuged at 100,000g for 50 minutes at 4°C. The supernatant from this latter spin was discarded. The remaining pellet (containing the microsomal membranes) was re-suspended in fresh buffer and its protein concentration determined (section 2.4.3), before being aliquoted, snap frozen with liquid nitrogen and stored at -80°C.

2.2.4. Cytosolic Fractions from Adult Male Rat Organs

Samples were prepared from brain, kidney, liver, testis, fat pads, heart and lungs that had been stored at -80°C. These were thawed on ice, DPBS with 1mM PMSF was added to them, they were cut up into small pieces, placed into a Potter homogeniser

and subjected to repeated mechanical homogenisation intermittently for 5-10 minutes. This homogenate was then centrifuged at 100,000g for 1 hour at 4^{o}C. The supernatant was collected and stored at -80^{o}C.

2.3. Preparation of Plasmid DNA for COS-7 Transfection

2.3.1. Maxipreps

Plasmids containing the coding sequences for human SPCA1d (hSPCA1d) (in pMT2 vector) and human SERCA2b (hSERCA2b) (in pMT2 vector) (both gifts from Dr. J. Vanoevelen; Katholieke Universiteit Leuven, Belgium), along with rabbit SERCA1b-EGFP (in pcDNA3.1(-) vector) (a gift from Dr. J. M. East, Southampton University, UK), human SMP30 (hSMP30) (in pcDNA3.1 vector), as well as control (i.e. no sequence insert present) pcDNA3.1(-) plasmid (the latter two plasmids were gifts from Prof. J. Lee; Pusan National University, Korea) and Prof. A Ishigami (Tokyo Metropolitan Institute of Gerontology, Japan), were purified using a Purelink HiPure Plasmid Filter Purification Maxiprep kit (Invitrogen) following manufacturer's instructions. Other DNA purification kits were also sometimes used, which were Qiagen QIAfilter Maxiprep kit and Sigma Genelute Endotoxin-Free Midiprep kit. In all three cases, DNA was purified from cultures of DH5-α cells transformed with these plasmids (section 2.11.5).

2.3.2. Quantification of Maxiprep DNA

Maxiprep DNA was quantified by measuring its absorbance at 260nm in duplicate using a spectrophotometer. The blank and buffer used to dilute the DNA was the elution buffer used to re-suspend the final pellet of DNA. The absorbance readings were averaged, and this average absorbance value was multiplied by 50 (a constant value in the calculation) and the dilution factor (used to dilute the maxiprep DNA with buffer in the cuvette). This calculation gave the concentration of DNA in the maxiprep in units of mg/ml.

2.3.3. Restriction Digest of Maxiprep DNA

Suitability of restriction endonucleases (BIOLINE) for digestion analysis of maxiprep DNA were checked using the NEB Cutter V2.0 web-based program (NEB) to note the number of DNA fragments that would be produced after digest and ensure most or all of them would be visible in a 0.8% w/v agarose gel by being at least ~1kb in size. The

expected digest DNA band sizes for hSPCA1d-pMT2, hSERCA2b-pMT2 and rabbit SERCA1b-pcDNA3.1(-) are shown by the restriction maps in figure 4.2.1.2. Those for hSMP30-pcDNA3.1(-) and control pcDNA3.1(-) are shown by the restriction map in figure 5.2.4.1.

Maxiprep DNA was diluted at a 1:5 ratio in autoclaved dH_2O before adding to the reaction mixture. A 10µl reaction volume was made with 5µl of diluted maxiprep DNA, 20 units of each restriction endonuclease, 1x reaction buffer (supplied with the enzymes) and autoclaved dH_2O. Restriction digest reactions were incubated in a 37°C water bath for 1 hour. The reaction mixtures were electrophoresed through a 0.8% w/v agarose gel afterwards (along with uncut diluted maxiprep DNA) and a 1kb DNA ladder, and stained (section 2.4.2).

2.4. Experiments on Samples from Mammalian Cells

2.4.1. PCR

Each 50µl PCR reaction mixture contained 2.5 units of BIOTAQ™, 1x NH_4 buffer (provided with the enzyme), 2mM dNTP mix, 1µl of cDNA sample prepared from A7r5 cells (section 2.2.1), $MgCl_2$, forward and reverse primers, and autoclaved dH_2O. Reaction reagents were purchased from BIOLINE and primers were made by Alta Bioscience (University of Birmingham, UK). Amount of primers (and references from which sequences were obtained), $MgCl_2$ concentrations, annealing temperatures (T_m) and number of cycles for each pair of primers used are listed in table 2.4.1.1. Primers for SPCA1 (all splice variants) and SERCA (all isoforms) were used. Both glyceraldehyde 3-phosphate dehydrogenase (GAPDH) (an enzyme of the glycolytic pathway) and β-actin (a contractility marker (Owens et al., 1986)) were also detected for using PCR. Ribosomal protein L19 (RPL19) PCR product levels were used to represent the amount of total cDNA content that was present in the samples (Al-Bader and Al-Sarraf, 2005). Sequences to all primers, which were all designed for rat mRNA, used are listed in table 2.4.1.2. The T_ms used for all primers were those quoted in their associated references ± 1°C. A sample of PCR products for SPCA1 was checked to ensure the correct mRNA sequences had been detected, by using their agarose gel extracts (section 2.10.1) and the SPCA1 PCR primers for DNA sequencing (section 2.10.5).

mRNA of Interest	Reference	Amount of Each Forward/ Reverse Primer Used (pmol)	[$MgCl_2$] (mM)	T_m (^oC)	Number of Cycles	Product size (bp)
SPCA1	(Missiaen et al., 2002a)	20	4	52.1	35	224
SERCA	(Varadi et al., 1996)	20	2	58.0	35	288
GAPDH	(Di Napoli et al., 2007)	100	2	60.0	28	400
β-actin	(Varadi et al., 1996)	3.5	2	58.0	28	255
RPL19	(Al-Bader and Al-Sarraf, 2005)	0.3	3	52.1	28	321

Table 2.4.1.1. PCR Conditions for Primers Used on A7r5 cDNA Samples

mRNA of Interest	Primer Sequences (5' to 3')	
	Forward Primer	Reverse Primer
SPCA1	AAACTGGAACCCTGACGAAG	TTGGCTTTCCCATCAGAGTG
SERCA	TGCCTGGTAGAGAAGATGAA	CCCTTCACAAACATCTTGCT
GAPDH	ACCACAGTCCATGCCATCAC	TCCACCACCCTGTTGCTGTA
β-actin	ATCCGTAAAGACCTCTATGC	ATTTGCGGTGCACGATGGAGG
RPL19	ATCGCCAATGCCAACTCT	GAGAATCCGCTTGTTTTTGAA

Table 2.4.1.2. Sequences of Primers Used on A7r5 cDNA Samples

Either a BIORAD MyCycler™ or BIOMETRA Personal Cycler thermocycler was used. For all primers, each cycle consisted of a melting step at 95^{o}C for 1 minute, an annealing step at specific temperatures (stated in table 2.4.1.1) for 1 minute and an extension step at 72^{o}C for 1 minute. An initial melting step prior to the first cycle of each PCR was done at 95^{o}C for 2 minutes. A final extension step at the end of the last cycle of each PCR was done at 72^{o}C for 10 minutes, and reaction mixtures were maintained at 4^{o}C following this last step temporarily before being stored at -80^{o}C.

2.4.2. Agarose Gel Electrophoresis

2% w/v agarose in TBE buffer (89.2mM Tris, 88.9mM boric acid and 2mM EDTA; pH 8.0), which was used for PCR products less than 1kb in size (c.f. 0.8% w/v agarose gels for plasmid DNA or its restriction digest fragments greater than or equal to 1kb in size), was heated until fully dissolved and then left to cool to approximately 40-50^{o}C (at which it was comfortable enough to hold the container with hand but still in liquid phase). The cooled solution was then poured into a mould with a well comb inserted and allowed to cool further to form a solid gel. The well comb was carefully removed (leaving well spaces into which samples could be loaded) and the gel was immersed into TBE buffer in an electrophoresis tank (with the wells closest to the cathode electrode).

10µl of PCR product was mixed with 2µl of 6x DNA loading buffer (0.25% w/v bromophenol blue, 0.25% w/v xylene cyanol FF and 30% v/v glycerol) and 10µl of this mixture was loaded into the gel for each sample. A 100bp DNA ladder (NEB) was also loaded. The loaded samples and ladder were electrophoresed through the gel at 90 volts until the band of purple colour from the DNA loading buffer was seen to have moved three-quarters of the way through the gel (towards the anode electrode). The gel was then removed from the tank and stained with Sybr Safe DNA stain (Invitrogen) for 1 hour with gentle agitation. The stained gel was viewed using a UV transluminator and images of the DNA fragments were captured using an UVP ImageStore 5000 system. Some gel images were analysed for pixel intensity of product fragments using ImageJ software (section 2.6).

2.4.3. Protein Estimation: The Bradford Assay

Protein Assay Reagent (BIO-RAD) was used to estimate the concentration of protein present in total cell lysates (section 2.2.2), microsomal membranes (section 2.2.3), nickel affinity column chromatography fractions (section 2.12.6) and dialysed/concentrated protein solutions (section 2.12.7-8). 1-30µl of sample was mixed with 170µl of working reagent and the total volume was made up to 200µl using dH_2O for each sample in wells of a 96-well plate. Mixtures were left to incubate at room temperature for 10 minutes before their absorbance at 590nm was read using a Dynatech MRX plate reader. Readings for each sample were done in triplicate. A calibration curve was constructed with absorbance readings from different amounts of bovine serum albumin (BSA) solution within a range of 0-15µg. This was used to convert the average absorbance readings of each sample into their protein concentration values.

2.4.4. SDS-PAGE

A BIORAD mini-PROTEAN® 3 system was used and manufacturer's instructions were followed to set up and use the apparatus. A 10% w/v acrylamide resolving gel was made from a mixture containing 3ml of resolving gel buffer (1.5M Tris and 0.4% w/v SDS; pH 8.8), 4ml of Ultra Pure Protogel (29.2% w/v acrylamide and 0.8% w/v bis-acrylamide; Geneflow), 5ml of dH_2O, 40µl of 10% w/v ammonium persulphate solution and 20µl of tetramethylethylenediamine (TEMED; Sigma). A 4% w/v acrylamide stacking gel was made from a mixture containing 1.5ml of stacking gel buffer (0.5M Tris and 0.4% w/v SDS; pH 6.8), 0.75ml of Ultra Pure Protogel, 3.75ml of dH_2O, 30µl of 10% w/v ammonium persulphate solution and 15µl of TEMED. A thin layer of saturated iso-butanol solution (made from mixing dH_2O and iso-butanol at a 1:1 ratio) was placed on top of the resolving gel to keep the top edge of the gel smooth once it had polymerised. Running buffer (192mM glycine, 25mM Tris and 0.1% w/v SDS) was used to fill the electrophoresis tank.

Each protein sample was mixed at a 1:1 ratio with sample loading buffer, which was made from sample buffer (125mM Tris, 4.6% w/v SDS and 20% w/v glycerol) and 2-mercaptoethanol mixed at a 20:1 ratio, along with a trace amount of bromophenol blue. Samples were then heated at 100^{o}C for 10 minutes before being loaded into the wells of a gel. Protein molecular weight markers (Sigma (10-250kDa) or NEB (2-212kDa, 7-175kDa)) were also loaded. Samples were electrophoresed

through the gel at 120 volts (~20mA) until the band of blue colour from the sample loading buffer had started to move out of the gel and into the running buffer. The gels were carefully separated from the glass plates and used either for Coomassie blue protein staining (section 2.4.5.) or Western blotting (section 2.4.6.).

2.4.5. Coomassie Blue Protein Staining

SDS-PAGE gels were immersed into a minimal volume of Coomassie blue protein stain (0.125% w/v Coomassie brilliant blue R250, 7.5% v/v glacial acetic acid and 45% v/v methanol) and left to incubate at room temperature for 1 hour with gentle agitation. Following this, the stain solution was remove and replaced with de-stain solution (5% v/v glycerol and 7.5% v/v glacial acetic acid), which was left to incubate with the gel at room temperature overnight to allow removal of background staining. Stained gels were imaged using a Kodak Electrophoresis Documentation & Analysis System 120, which included a Kodak DC290 Zoom Digital Camera and Kodak 1D (version 3.5.2) software.

2.4.6. Western blotting: Anti-SPCA1, Anti-SERCA & Anti-α-Actin

Proteins in SDS-PAGE gels were transferred onto nitrocellulose sheets at 30 volts (~400mA) using an Invitrogen XCell II blot module and following manufacturer's instructions. The transfer buffer used to soak the membranes and fill the tank was the same as the running buffer used for SDS-PAGE but with 20% v/v methanol added. Transfer took place for 1 hour. Once complete, nitrocellulose membranes were stained with Ponceau protein stain (0.1% w/v Ponceau-S, 0.1% w/v TCA and 1% v/v glacial acetic acid) for 5 minutes with gentle agitation. Excess stain was briefly washed off with dH_2O. The positions of the molecular weight markers were marked with a pencil onto the membranes before they were immersed in 5% w/v milk solution, which was made from semi-skimmed milk powder dissolved in TTBS buffer (25mM Tris-HCl (pH 8.0), 150mM NaCl and 0.05% v/v Tween-20). The membranes were then left to incubate at either room temperature for 1 hour with gentle agitation or 4^{o}C overnight to allow proteins in the milk solution to block non-specific binding sites.

For treatment with antibodies, the milk solution was discarded and the membranes were washed three times briefly with TTBS. Primary antibodies (specific to the protein of interest) were diluted in fresh TTBS buffer and incubated with the

membranes for 1.5 hours. Following this, the antibodies were discarded and the membranes were washed three times with TTBS, with each wash lasting for 5 minutes with gentle agitation. Fresh 5% w/v milk solution was incubated with the membrane for 30 minutes, discarded and the membrane washed three times briefly with TTBS. Horse radish peroxidase (HRP)-conjugated secondary antibodies (specific to the F_c region of the primary antibody) were diluted in fresh TTBS buffer at a ratio of 1:3000 and incubated with the membranes for 1 hour. The secondary antibodies were discarded afterwards and membranes were washed five times with TTBS, with each wash lasting for 5 minutes with gentle agitation.

Antibody-treated membranes were incubated with Immobilon™ Western chemiluminescent HRP substrate (Millipore) for 10 minutes in the dark. After substrate incubation, membranes were kept in the dark to be dried and wrapped with Saran wrap. Creases in the Saran wrap were kept as minimal as possible. The membranes were then stored in a film case to protect from light. Viewing of chemiluminescent protein bands were done using a BIO-RAD Fluor-S Max MultiImager, which was set to capture images once every minute for 10 minutes (to allow monitoring of image development) and to detect for chemiluminescence blotting at high sensitivity. Only the last image of the 10 minutes was used. Some images were analysed for pixel intensities of protein bands using ImageJ (section 2.6).

Dilution ratios for anti-SPCA1 (custom polyclonal antibody from BioCarta GmbH and as referenced previously (Wootton et al., 2004)), anti-SERCA (monoclonal Y1F4) (a gift from Dr. J.M. East; Southampton University, UK), anti-SERCA2 (monoclonal clone ILD8) (Abcam) and anti-α-actin (monoclonal clone 1A4) (Sigma) primary antibodies were 1:75, 1:800, 1:2500 and 1:800, respectively. With regards to secondary antibodies, anti-rabbit HRP was used for anti-SPCA1, and anti-mouse HRP was used for both anti-SERCA and anti-α-actin. The expected protein band sizes for SPCA1 and SERCA were both 100kDa (Wootton et al., 2004), α-actin was 42kDa (according to product literature from manufacturer) and SERCA-EGFP was 127kDa.

2.4.7. Ca^{2+}-ATPase Activity: The Phosphate Liberation Assay

The method was as described previously (Wootton and Michelangeli, 2006) with some modifications. Each assay consisted of a 200µl volume of reaction buffer

(45mM HEPES-KOH (pH 7.0), 6mM $MgCl_2$, 2mM NaN_3 (azide) and 0.25mM sucrose), which was supplemented with 1mM EGTA, 1µg ionophore A23187 and 2µM sodium vanadate. 1mM $CaCl_2$ was added for measurements of Ca^{2+}-dependent activity to give a free [Ca^{2+}] of 1µM. 1µM thapsigargin (Sigma) was added for measurements of thapsigargin-insensitive activity. Microsomal membranes were added at quantities of 20µg (A7r5) or 5-10µg (COS-7). 6mM ATP (Sigma) and 50µl of 6.5% w/v TCA solution were added to give negative control reactions with denatured membranes.

For experiments with bis-phenol, tetrabromobisphenol-A (TBBPA), trifluoroperazine (TFP), 2-aminoethoxydiphenyl-borate (2-APB) and bisphenol-A (BPA) (all purchased from Sigma, except bis-phenol (Pfaltz & Bauer), which were all prepared in DMSO, these was added to assay mixtures before initiating reactions and contributed to 0.1% of the total volume in each reaction mixture. The same was done with experiments that involved nicotinic acid adenine diphosphate (NAADP) and cyclic adenine diphosphate ribose (cADPR), except they were both prepared in dH_2O.

All reaction mixtures were incubated at 37^{o}C for 10 minutes before 6mM ATP was added to all except the controls to initiate activity. Reactions then remained at 37^{o}C to proceed for 90 minutes (A7r5) or 45 minutes (COS-7). Other time points were also tested for A7r5 (data not shown) and COS-7 (see section 4.2.4) membranes during optimisation trials. 50µl of 6.5% w/v TCA solution was added to stop reactions (at all except the negative controls), which were then incubated on ice for 10 minutes before they were centrifuged at 20,000g for 10 minutes at room temperature. For each reaction mixture, 100µl of supernatant was added to 150µl of copper acetate buffer (11.25% v/v glacial acetic acid, 0.25% w/v copper acetate and 0.2M sodium acetate; pH 4.0) in a well of a 96-well plate. To this, 25µl of 5% w/v ammonium molybdate was added and followed by 25µl of ELAN solution (2% w/v p-methyl-aminophenolsulphate and 5% w/v sodium sulphite). The assay mixtures were left to incubate at room temperature for 10 minutes before their absorbance of 850nm was read using a Dynatech MRX plate reader. A calibration curve was constructed with absorbance readings from different amounts of phosphate using KH_2PO_4 solution and within a range of 0-150nmol. This was used to convert the absorbance readings of the samples into values of amounts of phosphate.

For each reaction condition and Ca^{2+} concentration, each experiment consisted of three active assays and two negative control assays. The averaged value for the

control assays was subtracted from that for the active reactions to give the corrected amount of phosphate liberated for their associated reaction condition. The corrected values for the assays that contained no added $CaCl_2$ were then subtracted from that of their pair-matched assays that contained 1mM $CaCl_2$ to give the corrected amount of phosphate liberated that was Ca^{2+}-dependent. Each of these final values was then converted into a rate of amount of phosphate liberated/min/mg protein. Activity plots were produced using Prism (version 5) graph plotting software.

2.5. Fluorescence Microscopy with Mammalian Cells

2.5.1. Fluo-3 & Fluo-4 AM Single Cell Ca^{2+} Imaging

The method was as described previously (Ogunbayo et al., 2008) with some modifications. Hanks Balanced Salts Solution (HBSS; Sigma) (pH 7.2), which was supplemented with 4.5mM $NaHCO_3$ and 0.81mM $MgSO_4$, was used as the buffer for all steps. Supplementation with 1.26mM $CaCl_2$ or 1.26mM EGTA was done depending on if experiments required the presence or absence of extracellular Ca^{2+}, respectively, at both the wash and assay stage. Cells grown on coverslips (section 2.1.8) were loaded with 6μM Fluo-3 AM or 7.5μM Fluo-4 AM in HBSS that contained 1.26mM $CaCl_2$, 0.2mM sulfinpyrazone, 0.025% pluronic acid and 1% BSA. Incubation with dye lasted for 40 minutes, after which cells were washed with fresh HBSS that contained 0.2mM sulfinpyrazone for 10 minutes.

Each coverslip was transferred into a 3.5cm diameter Petri dish containing HBSS buffer, which was incubated at 37^{o}C using a heated stage at a Nikon TS-100F fluorescence microscope. 10x objective lens was used to view the cells. A Stellacam Astrovid^{3} was used to record videos (with an additional x10 magnification), which were saved onto a computer via connection with a Hauppage USB TV live video capture device and use of WinTV2000 software (Hauppage). The image capture rate for videos was one frame per second. Images were of 320x240 pixel resolution. Experiments started 1 minute after the start of video recording (to provide a stable baseline of fluorescence intensity) and total recording time for each experiment was either 5 or 10 minutes. A7r5 cells were treated with 10nM AVP (Bachem Biosciences) and COS-7 cells were treated with 10μM histamine (Sigma). 1μM thapsigargin was used to treat both A7r5 and COS-7 cells. A7r5 experiments also included those that involved their treatment with bis-phenol and 2-APB (section

2.4.7). All videos were analysed for their change in pixel intensity of individual cells over time, using ImageJ (section 2.6).

2.5.2. Immunofluorescence & Lectin Staining

Method was adapted from previous literature (Wootton et al., 2004). Cells grown on coverslips (section 2.1.8) were washed three times with DPBS between each incubation step. After discarding the media, cells were washed and fixed with 2% v/v formaldehyde in DPBS for 10-20 minutes at room temperature. Cells were then permeabilised with 0.1% v/v Triton X100 in DPBS for 5 minutes. Following this, anti-SPCA1, anti-SERCA (Y1F4) or custom-made anti-RGN (section 2.12.4) antibody was incubated with cells in DPBS at dilution ratios of 1:30-1:50, 1:50-1:100 and 1:100, respectively. FITC-conjugated secondary antibodies (Sigma) were incubated with cells for 1 hour afterwards at dilution ratios of 1:50-1:100. Tetramethylrhodamine (TMR)-conjugated wheat germ agglutinin (WGA) (Invitrogen) was incubated with A7r5 cells at 10µg/ml per coverslip for 1 hour.

After all labelling incubations, cells were washed three times with DPBS, once with dH_2O and excess liquid was dried off before being mounted onto glass slides using Hydramount (National Diagnostics). Cells were viewed and still images captured using the same set-up as used for single cell Ca^{2+} imaging (section 2.5.1), but at 640x480 resolution. This was the same still image capture set-up used to view rabbit SERCA1b-EGFP-pcDNA3.1(-)-transfected COS-7 cells. Immunofluorescence experiments with adult boar sperm cells (cleared of ejaculate fluid by centrifugation) were done as stated above but seeded onto gelatin-covered coverslips on the day of use.

2.6. ImageJ Analysis

Quantification of PCR product bands and chemiluminescent protein bands were done by analysing images of DNA-stained agarose gels (section 2.4.2) and HRP-subtrate-treated Western blot membranes (section 2.4.6), respectively, using ImageJ software (version 1.41e; National Institutes of Health USA). In all cases, the average pixel intensity of each band was measured and the size of the area of analysis was kept the same for all bands in a single image. The same was done for background measurements, whereby the area of the image selected, which was the same size as that used for the PCR products or protein bands, was in the same relative position

(above or below) its associated band but either did not contain any DNA staining (PCR products) or was not part of the membrane (Western blot bands). Background measurements were subtracted from their corresponding PCR product or protein band. For PCR products, values corrected for background were also made relative to the corrected values for RPL19 product bands, in the case of SPCA1, SERCA, RGN, GAPDH and β-actin. This latter step was done to correct for any differences in total cDNA content in the samples, which was represented by their content of RPL19 cDNA, and thus the corrected RPL19 product band used for calculation was from PCR with the same cDNA sample that was used in the PCR for the product band to be corrected for the total cDNA content of its corresponding sample.

Pixel intensity measurements from fluorescence microscopy video recordings were also done using ImageJ. For Fluo-3 experiments with A7r5 cells discussed in chapter 3, each frame in a video was converted into a stack with the software and these were collated in order of time of recording for analysis. Fluorescent cells were selected and their fluorescence was measured as the average pixel intensity of the selected area (i.e. the area covered by the whole of each cell) per frame in recording. Background measurements were also taken for each selected cell per frame by using the same-sized area of analysis (used to measure the cells) to measure the average pixel intensity of an area of the video that did not contain any cells and was as close to its associated cell as possible. The background value was subtracted from that of its corresponding cell for each stack and collated to give a plot of fluorescence intensity change over time using Microsoft Excel, to be referred to as a Ca^{2+} transient plot/trace, for each cell. All the values in this plot were made relative to the fluorescence intensity value at the time point prior to treatment addition (e.g. with thapsigargin or AVP), which is referred to as the basal level. The trace was also corrected for any photo-bleaching, which was recognised as a steady decrease of fluorescence intensity over time, by measuring the gradient of this decrease and subtracting it from the background-corrected measurements of its associated cell for each frame after multiplying the gradient value by the time point (in seconds) represented by the frame being calculated for. Average plots for each experiment were produced by averaging all the values obtained for all selected cells in its associated video recording after all corrections had been calculated. These were then used for calculating the kinetics of the rise and decay phases of Ca^{2+}-mediated AVP responses (table 3.2.4.4).

For all Fluo-4 experiments with COS-7 cells discussed in chapter 5 and Fluo-3 experiments with A7r5 cells discussed in chapter 4, the method of ImageJ analysis was modified from the above. Video recordings were opened directly in the ImageJ program using the AVI reader plug-in (via the 'Using Quicktime' option for importing files). Background noise was subtracted from whole recordings using the 'Subtract Background' function. Multiple cells were selected and measured for change in pixel intensity of the selected areas (i.e. whole cells) over time using the 'ROI manager' function. These measurements were saved as Excel files. The values from all cells from each experiment were averaged together to produce mean pixel intensity change over time, and these values were normalised to basal values and corrected for photo-bleaching as stated above.

2.7. Kinetics Measurements from Fluo-3 Fluorescence Microscopy Data

The time taken to achieve 50% of the maximum (i.e. peak) F/F_o value shown on the plots of mean F/F_0 over time was measured either between the start of treatment and peak response (i.e. half-maximal response) or between the peak response and beginning of the plateau at the end of the response (i.e. half-life of response decay). These measurements were made for each plot of mean F/F_o against time produced from recordings with A7r5 cells as stated in section 2.6.

2.8. Statistical Analysis

Standard errors of the means (S.E.M) were calculated for data from PCRs, Western blots, Ca^{2+}-ATPase activities and kinetics measurements from Fluo-3 experiments. For testing statistical significance (P), two-tailed equal variance Student's T-test (Microsoft Excel) was used for data from all experiments for A7r5 cells stated in chapter 3 except for measurements of Ca^{2+}-ATPase activities, whereby analysis of variance (ANOVA) with the general liner model (Minitab) was used for this exception (with advice from Dr. Jeremy Pritchard; University of Birmingham, UK). Two-tailed unequal variance Student's T-test was used for Fluo-3 data shown in chapter 4 due to differences in number of experiments for treatment with potential modulators (n=4) and thapsigargin/AVP (n=3).

2.9. PCR Experiments for Rat RGN

2.9.1. Rat cDNA Library Screen

The sequence of the forward primer was as referenced previously (Yamaguchi and Nakajima, 2002) and represents nucleotides 618-636 in the rat RGN coding sequence (although originally designed for the mouse RGN mRNA sequence). The sequence of the reverse primer was designed as follows:

5'-ACCCTGCATAGGAATATGG-3'

This latter sequence represents nucleotides 906-924 in the rat RGN coding sequence. This sequence for the reverse primer was used instead of that from the literature because the former complements better with the rat RGN mRNA sequence. The ClustalW web-based program (EBI) was used to check these primers would complement the rat RGN mRNA sequence that was retrieved from the Pubmed nucleotides databank (entry number NM_031546) (NCBI). The size of the PCR product for these primers was expected to be 307bp.

Each 50µl PCR mixture contained 2.5 units of BIOTAQ™, 1x NH_4 buffer, 2.5mM $MgCl_2$, 2mM dNTP mix, 20pmol of each primer and autoclaved dH_2O. The thermocyclers used were the same as those for PCR experiments with A7r5 cDNA samples (section 2.4.1). The initial melting step was 95^oC for 2 minutes. For the cycles, the melting step was 95^oC for 1 minute, the annealing step was 55^oC for 1 minute and extension step was 72^oC for 1 minute. The PCR lasted for 30 cycles. Reaction mixtures were temporarily maintained at 4^oC at the end of the last extension step, which lasted for 10 minutes at 72^oC, before being stored at -20^oC. PCR products were electrophoresed through a 2% w/v agarose gel with a 100bp DNA ladder and stained (section 2.4.2). Each sample in a partial rat cDNA library (prepared by Mrs. Rita Godfrey; University of Birmingham, UK) screened for the presence/absence of RGN mRNA was checked for their abundance in total cDNA using PCR with RPL19 primers (section 2.4.1). A gel extract sample of RGN PCR product was sequenced to ensure it did contain mRNA coding sequence for RGN (section 2.10.1 and 2.10.5)

2.9.2. Isolation of Full Length Rat RGN Coding Sequence

Primers for the full length coding sequence of rat RGN mRNA were designed from analysis of the mRNA sequence from the Pubmed nucleotides databank (entry

number NM_031546) and made by Alta Bioscience. The NEB Cutter V2.0 web program was used to find restriction sites suitable for cloning the rat RGN coding sequence into the pET21a expression vector (Novagen). NdeI and AvaI/XhoI restriction sites in the vector's multiple cloning site (MCS) was chosen because these sites are not present in the RGN coding sequence and so the latter would remain intact during restriction endonuclease treatment to obtain DNA fragments of both for ligation (section 2.10.3).

The sequence of the forward primer was as follows:

5'-**CCCTTT**CATATGTCTTCCATCAAGATTGAATGTG-3'

The sequence of the reverse primer was as follows:

5'**TAATAT**CTCGAG**[**AGTATGACCATCTAT**]**CCCTGCATAGGAATATGG-3'

Sequences in **bold** are non-coding and were included to aid digest by restriction endonucleases, which need non-specific sequences on either side of their preferred restriction site to allow them to bind strongly to the latter. Sequences underlined are the restriction sites, whereby the forward primer contains the NdeI restriction site and the reverse primer contains the AvaI/XhoI restriction site. The sequence in the square brackets (**[]**) (in the reverse primer) codes for an amino acid sequence that acts as a cleavage site (Ile-Asp-Gly-Arg-Thr) for Factor Xa protease. The primers were designed to obtain a full coding sequence from mRNA that could be cloned into a pET21a vector and be expressed to produce rat RGN protein that had a hexahistidine (Hisx6) tag at its C-terminus. The tag could then be used to purify the protein using nickel affinity chromatography (section 2.12.6) and the Factor Xa cleavage site would be used (if needed) to remove the tag after purification. The coding sequence for the Hisx6 tag is part of the pET21a plasmid at the 3' end of the multi-cloning site.

The thermocyclers used were the same as those for PCR experiments with A7r5 cDNA samples (section 2.4.1). The 50µl PCR mixture contained 50pmol of each of the above primers, 2.5 units of BIOTAQ™, 1x NH_4 buffer, 2mM $MgCl_2$, 2mM dNTP mix and 20ng of cDNA isolated from rat liver tissue (prepared by Mrs. Rita Godfrey; University of Birmingham, UK). The PCR lasted for 35 cycles. The

initial melting step was 95°C for 2 minutes. For the cycles, the melting step was 95°C for 1 minute, the annealing step was 60°C for 1 minute and the extension step was 72°C for 1 minute. Reaction mixtures were temporarily maintained at 4°C at the end of the last extension step, which lasted for 10 minutes at 72°C at the end of the last cycle, before being stored at -80°C.

The PCR mixtures were then electrophoresed through a 0.8% w/v agarose gel with a 1kb DNA ladder and stained (section 2.4.2). The expected PCR product size for full-length rat RGN coding sequence from mRNA was 0.94kb. DNA sequencing was done with gel extracts (section 2.10.1 and 2.10.5) of the PCR product to confirm the correct sequence was obtained using the LALIGN web-based program (EMBnet, Swiss Institute of Bioinformatics) for sequence alignment with the mRNA sequence used to design the primers. PCR products were stored at -20°C.

2.10. Preparation of Rat RGN Plasmids

2.10.1. Gel Extraction & Approximation of DNA Quantities

Extraction of PCR products (sections 2.4.1, 2.9.1 and 2.9.2) or restriction digest fragments of plasmid DNA (section 2.10.3) from agarose gels was done using a QIAquick Gel Extraction Kit (Qiagen) and following manufacturer's instructions for the microcentrifuge method. Several fragments of DNA were required to obtain a sufficient amount of extracted DNA. The final quantity of DNA obtained was approximated by electrophoresising the extraction product through either 0.8% or 2% w/v agarose gel (depending on the size of extracted DNA) (section 2.4.2) and comparing the product band intensity with that of its nearest marker from the DNA ladder (e.g. the 1kb marker for the 0.94kb full rat RGN coding sequence), the latter of which had a defined quantity of DNA that was known from the volume of DNA ladder loaded onto the gel and information given by the manufacturer.

For example, 0.5µg of 1kb DNA ladder contained 42ng of 1kb marker DNA. If a ~1kb product band (e.g. full rat RGN coding sequence) was judged by eye to be half the intensity of this marker, it was approximated that the amount of PCR product present in the band was 21ng. Dividing the amount of PCR product by its volume loaded into the gel for the same DNA band gave the concentration of DNA present in the gel extract. The same calculations were used to estimate DNA quantities for the purpose of DNA sequencing (section 2.10.5) and DNA ligation (section 2.10.2-3).

2.10.2. Ligation of Rat RGN Coding Sequence into pGEM-T Vector

The PCR product for the full coding sequence of rat RGN (0.94kb) extracted from agarose gels (sections 2.9.2 and 2.10.1) was inserted into a pGEM-T vector (Promega) following manufacturer's instructions for the pGEM-T Easy Vector System Kit. This was done to provide restriction sites at the 5' and 3' ends of the rat RGN coding sequence, which were used to insert the sequence into the pET21a vector later on (section 2.10.3). 25ng of pGEM-T vector was ligated with the gel-extracted PCR product at an 8:1 ratio, and the amount of PCR product used was calculated (as instructed in the manual provided with the kit) to be 61.6ng. The calculation used was as follows:

DNA insert amount (ng) =
((Vector amount (ng) x DNA insert size (kb)) / Vector size (kb)) x Insert:Vector ratio

pGEM-T empty vector and PCR product were initially mixed together and heated in a 55^{o}C heat block for 5 minutes (to improve ligation by melting the DNA) before 1x ligation buffer and 3 units of T4 DNA ligase (both provided in the kit) were added to complete the reaction mixture. Control reaction mixtures were also made in the same manner but with no insert DNA added. All reactions were incubated overnight in a 4^{o}C water bath. DH5-α cells were transformed (section 2.11.5) with the reaction mixtures afterwards and colonies on LB-agar plates from cells that had ligation reaction mixtures added to them were picked and grown overnight in LB cultures to use for minipreps (section 2.10.4). Control ligation reaction mixtures were expected to not produce colonies following its use for DH5-α transformation (due to absence of circularised plasmids).

A restriction digest with 10 units of AvaI and 20 units of NdeI (section 2.9.2) for 3µl of miniprep DNA in a total reaction volume of 10µl (the rest of the volume was made up with 1x reaction buffer (supplied with the enzymes) and autoclaved dH_2O) was done to check the correct plasmid was present. The reaction mixtures were incubated in a 37^{o}C water bath for 1 hour, before their contents were electrophoresed through a 0.8% w/v agarose gel and stained (section 2.4.2). The presence of two DNA gel fragments, one for rat RGN (0.94kb) and one for pGEM-T vector (3.0kb), after restriction digest of miniprep DNA, suggested the ligation was successful and the

pGEM-RGN plasmid was made. DNA sequencing (section 2.10.5) was done with the miniprep DNA to check the rat RGN coding sequence was present using the LALIGN web-based program.

2.10.3. Ligation of Rat RGN Coding Sequence into the pET21a Vector

Rat RGN coding sequence was excised out of the pGEM-RGN plasmid by doing a restriction digest with 10 units of AvaI and 20 units of NdeI (section 2.10.2). The same restriction digest reaction was also done for pET21a empty vector. Reaction mixtures were incubated in a 37^{o}C water bath for 1 hour, before they were electrophoresed through a 0.8% w/v agarose gel and stained (section 2.4.2). The DNA gel fragments corresponding to the RGN coding sequence (0.94kb) and pET21a vector (5.44kb) were extracted and the extracts were subjected to electrophoresis to approximate the amount of DNA they contained (section 2.10.1).

Ligation of rat RGN coding sequence into the linearised pET21a vector was done at a 7:1 ratio and the amount of insert DNA required was calculated in the same way as done for pGEM-T vector ligation (section 2.10.2). From this, 25ng of pET21a vector and 30.54ng of rat RGN coding sequence was used in the reaction mixture, which also contained 100 units of T4 DNA ligase (NEB), 1x reaction buffer (provided with the enzyme) and autoclaved dH_2O to make up the final reaction volume to 50µl. Note that the DNA and dH_2O were mixed first and heated in a 60^{o}C heat block for 10 minutes before the T4 DNA ligase and buffer were added. The reaction mixture was then incubated overnight in a 16^{o}C water bath.

After ligation, DH5-α cells were transformed with the reaction mixture (section 2.11.5) and colonies were grown overnight in LB cultures to use for minipreps (section 2.10.4). Restriction digests of the minipreps were done with 3µl of miniprep DNA, using 10 units of XhoI (an endonuclease that is specific to the same restriction site as AvaI) and 20 units of NdeI per 10µl reaction volume. Reaction mixtures were incubated in a 37^{o}C water bath for 1 hour, before their contents were electrophoresed through a 0.8% w/v agarose gel and stained (section 2.4.2) to check the correct DNA fragments were present. The pET21a-RGN plasmid was also sequenced (section 2.10.5) and minipreps of the plasmid were used to transform BL21 cells (section 2.11.5) after confirming it contained the correct sequences.

2.10.4. Minipreps

All minipreps of plasmid DNA for pGEM-RGN, pET21a-RGN and pET21a empty vector were done using a GenElute Plasmid Miniprep Kit (Sigma). Manufacturer's instructions were followed. A 5ml overnight LB culture of transformed DH5-α cells (carrying the plasmid of interest) (section 2.11.5) was used per miniprep. Elution of DNA was done with 100µl autoclaved dH_2O per miniprep. All minipreps were stored at -20^oC.

2.10.5. DNA Sequencing

The nucleotide sequences of PCR products and plasmids containing the full-length rat RGN coding sequence (sections 2.9.2, 2.10.2 and 2.10.3) were checked using the Plasmid-to-Profile service provided by the Genomics Laboratory (University of Birmingham, UK). The primers used were either those for the full rat RGN coding sequence (PCR product and pGEM-RGN plasmid) (section 2.9.2) or those used to screen the rat cDNA library (pET21a-RGN plasmid) (section 2.9.1). SPCA1 PCR products from A7r5 cDNA samples (section 2.4.1) and RGN PCR products from cDNA copies of total mRNA from adult male rat liver and testis (section 2.9.1) were also sequenced using the same service.

2.11. Bacterial Cell Culture

2.11.1. Sterilisation of Solutions & Culture-Handling Materials

All media (stored in glassware and sealed with either metal/plastic caps or foam bungs), some liquids (e.g. dH_2O) and some culture-handling materials purchased in non-sterile form (e.g. micropipette tips) were autoclaved as done for mammalian cell culture (section 2.1.1) before use with bacterial cultures. Filter sterilisation (where stated) was done using a 0.2µm pore filter with syringe, and the filtrate was stored in sterile containers. Work surfaces were cleaned using 70% v/v ethanol. A Bunsen burner flame was used to sterilise necks of glass bottles and flasks, glass spreaders and wire loops before and after use. The flame was also used to keep nearby work surfaces sterile. Glass spreaders and wire loops were pre-soaked with 100% v/v ethanol before fully sterilised with a Bunsen burner flame.

2.11.2. Making LB Media & LB-Agar

Luria-Bertani (LB) media (used for culturing DH5-α and BL21 E.coli strains, unless otherwise stated) was made with 10g/L tryptone (Oxoid), 5g/L yeast extract (Oxoid) and 5g/L NaCl, all dissolved in dH_2O. LB-agar was made by adding 1.5% w/v agar powder (Oxoid) to LB media. LB media was supplemented with 0.1mg/ml ampicillin (filter-sterilised) on the day of use for all cultures.

2.11.3. Setting LB-Agar Plates

To obtain three LB-agar plates, one bottle containing 75-80ml of LB-agar was placed in cold tap water and heated until all LB-agar had fully dissolved. Liquefied LB-agar was then left at room temperature to cool to approximately 40-50^{o}C (at which it was cool enough to hold the bottle in hand comfortably and while LB-agar was still in liquid state).

Once cooled, ampicillin solution (filter-sterilised) was added to give a final concentration of 0.1mg/ml. The antibiotic-supplemented LB-agar was poured into three 10cm diameter Petri dishes at approximately equal volumes. The plates were sealed with their lids and left to cool at room temperature next to a Bunsen burner flame until the LB-agar had solidified. Condensation was dried off the solid LB-agar by opening the lids slightly whilst still keeping the plates next to a Bunsen burner flame. Plates were used on the same day for plating DH5-α (section 2.11.5) or BL21 cells (section 2.12.1).

2.11.4. Making Stocks of Competent DH5-α Cells

A frozen glycerol stock (section 2.11.5) of already competent DH5-α cells (a gift from Dr. S. Whitehead; University of Birmingham, UK) was streaked onto a modified LB-agar plate using a wire loop and incubated in a 37^{o}C oven for 14-16 hours. The modified LB-agar consisted of 1.2% w/v agar in growth medium (20g/L tryptone, 5g/L yeast extract, 0.1M $NaCl_2$ and 10mM $MgSO_4$). The plates were set in the same way as normal agar plates (section 2.11.3) except that no ampicillin was added.

One colony was picked from the plate using a sterile pipette tip and transferred into 5ml of growth media, which was then maintained at 37^{o}C in a shaking incubator. A few of such cultures were set up for growth. Absorbance readings at 650nm were taken of 1ml samples from the 5ml cultures every 30 minutes until the O.D. values

were within the range of 0.2-0.6. 4ml of combined cultures were then used to inoculate 100ml of fresh 37^{o}C pre-warmed growth media, which was then maintained at 37^{o}C in the shaking incubator. Absorbance readings at 650nm were taken of 1ml samples from the 100ml culture until O.D. values were within the range of 0.5-0.9. Following this, all the remaining culture was used to inoculate 500ml of fresh growth media, which was maintained at 37^{o}C in the shaking incubator and absorbance readings at 650nm were taken of 1ml samples from this latter culture until O.D. values were within the range of 0.6-0.8.

All solutions and culture-handling materials were kept on ice from hereon. Note that centrifuge bottles had been rinsed with ethanol and dH_2O before being autoclaved to sterilise thoroughly before use. The 500ml culture was placed on ice to be chilled for 5 minutes before being centrifuged at 6,700g for 5 minutes at 4^{o}C. The media was discarded and the cell pellet was re-suspended in 100ml of TfBI solution (filter-sterilised) (30mM $KC_2H_3O_2$, 10mM $RbCl_2$, 50mM $MnCl_2$ and 1.5% v/v glycerol; pH 5.8 using 0.2M acetic acid). The cell suspension was left on ice for 1.5 hours before being centrifuged as before. TfBI solution was then discarded, the cell pellet was re-suspended in TfBII solution (filter-sterilised) (10mM MOPS, 75mM $CaCl_2$, 10mM $RbCl_2$ and 15% v/v glycerol; pH 6.5 using KOH) and left on ice for 2 hours. The cell suspension was then aliquoted, snap frozen with liquid nitrogen and stored at -80^{o}C.

2.11.5. Transformation of Competent E.coli Cells & Making Glycerol Stocks

DH5-α cells were transformed with plasmid DNA needed for minipreps (section 2.10.4) and maxipreps (section 2.3.1). These were pGEM-RGN, pET21a-RGN, control pET21a and all plasmids used for over-expression in COS-7 cells (section 2.3.1). BL21 cells (a gift from Dr. Simon Whitehead; University of Birmingham, UK) transformed with pET21a-RGN were used for over-expression of recombinant RGN protein.

Frozen competent cells were thawed on ice and kept at ice-cold temperatures at all times (unless otherwise stated). Failure to do this resulted in their loss of competence (i.e. weakened their ability to take up plasmid DNA). 50-100µl of thawed competent cells was mixed by gentle pipetting with 50ng-1µg of plasmid DNA in a sterile tube and incubated on ice for 60 minutes. A separate sterile tube of competent cells with no added DNA was used as a negative control. Following this, both DNA-

treated and control cells were heat-shocked by incubating in a 42°C water bath for 2 minutes and then incubated on ice for a further 2 minutes. 0.5-1ml of LB media was added to the cells and incubated in a shaking incubator at 37°C for 90 minutes. 20-50µl of these cultures were then plated onto ampicillin-supplemented LB-agar plates using a sterile glass spreader and incubated overnight in a 37°C oven. After viewing (and using) colonies the next day, the plates were wrapped with Parafilm and stored at 4-6°C for up to 3 weeks for later use. Control cells were expected not to form colonies (due to absence of ampicillin resistance).

Colonies were picked to inoculate either 5ml or 50ml of LB media and cultures were grown overnight in a shaking incubator maintained at 37°C. 5ml cultures were then used for minipreps. 50ml cultures were used to set up 200ml overnight cultures for maxipreps, whereby 10ml from the 50ml overnight culture was used to inoculate 200ml of fresh LB media. Glycerol stocks of transformed cells were made for future use by mixing at a 1:1 ratio of cell culture with 50% v/v glycerol and stored at -80°C. Cells were plated onto LB-agar plates from glycerol stocks by picking a small amount of the frozen stock with a sterile wire loop and streaking this onto the plate, which were then incubated in a 37°C oven overnight, or inoculating 5-50ml of ampicillin-supplemented LB media and grown at 37°C in a shaking incubator.

2.12. Production, Use & Purification of Recombinant RGN Protein

2.12.1. IPTG Induction of pET21a-RGN-Transformed BL21 Cells

Glycerol stocks of BL21 cells transformed with pET21a-RGN plasmid (section 2.11.5) were streaked onto LB-agar plates. Colonies were picked to inoculate 50ml of LB media, which was maintained at 37°C overnight in a shaking incubator. 10ml of the overnight culture was used to inoculate 200ml of fresh LB media, which was then maintained at 37°C in a shaking incubator and readings of its absorbance at 600nm was taken every 30 minutes from 1ml samples. Once O.D. values reached 0.7-1.0, cells were induced to synthesise recombinant RGN by adding isopropyl β-D-1-thiogalactopyranoside (IPTG) solution (filter-sterilised) (BIOLINE) to the culture, which was then incubated in a shaking incubator for a chosen period of time and temperature. A range of IPTG concentrations, as well as incubation times and temperatures were tested during optimisation (see section 5.2.10). The final conditions used for induction were 0.25mM IPTG, 17°C and overnight culture for

production of inclusion bodies. After the induction period, cultures were centrifuged at 11,900g for 20 minutes at 4^{o}C, the media was discarded and the pellet was stored at -20^{o}C.

2.12.2. Sonication of BL21 Pellets & Solubilisation of Inclusion Bodies

Frozen pellets of induced BL21 cells were thawed and 10ml of TED buffer (50mM Tris-HCl (pH 8.0), 1mM EDTA and 1mM DTT) was added to each pellet. The cells were re-suspended and sonicated once every minute for 15 seconds over a total period of 10 minutes. 10ml of fresh TED buffer, followed by 1mM PMSF, was added to the total cell lysate, which was then centrifuged at 20,000g for 20 minutes to separate inclusion bodies and soluble proteins. To solubilise the inclusion bodies prior to Ni^{2+} affinity column chromatography (section 2.12.6), the supernatant was removed and solubilisation buffer (0.1M NaH_2PO_4, 8M urea and 5mM DTT; pH 8.0) was used to re-suspend the pellet. The solubilised pellet was then centrifuged at 100,000g for 45 minutes and the resulting supernatant (containing the solubilised inclusion bodies) was collected.

2.12.3. Preparation of Dialysis Tubing

New dialysis tubing had to be treated before use. Hot dH_2O was supplemented with 5% w/v $NaHCO_3$ and 1mM EDTA. The solution was kept on a hot plate with constant stirring until it was 70^{o}C. New dialysis tubing was then added and kept in the solution for 1 hour with gentle stirring. Following this, the dialysis tubing was removed and washed thoroughly with fresh dH_2O before being stored in 20% v/v ethanol; the latter had to be thoroughly washed off with dH_2O before using the dialysis tubing.

2.12.4. Antibody Production for Anti-RGN

Recombinant RGN protein isolated during optimisation trials of its purification was used to produce an antibody that recognised all RGN protein. A BL21 pellet was sonicated and the cell lysate centrifuged as described above (section 2.12.2). Inclusion bodies (within the pellet obtained from centrifugation at 20,000g) were solubilised with 6M urea dissolved in 50mM Tris-HCl buffer (pH 7.2) and stored overnight at -20^{o}C. Following this, 2ml of this protein solution was thawed on ice, transferred into dialysis tubing and kept in 2.5L dialysis buffer (50mM Tris-HCl (pH 7.2) with 15% v/v glycerol) overnight at 4-6^{o}C with constant gentle stirring.

After dialysis, the protein solution was subjected to SDS-PAGE and the gels were stained for proteins (section 2.4.5). An abundant 33kDa protein band from the protein sample was excised from the gel with a scapel and used for FT-ICR mass spectrometry analysis (Proteomics Laboratory; The University of Birmingham, UK), which confirmed the identity its protein contents to be rat RGN. The same FT-ICR service was used to identify of the protein contents of a 66kDa Coomassie-stained gel band from the total cell lysate of adult boar sperm (section 5.2.6). SDS-PAGE and Coomassie blue staining was repeated with the same recombinant RGN sample, and multiple 33kDa protein bands were excised and sent to Covalab (UK) for antibody production.

Two rabbits were each immunised with the 33kDa protein and boosted 14 and 28 days after the initial immunisation. Later on, one of the two rabbits was chosen for a further two immunisations at 74 and 88 days after the first immunisation. Blood sera taken from the rabbit(s) before immunisation (the 'pre-immune' bleed) and on the days of the three or five immunisations were received for testing via Western blotting method (section 2.12.5).

2.12.5. Western blotting with Anti-Hisx6 & Anti-RGN Antibodies

Basic procedure for Western blotting was as described before (section 2.4.6). Monoclonal mouse anti-Hisx6 (clone HIS-1; Sigma) was used at a dilution ratio of 1:1500. Custom-made anti-RGN polyclonal rabbit antibody (Covalab) was used at dilution ratios ranging between 1:75 and 1:750 during optimisation trials with day 88 and final bleeds, whereas a dilution ratio of 1:50 was used with days 0 and 39 bleeds. All secondary antibodies were used at a dilution ratio of 1:3000. For the detection of RGN, either with or without Hisx6-tag, the protein band's expected size was 33kDa (Yamaguchi, 2005).

2.12.6. Nickel Affinity Column Chromatography

All column chromatography was done using a BIORAD ECONO pump system. All column washes and runs were done at a flow rate of 0.3ml/min and for 60 minutes each. A fast flow rate of 15.2ml/min was used to rinse tubing only and the column would be detached from these during the use of this latter flow rate. Each time a new buffer or solution was to be used to wash the column, it would be used to rinse tubing at fast flow rate for 2 minutes first. HIS-Select Nickel Affinity Gel (Sigma) was

packed into a chromatography column to give a 2ml resin bed volume, washed first with dH_2O and then equilibration buffer (same as solubilisation buffer (section 2.12.2)). Excess of the latter was removed afterwards to leave approximately 0.5ml at the top of the resin gel.

Solubilised inclusion bodies (section 2.12.2) were applied to the top of this resin gel (with care taken not to disrupt its packing), washed through the column with equilibration buffer, followed by wash buffer (equilibration buffer at pH 6.2) and elution buffer (equilibration buffer at pH 4.5). The 60 minutes of each of the latter three column washes (i.e. equilibration, wash and elution) consisted of the first 30 minutes of eluant being discarded into waste and the last 30 minutes of eluant being collected as the sample. These three samples were then subjected to SDS-PAGE and the gels were stained for proteins (section 2.4.5). The fraction with both a good amount of 33kDa protein and minimal content of contaminating proteins was selected as a good sample of RGN to use for refolding (section 2.12.7).

2.12.7. Protein Refolding

The His-column fraction determined to contain the most and purest amount of RGN (section 2.12.6) was used for refolding experiments. For the one-step dialysis refolding method, the fraction was diluted to 0.1mg/ml protein concentration with the column buffer used to elute it off the column, 10ml of the diluted protein solution was transferred into dialysis tubing (section 2.12.3) and dialysed overnight at 4^oC with gentle stirring in 5L of 50mM Tris-HCl (pH 8.0) buffer containing 1mM DTT and 15% v/v glycerol. For the crash dilution method of refolding, the chosen column fraction was rapidly diluted at a 1:5 ratio by adding 50mM Tris-HCl (pH 8.0) buffer, which was supplemented with 5mM DTT and 10% v/v glycerol, to it whilst gently stirring to give a final protein concentration of 0.1mg/ml, then left for 10 minutes at 4^oC still stirring. Following this incubation, 5ml of the dilution refolded protein was dialysed in 5L of 50mM Tris-HCl (pH 7.2) buffer, containing 5% glycerol, overnight (with 5ml of sample in dialysis bag) and concentrated (section 2.12.8). Protein solutions from refolding attempts were snap frozen with liquid nitrogen and stored at -80^oC.

2.12.8. Protein Concentrating

Vivaspin 20 centrifugal concentrators (Sartorius) were used to concentrate dialysed RGN protein. All centrifugation steps were 5000g for 30 minutes at 15^{o}C. Each concentrator was first filled with 5ml of 50mM Tris-HCl (pH 8.0), centrifuged and all buffer discarded afterwards to wash the sample reservoir. This reservoir was then re-filled with the dialysed protein solution and centrifuged again. Centrifugation of the protein sample was repeated until its volume was reduced by 10-fold. Following this, the concentrated sample was retrieved from the reservoir to have its protein concentration estimated (section 2.4.3), before it was aliquoted, snap frozen with liquid nitrogen and stored at -80^{o}C.

2.12.9. Circular Dichroism (CD) Spectroscopy

Cl^- contents of protein samples had to be reduced by dialysis in 50mM Tris buffer, with pH adjusted using phosphoric acid (pH 8.0), overnight at 4^{o}C. Each sample was then analysed using a Jasco J715 spectropolarimeter (with Spectra Manager v.1.07.02 program) in quartz cuvettes (0.2mm pathlength), using 190-260nm wavelength range and 16 repeat readings. Such measurements were also done for fresh dialysis buffer (used in section 2.12.7) without added protein as controls, the values of which were subtracted from those for protein samples to correct for effects of buffer and background. Absorbance spectra were measured to monitor linearity of light absorbance at all samples. The K2D2 web-based program (Ontario Genomics Innovation Centre) was used to analyse CD spectra for protein samples to predict contents of secondary structure.

CHAPTER 3.

SPCA EXPRESSION & ACTIVITY IN A7r5 CELLS CULTURED IN NORMAL & HIGH GLUCOSE MEDIA

CHAPTER 3.
SPCA EXPRESSION & ACTIVITY IN A7r5 CELLS CULTURED IN NORMAL & HIGH GLUCOSE MEDIA

3.1. Introduction

Diabetes mellitus can cause cardiovascular diseases, by promoting pathological processes, such as the formation of atherosclerotic plaques (Rader and Daugherty, 2008). Such diseases are characterised by the dis-regulation of calcium homeostasis in vascular cells (Levy, 1999), with examples such as higher than normal basal intracellular [Ca^{2+}] in rat cardiomyocytes and altered hormone-induced Ca^{2+} signalling in human vascular smooth muscle cells (Fleischhacker et al., 1999). This has been attributed to altered expression and/or activity of Ca^{2+}-binding proteins, which has been exemplified by increased enzymatic activity of calpain in endothelial cells (Stalker et al., 2005) and decreased expression of SERCA in heart tissue (Teshima et al., 2000) of diabetic rats.

Vascular smooth muscle cells (VSMCs) can also exhibit diabetes-associated abnormalities in Ca^{2+} homeostasis during the progression of cardiovascular disease, which has been exemplified by, for example, observations of higher than normal basal intracellular [Ca^{2+}] (Barbagallo et al., 1995) and increased SERCA activity (Tong et al., 2008) in rat-derived cells. In addition to this, VSMCs have been noted in previous studies to have enhanced secretory activity and produce higher than normal amounts of extracellular matrix proteins, such as collagen (Mazzone et al., 2008). This vascular cell type is specialised to assist the control of blood vessel diameter and structural modelling of blood vessel walls, both of which are required to adapt to changes in blood flow through the cardiovascular system (Rensen et al., 2007). VSMCs can exist in two phenotypic states, contractile and secretory (the latter also known as ‘synthetic’), both in healthy and diseased vascular tissue (Archer, 1996). However, it is characteristic of vascular diseases for proliferative secretory VSMCs to dominate more in its associated cell population than their more differentiated contractile counterparts (Thyberg et al., 1990). One of the likely consequences of this phenotypic switch of a VSMC population is higher than normal inflammation of

blood vessel walls and this is a major factor that promotes atherosclerotic plaque formation (Mazzone et al., 2008).

One protein that is involved in both Ca^{2+} homeostasis and secretory function in cells is SPCA (Wuytack et al., 2003), which is also relatively highly expressed in cardiovascular tissue, such as from heart and aorta (Wootton et al., 2004). SPCA is important for establishing a store of Ca^{2+} in the Golgi apparatus, which is required by Ca^{2+}-dependent enzymes that are essential for post-translational modification of proteins in transit through the secretory pathway. An example would be casein kinase (Szymanski and Farrell, 1982), which controls matrix gamma-carboxyglutamic acid protein trafficking via it's phosphorylation in human VSMCs (Wajih et al., 2004). Ca^{2+} in the Golgi apparatus can also be used to promote protein-protein interactions required for their secretion, such as that between osteoprotegerin and von Willebrand factor in human vascular endothelial cells (Shahbazi et al., 2007).

Despite the relationship between Golgi apparatus Ca^{2+} stores and protein secretion being relatively well established, with some links to cardiovascular disease also suggested, it is unknown if SPCA activity and/or expression is involved in diabetes-related vascular pathology, like other similar Ca^{2+}-binding proteins such as those mentioned above. However, one study has suggested that altered SPCA expression levels could contribute to the pathological effects of diabetes in pancreatic β-cells by affecting glucose-stimulated insulin secretion (Mitchell et al., 2004). Furthermore, another study has shown the Golgi apparatus can influence the proliferative state of VSMCs (Thyberg, 1998). Thus there is evidence to suggest SPCA and the Golgi apparatus could play a role in diabetes-related vascular disease.

The aim of the present study was to establish if SPCA expression and/or activity can be altered in VSMCs maintained under a hyperglycaemic state, which resembles that in diabetes, compared to the normal euglycaemic state of cellular glucose availability. An aortic VSMC cell line, A7r5, was grown in media either supplemented with a normal (5.55mM; "NG") or high (25mM; "HG") glucose concentration to produce experimental models of the two states for this study. Only SPCA1 expression and localisation was studied because it has been shown in a previous study that aortic vascular cells are unlikely to express the SPCA2 isoform (Vanoevelen et al., 2005).

3.2. Results

3.2.1. Expression Levels of SPCA1, SERCA, GAPDH & β-Actin mRNA in A7r5 Cells Cultured in Normal & High Glucose Media

PCR was used to measure the amount of mRNA that encoded SPCA1, SERCA, GAPDH and β-actin in A7r5 cells grown in media supplemented with either a normal (5.5mM; NG) or high (25.0mM; HG) concentration of glucose. SPCA1 (all splice variants) was the main subject of interest. SERCA (all isoforms and splice variants) mRNA levels were also measured to see if it was affected by a difference in A7r5 media glucose concentration and how it relates to any change in SPCA1 mRNA levels. Amounts of RPL19 mRNA were measured as a control for the total amount of transcripts that was present in each sample and thus allowed correction for any differences in this factor. RPL19 was chosen as the control because it is a commonly used control for similar experiments and was unlikely to be affected by a change in glucose availability to A7r5 cells because it encodes for a housekeeping ribosomal protein (Al-Bader and Al-Sarraf, 2005).

GAPDH and β-actin mRNA levels are two other commonly used controls for PCR reactions (Al-Bader and Al-Sarraf, 2005). However, their suitability as controls in the present study were questionable due to their associated functions. GAPDH is an enzyme that is part of the glycolytic pathway and it was suspected to be possible that any changes in basal metabolism, caused by a change in glucose availability, may affect its mRNA expression levels. β-actin (a cytoskeletal protein) has been previously used as a phenotype marker in VSMCs due to its involvement in their contractility (Owens et al., 1986) and so its transcript levels were not used as a control for the present study in case of any changes in A7r5 phenotype from culture in media with different glucose concentrations. However, both GAPDH and β-actin mRNA levels were still monitored in the present study to see if such effects to their mRNA abundance did occur under the experimental conditions used.

The use of cDNA copies of mRNA extracts from A7r5 cells, rather than the direct use of the latter, to measure for changes in mRNA expression was implemented due to the greater stability of cDNA compared to mRNA. The cycle numbers deemed to be appropriate for observing any differences in PCR product levels between

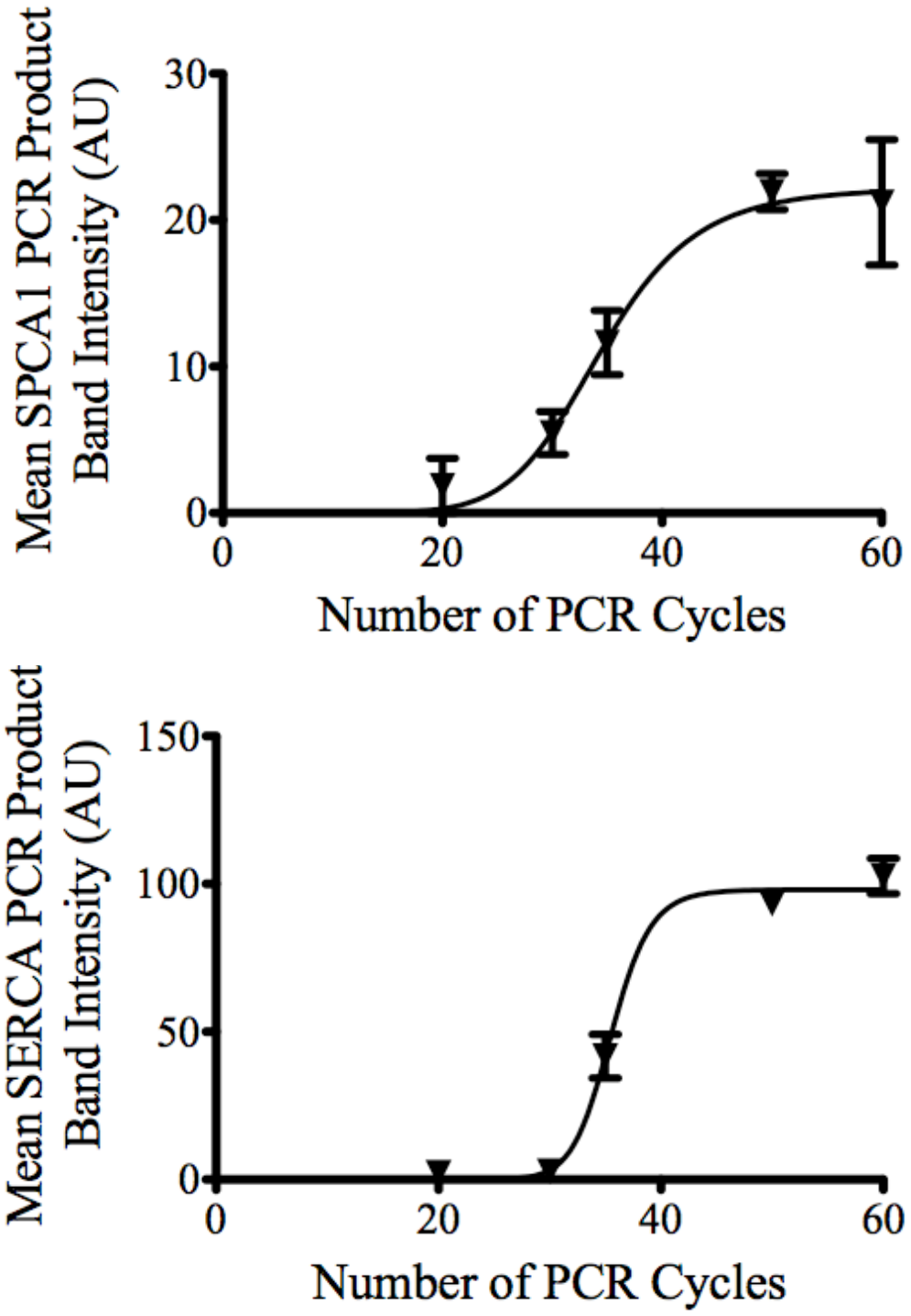

Figure 3.2.1.1. Effect of PCR Cycles on Amount of PCR Product for SPCA1 & SERCA Primers

Figure 3.2.1.1. Effect of PCR Cycles on Amount of PCR Product for SPCA1 & SERCA Primers

PCRs with SPCA1 and SERCA primers and cDNA samples from NG cells were done using 20, 30, 35, 50 and 60 cycles. The reaction mixtures were subjected to agarose gel electrophoresis. The PCR product band intensities from DNA-stained gels were measured from two replicate PCRs (one for each cDNA sample preparation from A7r5 cells) for each cycle number and the mean value was calculated. Error bars represent the spread of data.

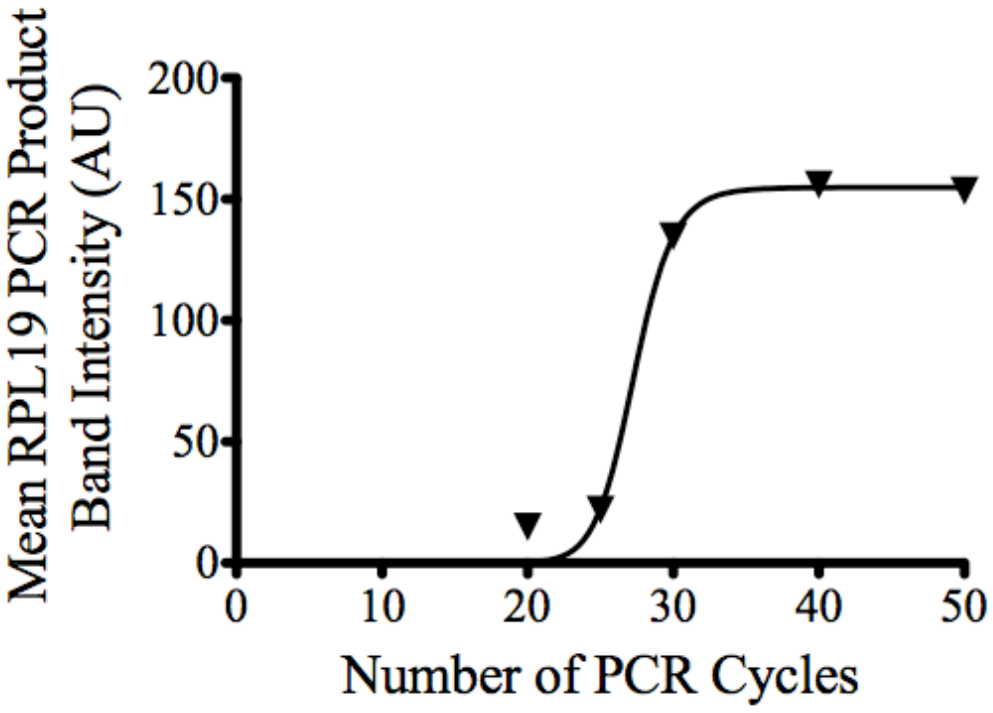

Figure 3.2.1.2. Effect of PCR Cycles on Amount of PCR Product for RPL19 Primers

PCR with RPL19 primers and cDNA samples from NG cells were done to test the effect of cycle numbers in the same way as represented in figure 3.2.1.1. The cycle numbers used were 20, 25, 30, 40 and 50. The same measurements and calculations were also used. (Error bars for the spread of data are present though not visible due to their low values.)

samples were determined for SPCA1 and SERCA (figure 3.2.1.1) as well as RPL19 (figure 3.2.1.2). For each of these three transcripts of interest, the cycle number for their PCRs was selected within the linear range of their associated plot of mean PCR product band intensity against cycle number, each of which was produced using cDNA samples from NG cells. From this, 35 cycles was used for SPCA and SERCA primers, while 28 cycles was used for RPL19 primers. A cycle number in this range on each plot avoids saturation of PCR product amount and yet still produce enough transcripts for measurements to be made from. The cycle number used for β-actin primers (i.e. 28 cycles) is comparable to that previously determined as optimal (30 cycles) and details of the associated experiments done to select this cycle number, which were similar to what was done in the present study for SPCA1, SERCA and RPL19, are in the literature from which the sequences of the primer pairs were obtained (Varadi et al., 1996). The cycle number used for PCR with GAPDH primers was set as the same as that for RPL19 and β-actin primers, which was lower than that used previously as stated in the literature from which its primer sequences were obtained (35 cycles) (Di Napoli et al., 2007). All cycle numbers are summarised in table 2.4.1.1.

For the use of β-actin and GAPDH primers, the PCR conditions were the same as those quoted in the literature from which their sequences were obtained, except with a lower PCR cycle number of 28 (i.e. same as that for RPL19 primers) in both cases. Both pairs of primers had been used to indicate total mRNA quantity for PCR reactions in the studies described in their associated literature, and thus the cycle numbers that had been used had been optimised (as done in the present study for SPCA1, SERCA and RPL19 described above) to avoid production of saturated amounts of PCR products. Hence to use a lower PCR cycle number than that quoted in both cases was unlikely to produce saturated PCR product quantities.

PCR product band intensities determined from images of DNA-stained agarose gels like those at figure 3.2.1.3B were measured from three replicate PCRs for each primer pair, whereby one replicate represented one sample of cDNA obtained from one culture of cells and thus three cell cultures were used in total for each of the two glucose culture conditions. The mean of replicates for each primer pair used were calculated and those measured for samples from HG cells were made relative to equivalent values measured for samples from NG cells. These relative values were

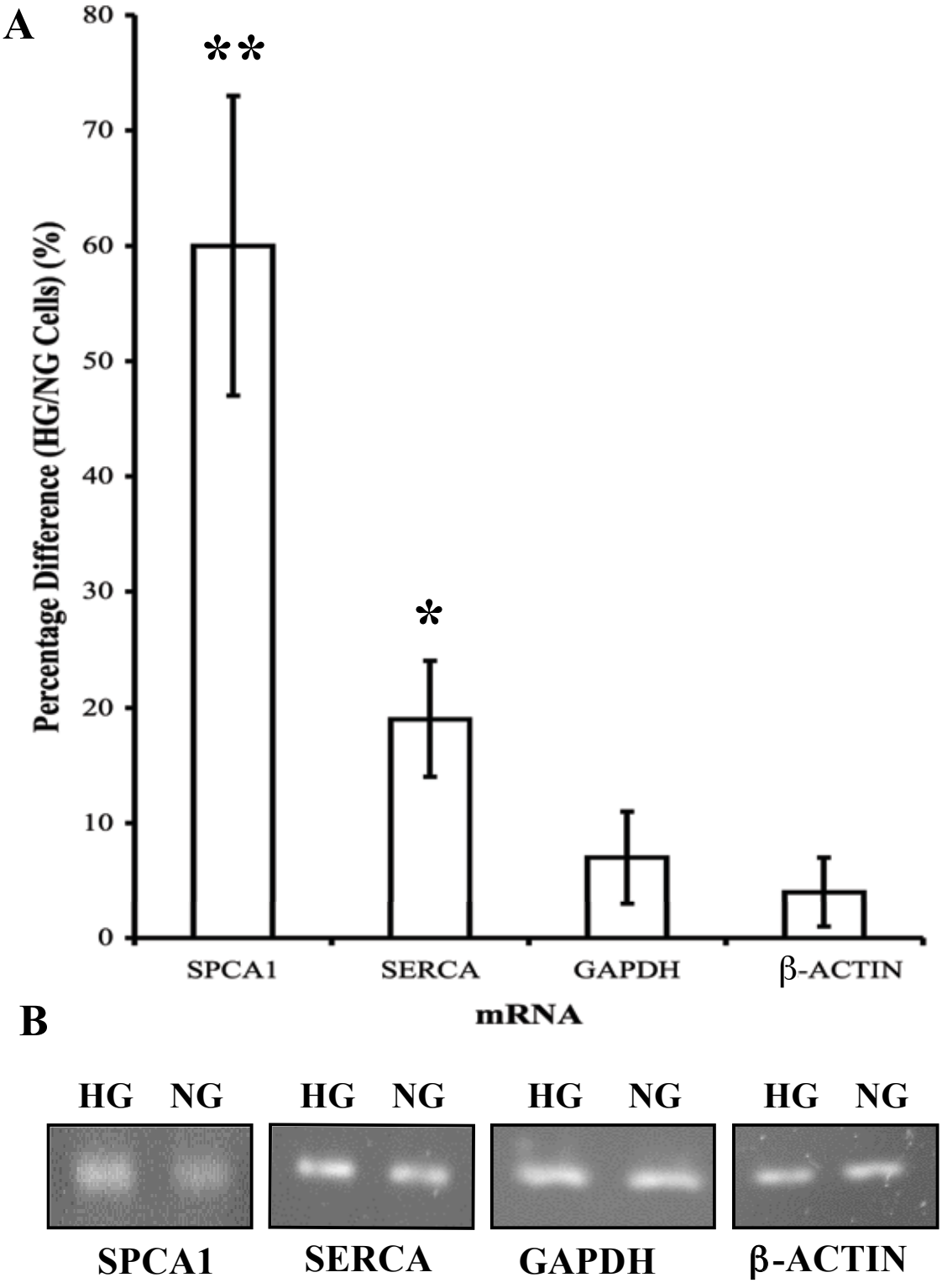

Figure 3.2.1.3. PCR Analysis of SPCA1, SERCA, GAPDH & β-Actin mRNA Expression Levels in A7r5 Cells Cultured in Normal & High Glucose Media

Figure 3.2.1.3. PCR Analysis of SPCA1, SERCA, GAPDH & β-Actin mRNA Expression Levels in A7r5 Cells Cultured in Normal & High Glucose Media

(A) Three PCR reactions were done for each primer pair and glucose culture condition, using cDNA copies of mRNA extracts from three pairs of NG and HG A7r5 cell cultures. PCR product band intensities from images of DNA-stained gels were measured for each PCR, corrected for background and made relative to equivalent measurements made for RPL19 PCR product bands to correct for any differences in total amount of cDNA in samples. Corrected values for HG cells were made relative to those from their pair-matched NG cells. Mean values of replicate PCR reactions were calculated for each primer pair and glucose culture condition, and converted to the percentage difference values shown. Error bars indicate S.E.M. Significant P-values calculated from two-tailed equal variance Student's T-test are indicated by * ($P<0.05$) and ** ($P<0.01$).

(B) DNA-stained gels of PCR product bands, which show typical band intensities observed for each of the four transcripts of interest from NG and HG cell samples of cDNA-copied mRNA extracts. The sizes of these DNA bands were those stated in table 2.4.1.1 when compared to positions of markers from a 100bp DNA ladder.

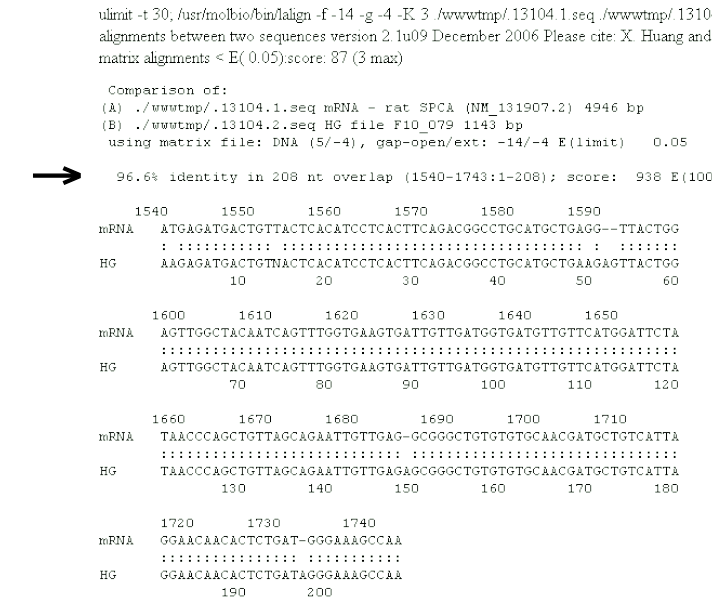

HG

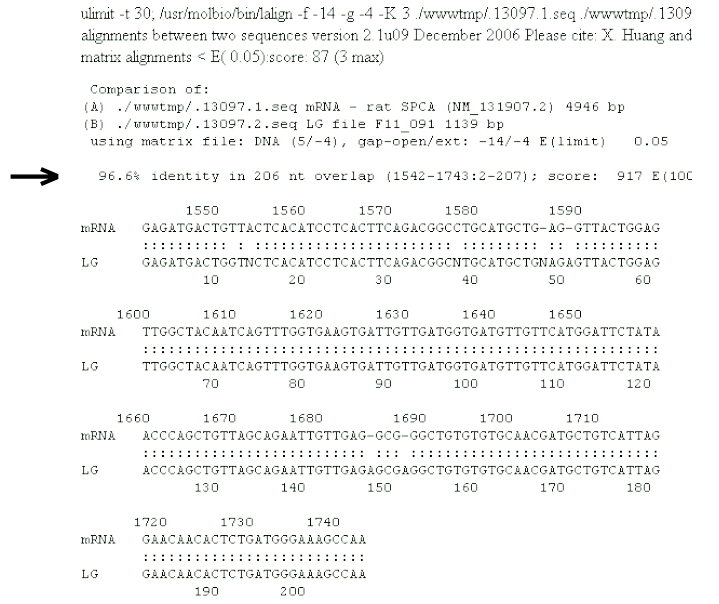

NG

Figure 3.2.1.4. Sequence Alignment Between SPCA1 PCR Products From HG/NG Cells & Rat SPCA1 mRNA

Figure 3.2.1.4. Sequence Alignment Between SPCA1 PCR Products From HG/NG Cells & Rat SPCA1 mRNA

Sequences of SPCA1 PCR products for both "HG" and "NG" cells were aligned against that for rat SPCA1 (listed as '*Rattus norvegicus* ATP2C1') from the Pubmed nucleotide databank (entry number NM_131907.2). Values indicated by the arrows show the percentage of sequence between the PCR product and databank entry that was found to be the same as each other.

converted into percentages of mean band intensity measured from HG cells samples compared to NG cells (HG/NG), which are shown in figure 3.2.1.3A with S.E.M values represented by the error bars.

From this, it was observed that HG cells contained 60 ± 13% more SPCA1 mRNA than NG cells. HG cells were also 19 ± 5% more abundant in their SERCA mRNA content than NG cells. On the other hand, GAPDH and β-actin mRNA levels showed minimal change, whereby increases of 7 ± 4% and 4 ± 3% were observed, respectively. Student's T-test analysis determined the difference in SPCA1 ($P<0.01$) and SERCA ($P<0.05$) transcript levels between NG and HG levels to be significant, whereas those for GAPDH and β-actin ($P>0.05$) were not significant. The SPCA1 PCR product for both HG and NG cells were both sequenced and confirmed to represent the presence of SPCA1 mRNA coding sequence (figure 3.2.1.4).

3.2.2. Expression Levels of SPCA1, SERCA & α-Actin Protein in A7r5 Cells Cultured in Normal & High Glucose Media

Western blots of total cell lysates from A7r5 cells were repeated twice for each sample. Three samples were used for the detection of each of three proteins of interest and for each glucose culture condition. Total protein levels of each chemiluminescent protein band, like those in figure 3.2.2.1B, were deemed to be the same for all bands on the same blot by ensuring the same amount of protein was loaded at their corresponding SDS-PAGE gels. The amount of α-actin protein detected would also serve as a loading control as well as a VSMC marker. The mean of corrected protein band intensity values were calculated, and those representing measurements of samples from HG cells were made relative to equivalent values obtained for samples from NG cells. Such relative values were converted into percentage values of mean difference in amount of protein of interest in HG cells compared to NG cells (HG/NG), which are shown with their S.E.M values represented by the error bars in figure 3.2.2.1A.

The data presented shows a difference of 15 ± 5% more SPCA1 protein detected in total cell lysates from HG cells compared to those isolated from NG cells. Furthermore, SERCA and α-actin protein levels were found to be 9 ± 4% and 2 ± 4%, respectively, higher in samples from HG cells than those of NG cells. However, Student's T-test analysis determined the difference observed for SPCA1 protein levels

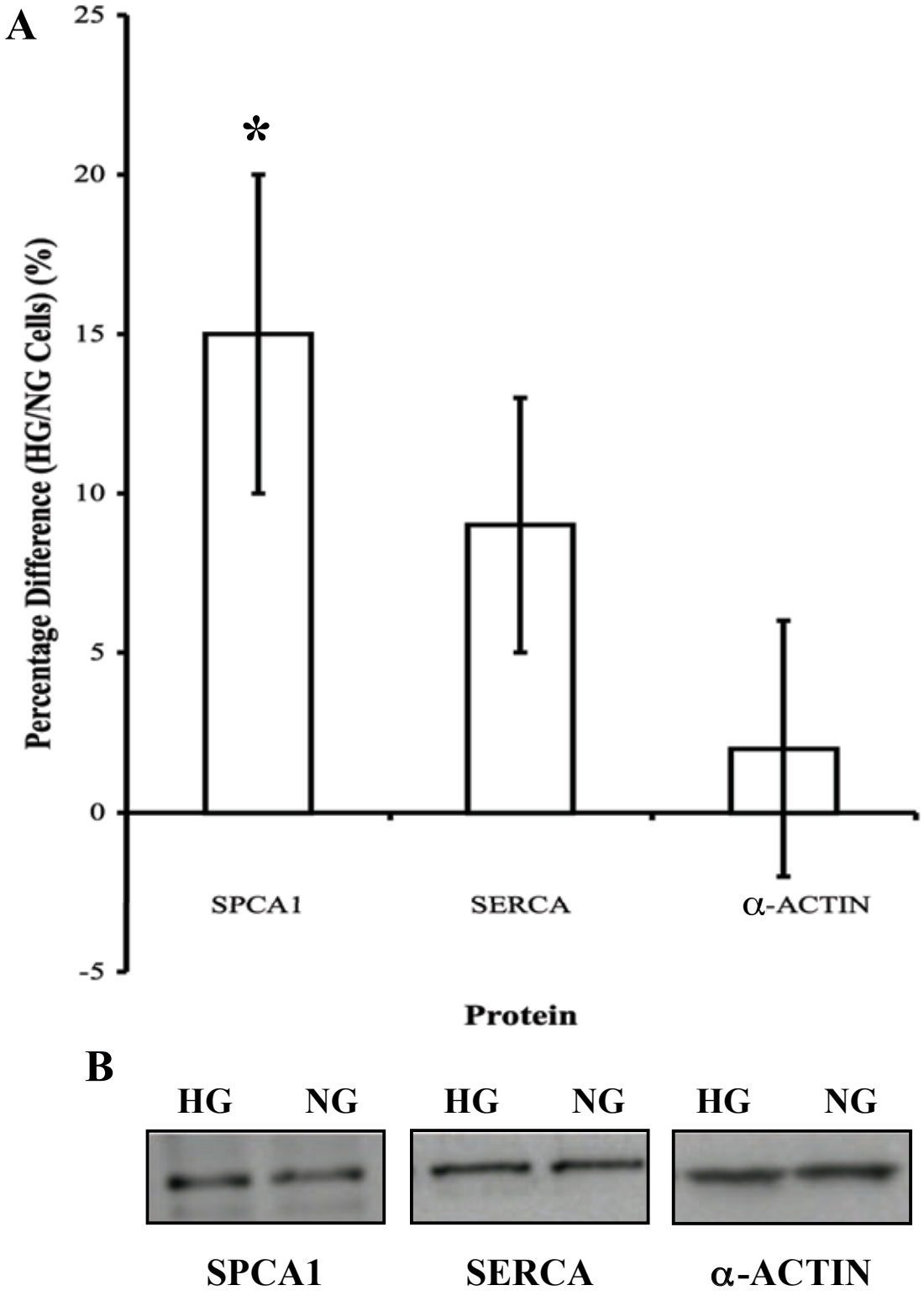

Figure 3.2.2.1. Western Blot Analysis of SPCA1, SERCA & α-Actin Protein Expression Levels in A7r5 Cells Cultured in Normal & High Glucose Media

Figure 3.2.2.1. Western Blot Analysis of SPCA1, SERCA & α-Actin Protein Expression Levels in A7r5 Cells Cultured in Normal & High Glucose Media

(A) Two Western blots were done for each primary antibody and total cell lysate sample. Three pairs of NG and HG cell cultures were used for sample collection. Chemiluminescent protein band intensities from images of HRP substrate-treated blots were measured for each sample, corrected for background, and values from HG cells were made relative to those for their pair-matched NG cells. Mean values from replicate Western blots were calculated for each protein of interest and glucose culture condition, and converted to the percentage difference values shown. Error bars indicate S.E.M. A significant P-value calculated from two-tailed equal variance Student's T-test is indicated by * ($P<0.05$).

(B) Chemiluminescent protein bands from HRP substrate-treated Western blots, which show typical band intensities observed for each of the three proteins of interest from NG and HG total cell lysate samples. Their molecular mass were approximately 100kDa for both SPCA1 and SERCA, and 42kDa for α-actin.

between HG and NG cells to be significant ($P<0.05$), whereas those for SERCA and α-actin were not significant. The lack of difference in α-actin protein levels between NG and HG samples indicated there was no significant difference in their amounts of total protein that were blotted onto the analysed membranes.

3.2.3. Measurements of Ca^{2+}-Dependent ATPase Activity from Microsomal Membranes of A7r5 Cells Cultured in Normal & High Glucose Media

Microsomal membranes were prepared from three cultures of A7r5 cells for each of the two glucose culture conditions tested. Triplicate Ca^{2+}-dependent ATPase activity measurements were made for each preparation of microsomal membranes, either in the absence or presence of 1μM thapsigargin in reaction mixtures. All activities were corrected for any effects from the physical presence of membranes and reagents on the phosphate liberation assay used, by subtracting values from the two following types of control reactions: those with (1) active membranes in the absence of Ca^{2+}, and (2) the presence of denatured membranes.

In all experiments, 2mM azide was used to inhibit Ca^{2+}-independent ATPase activity and Ca^{2+} uptake processes from any contaminating mitochondria that may have been present in the microsomal membrane preparations. 2μM vanadate was also used in all reaction mixtures to inhibit any PMCA activity that may have been present in the samples. Thus the Ca^{2+}-dependent ATPase activities that were measured were either from a combination of SERCA and SPCA (in the absence of thapsigargin), or from SPCA alone (in the presence of thapsigargin). Note that the assay used did not discriminate between the splice variants and isoforms of both SPCA and SERCA. 1μM thapsigargin was selected for use based on data from literature of a previous study, which has shown this concentration of thapsigargin inhibits all SERCA activity without affecting SPCA1 activity at all (Dode et al., 2006). Although 1μM thapsigargin can reduce SPCA2 activity by 40% as demonstrated in the same study, it was not considered to be problematic for the purpose of the present study because SPCA2 expression in aortic and other vascular cells has been shown to be non-detectable (Vanoevelen et al., 2005).

From the data presented in table 3.2.3.1 of all mean Ca^{2+}-dependent ATPase activities calculated from measurements of phosphate liberation from Ca^{2+}- and ATP-stimulated A7r5 microsomal membranes, the overall mean activities for all three

Mean Ca^{2+}-Dependent ATPase Activity (nmol/min/mg protein) ± S.E.M				
Membrane Preparation	**No Thapsigargin**		**1μM Thapsigargin**	
	NG	**HG**	**NG**	**HG**
1	3.2 ± 0.5	3.1 ± 0.7	0.62 ± 0.09	1.05 ± 0.17
2	4.1 ± 1.6	2.7 ± 0.4	0.38 ± 0.07	2.89 ± 1.21
3	4.4 ± 0.5	3.7 ± 0.2	1.26 ± 1.17	1.63 ± 0.48

Table 3.2.3.1. Mean Ca^{2+}-dependent ATPase Activities Associated with Three Preparations of Microsomal Membranes from Normal & High Glucose-Cultured A7r5 Cells in the Absence & Presence of Thapsigargin

Three activity measurements were made for each membrane preparation and glucose culture condition, from which mean values were calculated and are presented with S.E.M values.

preparations of membranes from NG and HG cells were 3.9 ± 0.5 and 3.2 ± 0.4 nmol/min/mg protein, respectively, in the absence of thapsigargin. Equivalent mean activities in the presence of 1μM thapsigargin for NG and HG cells were 0.75 ± 0.27 and 1.86 ± 0.55 nmol/min/mg protein, respectively. Statistical testing using analysis of variance (ANOVA) showed differences between the three mean activities for each of NG and HG cells-derived microsomal membranes were not statistically significant from reactions done in the absence of thapsigargin. On the other hand, differences between equivalent mean activities from reactions done in the presence of thapsigargin were found to be significant ($P<0.05$), with higher thapsigargin-insensitive activity from HG, compared to NG, membranes. This latter observation was consistent with an higher SPCA activity in HG, compared to NG, membranes.

3.2.4. Fluo-3-Based Ca^{2+} Measurements in Single Cells from A7r5 Normal & High Glucose Cultures

NG and HG cells loaded with Fluo-3 Ca^{2+}-sensitive fluorescent dye were viewed using fluorescence microscopy and video recordings of their Ca^{2+}-mediated responses to AVP in the absence and presence of thapsigargin were analysed. Changes in fluorescence were measured from 10 cells for each experiment and four experiments were done for each AVP treatment (i.e. in the absence and presence of thapsigargin) and glucose culture condition. Four averaged plots (one for each experiment) of relative changes in fluorescence over time, for each agonist treatment and glucose culture condition, are presented in figures 3.2.4.1-3.2.4.3.

Analysis of Ca^{2+} transients produced by thapsigargin in NG and HG cells shown in figure 3.2.4.1 indicate there was no major difference observed between the cells from the two glucose culture conditions tested, since the general average response profile from all experiments is near the same and mean peak heights of change in F/F_0 were 0.41 ± 0.06 for NG cells and 0.40 ± 0.05 for HG cells. Student's t-test of these values confirm no statistical significance in the difference observed for these values between NG and HG cells from the four experiments for each glucose culture condition ($P>0.05$). The same lack of difference was also observed from NG and HG cells that were treated with AVP in the absence the thapsigargin, as shown in figure 3.2.4.2. Again, the response profiles for all experiments in the latter case were, on average, the same as each other and resembled typical profiles observed previously (Byron and Taylor, 1995). Furthermore, the mean peak heights of change in F/F_0 were

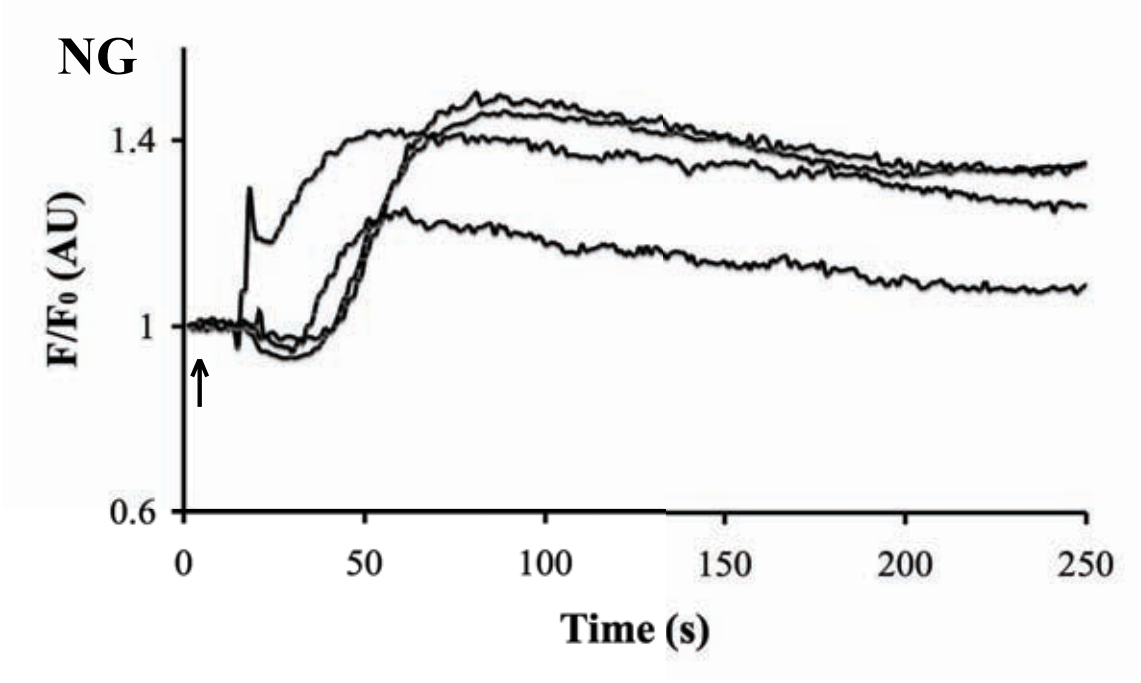

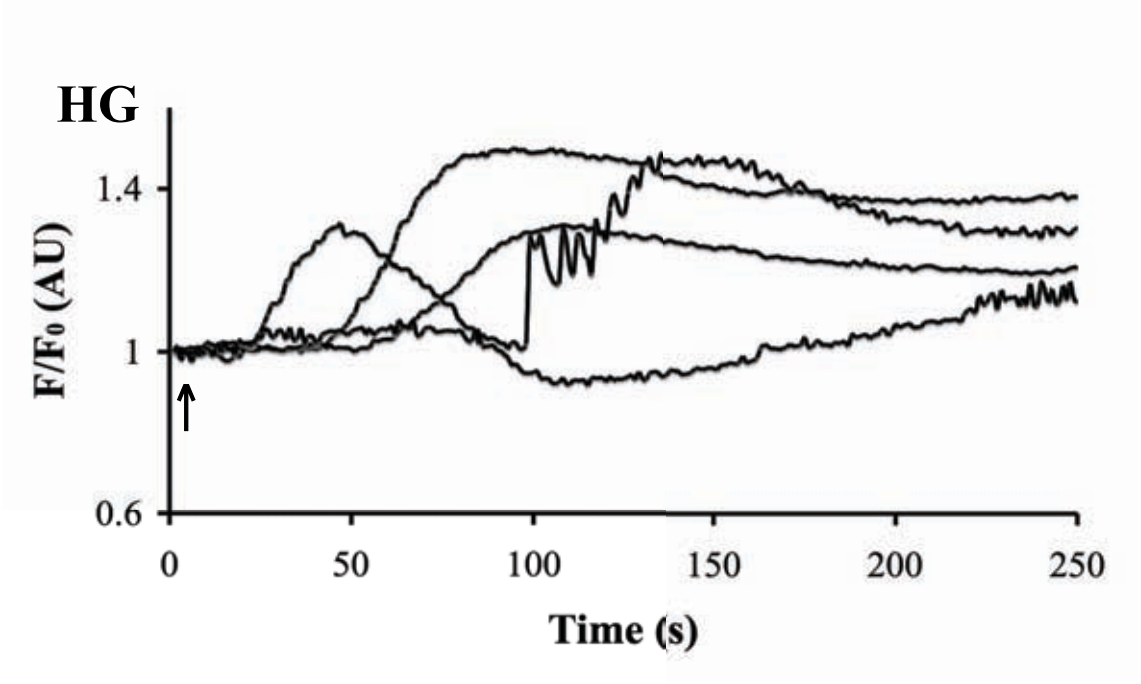

Figure 3.2.4.1. Thapsigarigin-Stimulated Ca^{2+} Transients in A7r5 Cells Cultured in Normal & High Glucose Media

Figure 3.2.4.1. Thapsigarigin-Stimulated Ca^{2+} Transients in A7r5 Cells Cultured in Normal & High Glucose Media

Changes in [Ca^{2+}] within A7r5 cells grown in either normal ("**NG**") or high ("**HG**") glucose-supplemented media were detected by monitoring Fluo-3 fluorescence levels in dye-loaded cells. Each trace represents mean values calculated from 10 cells. Arrows indicate the time-point at which 1μM thapsigargin was added.

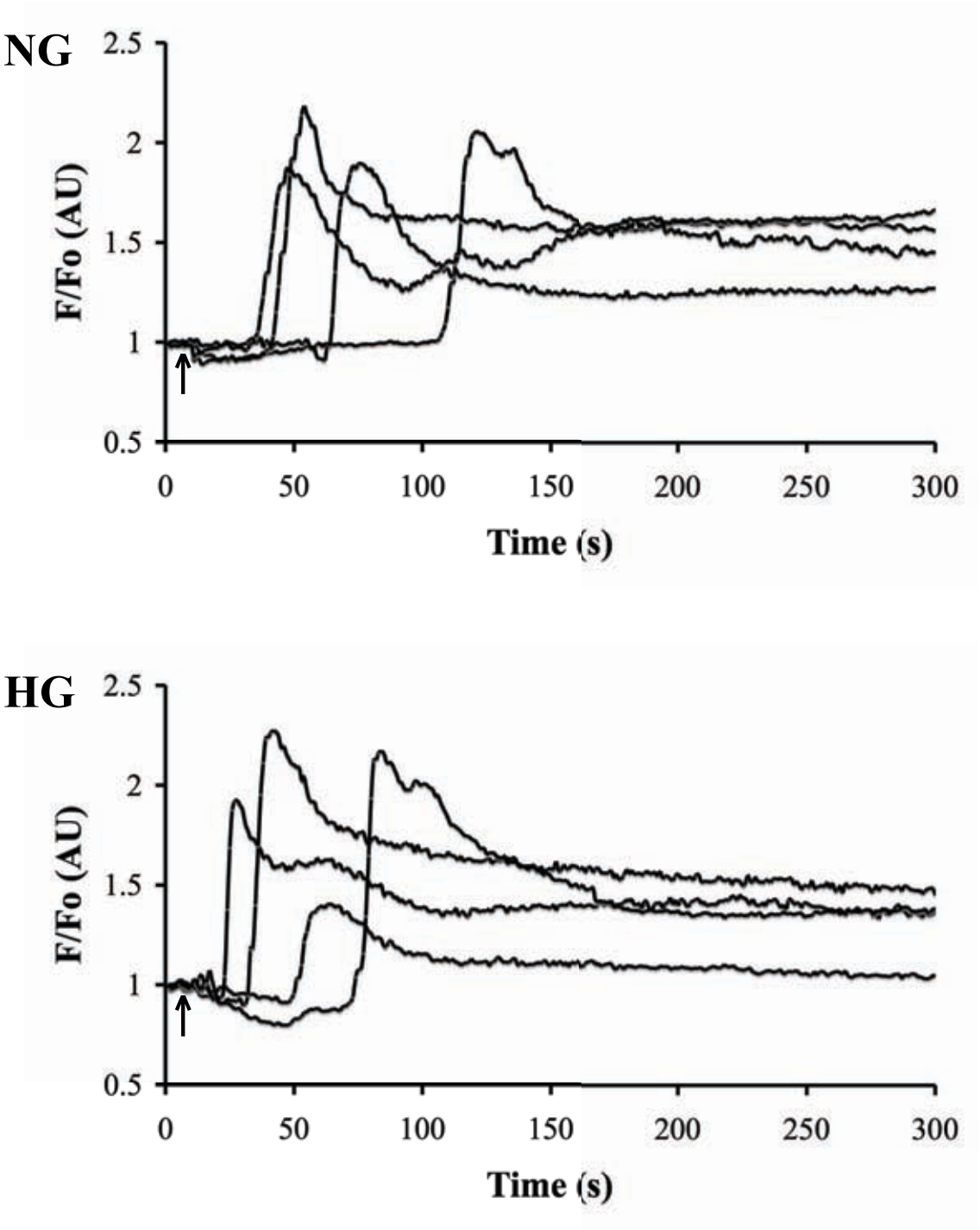

Figure 3.2.4.2. AVP-Stimulated Ca^{2+} Transients in A7r5 Cells Cultured in Normal & High Glucose Media (No Thapsigargin Pre-Treatment)

Figure 3.2.4.2. AVP-Stimulated Ca^{2+} Transients in A7r5 Cells Cultured in Normal & High Glucose Media (No Thapsigargin Pre-Treatment)

Changes in [Ca^{2+}] within A7r5 cells grown in either normal ("**NG**") or high ("**HG**") glucose-supplemented media were detected by monitoring Fluo-3 fluorescence levels in dye-loaded cells. Each trace represents mean values calculated from 10 cells. Arrows indicate the time-point at which 10nM AVP was added.

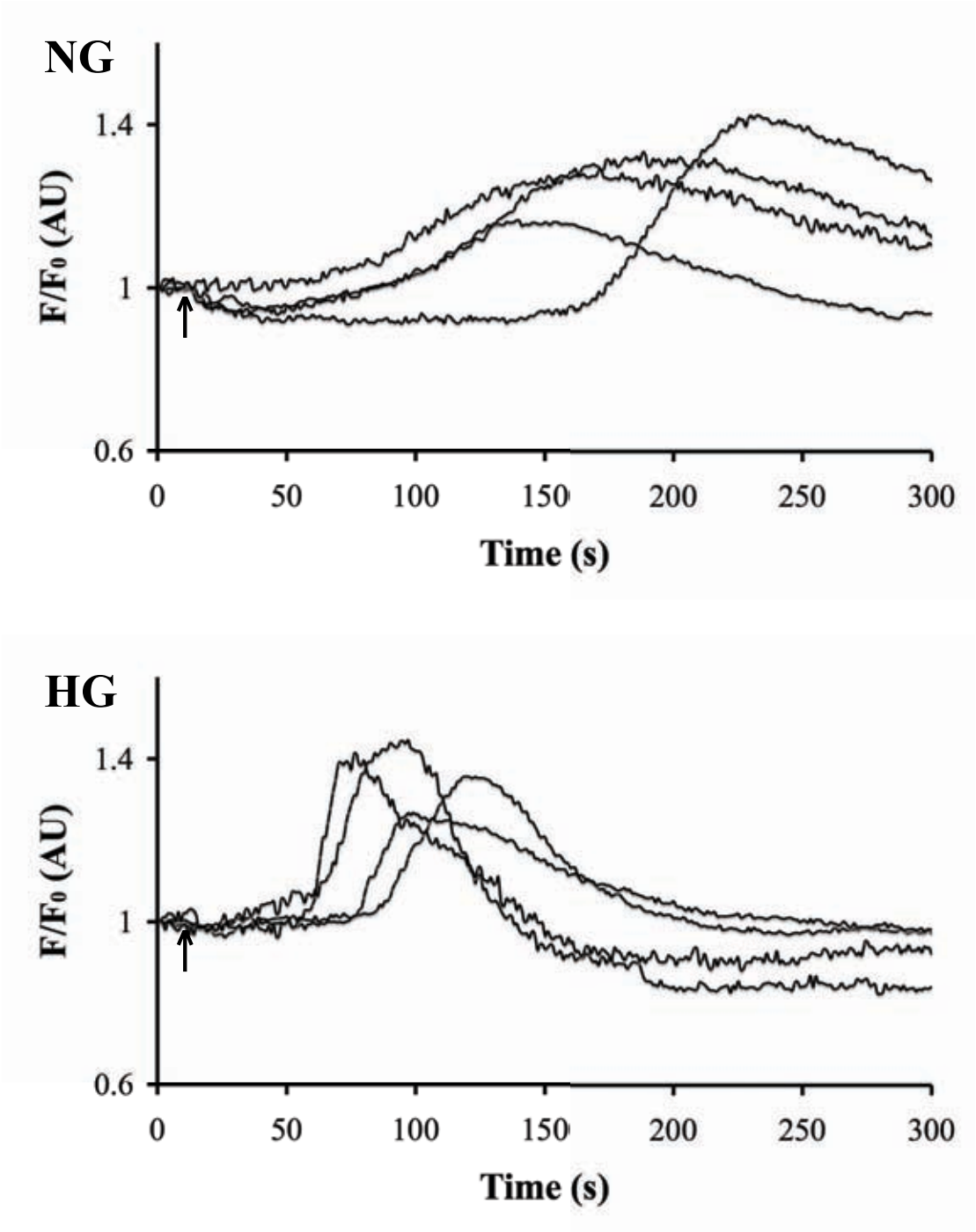

Figure 3.2.4.3. AVP-Stimulated Ca^{2+} Transients in A7r5 Cells Cultured in Normal & High Glucose Media (Pre-Treatment with Thapsigargin)

Figure 3.2.4.3. AVP-Stimulated Ca^{2+} Transients in A7r5 Cells Cultured in Normal & High Glucose Media (Pre-Treatment with Thapsigargin)

Changes in [Ca^{2+}] within A7r5 cells grown in either normal ("**NG**") or high ("**HG**") glucose-supplemented media were detected by monitoring Fluo-3 fluorescence levels in dye-loaded cells. Each trace represents mean values calculated from 10 cells. Arrows indicate the time-point at which 10nM AVP was added. Cells were pre-treated with 1μM thapsigargin for 5 minutes before the addition of AVP. The thapsigargin response was recorded to ensure this pre-treatment was effective on the cells (but profiles for which are not presented here).

1.14 ± 0.13 for NG cells and 0.98 ± 0.20 for HG cells, which were found to not be statistically significant in their difference to each other according to Student's T-test analysis ($P>0.05$).

On the other hand, figure 3.2.4.3 does show a difference in mean Ca^{2+}-mediated responses to AVP after pre-treatment with thapsigargin between NG and HG cells, whereby their associated response profiles indicate both faster rise and fall phases of change in intracellular [Ca^{2+}] were recorded following AVP stimulation in HG cells compared to NG cells. This difference was further analysed by measuring the kinetics of both phases from the response profiles shown in figure 3.2.4.3. Both the time taken to reach half-maximal response and half-life of decay in response to AVP were measured from each of the four mean response profiles and the mean values of these were calculated for each glucose culture condition, which are shown in table 3.2.4.4 with their S.E.M values. Student's T-test analysis showed the difference between NG and HG cells for both kinetics measurements were statistically significant ($P<0.05$).

The mean peak heights of change in F/F_0 for these Ca^{2+}-mediated AVP responses were not found to be statistically significant ($P>0.05$), whereby values of 0.32 ± 0.06 and 0.39 ± 0.04 were obtained for NG and HG cells, respectively. However, by making the mean peak heights of change in F/F_0 from thapsigargin pre-treated cells relative to those from cells that were stimulated with AVP in the absence of thapsigargin, it can be shown that, on average, 28% and 40% of Ca^{2+}-mediated response to this agonist is insensitive to thapsigargin treatment in NG and HG cells, respectively. These differences between the two AVP treatments were found to be statistically significant from Student's T-test calculation for both NG ($P<0.05$) and HG ($P<0.01$) cells.

Two types of control experiments were done to further investigate where the AVP-stimulated Ca^{2+} release originated from following thapsigargin treatment. Only HG cells were used for these. All control experiments lasted 10 minutes each and, like the experiments discussed above, involved thapsigargin treatment 1 minute after initiating their recording. One experiment involved treating the cells again with 1μM thapsigargin four minutes after the first treatment, instead of AVP, in the absence of extracellular Ca^{2+}. This showed whether or not thapsigargin-sensitive Ca^{2+} release was still possible after one treatment of A7r5 cells with 1μM of this SERCA inhibitor.

Kinetics Measurements from Ca^{2+} Transient Profiles of AVP Responses in Thapsigargin Pre-treated A7r5 Cells		
	NG	**HG**
Time taken to reach half-maximal response (s)	48.3 ± 5.1	18.2 ± 3.2
Half-life of decay in response (s)	76.9 ± 7.4	39.7 ± 5.7

Table 3.2.4.4. Kinetics Measurements from Mean Ca^{2+} Transient Plots of AVP Stimulation in Thapsigargin Pre-Treated A7r5 Cells Cultured in Normal & High Glucose Media

Measurements were taken from the rise and fall phases of Ca^{2+}-mediated AVP response shown in the four traces of each graph at figure 3.2.4.3. Mean values were calculated for each of the two glucose culture conditions and are presented ± S.E.M.

The result of these experiments showed no further Ca^{2+} release (data not shown). The other experiment was the same as the 10-minute experiments discussed above (i.e. thapsigargin treatment at 1 minute and AVP treatment at 5 minutes after initiation) except that they were also done in the absence of extracellular Ca^{2+}. These latter control experiments showed that it was indeed possible to produce AVP-stimulated Ca^{2+} release following a visible Ca^{2+} response to thapsigargin treatment even in the absence of extracellular Ca^{2+} (see chapter 4 for figure 4.2.6.1).

3.2.5. Immunofluorescence Detection of SPCA1, SERCA & Golgi Apparatus Localisation in A7r5 Cells Cultured in Normal & High Glucose Media

Figure 3.2.5.1 shows images taken of A7r5 cells that were fixed, permeabilised and treated with either antibodies or WGA for the detection of SPCA1, SERCA and the Golgi apparatus. WGA is a lectin that binds to glycoproteins highly abundant at the Golgi apparatus (Wright, 1984) and, more specifically, has been found to localise its binding at trans-Golgi membranes (Iida and Page, 1989). Analysis of images treated with antibodies against SPCA1 showed no detectable difference between NG and HG cells with regards to SPCA1 localisation. The same conclusion was made for the detection of SERCA in cells from the same two glucose culture conditions.

Comparison of SPCA1 localisation to that for the Golgi apparatus shows SPCA1 is most likely to be located at this organelle because they shared very similar perinuclear distribution patterns of fluorescence. This was in contrast to SERCA's more diffuse pattern of staining, which was observed in both NG and HG cells.

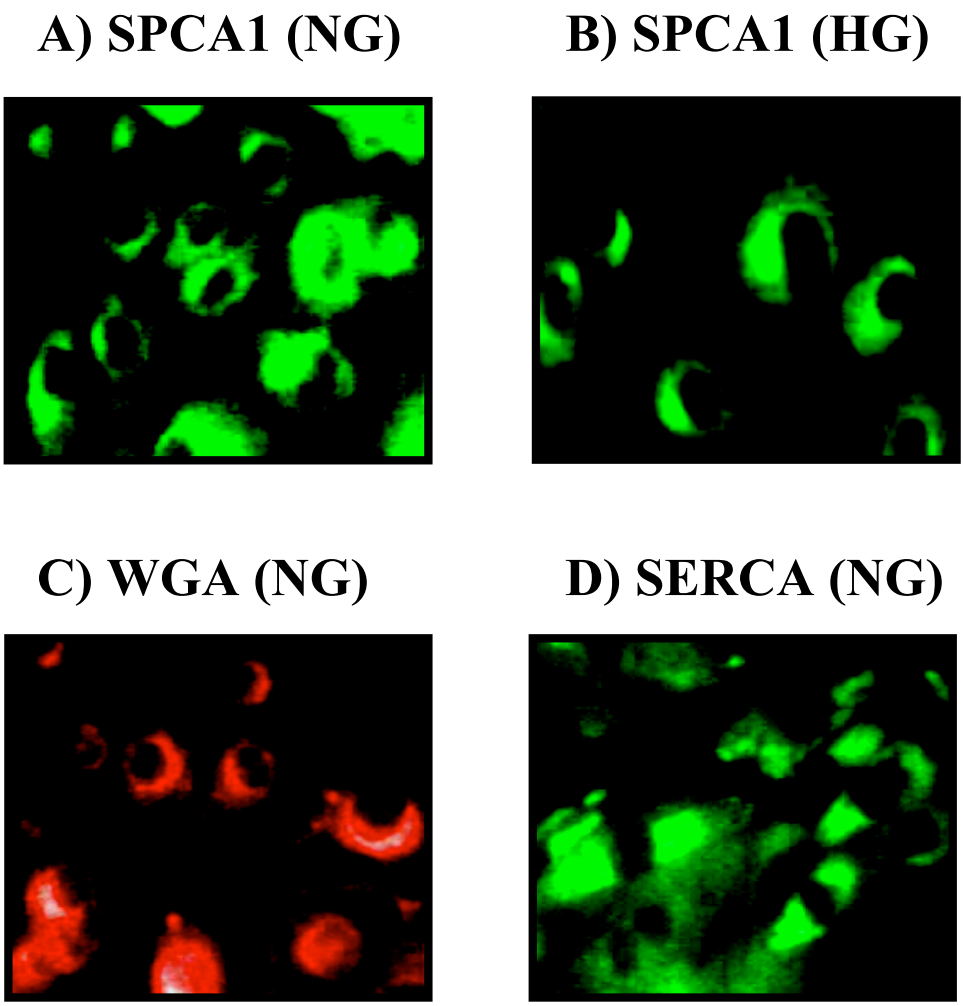

Figure 3.2.5.1. Localisation of SPCA1, SERCA & the Golgi Apparatus Within A7r5 Cells Cultured in Normal & High Glucose Media Using Fluorescently-Tagged Antibodies & Wheat Germ Agglutinin

Figure 3.2.5.1. Localisation of SPCA1, SERCA and the Golgi Apparatus Within A7r5 Cells Cultured in Normal & High Glucose Media Using Fluorescently-Tagged Antibodies & Wheat Germ Agglutinin

A7r5 cells cultured in normal ("**NG**") and high ("**HG**") glucose media were fixed with formaldehyde, permeabilised with Triton X100 and incubated with either antibodies specific for the detection of SPCA1 or SERCA, or WGA. The latter binds and therefore labelled glycoproteins abundant in the Golgi apparatus. Fluorescence was detected from either FITC-conjugated secondary antibodies or the TMR conjugated to WGA. Both SPCA1 detection in (A) NG and (B) HG cells are shown. (C) Golgi apparatus and (D) SERCA detection has been shown for NG cells, which showed the same distribution of fluorescence as observed for HG cells (latter not shown).

3.3. Discussion

PCR and Western blotting experiments have shown SPCA1 abundance at the mRNA and protein levels, respectively, were significantly higher than normal in A7r5 cells cultured in high glucose (HG), compared to normal glucose (NG), media. Lack of alteration in β-actin and GAPDH mRNA levels indicate both phenotype and activities of glucose metabolic pathways did not differ greatly between NG and HG cells. Thus, the difference in SPCA1 expression levels observed between A7r5 cells cultured under the two glucose conditions tested were unlikely to have been due to differences caused by a phenotypic switch nor altered ATP utilisation of the SPCA1 Ca^{2+}-ATPase. Furthermore, positive detection of α-actin, a VSMC marker, in all samples from NG and HG cells confirm they were both representative of VSMCs. Overall, this suggests glucose availability itself can affect the expression levels of SPCA1 in VSMCs.

It was notable that an approximate 60% difference in SPCA1 mRNA levels only reflected a difference of about 15% at the protein level. A similar discrepancy has been observed in a previous study that showed SPCA expression levels differ between brain and mammary tissues of rats, whereby the latter was found to express 7-8 times more of its mRNA but only 2-3 times more of its protein compared to the former (Reinhardt et al., 2000). The authors of this study attributed the difference in protein turnover rates (i.e. SPCA1 protein turnover was faster in mammary tissue compared to that of brain), which could also explain the discrepancy between SPCA1 mRNA and protein levels in the present study.

Another possible explanation for the difference observed between SPCA1 mRNA and protein levels refers to transcriptional control of the gene that encodes SPCA1, whereby its transcription factors may have had more enhanced activity for the promotion of this gene's expression in HG cells. This should be considered since it has been previously shown that both Sp1 (Han and Kudlow, 1997) and YY1 (Hiromura et al., 2003), the transcription factors of the SPCA1 gene in humans (Kawada et al., 2005), are more active in VSMCs grown in high glucose, compared to normal glucose, media. A7r5 cells can express the Sp1 transcription factor (Teunissen

et al., 2003). The observations made of Sp1 and YY1 were, in both cases, attributed to their glycosylation states. It is well established that the hyperglycaemic state can promote hyper-glycosylation of proteins in vascular cells (Aronson, 2008). Thus it is possible that differences in SPCA1 mRNA levels would not have been directly proportional to its proteins levels between NG and HG cells because of over-active promoter activity of its gene transcription factors, caused by changes to their glycosylation states, if combined with a near-maximal rate of either mRNA translation or protein turnover.

Differences in SPCA1 expression levels correlated well with levels in thapsigargin-insensitive Ca^{2+}-dependent ATPase activity measured from microsomal membranes. HG cells showed approximately 2-fold higher activity levels than NG cells. However, like SPCA1 mRNA levels, this relationship between protein expression and activity appeared to be disproportionate. One possible explanation for this discrepancy is that NG and HG cells expressed different amounts of different SPCA1 splice variants, which have been shown to exist in rats (Gunteski-Hamblin et al., 1992) and, for human splice variants, do differ in their kinetic properties (Dode et al., 2005). Here it should be emphasised that the anti-SPCA1 antibody used in Western blotting experiments recognised all rat SPCA1 splice variants (Wootton et al., 2004) and any differences in the amount of each available splice variant present in NG and HG cells was not identifiable in the present study. Thus the disproportional difference observed between SPCA protein expression and activity could have been attributed to HG cells expressing more of those variants with greater Ca^{2+}-ATPase activity than NG cells.

Lack of significant difference between NG and HG cells with regards to their total Ca^{2+}-dependent ATPase activities, despite a difference observed for thapsigargin-insensitive activities, suggested SERCA activity might have compensated for the difference in SPCA activity. This was a possibility since it has been shown previously that alterations to SPCA1 levels can influence that of SERCA in the opposite manner, which is exemplified by SPCA over-expression in COS-7 cells (Reinhardt et al., 2004). An apparent conflict of this possibility with the lack of significant difference between NG and HG cells with regards to their SERCA protein levels. However, this could be explained by factors such as differences in lipid composition of ER and/or Golgi apparatus membranes between NG and HG cells. It is well established that the

lipid components of ER membranes can affect SERCA function (Lee, 1998) and that the composition of lipids in the Golgi apparatus membranes are distinctly different from those of ER (Lev, 2005). It may be possible that glucose availability can affect lipid synthesis activity at the ER and/or Golgi apparatus, which would lead to changes in the structural integrity of their membranes that could, in turn, influence SERCA and SPCA activity without the need to change their protein abundance.

The kinetics of Ca^{2+}-mediated responses to AVP stimulation in A7r5 cells cultured under the two glucose conditions tested demonstrate a clear difference between NG and HG cells after thapsigargin pre-treatment. The faster rise and decay phases of AVP-stimulated Ca^{2+} transients in HG, compared to NG, cells was consistent with higher than normal SPCA expression and activity levels. For the rise phase, a faster than normal increase in intracellular [Ca^{2+}] could be attributed to larger thapsigargin-insensitive agonist-releasable stores after depletion of ER stores, following SERCA inhibition, which is most likely to have resided at the Golgi apparatus (Missiaen et al., 2002, Baron et al., 2009, Lissandron et al., 2010). Note that AVP-stimulated Ca^{2+} transients are initiated by intracellular Ca^{2+} release and this is a pre-requisite of Ca^{2+} entry from extracellular medium that follows to form the rise phase (Byron and Taylor, 1995). Thus faster than normal time taken to reach half-maximal response in HG, compared to NG, cells could have resulted from there being more thapsigargin-insensitive SPCA activity in HG cells and subsequently greater compensatory effect following the loss of SERCA-controlled agonist-releasable Ca^{2+} stores. Higher than normal SPCA activity at the Golgi apparatus Ca^{2+} stores in HG cells would have aided the recovery of resting Ca^{2+} levels after thapsigargin treatment better than NG cells. This is because HG cells would have been made more efficient at removing and storing the Ca^{2+} released from the ER by having more active Ca^{2+}-ATPase activity available, which would explain the faster than normal decay phase of AVP-stimulated Ca^{2+} transients in HG cells.

The physiological consequence of having the types of Ca^{2+} responses observed for AVP stimulation in A7r5 cells cultured in normal and high glucose media is evident when considering the role of Ca^{2+} in VSMC contraction. VSMCs in blood vessel walls contract and relax to alter their diameter in order to adjust to changes in blood flow. The more sustained a rise in intracellular [Ca^{2+}] maintained in VSMCs, the

more prolonged their contractile response will be. Thus by having faster than normal rates of rise and fall in intracellular [Ca^{2+}] following vasoactive hormone stimulation, like those observed in HG cells, the contraction of VSMCs is likely to be maintained for shorter periods of time and so thus would be less contractile. This would correspond well with the secretory phenotype of VSMCs in cardiovascular diseases, such as those induced by type II diabetes mellitus. Furthermore, enhanced SPCA1 activity could also increase the population of cells in the secretory phenotype in vascular smooth muscle tissue, by promoting abnormal levels of synthesis and/or post-translational modification of secretory proteins due to its role in controlling the luminal Ca^{2+} store of the Golgi apparatus.

With regards to lack of significant difference in Ca^{2+} responses produced as a result of AVP treatment to NG and HG cells that had not been pre-treated with thapsigargin, this result was consistent with there also being no difference between their total microsomal membrane Ca^{2+}-dependent ATPase activities. This again leads to the suggestion that SERCA activity compensated for alterations of SPCA1 activity to make total intracellular Ca^{2+}-ATPase activity the same between NG and HG cells, and thus initiated AVP-stimulated Ca^{2+} responses with the same degree of intensity. The lack of significant difference in thapsigargin-stimulated Ca^{2+} transients does not necessarily disprove of this possibility, since it only demonstrates the Ca^{2+} storage capacity of the ER, not SERCA activity in hormone-mediated signalling, is the same between resting NG and HG cells.

The visualisation of SPCA1 localisation in NG and HG cells, along with that of the Golgi apparatus (using WGA) and SERCA, demonstrate alternations in SPCA1 expression and activity did not affect its localisation in A7r5 cells, cultured under the two glucose conditions tested, to a visually significant extent. This would agree well with the low amount of change in SPCA1 protein abundance detected. Furthermore, it was confirmed that SPCA1 localises to the Golgi apparatus in A7r5 cells and its intracellular distribution patterns differ to that of SERCA, which emphasised the point that these two Ca^{2+}-ATPases play roles at different organelles.

Finally, two additional points should be noted from the data presented here. Firstly, it is widely known that some observations made with cell lines, like A7r5 cells, may not

necessarily occur in intact tissue, and so the experiments in the present study need to be repeated in the context of primary VSMCs and animal models to establish the role of SPCA in diabetes-associated cardiovascular diseases with greater certainty. With regards to the A7r5 cell-line specifically, this study has demonstrated these cells contain significantly detectable agonist-releasable Ca^{2+} stores that are not controlled by SERCA. Such stores in A7r5 cells had been disputed to exist due to conflicting observations from previous studies (Missiaen et al., 2002, Vanoevelen et al., 2004). However, the data presented here has confirmed their existence.

To summarise, the present study has shown that A7r5 cells cultured in high, compared to normal, glucose media demonstrate: (1) higher SPCA1 expression, both at the mRNA and protein level; (2) higher thapsigargin-insensitive Ca^{2+}-dependent ATPase activity at microsomal membranes; and (3) faster rates of rise and fall phases of AVP-stimulated Ca^{2+} responses in intact cells following thapsigargin treatment. Together, these findings suggest glucose availability to VSMCs can mediate control on SPCA1 expression and activity, which can influence the Ca^{2+}-handling ability of the Golgi apparatus of these cells. The hyperglycaemic condition is likely to promote increased SPCA1 expression and activity in VSMCs, which could lead to increased Ca^{2+}-handling activity in the Golgi apparatus and decreased responsiveness to vasoactive hormones, at least by this organelle. SPCA may play a role in diabetes-related vascular pathology in VSMCs due to its responsiveness to glucose availability in these cells, as demonstrated with the A7r5 cell-line, which has been shown to cause alterations in Ca^{2+} homeostatic mechanisms that could potentially lead to the features of reduced contractility and increased secretory behaviour of these cells.

CHAPTER 4.

FINDING INHIBITORS & MODULATORS OF HUMAN SPCA

CHAPTER 4.
FINDING INHIBITORS & MODULATORS OF HUMAN SPCA

4.1. Introduction

SPCA is a Ca^{2+}-ATPase that is localised at the Golgi apparatus and provides this organelle with Ca^{2+} for its secretory pathway-related functions, such as the post-translational modification of proteins (Ramos-Castaneda et al., 2005) and promoting the formation of Ca^{2+}-containing secretory vesicles (Reinhardt and Horst, 1999). Previous studies have also shown SPCA activity can contribute to agonist-stimulated Ca^{2+}-signalling in, for example, rat pancreatic β-cells (Mitchell et al., 2004) and human neutrophils (Baron et al., 2009). This Ca^{2+}-ATPase exists in the form of different splice variants (e.g. SPCA1a-d in humans) and isoforms (SPCA1-2 in humans), which have different kinetic properties (Dode et al., 2005, Dode et al., 2006) and tissue distribution (Vanoevelen et al., 2005, Xiang et al., 2005).

SPCA was first identified as PMR1, a plasma membrane related Ca^{2+}-ATPase expressed in yeast and suggested to play a role in the secretory pathway due to its ability to affect glycosylation of proteins in transit through the Golgi apparatus (Rudolph et al., 1989). Since then, its expression has been detected in a number of other organisms, including Drosophila (Southall et al., 2006), sea urchin (Gunaratne and Vacquier, 2006) and pigs (Sepulveda et al., 2007). SPCA1 is regarded as a house-keeping protein because it has been found to be widely expressed in various types of human-derived tissues (Vanoevelen et al., 2005). Its expression in humans has most notably been linked to the skin condition, Hailey-Hailey disease (HHD) (Hu et al., 2000, Sudbrak et al., 2000). The transcription factors that control its gene expression in humans have been identified as Sp1 and YY1 (Kawada et al., 2005).

Previous studies on SPCA activity have relied on the use of inhibitors for its related Ca^{2+}-ATPases, such as SERCA with thapsigargin (Vanoevelen et al., 2004), to allow differentiation between their very similar activities in cells. Another method that has been used is artificial manipulation of its expression, either by increasing (Missiaen et al., 2002) or decreasing (Van Baelen et al., 2003) its levels. SPCA1 knockout mice have also been produced (Okunade et al., 2007). However, there are notable problems

with the use of some of these techniques. For example, over-expression of SPCA has been shown to result in some of its localisation at the ER, as well as altered expression levels of other Ca^{2+}-binding proteins that include PMCA and CALNUC (Reinhardt et al., 2004). The use of thapsigargin has resulted in conflicting results with regards to the effect of agonist-stimulation on Ca^{2+} release from the Golgi apparatus, which has recently been attributed to differences in the concentration used of this inhibitor (Baron et al., 2009). Use of inhibitors for other Ca^{2+}-binding proteins instead of those for SPCA is likely to reflect more on the effect of loss in activity of the former, rather than enhanced visibility of the latter's, especially in studies involving intact cells. Unfortunately, a well-characterised specific SPCA inhibitor has yet to be found.

The aim of the present study was to test the effects of seven possible SPCA1 modulators, which were in the form of either synthetic compounds or naturally occurring molecules (figure 4.1.1). The experimental model chosen for use was microsomal membranes from COS-7 cells that over-expressed hSPCA1d (the longest splice variant of SPCA1 from humans (Fairclough et al., 2003)). Comparisons were made with microsomal membranes prepared from COS-7 cells that over-expressed the ubiquitous hSERCA2b (the most commonly found and longest slice variant of SERCA in humans (Dhitavat et al., 2003)). Any of these compounds that were able to inhibit hSPCA1d but not hSERCA2b activity, over a similar concentration range, may be considered as potentially valuable tools in future studies on SPCA. A7r5 cells, which express both SPCA and SERCA endogenously, were also used to observe the effects of these potential modulators.

Five synthetic compounds were tested, which were bis(2-hydroxy-3-tert-butyl-5-methyl-phenyl)methane (bis-phenol), tetrabromobisphenol-A (TBBPA), trifluoroperazine (TFP), 2-aminoethoxydiphenyl-borate (2-APB) and bisphenol-A (BPA). Bis-phenol has been suggested in the literature to be able to inhibit SPCA activity because of its ability to inhibit thapsigargin-insensitive Ca^{2+}-ATPase activity in rat cerebellar microsomes (Brown et al., 1994) and inhibit Ca^{2+}-ATPase activity in human spermatozoa that do not express SERCA (Harper et al., 2005). A specific concentration of bis-phenol that can be used to differentiate between the two Ca^{2+}-ATPases (i.e. inhibit SPCA but not SERCA) has yet to be firmly established. The

other four synthetic compounds have all been previously shown to inhibit SERCA activity (TBBPA (Ogunbayo and Michelangeli, 2007), TFP (Engelender and DeMeis, 1996), 2-APB (Bilmen et al., 2002) and BPA (Hughes et al., 2000). It was of interest to see whether or not SERCA's sensitivity to these four compounds differs to that of SPCA in order to infer any structural differences between the two Ca^{2+}-ATPases, as well as finding an inhibitor that could block SPCA activity better than SERCA. Nicotinic acid adenine diphosphate (NAADP) and cyclic adenine diphosphate ribose (cADPR) are both naturally occurring molecules that are believed to be able to release intracellular Ca^{2+} stores by acting as potential second messengers (Lee and Aarhus, 1995, Dargie et al., 1990). Ca^{2+} release is believed to occur at the ER and acidic lysosomal stores by cADPR and NAADP, respectively (Galione and Churchill, 2002, Gerasimenko et al., 2006). However, these findings are relatively novel, yet to be fully ascertained in both cases and thus there is still some scope in possibility for other Ca^{2+} stores to be affected by these two second messengers. Thus they were also tested on hSPCA1d activity to see if they influence Ca^{2+} storage at the Golgi apparatus by acting on this Ca^{2+}-ATPase.

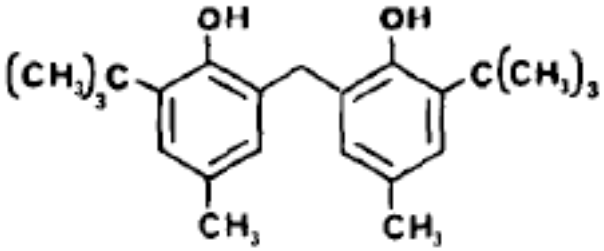

Bis(2-hydroxy-3-tert-butyl-
5-methyl-phenyl)methane
(Bis-phenol)

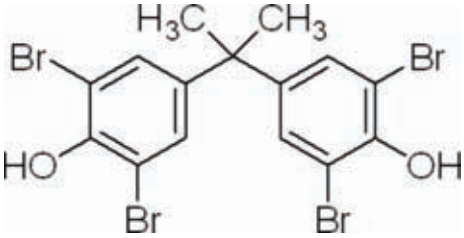

Tetrabromobisphenol-A
(TBBPA)

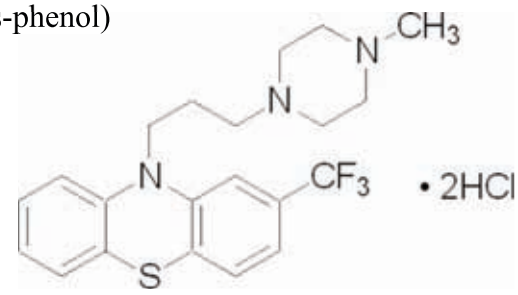

Trifluoroperazine
(TFP)

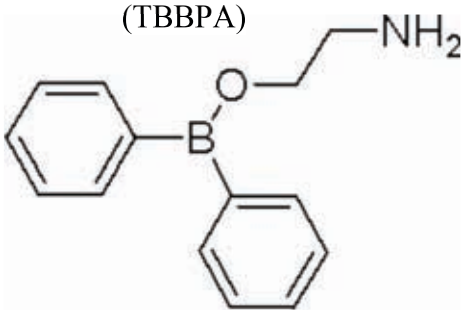

2-aminoethoxydiphenyl-borate
(2-APB)

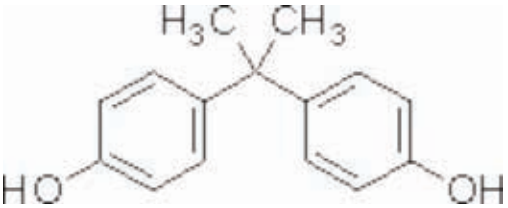

Bisphenol-A
(BPA)

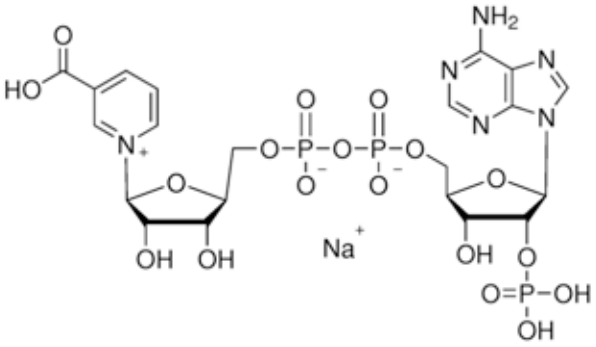

Nicotinic Acid Adenine Diphosphate
(NAADP)

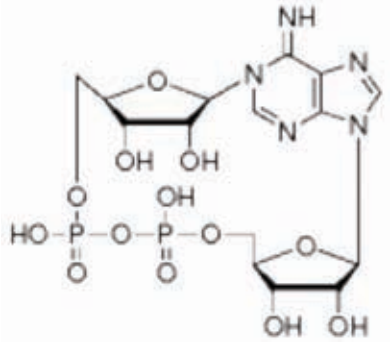

Cyclic Adenine Diphosphate
(cADPR)

Figure 4.1.1. The Seven Potential SPCA Inhibitors & Modulators

4.2. Results

4.2.1. Optimisation of hSPCA1d, hSERCA2b & Rabbit SERCA1b-EGFP Over-Expression in COS-7 Cells

Figure 4.2.1.1 shows successful digests for hSPCA1d-pMT2, hSERCA2b-pMT2 and rabbit SERCA1b-EGFP-pcDNA3.1(-) expression plasmids. Uncut plasmid DNA counterparts for hSPCA1d-pMT2 and rabbit SERCA1b-EGFP-pcDNA3.1(-) are also shown. The 'streaky' staining of undigested plasmid DNA, which had also been observed for hSERCA2b-pMT2 uncut plasmid, was due to supercoiling of circular DNA interfering with its movement through agarose gels and is a normal observation. For hSERCA2b-pMT2, only three of the six possible DNA bands produced from a HindIII restriction digest were visible on a 0.8% w/v agarose gel as the other three DNA fragments were less than 0.5kb and thus too small to be visible.

COS-7 cells were chosen for this study because they are easy to culture and transfect. Furthermore, this is the same cell line that was used in a previous study on the effects of over-expressing rat SPCA on Ca^{2+} homeostasis (Reinhardt et al., 2004). Rabbit SERCA1b-EGFP-pcDNA3.1(-) transfection was done to allow visualisation of transfection efficiency in intact COS-7 cells with the Genejuice reagent, which was assumed would be similar for the hSPCA1d/hSERCA2b-pMT2 plasmids. Figure 4.2.1.3A shows a Western blot of microsomal membranes prepared from COS-7 cells that were either transfected with rabbit SERCA1b-EGFP-pcDNA3.1(-) plasmid DNA or not transfected. Transfection was done using a 18μg:54μl ratio of plasmid DNA-to-transfection reagent in 10cm diameter Petri dishes, which were filled with 10ml of media, as a starting point for optimisation. Microsomal membranes were prepared 48 hours after transfection. Observation of 127kDa protein bands from microsomal membrane samples indicated the presence of SERCA-EGFP protein, whereby the molecular weights of SERCA and EGFP as separate proteins are approximately 100kDa (Wootton et al., 2004) and 27kDa (Muller-Taubenberger and Anderson, 2007), respectively. 127kDa bands were only detected in samples obtained from rabbit SERCA1b-EGFP-pcDNA3.1(-)-transfected COS-7 cells. Other protein bands on the Western blots that were not 127kDa in size were considered a result of non-specific binding of antibodies, except for 100kDa bands which were assumed to be representing endogenous SERCA expression in COS-7 cells.

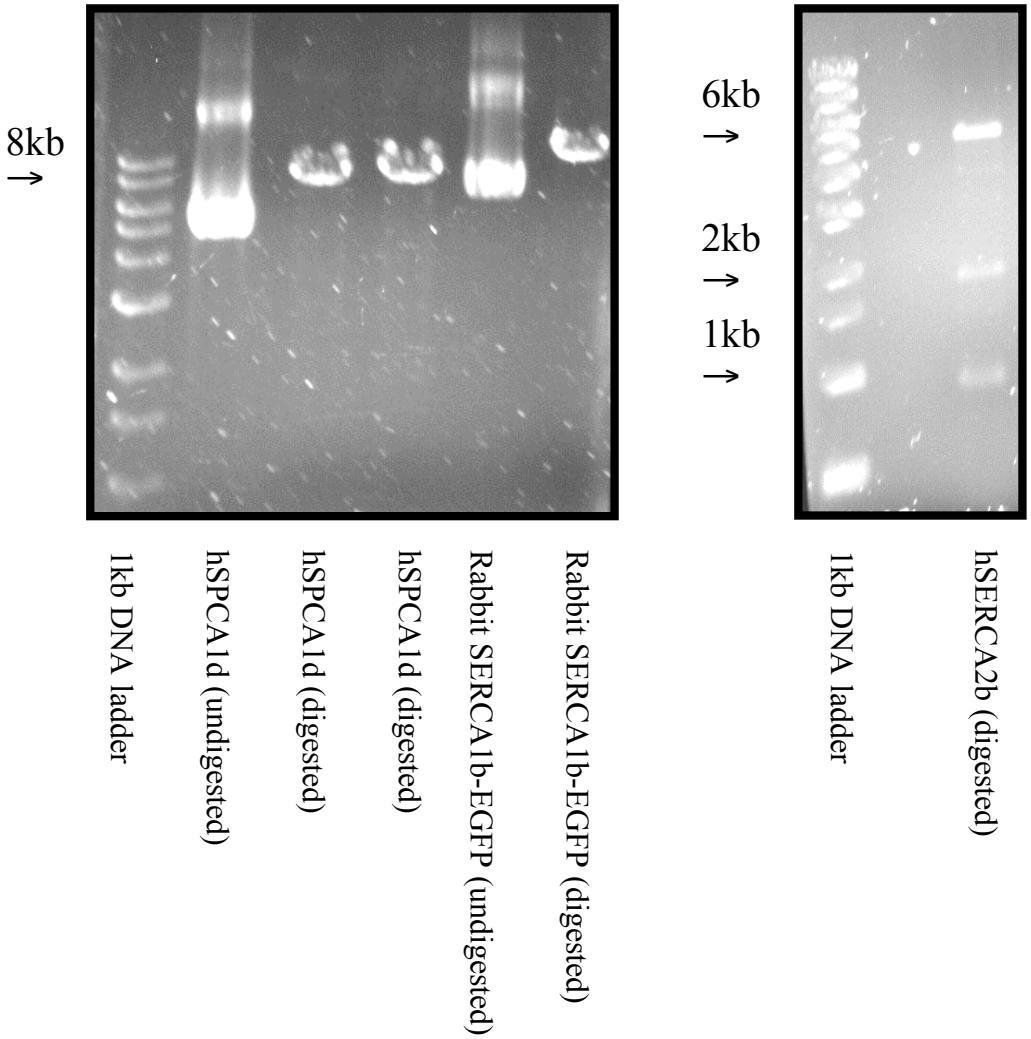

Figure 4.2.1.1. Restriction Digests for hSPCA1d-pMT2, hSERCA2b-pMT2 & Rabbit SERCA1b-EGFP-pcDNA3.1(-) Plasmids

Minipreps of hSPCA1d-pMT2 ("hSPCA1d"), hSERCA2b-pMT2 ("hSERCA2b") and rabbit SERCA1b-EGFP-pcDNA3.1(-) ("Rabbit SERCA1b-EGFP") plasmid DNA were digested with restriction endonucleases indicated on their associated restriction maps at figure 4.2.1.2. Restriction digest fragments ("digested") were electrophoresed alongside undigested DNA ("undigested"). The position of expected DNA band sizes are indicated at each gel image. All samples were loaded at equal volumes in each lane.

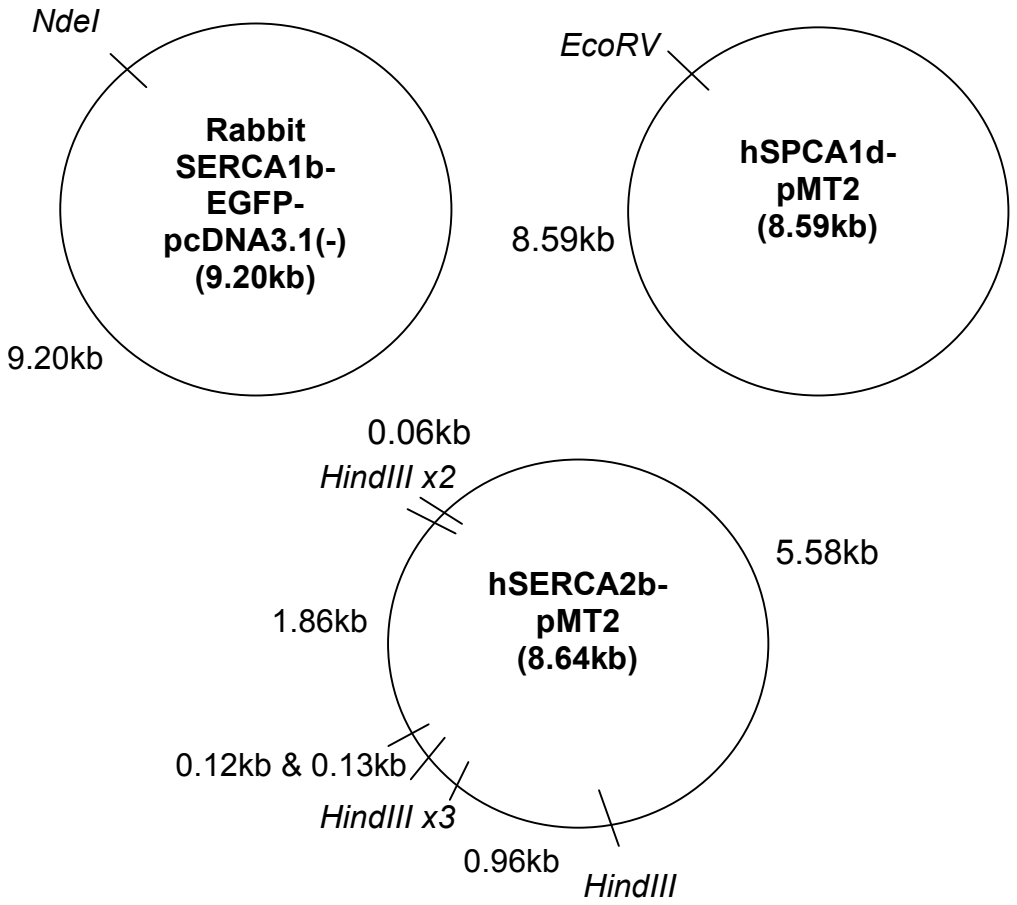

Figure 4.2.1.2. Restriction Maps for hSPCA1d-pMT2, hSERCA2b-pMT2 & Rabbit SERCA1b-EGFP-pcDNA3.1(-) Plasmids

The restriction maps associated with figure 4.2.1.1.

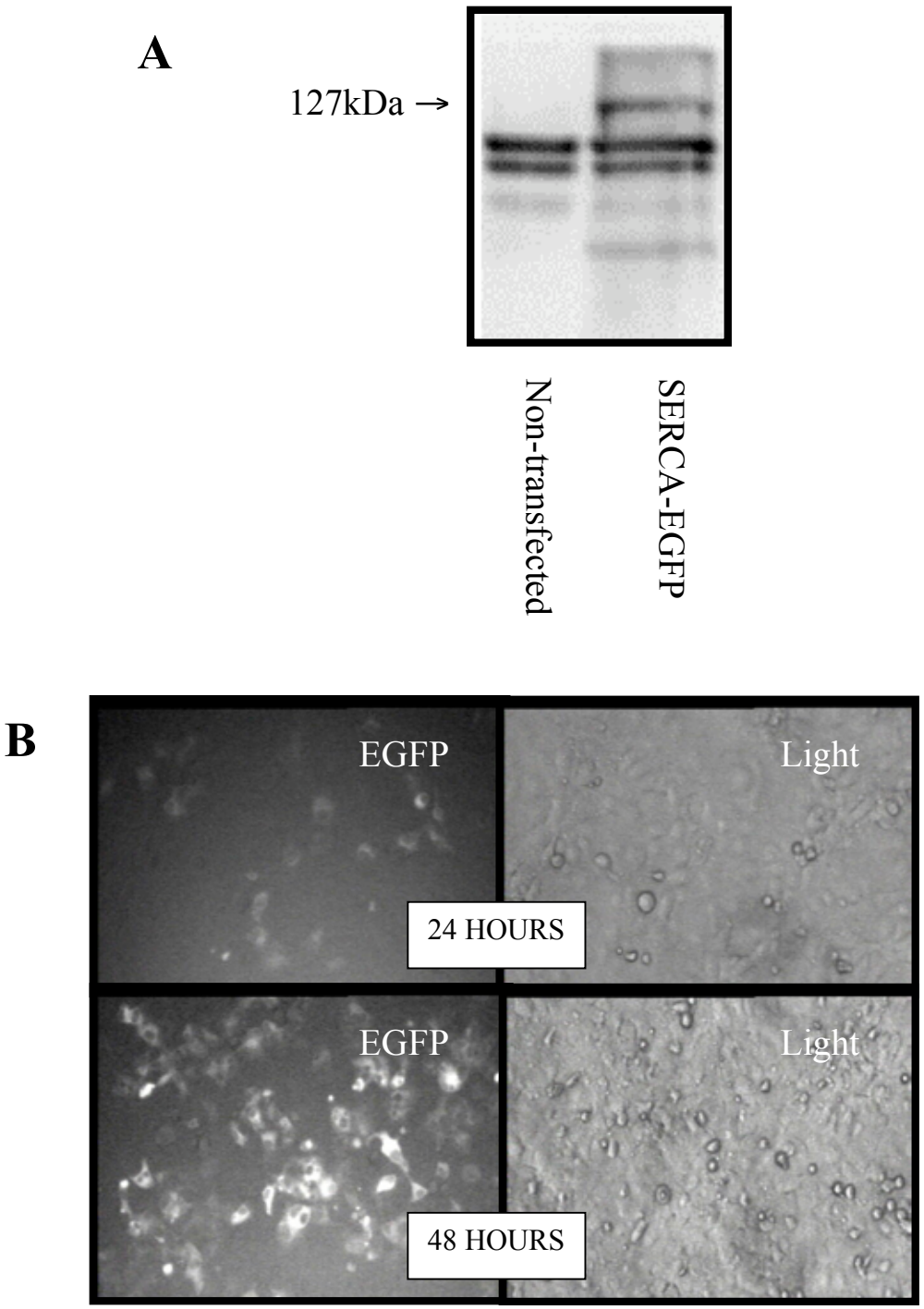

Figure 4.2.1.3. Western Blots & GFP Fluorescence Microscopy Images for Detection of SERCA-EGFP Over-Expression in COS-7 Cells Transfected with Rabbit SERCA1b-EGFP-pcDNA3.1(-) Plasmid

Figure 4.2.1.3. Western Blots & GFP Fluorescence Microscopy Images for Detection of SERCA-EGFP Over-Expression in COS-7 Cells Transfected with Rabbit SERCA1b-EGFP-pcDNA3.1(-) Plasmid

(A) A Western blot showing SERCA-EGFP was detected in microsomal membranes prepared from COS-7 cells transfected with rabbit SERCA1b-EGFP-pcDNA3.1(-) plasmid ("SERCA-EGFP"), along with those isolated from non-transfected cells ("non-transfected"), using anti-SERCA (Y1F4). 20μg of total protein from each sample was loaded into each lane. The position of the expected 127kDa protein band of rabbit SERCA1b-EGFP is indicated.

COS-7 cells were seeded at a density of $1.2x10^6$ cells per 10cm diameter plate and transfected 24 hours later with a 18μg:54μl ratio of plasmid DNA (μg)-to-transfection reagent (μl) per plate. Microsomal membranes were prepared 48 hours after transfection.

(B) Microscopy images taken of COS-7 cells 24 and 48 hours after being transfected with rabbit SERCA1b-EGFP-pcDNA3.1(-) plasmid DNA. Detection of GFP fluorescence ("EGFP") confirmed successful expression of SERCA1b-EGFP protein. Light microscopy ("Light") images were used to observe for morphology and population of transfected and non-transfected cells. Non-transfected cells showed no GFP fluorescence under the same culture conditions.

COS-7 cells were seeded at a density of $2x10^5$ cells per well of a 6-well plate and transfected 24 hours later with a 3μg:9μl ratio of plasmid DNA-to-transfection reagent per well. Transfected cells were viewed with a fluorescence microscope 24 and 48 hours after transfection.

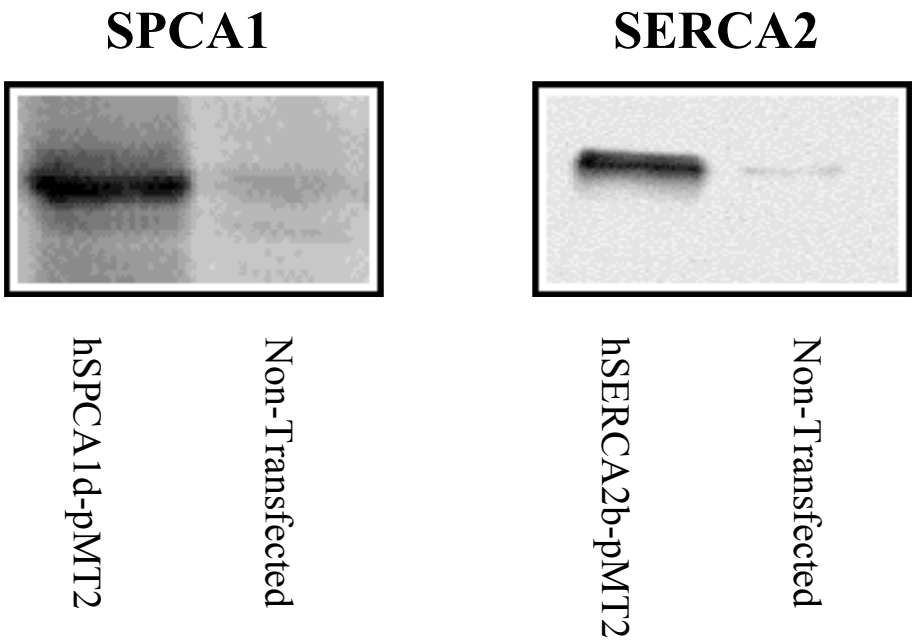

Figure 4.2.1.4. Western Blots of Microsomal Membranes Prepared From COS-7 Cells Transfected with hSPCA1d-pMT2 & hSERCA2b-pMT2 Plasmids

Detection of SPCA1 and SERCA2 protein levels in microsomal membranes prepared from "hSPCA1d/hSERCA2b-pMT2" transfected cells and "non-transfected" cells. Each lane was loaded with 20μg of total protein for each sample. SPCA1 was detected using anti-SPCA1 and SERCA2 was detected using anti-SERCA2.

Cells were seeded at a density of $1.2x10^6$ cells per 10cm diameter plate and transfected with a 18μg:54μl ratio of plasmid DNA-to-transfection reagent ratio 24 hours later. Microsomal membranes were prepared 48 hours after transfection.

Figure 4.2.1.3B shows the use of EGFP fluorescence to detect SERCA1b-EGFP-pcDNA3.1(-) transfection efficiency in intact COS-7 cells. Non-transfected cells were shown to not emit GFP fluorescence. GFP fluorescence was successfully detected from SERCA1b-EGFP-pcDNA3.1(-)
transfected COS-7 cells and thus rabbit SERCA1b over-expression was confirmed to be possible in these cells using the transfection ratio of DNA-to-reagent tested.

The amount of fluorescence observed from the transfected cells varied depending on the length of time between transfection and viewing at the microscope. 20-30% transfection efficiency was observed from cells following 24 hours after transfection, whereas 60-80% efficiency was observed from cells following 48 hours after transfection. From this, it was decided that all experiments with transfected COS-7 cells would be done 48 hours after transfection. Indeed these optimised transfection conditions allowed for the production of microsomal membranes with detectable amounts of over-expressed SPCA1 and SERCA2 protein, as shown by Western blots in figure 4.2.1.4, from COS-7 cells transfected with hSPCA1d-pMT2 and hSERCA2b-pMT2 plasmids, respectively.

4.2.2. Ca^{2+}-Dependent ATPase Activity Measurements with Microsomal Membranes Prepared from Rabbit SERCA1b-EGFP-pcDNA3.1(-)-Transfected COS-7 Cells

The Ca^{2+}-dependent ATPase activity from microsomal membranes of rabbit SERCA1b-EGFP over-expressing COS-7 cells was measured to ensure the transfection and microsomal membrane preparation methods used together could successfully produce microsomal membranes that contained such activity at a measurable level that would predominantly originate from the over-expressed Ca^{2+}-ATPase. Such measurements were made using the phosphate liberation method. This activity was also measured with microsomal membranes from non-transfected cells.

Mean activities for each membrane preparation and thapsigargin treatment condition were calculated from three assays. These mean activities are presented in table 4.2.2.1 with their S.E.M values. From this, differences in Ca^{2+}-dependent ATPase activities, which were measured in the absence of thapsigargin, observed

Microsomal Membrane Ca^{2+}-ATPase Activity ± SEM (nmol/min/mg protein)			
No Thapsigargin		**1μM Thapsigargin**	
Transfected	**Non-Transfected**	**Transfected**	**Non-Transfected**
21.53 ± 1.86	3.4 ± 0.32	2.01 ± 1.05	1.06 ± 0.87

Table 4.2.2.1. Ca^{2+}-ATPase Activity Measurements from Microsomal Membranes of SERCA1b-EGFP-pcDNA3.1(-)-Transfected & Non-Transfected COS-7 Cells

Activity measurements were made in either the presence or absence of 1μM thapsigargin in reaction mixtures. Each mean activity was calculated from nine assays with one microsomal membrane preparation. S.E.M values are shown.

between non-transfected and SERCA1b-EGFP-pcDNA3.1(-)-transfected COS-7 cells were found to be statistically significant according to Student's T-test ($P<0.01$). On the other hand, differences observed from activities measured in the presence of 1μM thapsigargin (a concentration of thapsigargin that has been shown in inhibit SERCA activity as stated in section 3.2.3) were not statistically significant between microsomal membranes from non-transfected and rabbit SERCA1b-EGFP-pcDNA3.1(-)-transfected cells ($P>0.05$). This indicated that SERCA1b-EGFP over-expression was successful and the same transfection conditions were subsequently used for hSPCA1d/hSERCA2b-pMT2 plasmids.

4.2.3. Ca^{2+}-Dependent ATPase Activity Measurements with Microsomal Membranes Prepared from COS-7 Cells Over-Expressing hSPCA1d & hSERCA2b

For both hSPCA1d and hSERCA2b, Ca^{2+}-dependent ATPase activities in the presence and absence of 1μM thapsigargin were measured from three preparations of microsomal membranes. Such activities from microsomal membranes prepared from non-transfected cells were also measured and these values were subtracted from those of their counterpart membranes that had the over-expressed human Ca^{2+}-ATPase, so that only activity from the latter would be presented. Western blotting was used on samples of all membrane preparations to confirm over-expression was successful at protein level. The mean activity values, each calculated from six assays, are shown in table 4.2.3.1 along with their S.E.M values for both hSPCA1d and hSERCA2b. Student's T-test confirmed no difference between the two conditions of thapsigargin treatment for all three hSPCA1d microsomal membrane preparations ($P>0.05$). This indicated no measurable inhibition of Ca^{2+}-dependent ATPase activity from microsomal membranes of hSPCA1d-pMT2-transfected cells and such thapsigargin-insensitive activity was interpreted as that from over-expressed hSPCA1d protein. On the other hand, the presence of 1μM thapsigargin in reaction mixtures with microsomal membranes from hSERCA2b-over-expressing cells inhibited virtually all Ca^{2+}-dependent ATPase activity for all three preparations, which demonstrated that such activity originated from thapsigargin-sensitive over-expressed hSERCA2b protein.

Microsomal Membrane Ca2+-ATPase Activity ± S.E.M. (nmol/min/mg protein)				
	hSPCA1d		hSERCA2b	
Membrane Preparation	**No Thapsigargin**	**1µM Thapsigargin**	**No Thapsigargin**	**1µM Thapsigargin**
1	26.16 ± 2.95	16.40 ± 2.07	15.55 ± 0.79	1.08 ± 0.50
2	22.03 ± 2.43	25.18 ± 1.94	15.56 ± 1.90	0
3	22.63 ± 1.05	25.17 ± 1.82	12.60 ± 1.56	0.98 ± 0.80

Table 4.2.3.1. Ca^{2+}-ATPase Activity Measurements from Three Preparations of Microsomal Membranes from hSPCA1d- & hSERCA2b- Over-Expressing COS-7 Cells

Activity measurements were made in either the presence or absence of 1µM thapsigargin in reaction mixtures. Each mean activity was calculated from six assays for each microsomal membrane preparation. S.E.M values are shown.

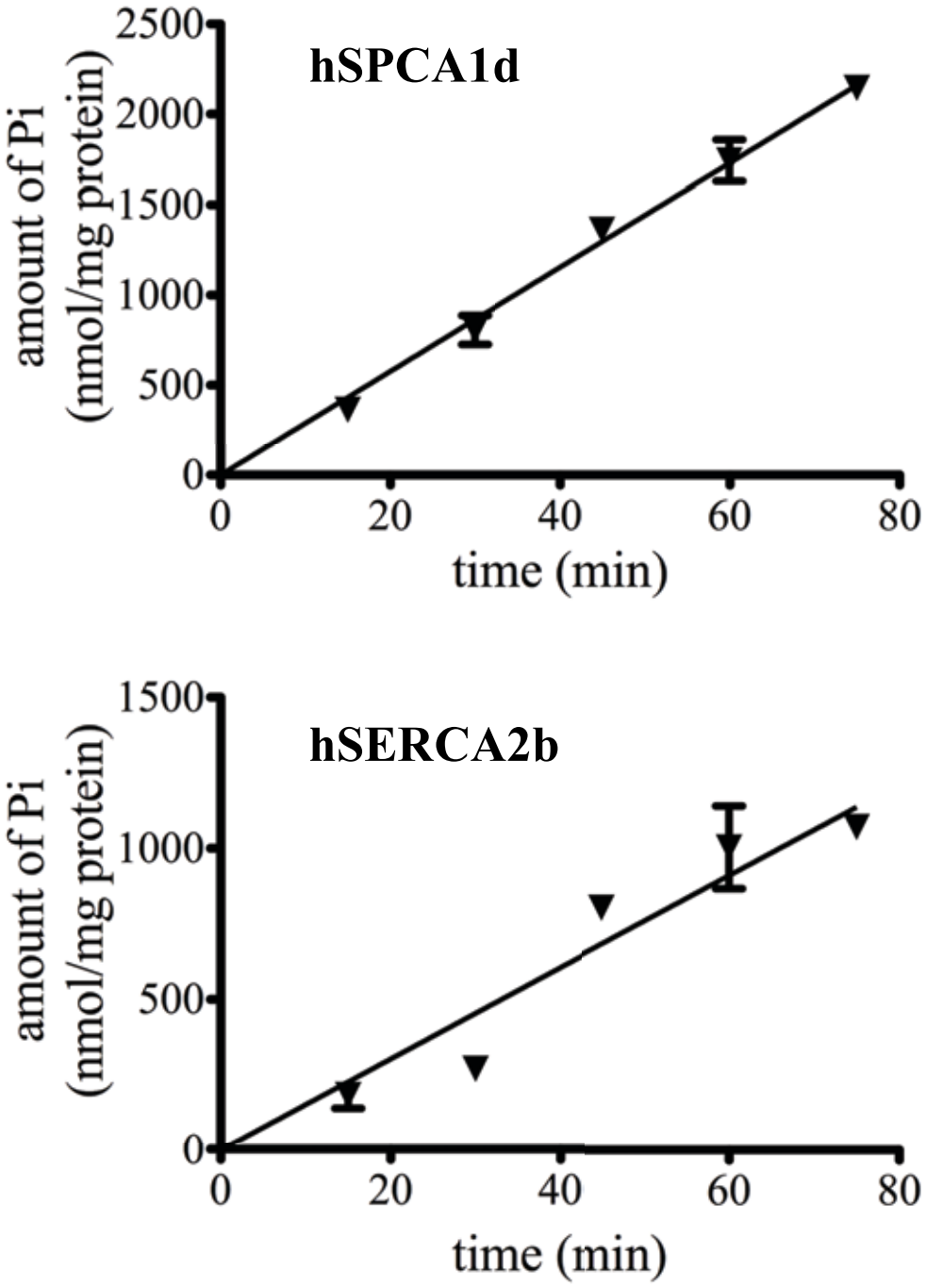

Figure 4.2.4.1. Time-Dependence of Mean Ca^{2+}-ATPase Activities From hSPCA1d & hSERCA2b in Microsomal Membranes

Figure 4.2.4.1. Time-Dependence of Mean Ca^{2+}-ATPase Activities From hSPCA1d & hSERCA2b in Microsomal Membranes

Ca^{2+}-stimulated ATPase activities were measured from microsomal membranes after 15, 30, 45, 60 and 75 minutes of ATP addition. Mean activities were taken from six replicate assays and one microsomal membrane preparation for each time point and error bars indicate S.E.M values. 1μM thapsigargin was added to reaction mixtures that contained "hSPCA1d" membranes, whereas no thapsigargin was added to those with "hSERCA2b" membranes.

4.2.4. Optimisation of Assay Time Length for Ca^{2+}-Dependent ATPase Activity Measurements of Microsomal Membranes from hSPCA1d- & hSERCA2b-Over-Expressing COS-7 Cells

Figure 4.2.4.1 shows the plot obtained from hSPCA1d membranes, which were treated with thapsigargin and thus values represent Ca^{2+}-dependent ATPase activity specific to this thapsigargin-insensitive protein. Figure 4.2.4.1 also shows the plot obtained from hSERCA2b membranes without the presence of thapsigargin in their reaction mixtures. Both plots represent mean Ca^{2+}-dependent ATPase activities measured from reactions that lasted for different durations of time. These were required to determine the optimal length of reaction time to use for the assay in order to measure any differences in activity when experimental conditions were altered, such as with the presence of potential inhibitors. From this, 45 minutes was selected as a suitable length of reaction time because it is within the linear range of values obtained for both hSPCA1d and hSERCA2b, which meant 45 minutes was enough time to both produce sufficiently measurable amounts of activity and not reach plateau due to substrate utilisation or product inhibition.

4.2.5. The Effects of Bis-phenol, TBBPA, TFP, 2-APB, BPA, cADPR & NAADP on Ca^{2+}-Dependent ATPase Activities of Microsomal Membranes from hSPCA1d- & hSERCA2b- Over-Expressing COS-7 Cells

Plots of mean thapsigargin-insensitive Ca^{2+}-dependent ATPase activities against different concentrations of bis-phenol (figure 4.2.5.1), TBBPA (figure 4.2.5.2), TFP (figure 4.2.5.3), 2-APB (figure 4.2.5.4), BPA (figure 4.2.5.5), cADPR (figure 4.2.5.6) and NAADP (figure 4.2.5.7) present in the reaction mixtures with hSPCA1d membranes are shown. Plots of mean Ca^{2+}-dependant ATPase activities (without thapsigargin treatment) against different concentrations of bis-phenol (figure 4.2.5.1), TBBPA (figure 4.2.5.2) and TFP (figure 4.2.5.3) measured from the present study are also shown for hSERCA2b membranes alongside their hSPCA1d counterparts. The data for 2-APB inhibition of hSERCA2b membranes was obtained from a previous study (Wootton and Michelangeli, 2006) (figure 4.2.5.4).

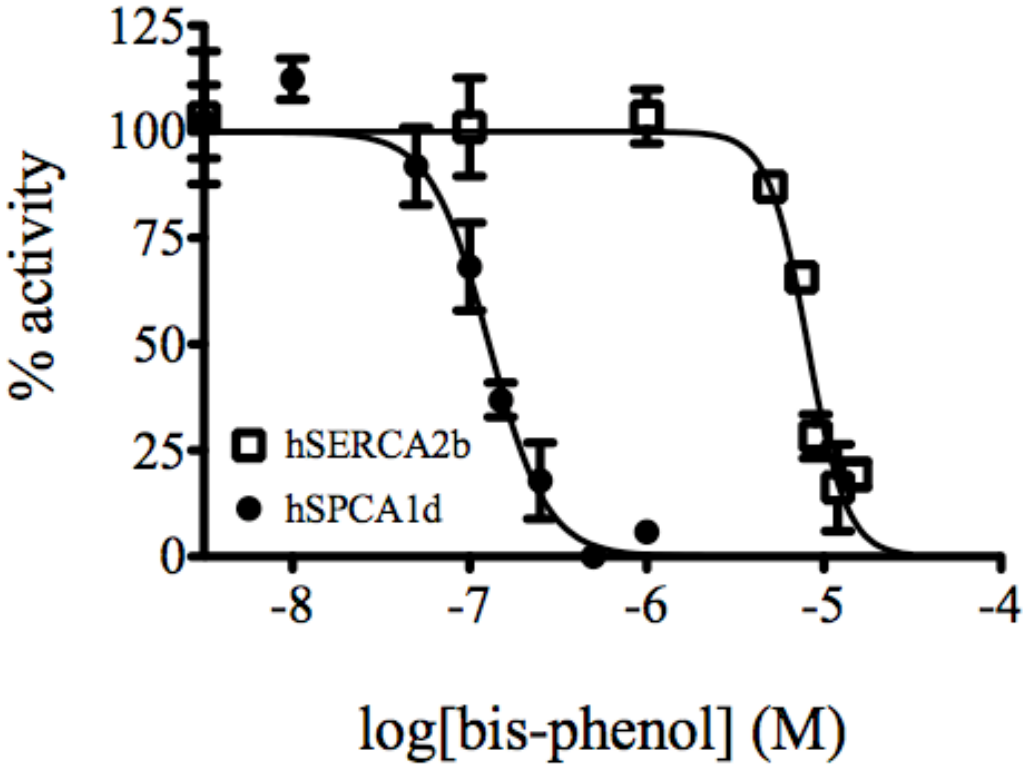

Figure 4.2.5.1. Effect of Different Bis-phenol Concentrations on Mean Ca^{2+}-ATPase Activities From Microsomal Membranes of hSPCA1d- & hSERCA2b- Over-Expressing COS-7 Cells

Percentage activity was calculated from making activity measurements in the presence of bis-phenol relative to those of vehicle (DMSO) control. DMSO content in all assays was 0.1% of their total volume. Mean activities were measured from three replicate assays for each bis-phenol concentration tested. Error bars indicate S.E.M values. Assay mixtures for "hSPCA1d" membranes contained 1μM thapsigargin and those for "hSERCA2b" membranes did not contain thapsigargin.

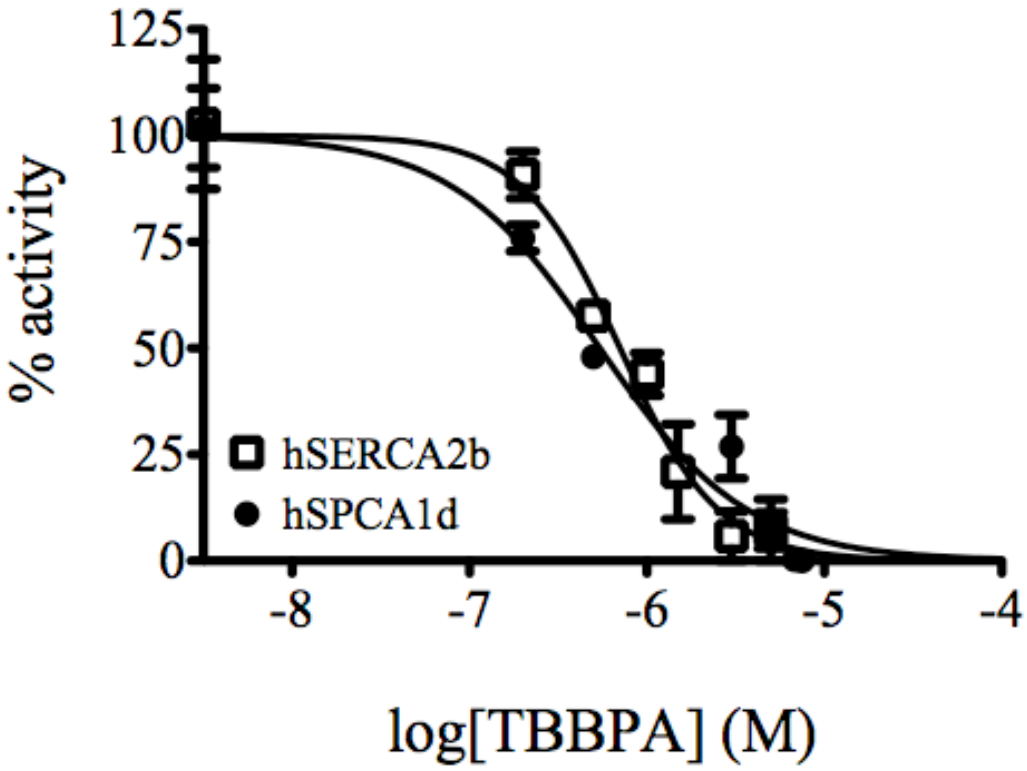

Figure 4.2.5.2. Effect of Different TBBPA Concentrations on Mean Ca^{2+}-ATPase Activities From Microsomal Membranes of hSPCA1d- & hSERCA2b- Over-Expressing COS-7 Cells

Percentage Ca^{2+}-dependent ATPase activities measured from hSPCA1d and hSERCA2b membranes in reaction mixtures that contained TBBPA at different concentrations. Mean activities were measured from three replicate assays for each TBBPA concentration tested and percentage activities calculated in the same way as stated for figure 4.2.5.1. Error bars indicate S.E.M values. Assay mixtures for hSPCA1d membranes contained 1μM thapsigargin and those for hSERCA2b membranes did not contain thapsigargin.

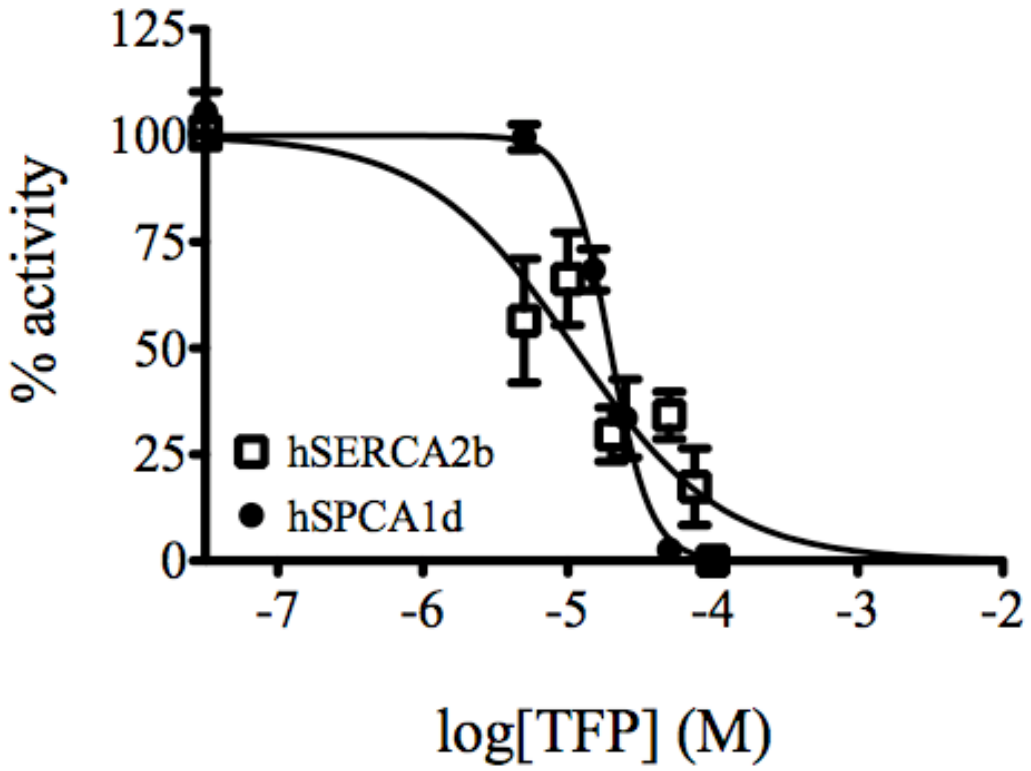

Figure 4.2.5.3. Effect of Different TFP Concentrations on Mean Ca^{2+}-ATPase Activities From Microsomal Membranes of hSPCA1d- & hSERCA2b- Over-Expressing COS-7 Cells

Percentage Ca^{2+}-dependent ATPase activities measured from hSPCA1d and hSERCA2b membranes in reaction mixtures that contained TFP at different concentrations. Mean activities were measured from three replicate assays for each TFP concentration tested and percentage activities calculated in same way as stated for figure 4.2.5.1. Error bars indicate S.E.M values. Assay mixtures for hSPCA1d membranes contained 1μM thapsigargin and those for hSERCA2b membranes did not contain thapsigargin.

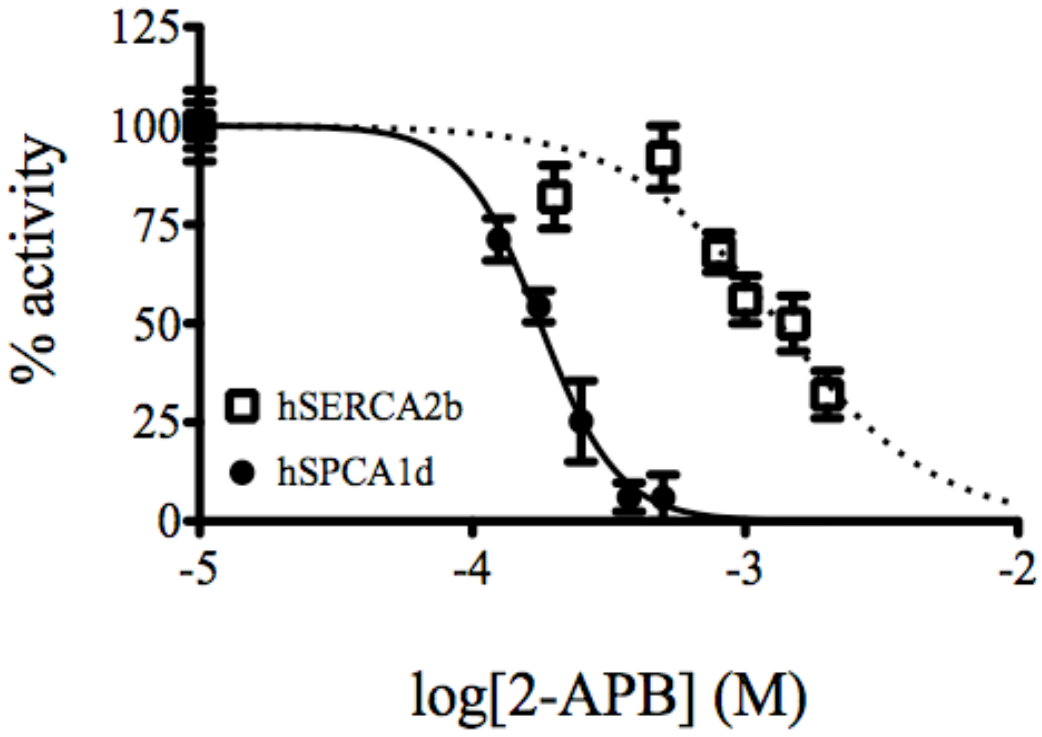

Figure 4.2.5.4. Effect of Different 2-APB Concentrations on Mean Ca^{2+}-ATPase Activities From Microsomal Membranes of hSPCA1d- & hSERCA2b- Over-Expressing COS-7 Cells

Percentage Ca^{2+}-dependent ATPase activities measured from hSPCA1d and hSERCA2b membranes in reaction mixtures that contained 2-APB at different concentrations. Mean activities were measured from three replicate assays for each 2-APB concentration tested and percentage activities calculated in same way as stated for figure 4.2.5.1. Error bars indicate S.E.M values. Assay mixtures for hSPCA1d membranes contained 1µM thapsigargin and those for hSERCA2b membranes did not contain thapsigargin. The data for hSERCA2b membranes was obtained from a previous study (Wootton and Michelangeli, 2006) (emphasised by the dotted line).

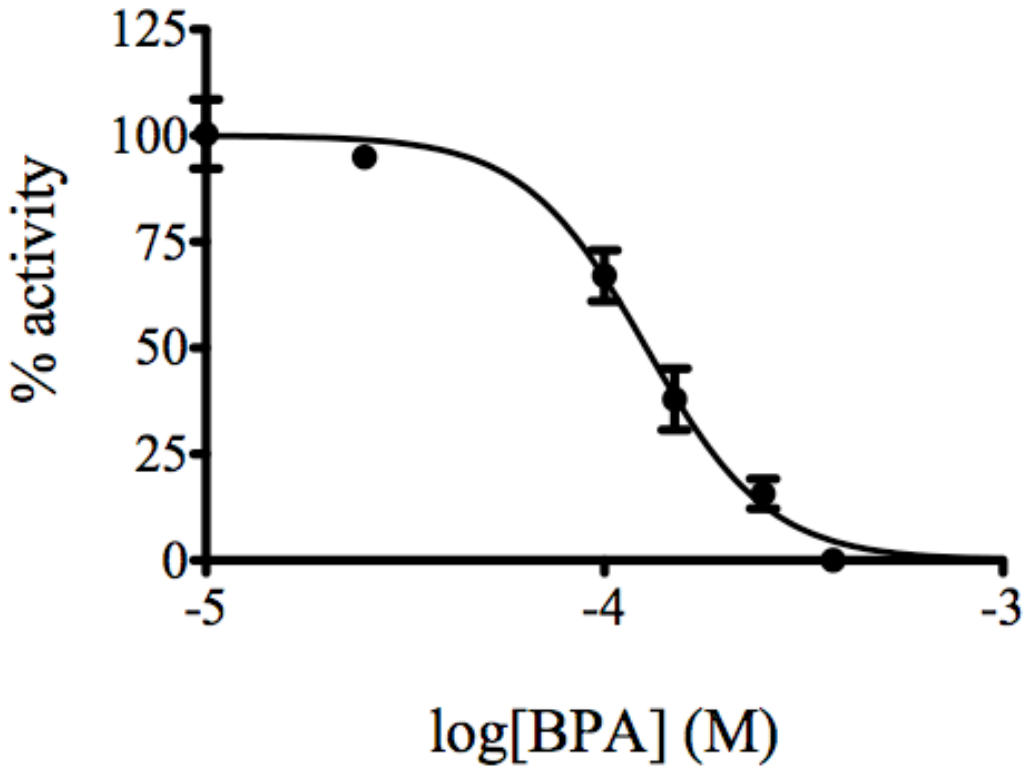

Figure 4.2.5.5. Effect of Different BPA Concentrations on Mean Ca^{2+}-ATPase Activities From Microsomal Membranes of hSPCA1d-Over-Expressing COS-7 Cells

Percentage activity was calculated from making activity measurements in the presence of BPA relative to those of vehicle (DMSO) control in the same way as stated for figure 4.2.5.1. Mean activities were measured from three replicate assays for each BPA concentration tested. Error bars indicate S.E.M values. 1μM thapsigargin was added to reaction mixtures.

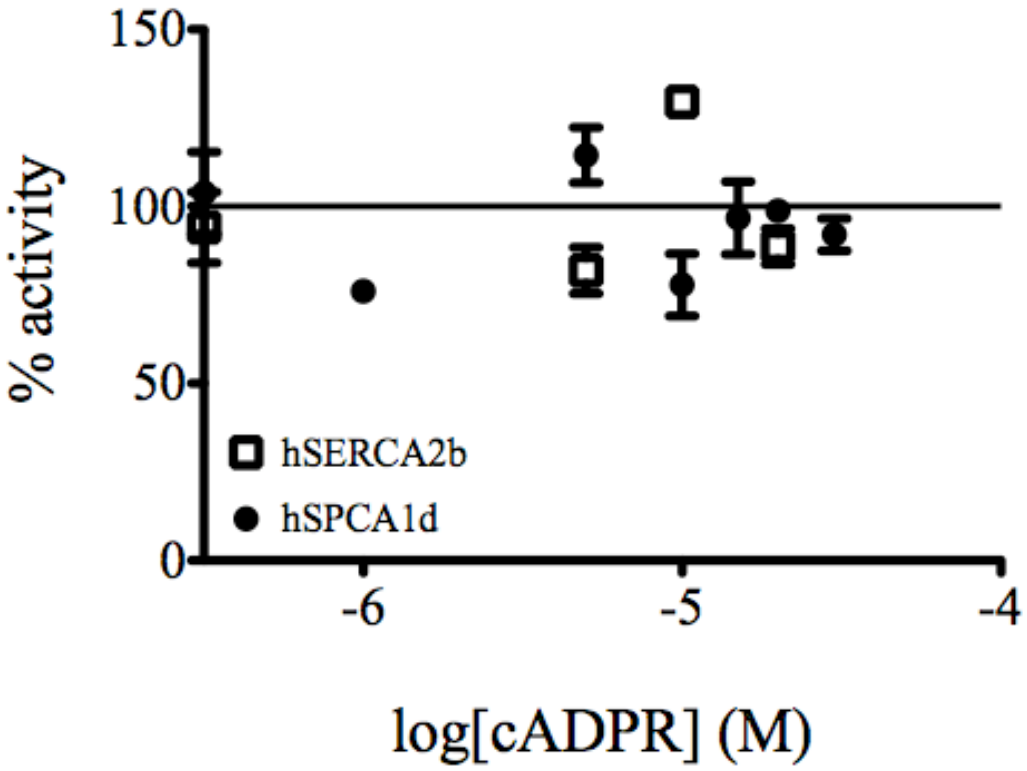

Figure 4.2.5.6. Effect of Different cADPR Concentrations on Mean Ca^{2+}-ATPase Activities From Microsomal Membranes of hSPCA1d- & hSERCA2b- Over-Expressing COS-7 Cells

Percentage Ca^{2+}-dependent ATPase activities measured from hSPCA1d and hSERCA2b membranes in reaction mixtures that contained cADPR at different concentrations. Mean activities were measured from three replicate assays for each cADPR concentration tested and made relative to those of vehicle (dH_20) controls to calculate percentage activities. Error bars indicate S.E.M values. Assay mixtures for hSPCA1d membranes contained 1μM thapsigargin and those for hSERCA2b membranes did not contain thapsigargin.

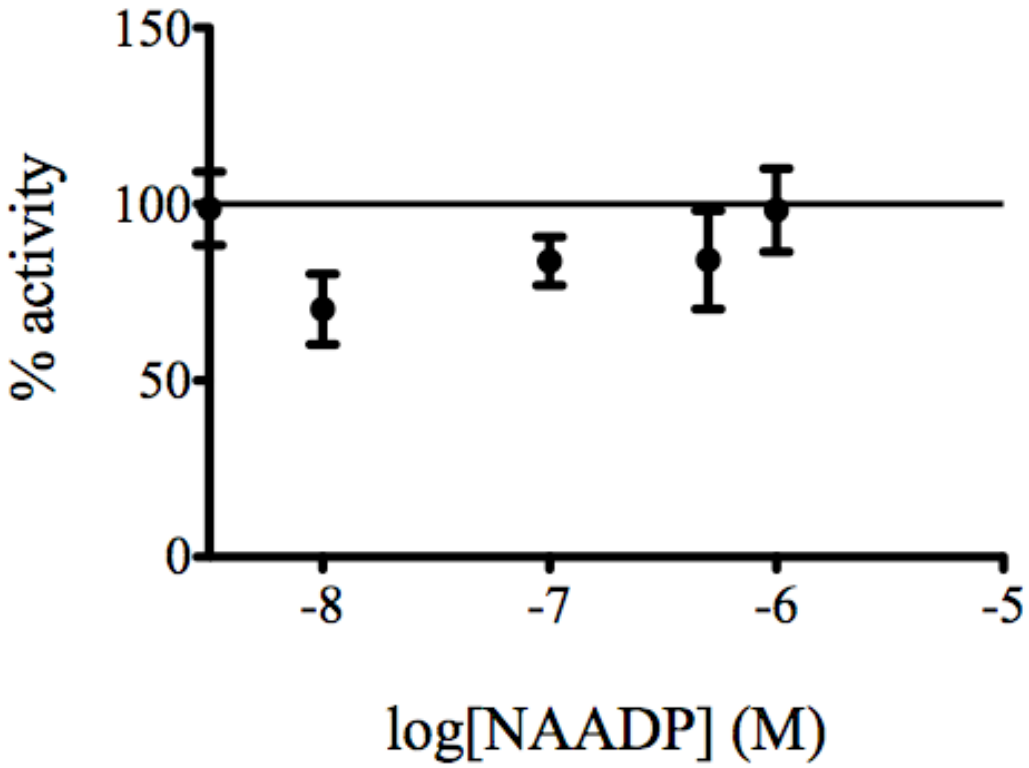

Figure 4.2.5.7. Effect of Different NAADP Concentrations on Mean Ca^{2+}-ATPase Activities From Microsomal Membranes of hSPCA1d-Over-Expressing COS-7 Cells

Percentage activities were calculated in the same way as stated for figure 4.2.5.6. Mean activities were measured from three replicate assays for each NAADP concentration tested. Error bars indicate S.E.M values. 1µM thapsigargin was added to reaction mixtures.

IC_{50} Values of hSPCA1d & SERCA Inhibitors (± S.E.M)

INHIBITOR	hSPCA1d (M)	hSERCA2b (M)	Fold difference $\left(\frac{IC_{50}\ hSERCA2b}{IC_{50}\ hSPCA1d}\right)$
Bis-phenol	1.3×10^{-7} ($\pm 9.0 \times 10^{-9}$)	8.1×10^{-6} ($\pm 3.8 \times 10^{-7}$)	62
TBBPA	5.4×10^{-7} ($\pm 8.3 \times 10^{-8}$)	7.1×10^{-7} ($\pm 7.0 \times 10^{-8}$)	1.3
TFP	2.0×10^{-5} ($\pm 9.0 \times 10^{-7}$)	1.1×10^{-5} ($\pm 3.1 \times 10^{-6}$)	0.6
2-APB	1.8×10^{-4} ($\pm 5.0 \times 10^{-6}$)	1.5×10^{-3} ($\pm 2.0 \times 10^{-4}$)	7.2
BPA	1.3×10^{-4} ($\pm 5.5 \times 10^{-6}$)	*2.3×10^{-4} ($\pm 3.0 \times 10^{-5}$)	*1.8

Table 4.2.5.8. IC_{50} Values of Inhibitors for hSPCA1d & SERCA

IC_{50} values ± S.E.M for all except BPA's value for SERCA were calculated using Prism graph plotting software, which was used to produce the plots shown in figures 4.5.5.1-7. The IC_{50} value for BPA's inhibitory effect on hSERCA2b was not available and so that for *rabbit SERCA1a, taken from a previous publication (Kirk et al., 2003), is shown in the above table instead.

Activities had been measured from control microsomal membranes in all cases, which were isolated from non-transfected cells, in the same manner as those that contained over-expressed protein. Any activity found in these control membranes was subtracted from the equivalent activities measured from their pair-matched hSPCA1d/hSERCA2b membranes. IC_{50} values calculated from the plots shown in figures 4.2.5.1-5 are given in table 4.2.5.8.

Bis-phenol (figure 4.2.5.1) was shown to be the most potent inhibitor out of the seven compounds tested and also gave the largest difference in its IC_{50} values between hSPCA1d and hSERCA2b, which showed this compound was 62 times more potent on hSPCA1d than hSERCA2b membranes. Using data from a previous study on the inhibitory effect of 2-APB on hSERCA2b (also when over-expressed in COS-7 cells) (Wootton and Michelangeli, 2006), the present study has also shown inhibition by 2-APB (figure 4.2.5.4) is 7.2 times more potent on hSPCA1d than hSERCA2b membranes.

On the other hand, less substantial differences in inhibitory potency between hSPCA1d and hSERCA2b was observed for both TBBPA (figure 4.2.5.2) and TFP (figure 4.5.2.3), and thus these two compounds are unlikely to be able to discriminate between the activities of these two Ca^{2+}-ATPases. For BPA (figure 4.2.5.5), its IC_{50} value for hSERCA2b has not been determined in both past and present study. To date, the nearest match that can be obtained for comparison is the IC_{50} value for SERCA1a, which has been measured using rabbit skeletal muscle SR (Kirk et al., 2003), and this value shows no substantial difference to that for hSPCA1d. Thus, like TBBPA and TFP, it is unlikely that BPA can be used as an inhibitor specific to hSPCA1d.

Ca^{2+}-ATPase activities measured from hSPCA1d membranes incubated with 0-30μM cADPR (figure 4.2.5.6) or 0-1μM NAADP (figure 4.2.5.7) did not appear to notably deviate from the control activity levels. Ca^{2+}-ATPase activity measurements were also made from hSERCA2b membranes in the presence of 5, 10 and 20μM cADPR, which showed this second messenger made no significant difference to such activity at these concentrations when compared to control activities. Thus both cADPR and NAADP demonstrated no influence on hSPCA1d activity and the present study preliminarily also suggests cADPR does not act on hSERCA2b activity.

4.2.6. The Effects of Bis-phenol & 2-APB on Intracellular Ca^{2+} Mobilisation in A7r5 Cells Detected by Fluo-3 Fluorescence Microscopy

A7r5 cells were used to investigate the effects of bis-phenol and 2-APB on mobilisation of internal Ca^{2+} stores in intact cells because this cell-line has been found to express both SERCA and SPCA endogenously (see section 3.2.1-2). All experiments were done in the absence of extracellular Ca^{2+} so that its effects would not obscure those from intracellular Ca^{2+} stores. Three types of responses were assessed, which were (i) response to 1μM thapsigargin after 10-minute pre-treatment with potential inhibitor, (ii) response to potential inhibitor after 10-minute pre-treatment with 1μM thapsigargin, and (iii) response to potential inhibitor without any pre-treatment. The concentration used for each of the five compounds was that which gave 100% inhibition of hSPCA1d at isolated microsomal membranes, as indicated from phosphate liberation assay data presented above (section 4.2.5).

For 1.5μM bis-phenol, Ca^{2+} mobilisation in A7r5 cells was only observable as response type (i) (figure 4.2.6.2). The mean peak height of response calculated for 1μM thapsigargin, after 10-minute pre-treatment with 1.5μM bis-phenol, was 0.58 ± 0.03, which was found to not be significantly different via Student's T-test ($P>0.05$) to that obtained from cells that were treated with 1μM thapsigargin with no pre-treatment (0.70 ± 0.04) (figure 4.2.6.1). The shape, timing and duration of these response profiles were also qualitatively almost identical. This altogether suggested 1.5μM bis-phenol treatment of intact A7r5 cells was unable to inhibit SPCA activity, at least at the time period monitored (5 minutes). It is possible that bis-phenol-stimulated Ca^{2+} mobilisation would have been observed if the duration of experiments was extended.

500μM 2-APB (figure 4.2.6.3) was able to produce Ca^{2+}-mediated responses of all three types that were observed for. The mean peak heights in Fluo-3 fluorescence intensity change in response to 1μM thapsigargin after pre-treatment with 2-APB was 63% lower (0.26 ± 0.04) (figure 4.2.6.3 (i)) than that shown from control thapsigargin experiments (0.70 ± 0.04) (figure 4.2.6.1), suggesting a proportion of thapsigargin-releasable Ca^{2+} stores had been emptied during the 10-minute pre-treatment period by 2-APB inhibition of SERCA. Furthermore, the cytosolic Ca^{2+} concentration of 2-APB pre-treated cells returned closer to basal levels

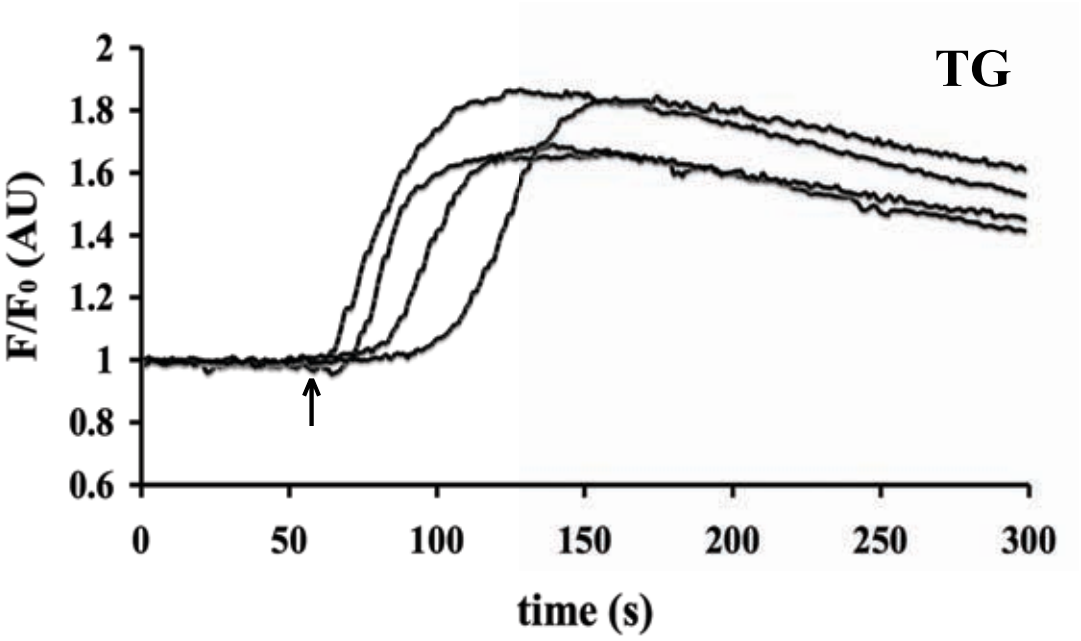

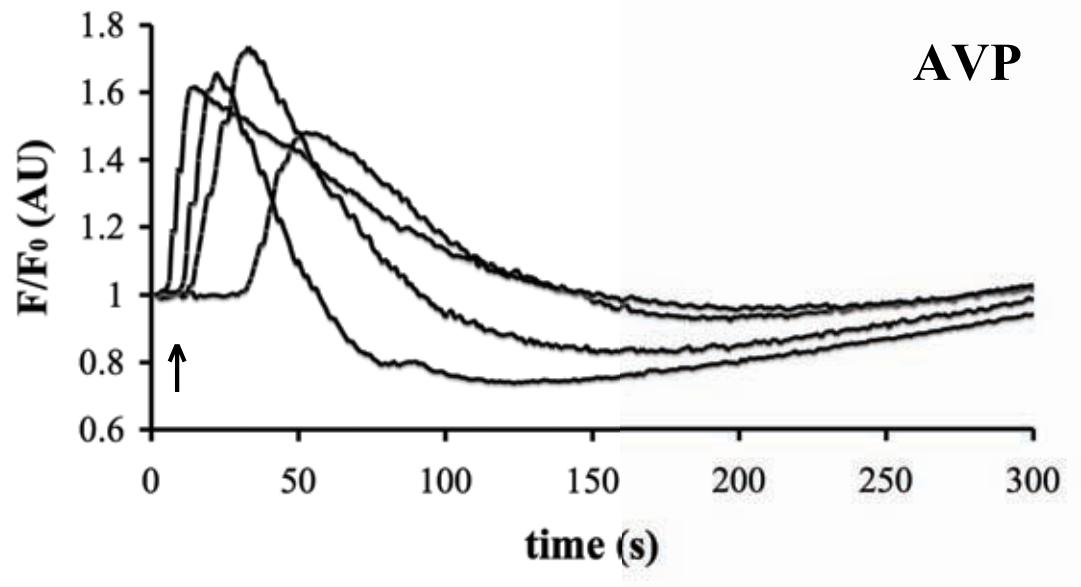

Figure 4.2.6.1. Ca^{2+}-Mediated Responses to 1μM Thapsigargin & Thapsigargin-Insensitive 10nM AVP Response by A7r5 Cells in the Absence of Extracellular Ca^{2+}

Figure 4.2.6.1. Ca^{2+}-Mediated Responses to 1μM Thapsigargin & Thapsigargin-Insensitive 10nM AVP Response by A7r5 Cells in the Absence of Extracellular Ca^{2+}

1μM thapsigargin response with no prior treatment ("TG"), and 10nM AVP response following response to 1μM thapsigargin ("AVP"). Each trace represents mean data measured from 25 cells. Arrows indicate time-point at which treatment was added. Mean peak heights ± S.E.M were 1.03 ± 0.07 and 0.92 ± 0.08 for "TG" and "AVP" responses, respectively.

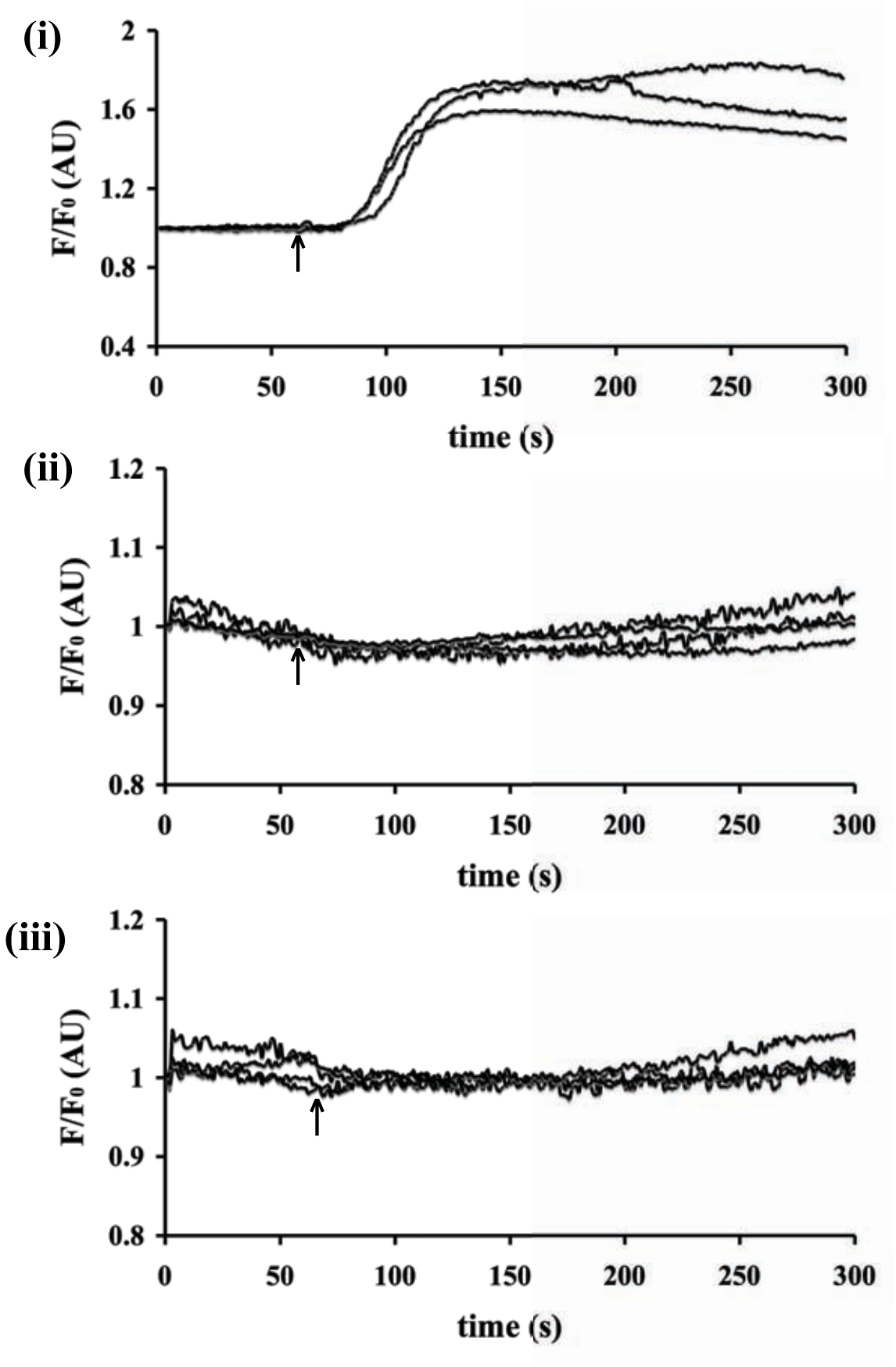

Figure 4.2.6.2. Bis-phenol Effects on Intracellular Ca^{2+} Mobilisation in A7r5 Cells

Figure 4.2.6.2. Bis-phenol Effects on Intracellular Ca^{2+} Mobilisation in A7r5 Cells

The plots show (i) 1μM thapsigargin response after 1.5μM bis-phenol pre-treatment, (ii) 1.5μM bis-phenol response after 1μM thapsigargin pre-treatment, and (iii) 1.5μM bis-phenol response with no pre-treatment. Each trace represents mean data measured from 25 cells. Positions of arrows indicate time point at which treatment was added to cells. Mean peak height ± S.E.M for response type (i) was 0.58 ± 0.03, while no response was detected for types (ii) and (iii).

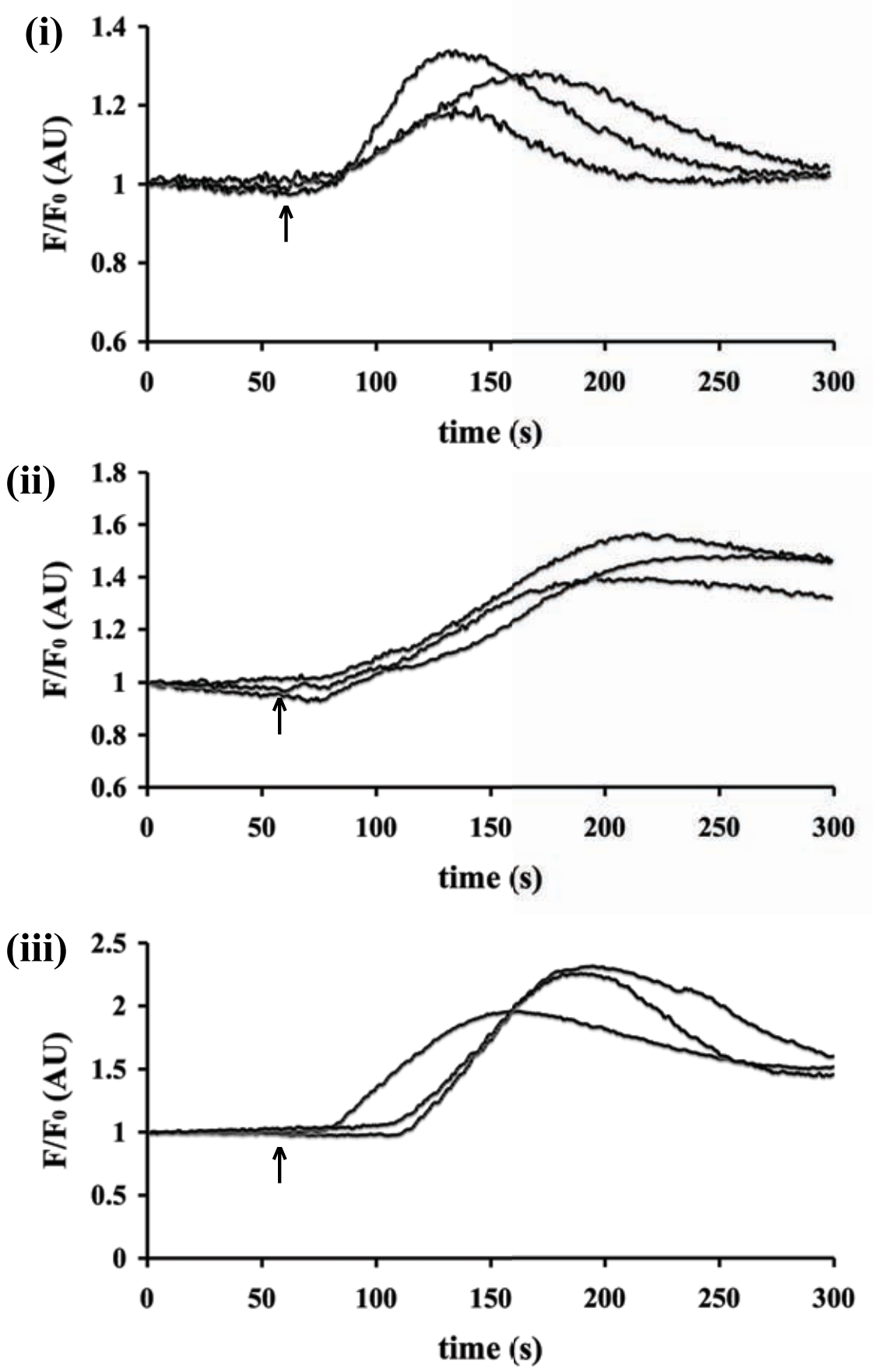

Figure 4.2.6.3. 2-APB Effects on Intracellular Ca^{2+} Mobilisation in A7r5 Cells

Figure 4.2.6.3. 2-APB Effects on Intracellular Ca^{2+} Mobilisation in A7r5 Cells

The plots show (i) 1μM thapsigargin response after 500μM 2-APB pre-treatment, (ii) 500μM 2-APB response after 1μM thapsigargin pre-treatment, and (iii) 500μM 2-APB response with no pre-treatment. Each trace represents mean data measured from 25 cells. Positions of arrows indicate time point at which treatment was added to cells. Mean peak heights ± S.E.M were (i) 0.26 ± 0.04, (ii) 0.45 ± 0.04 and (iii) 1.23 ± 0.13.

after thapsigargin response than cells that had not been pre-treated. Student's T-test showed a significant difference in mean peak height values from these two conditions of thapsigargin response ($P<0.05$) in A7r5 cells. 2-APB response after 10-minute pre-treatment with 1μM thapsigargin produced a mean peak height value of 0.45 ± 0.04 (figure 4.2.6.3 (ii)), which was found to be border-line statistically not significant in its difference ($P>0.05$, where $P=0.06$) to the mean peak height value of 0.62 ± 0.05 obtained from A7r5 control responses to 10nM AVP (figure 4.2.6.1). However, the thapsigargin-insensitive response profile for 2-APB was notably different to that for the control AVP response, whereby the former showed no decline phase in cytosolic Ca^{2+} levels after the rise phase, unlike AVP. The mean height of response to 2-APB without pre-treatment was 1.23 ± 0.13 (figure 4.2.6.3 (iii)), which was 1.7 times larger than the mean peak heights of response (i) and (ii) combined together, as well as being almost twice as large as the mean peak height for thapsigargin-insensitive Ca^{2+} mobilisation by 10nM AVP stimulation in the absence of extracellular Ca^{2+}. Thus it was likely that 500μM 2-APB did not just empty Ca^{2+} stores that were controlled by SPCA in the absence of pre-treatment.

4.3. Discussion

Successful over-expression of active hSPCA1d and hSERCA2b protein, along with their isolation and detection in the microsomal membranes of transfected COS-7 cells, has allowed for the testing of seven potential modulators of human microsomal Ca^{2+}-ATPases in the present study. From this, it was found that neither of the two putative second messengers tested (cADPR and NAADP) were able to alter hSPCA1d activity at the concentrations tested. On the other hand, all five synthetic compounds that were tested (i.e. bis-phenol, TBBPA, TFP, 2-APB and BPA) did inhibit hSPCA1d activity, although to different extents.

Bis-phenol and 2-APB stood out from the other three inhibitors because the differences in their potency in inhibiting hSPCA1d and hSERCA2b activity were substantially larger than those of the other three compounds. Bis-phenol and 2-APB inhibited hSPCA1d activity by 62- and 7.2-fold, respectively, better than hSERCA2b activity. 1.5μM bis-phenol was able to inhibit 100% of hSPCA1d activity of isolated membranes (whilst having no effect of hSERCA2b activity) but was unable to release Ca^{2+} stores from A7r5 cells at this concentration. In contrast, 500μM 2-APB, was able to inhibit hSPCA1d without affecting the hSERCA2b activity, as well as mobilise thapsigargin-insensitive Ca^{2+} stores in A7r5 cells. However, pre-treatment with 500μM 2-APB did decrease the amount of intracellular Ca^{2+} that was releasable by thapsigargin treatment of A7r5 cells.

The discrepancy between studies on isolated membranes and intact A7r5 cells (the latter of which has been demonstrated to express SPCA endogenously (see chapter 3)) with regards to bis-phenol inhibition of SPCA may have been caused by its highly hydrophobic nature, which would have made it difficult for bis-phenol to reach SPCA at the Golgi apparatus inside intact cells, in contrast to being more able to be in direct contact with SPCA at isolated membranes. Thus further optimisation is likely to be required in order to identify a concentration of bis-phenol (above 1.5μM) that is effective at inhibiting SPCA in intact cells. Though higher concentrations of bis-phenol could also influence the activities of other proteins involved in Ca^{2+} homeostasis and future studies will have to take this into consideration. In addition to

this, it should be noted that a previous study on HL60 cells showed bis-phenol can cause Ca^{2+} mobilisation in these cells, but such an event was often observed to occur after a substantial time delay between time point of applying bis-phenol to cells and response onset (Brown et al., 1994). Thus it may be well advised to repeat experiments with 1.5μM bis-phenol on A7r5 cells, but extend the duration of experiments beyond 5 minutes.

The ability of A7r5 cells to respond to 1μM thapsigargin after pre-treatment with 500μM 2-APB demonstrated this compound can affect intracellular Ca^{2+} stores at this concentration (which can inhibit 100% hSPCA1d activity at isolated membranes) and cannot empty SERCA-controlled Ca^{2+} stores completely in intact cells. However, the 63% reduction in thapsigargin-releasable Ca^{2+} stores after pre-treatment of A7r5 cells with 500μM 2-APB conflicted with data obtained from isolated membranes, whereby the use of the latter demonstrated this concentration is three times lower than its IC_{50} value for hSERCA2b. Two explanations for this discrepancy could be made from taking into account 2-APB's effects on other proteins involved in Ca^{2+} homeostasis. 100μM 2-APB is able to inhibit IP_3R and 30μM 2-APB can inhibit store-operated Ca^{2+} entry, both cases in permeabilised mouse pancreatic acinar cells (Choi et al., 2010a). These other effects potentially make 500μM 2-APB (or even lower concentrations of this compound) unsuitable for use as an inhibitor specific to SPCA in intact cells. This is certainly a highly likely possibility when taking into consideration the substantial amount of Ca^{2+} that was released in A7r5 cells following stimulation with 500μM 2-APB in the absence of any pre-treatment, which showed a visibly significant difference to the thapsigargin-insensitive response these cells had to this compound, and thus likely to have been caused by 2-APB emptying Ca^{2+} stores that are unlikely to be associated with SPCA in intact A7r5 cells.

Another peculiar observation made from 2-APB's Ca^{2+}-mediated responses in intact A7r5 cells was the difference in amount of decline of cytosolic Ca^{2+} levels after reaching peak response to 1μM thapsigargin (after 2-APB pre-treatment) and 500μM 2-APB (after thapsigargin pre-treatment). The response to thapsigargin involved a visible decline back to basal levels by the end of the experiments, but the response to 2-APB did not decline significantly after reaching peak levels before the end of

experiments. Ca^{2+} transporters that could aid recovery of cytosolic Ca^{2+} back to basal levels and also be active in the absence of SPCA and SERCA activity would be PMCA and the mitochondrial Ca^{2+} uniporter. It would appear that neither of these alternative Ca^{2+} transporters were inhibited when A7r5 cells responded to thapsigargin following pre-treatment with 2-APB. However, the same could not be said for the thapsigargin-insensitive 2-APB responses observed in A7r5 cells and it is unlikely the reason could be due to activation of mitochondrial Ca^{2+} release (in the event of Ca^{2+} overload) because the peak amount of Ca^{2+} released by 2-APB was not significantly different to that released by AVP following thapsigargin pre-treatment. It has been noted in the past that 100μM 2-APB can decrease the rate of mitochondrial Ca^{2+} uptake (Peppiatt et al., 2003). This would again suggest 500μM 2-APB does not act specifically on SPCA in intact A7r5 cells and further experiments will be required to understand why the shape of these Ca^{2+} response profiles were notably different in the ways that were observed.

The difference in susceptibility to bis-phenol inhibition between hSPCA1d and hSERCA2b are likely to be related to the differences they have in the kinetic properties of their Ca^{2+}-ATPase activities. A past study on bis-phenol inhibition of SERCA in isolated rat skeletal muscle SR suggested bis-phenol hinders SERCA's activity by binding to its E2 state, where its affinity for Ca^{2+} is at its lowest (Sokolove et al., 1986, Brown et al., 1994). Factors such as a decrease in pH and increasing membrane fluidity by adding Triton-X100 to the rat SR were also noted to decrease the potency of bis-phenol inhibition at SERCA in this study. It has been shown in another study that hSPCA1d has a faster rate of Ca^{2+} dissociation than rabbit SERCA1a, and thus favours the E2 state more than SERCA1a (Dode et al., 2005). In addition to this, hSPCA1d activity was also shown to be relatively insensitive to pH changes in this latter study, which was attributed to the greater stability its Ca^{2+}-binding site has when not bound with Ca^{2+}. These past findings can be taken together to suggest that bis-phenol can inhibit hSPCA1d with 62-fold greater potency than hSERCA2b because the probability of finding hSPCA1d in the E2 state is greater than it is for hSERCA2b. Another difference that has been noted between the kinetic properties of hSPCA1d and rabbit SERCA1a, which may also be applicable to hSERCA2b, is that hSPCA1d has a slower rate of dephosphorylation than rabbit

SERCA1a (Dode et al., 2005), which is a step that is required to promote the conformational change of both Ca^{2+}-ATPases from the E2 state back to the E1 state, and is another factor that would keep hSPCA1d in the E2 state longer than it would for rabbit SERCA1a.

With regards to the effect of Triton-X100 that was noted in the study on rat SR (Sokolove et al., 1986), this could be taken into account with hSPCA1d's lack of pH sensitivity because the latter has been attributed to the membranes of the Golgi apparatus having a higher content of sterols and sphingolipids than those of the ER, which would make the former membranes more rigid and thus more capable of stabilising and maintaining hSPCA1d in the E2 state for a longer period of time. Again, this would support the idea that bis-phenol inhibits hSPCA1d better (when compared to hSERCA2b) because both hSPCA1d and bis-phenol favour the E2 state. A more rigid membrane at the Golgi apparatus may also mean a slower rate of transition from the E2 state back to the E1 state for hSPCA1d than hSERCA2b, because such a transition requires the Ca^{2+}-ATPase to make a major conformational change to move its Ca^{2+}-binding sites from the luminal side to the cytosolic side of the membrane it is embedded in. By making the membrane of rat SR more fluid with Triton-X100 (as done in the aforementioned study) it is likely to make it easier for SERCA to convert between the E1 and E2 states, which could reduce the probability the E2 state being available for interaction with bis-phenol, especially if it is the case that the E2 state is far less stable for SERCA than it is for SPCA.

The lesser but still significant ability of 2-APB to inhibit hSPCA1d 7.2-fold better than hSERCA2b may also be associated with differences in the kinetic properties of these two Ca^{2+}-ATPases. A previous study has suggested 2-APB inhibits SERCA in rabbit skeletal muscle SR by hindering its formation of a phospho-enzyme intermediate, which was attributed to 2-APB decreasing its rate of phosphoryl group transfer (Bilmen et al., 2002). Another study has shown hSPCA1d has a slower ATP turnover rate than hSERCA2b, which was attributed to a higher apparent Ca^{2+} affinity that slows down the rate of hSPCA1d dephosphorylation (Dode et al., 2005). Taken together, it could be interpreted that 2-APB binds these two Ca^{2+}-ATPases when they are in conformations that do not promote the process of phosphoryl group transfer, and its preference to do so when still phosphorylated and/or Ca^{2+}-bound (i.e. in the

E1-P(Ca^{2+}) state) may be the reason why 2-APB is 7.2-fold more potent at inhibiting hSPCA1d than hSERCA2b. It has been suggested that 2-APB binds near the L67 loop of SERCA (Wootton and Michelangeli, 2006), which can influence both SERCA phosphorylation and its Ca^{2+} affinity (Zhang et al., 2001). This may also be the case for SPCA, though further studies would be required to ascertain this and would be of interest to do in order to further define any structural differences between SERCA and SPCA that result in their kinetic properties being different.

The present study has demonstrated 1-40μM cADPR does not affect hSPCA1d activity, which has not been shown before. In addition to this, data from preliminary experiments with hSERCA2b suggested cADPR also does not have an effect on this Ca^{2+}-ATPase in isolated membranes too. This would conflict with at least two past studies that have suggested cADPR can increase SERCA activity in intact xenopus oocytes (Yamasaki-Mann et al., 2009) and in isolated dog heart SR (Lukyanenko et al., 2001). This contrast between the present and past studies may be explained by differences in (i) the organisms used for their experiments, (ii) SERCA isoforms involved (SERCA1 in SR vs. SERCA2 in microsomes), (iii) the type of sample used (intact cells (Xenopus oocytes) vs. isolated membranes), and/or (iv) the form of cADPR used (non-metabolisable 3-Deaza-cADPR (microinjected into xenopus ooctyes) vs. standard cADPR (added to cell-free reaction mixtures containing microsomal membranes)). On the other hand, a third past study has shown that cADPR does not bind directly to isolated microsomes from both dogs and rabbits, and thus suggested this second messenger does not act directly on SR to cause Ca^{2+} release (Copello et al., 2001). Ideally, more hSERCA2b activity measurements in the presence of a wider range of cADPR concentrations is needed to give a more ascertained answer to the question of whether or not this second messenger can change SERCA activity according to the experimental model tested in the present study.

The lack of effect on hSPCA1d activity by 0.01-1μM NAADP in the present study has not been demonstrated before. Most past studies on NAADP have focused on its ability to mobilise Ca^{2+} from either the ER or lysosomes (Singaravelu and Deitmer, 2006, Macgregor et al., 2007, Steen et al., 2007, Zhang and Li, 2007), and it has been

debated which of these organelles is the source of intracellular Ca^{2+} that gets released in the presence of NAADP. There has been one study that has suggested NAADP-illicted Ca^{2+} release is unlikely to involve the Golgi apparatus because it showed brefeldin A (a compound that disrupts Golgi apparatus integrity by promoting its vesiculation) does not affect the ability of NAADP to release intracellular Ca^{2+} stores in permeabilised mouse pancreatic acinar cells (Gerasimenko et al., 2006). However, the use of brefeldin A may not have been ideal because an earlier study showed this compound is unable to alter ATP-stimulated Ca^{2+} oscillations in thapsigargin-pre-treated COS-1 cells that were made to over-express C.elegans SPCA (Missiaen et al., 2001). In both cases, it also has to be taken into consideration whether or not NAADP could act on other proteins involved in Ca^{2+} homeostasis to indirectly influence Ca^{2+} release from SPCA-controlled stores, due to the use of whole cells. In the present study, it has been shown that NAADP does not affect hSPCA1d activity of isolated microsomes and thus unlikely to act on hSPCA1d directly.

In conclusion, it appears to be highly promising that bis-phenol can be used as a SPCA-specific inhibitor, at least at a concentration of 1.5μM at isolated microsomal membranes. Further optimisation of its concentration will be required to find one suitable for use on intact cells, which is most likely to be above 1.5μM. 2-APB has also been identified as a compound that can inhibit hSPCA1d without affecting hSERCA2b activity (over the same concentration range) in isolated membranes. However, as a result of the present study, it is not recommended for use as a SPCA inhibitor in intact cells due to the influence it is likely to have on non-SPCA-controlled Ca^{2+} stores. An inhibitor that can specifically inhibit SPCA is needed to assist further research on this Ca^{2+}-ATPase, especially when experiments will involve observing the effects of its activity in the presence of other proteins that can influence Ca^{2+} homeostasis (e.g. SERCA, PMCA). A SPCA-specific inhibitor could also be potentially used as a template for drug design to aid treatment of medical conditions that have been associated with increased expression and/or activity of SPCA, such as diabetes and neurological diseases.

CHAPTER 5.

THE ROLE OF RGN (SMP30) IN MAMMALIAN Ca^{2+} HOMEOSTASIS: OVER-EXPRESSION & RECOMBINANT STUDIES

CHAPTER 5.
THE ROLE OF RGN (SMP30) IN MAMMALIAN Ca^{2+} HOMEOSTASIS: OVER-EXPRESSION & RECOMBINANT STUDIES

5.1. Introduction

Regucalcin (RGN; also known as senescence marker protein 30 (SMP30)) is a protein that is believed to contribute to Ca^{2+} homeostasis by interacting with other Ca^{2+}-dependent proteins, such as SERCA (Yamaguchi and Nakajima, 2002) and nuclear protein tyrosine phosphatase (Tobisawa and Yamaguchi, 2003b). It has been noted that RGN is expressed in a number of tissues, such as brain (Fujita, 1999), liver (Yamaguchi, 2000b) and prostate (Maia et al., 2008). Furthermore, RGN is believed to be able to localize in the nucleus (Omura and Yamaguchi, 1999) and mitochondria (Yamaguchi et al., 2008b), as well as being primarily a cytosolic protein (Yamaguchi and Yamamoto, 1978). Links to various medical conditions, ranging from Alzheimer's disease (Sun et al., 2006) to breast cancer (Maia et al., 2009), have been made and with association to changes in RGN expression levels. The crystal structure of human RGN was recently published (Chakraborti and Bahnson, 2010) and dispelled the argument against its ability to bind Ca^{2+} (Kondo et al., 2004, Yamaguchi, 2000a).

A multitude of studies have focused on the effects of RGN's presence on cellular events, such as Ca^{2+} transport into the ER (Yamaguchi, 2000a) and Ca^{2+}-mediated gene transcription (Yamaguchi, 2000b), but virtually none have shown how RGN interacts with other proteins to produce these observations. It is unknown how it influences the activities of Ca^{2+}-dependent transporters and enzymes. RGN could possibly play a part in agonist-induced Ca^{2+}-mediated signaling pathways, by being involved in protein-protein interactions, or simply act by binding and sequestering Ca^{2+}. Most of the focus has been on RGN expression levels, specifically its changes during aging (Ishigami, 2010, Maruyama et al., 2010) and in diseases (Doran et al., 2006, Maia et al., 2009, Park et al., 2010), rather than the study of its molecular features. Furthermore, RGN has been shown to function as a gluconolactonase (Kondo et al., 2008, Arai et al., 2009, Kashio et al., 2009, Koike et al., 2010). Recent research has also mainly focused on the mouse model, which was first used to

demonstrate RGN's role in vitamin C synthesis (Ishigami et al., 2002). The problem this produces is that it removes focus on the role of RGN in humans because the human body does not possess the ability to synthesise vitamin C. This may change now that the Ca^{2+}-bound RGN crystal structure has been made available, along with results from biochemical studies that suggest RGN's ability to bind Ca^{2+} is unlikely to be related to its role as a gluconolactonase because its K_d for Ca^{2+}-binding has been determined to be far above those found under physiological resting conditions in the cell cytosol (0.57 ± 0.25mM) (Chakraborti and Bahnson, 2010).

Most biochemical experiments have involved the use of cell-free based assays. Although efforts had been made in these studies to make the conditions used physiologically relevant, whole cell studies would still be more favourable if the true biological role of RGN in tissues are to be examined. Only two studies have involved the use of intact cells to investigate the effect of RGN's function in vivo in relation to calcium movement, and in both cases it was suggested that RGN over-expression increases PMCA activity (Fujita et al., 1998, Son et al., 2008). One of these studies also suggested RGN over-expression has no effect on thapsigargin response in a mouse carcinoma cell line, P19, though the experiments used to demonstrate this only monitored the first 60 seconds of thapsigargin response (Son et al., 2008). Finally, although RGN expression has been detected in 10 out of 14 different types of tissues (Fujita et al., 1996, Ichikawa and Yamaguchi, 2004, Tobisawa and Yamaguchi, 2003a, Yamaguchi et al., 2005, Doran et al., 2006, Maia et al., 2009), additional types of tissues/cells need to be tested to get a better profile of its distribution.

The present study aimed to address some of the gaps in RGN research that have been highlighted above, with specific focus on finding out whether RGN can contribute to the formation and/or delivery of Ca^{2+} signaling cascades, and/or control of intracellular Ca^{2+} stores. An attempt was also made to identify other tissues that express RGN endogenously at the mRNA and/or protein level(s). The production of recombinant rat RGN and an anti-RGN antibody, along with the use of an intact cell model that over-expresses human RGN, were involved in the work to be discussed here.

5.2. Results

5.2.1. Distribution & Abundance of RGN mRNA Expression Levels in Different Rat Tissues

RGN mRNA expression levels were measured from cDNA copies of total mRNA from 14 different cell/tissue samples to examine its pattern of distribution across different types of organs. Figure 5.2.1.1 shows PCR product bands that represent the detection of either RGN or RPL19 mRNA sequences in a number of cDNA samples from different rat tissues, whereby the cDNA samples were copies of total mRNA extracts from these tissues. From this, it was observed that transcripts of RGN mRNA were detected in adult tissue samples from aorta, testes, skeletal muscle, brain, cerebellum, kidney and liver. RGN mRNA transcripts were also detected in tissue samples of juvenile rats; from heart, Sertoli cells, testes, germ-line cells (spermatogonia) and myeloid cells. RGN PCR was also done with cDNA copies of total mRNA from lungs and heart of adult rats, but the RGN mRNA transcript was not detected despite reasonable levels of RPL19 PCR product shown both in figure 5.2.1.1 and in repeat experiments. It was curious to see that RGN transcript could be detected in the adult rat aorta cDNA sample but not in that of heart. Amount of RPL19 PCR product at adult heart was only slightly lower than at adult aorta and thus difference in amount of total mRNA in samples was unlikely to have contributed to the difference in RGN levels.

Tissues that had not previously been shown to express RGN mRNA in rats (underlined at figure 5.2.1.1) included samples from the male reproductive system of both adult and juvenile rats. Adult testes showed a striking amount of RGN mRNA detection and this was the case for four different cDNA samples from this tissue type (prepared on different days from different adult rats) that were tested. Furthermore, juvenile testes were shown to express RGN mRNA, along with germ cells and myeloid cells. As control experiments, the sequence of RGN PCR products from both adult rat testes and liver (the latter as a positive control) were checked and confirmed they did indeed represent the mRNA sequence for RGN (figure 5.2.1.2A). A control PCR was also done with the same two samples of cDNA, which involved the use of primers that would produce the full-length RGN mRNA coding sequence as its PCR product if it were present. Indeed, this full-length RGN transcript was detected in both adult rat testes and liver samples (figure 5.2.1.2B). It should be noted that although it

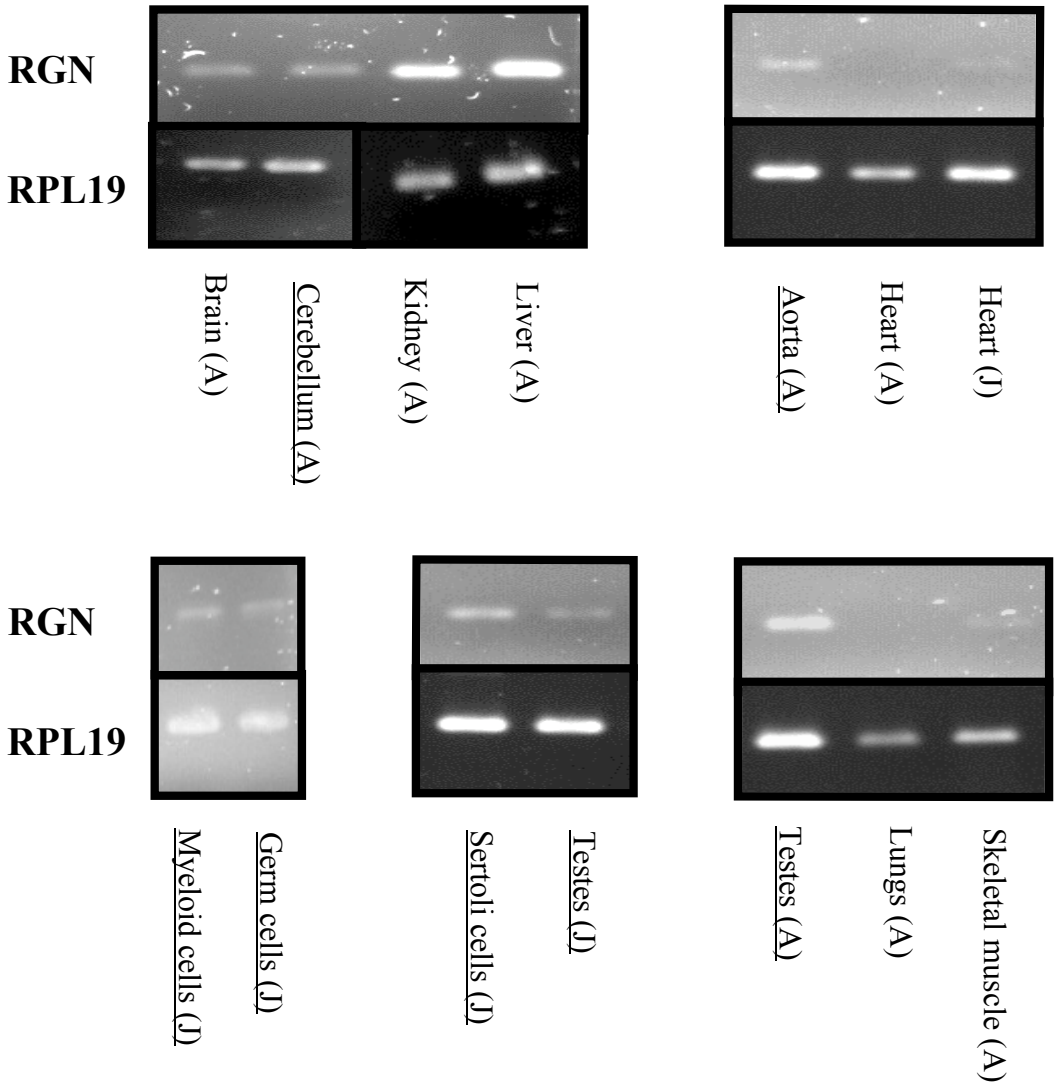

Figure 5.2.1.1. RGN mRNA Expression in Different Rat Tissues

Figure 5.2.1.1. RGN mRNA Expression in Different Rat Tissues

For each type of tissue represented, PCR products for RGN and RPL19 mRNA were produced using cDNA copies of total mRNA from either male rat adults ("A") or juveniles ("J"). Tissue types with their names underlined indicate those that had not been screened in previously published studies.

The PCR product bands were of their predicted sizes, which were 307bp for RGN and 321bp for RPL19. All samples were loaded at equal volumes in each lane.

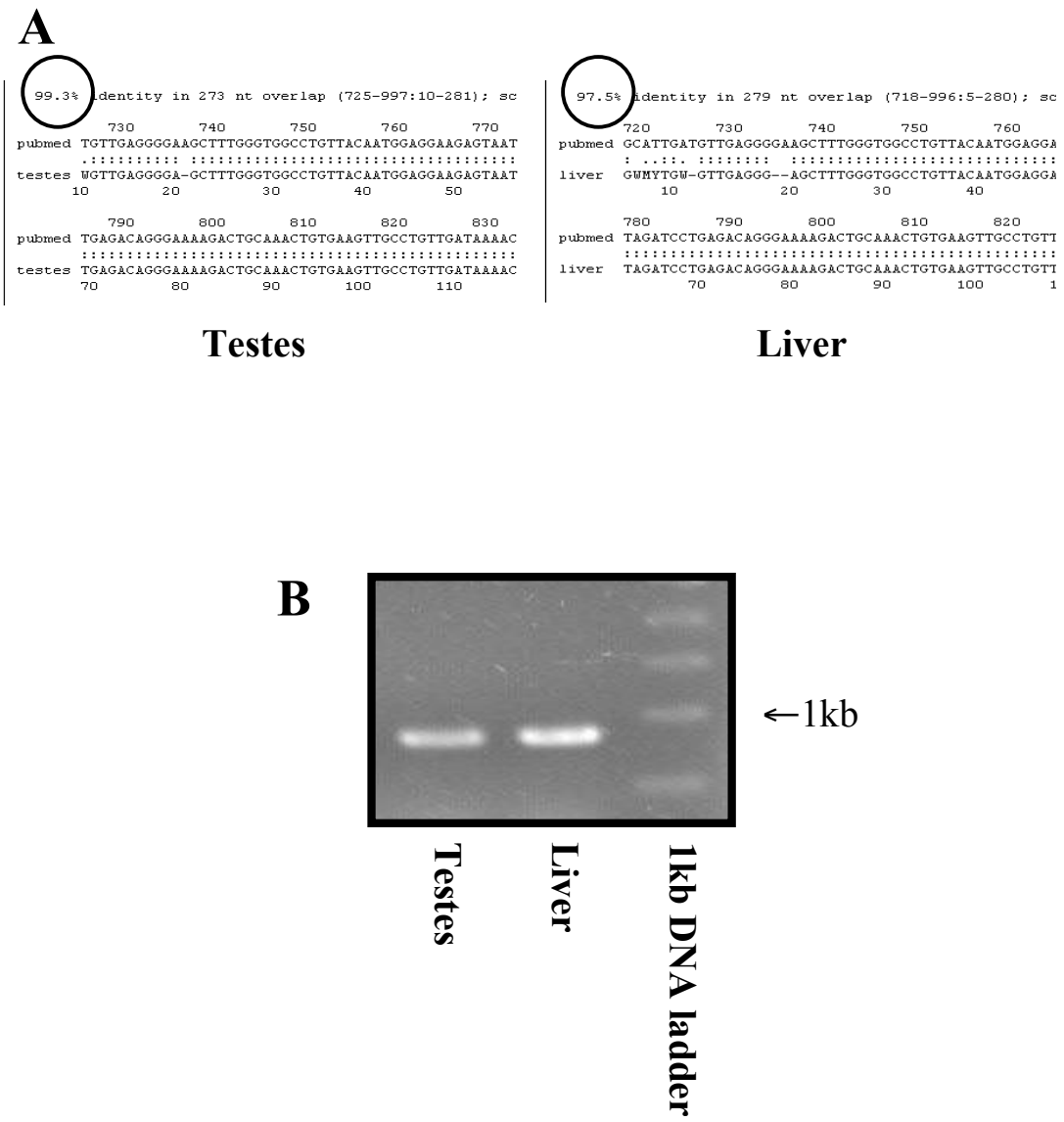

Figure 5.2.1.2. Control PCR & DNA Sequencing with RGN mRNA Transcript Copies from Adult Rat Liver & Testes

Figure 5.2.1.2. Control PCR & DNA Sequencing with RGN mRNA Transcript Copies from Adult Rat Liver & Testes

(A) The DNA sequences of 307bp RGN PCR products for both adult rat testes and liver (presented in figure 5.2.1.1) (as labelled) were aligned with the rat RGN mRNA sequence from the Pubmed nucleotide databank (entry number NM_031546). The percentage alignment match for the region that the PCR products encode between these sequences is circled in both cases.

(B) PCR products of full-length RGN mRNA coding sequence (0.94kb) for adult rat testes and liver (as labelled), which were obtained from the same cDNA copies of total mRNA used for PCR of the shorter 307bp RGN product given in figure 5.2.1.1. The lane of 1kb DNA ladder is as labelled and the position of the 1kb marker is indicated.

has been previously shown RGN is expressed in adult rat brain (Yamaguchi et al., 1999), specific areas of RGN mRNA expression within this organ, such as the cerebellum examined in the present study, had not been previously shown.

5.2.2. Extraction of Full-Length Rat Liver RGN Coding Sequence & Insertion into *E.coli* Expression Vector for Recombinant Protein Production

Western blot detection for RGN protein levels in a number of different rat tissue samples was intended to be done after the PCR experiments presented above (section 5.2.1). For this, an anti-RGN antibody was required. It was decided that such an antibody would be custom-made, with the use of recombinant rat RGN as the antigen, after commercially available anti-RGN antibodies were tried and proved to be poor at detecting RGN in cytosolic fraction samples from rat liver, which is an organ that expresses this protein at abundant levels (Yamaguchi and Isogai, 1993). Both would be produced as part of the present study. Production of recombinant rat RGN firstly required the construction of a bacterial expression plasmid that contained the full-length mRNA coding sequence for rat RGN.

Full-length RGN coding sequence was isolated from cDNA copies of total mRNA extracts from adult rat liver using PCR. The use of transcripts from mRNA extracts ensured the sequence obtained did not contain any non-coding regions, and thus allowed it to be expressed using an E.coli expression vector because post-transcriptional mRNA processing is not possible in an E.coli expression system for the production of recombinant proteins. The optimal T_m for producing transcripts of the sequence was determined to be 60^oC, with the use of 2mM $MgCl_2$ and 35 cycles.

0.94kb PCR products made using the optimised PCR conditions were purified by gel extraction and the resulting gel extracts were analysed by DNA sequencing, which confirmed the correct coding sequence for rat RGN had been isolated in full. Sequence alignment of the PCR product with rat RGN mRNA coding sequence obtained from the Pubmed nucleotide databank (entry number NM_031546) showed 100% match between these two sequences. Subsequently, the PCR product obtained was used for ligation into the pGEM-T vector, which allowed it to be moved into the pET21a expression vector later on, by providing restriction sites to produce sticky 5' and 3' ends outside of the RGN coding sequence for ligation into the latter.

Figure 5.2.2.1A shows the gel extract of full-length RGN coding sequence that was inserted into the pGEM-T vector, along with successful AvaI and NdeI double

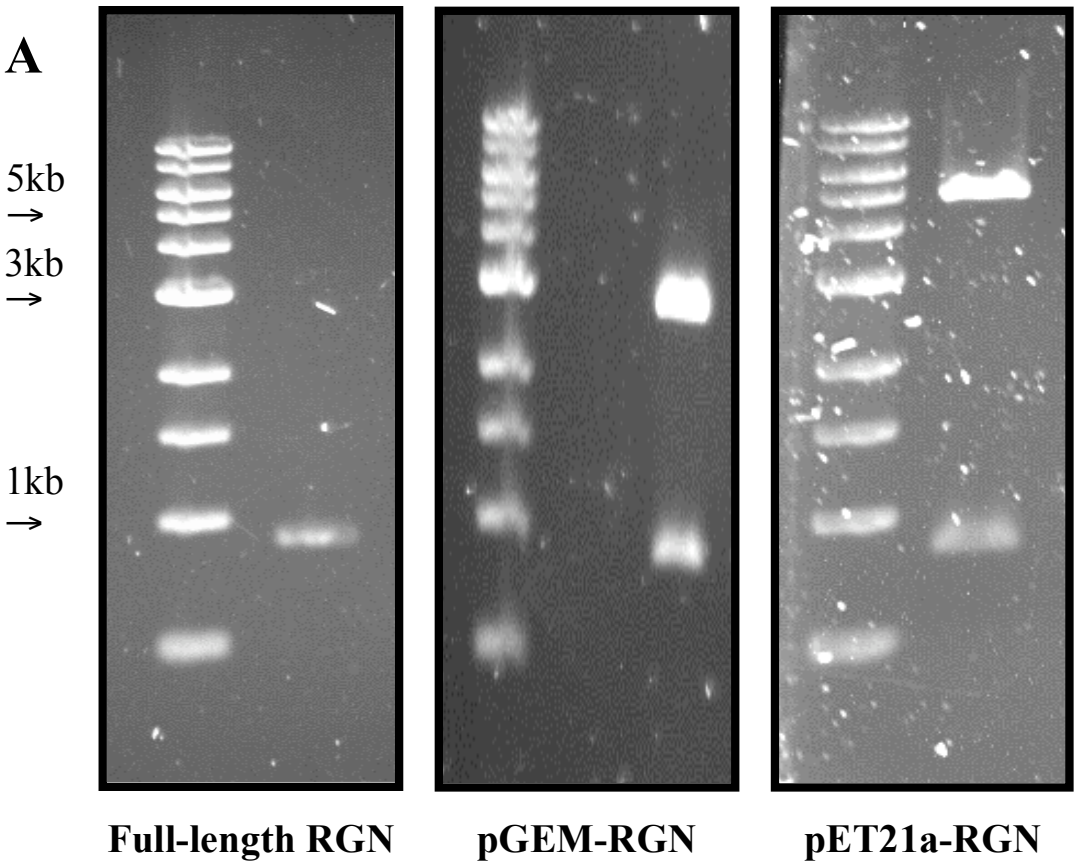

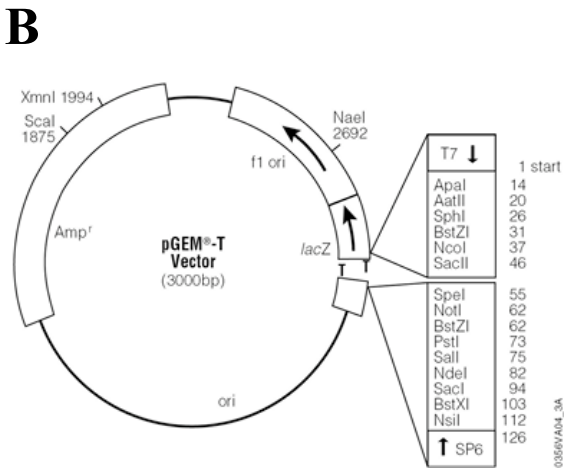

Figure 5.2.2.1. Extraction of Full-Length Rat RGN Coding Sequence & Insertion into pGEM-T & pET21a Vectors

Figure 5.2.2.1. Extraction of Full-Length Rat RGN Coding Sequence & Insertion into pGEM-T & pET21a Vectors

(A) Gel extract of full-length RGN coding sequence (left) produced by PCR with cDNA copies of total mRNA from adult rat liver, which was ligated with the pGEM-T vector to produce pGEM-RGN. Restriction digest with AvaI and NdeI of pGEM-RGN (middle) produced sticky ends on either side of the RGN coding sequence to allow its insertion into the pET21a vector to produce pET21a-RGN, which was digested with the same restriction enzymes (right). Two lanes are shown at each image, whereby the lane of the left shows 1kb DNA ladder and the lane of the right shows digested DNA. 1kb, 3kb and 5kb DNA marker positions are indicated on the left of the figure and are applicable to all three images.

(B) Restriction maps for pGEM-T (Promega) and pET21a (Novagen) vectors.

restriction digest of the resulting pGEM-RGN plasmid. This double digest was required to produce complementary sticky ends that allowed insertion of the RGN coding sequence into a pET21a bacterial expression vector. The final expression plasmid, pET21a-RGN, was produced and its successful AvaI and NdeI double restriction digest is also shown. Note that the recombinant rat RGN coding sequence was engineered to include a hexahistidine (Hisx6) tag at the protein's C-terminus, which was done by inserting the RGN coding sequence into the pET21a vector at the latter's multi-cloning site without a termination sequence, so that the vector's intrinsic Hisx6 tag coding sequence would be attached to the inserted RGN coding sequence at the latter's 3' end. This modification to the rat RGN sequence was made to aid identification and subsequent purification of the recombinant protein.

Sequences of DNA from minipreps of both pGEM-RGN and pET21a-RGN were checked by alignment with the same rat RGN coding sequence from the Pubmed nucleotide databank used for alignment with the original full-length rat RGN PCR product that was inserted into these plasmids. Detailed analysis showed that the two sequences shared 100% identity with that from the Pubmed nucleotide databank. The pET21a-RGN plasmid was subsequently used to transform a BL21 strain of E.coli, which is commonly used for recombinant protein expression, to produce bacteria that can express recombinant Hisx6-tagged rat RGN following IPTG induction.

5.2.3. Anti-RGN Antibody Production from Recombinant Rat RGN Protein

The RGN antigen, in the form of recombinant rat RGN, required to generate an anti-RGN antibody, was produced from pET21a-RGN-transformed BL21 cells by adding 0.25mM IPTG to their culture media and growing them overnight at 17^{o}C. Following this, the cells were isolated from their culture media by centrifugation at 6000g, sonicated and their cell lysates centrifuged at 20,000g to separate soluble proteins (supernatant) from cell debris and inclusion bodies (pellet). SDS-PAGE and Western blot analysis (latter with the use of a anti-Hisx6 antibody) of these fractions (figure 5.2.3.1) showed the recombinant RGN was located in the 20,000g spin pellet, which indicated it was expressed in the form of inclusion bodies (i.e. mis-folded protein). In order to separate the recombinant RGN from cell debris in this pellet, it was solubilised using 6M urea (a denaturing agent) and centrifuged at 100,000g to produce supernatant that contained the solubilised inclusion bodies. The 6M urea content in the supernatant was removed from the recombinant RGN by dialysis and

the latter's presence in the form of a relatively pure over-expressed 33kDa protein was confirmed by SDS-PAGE, the identity of which was also ascertained to be rat RGN by FT-ICR analysis (figure 5.2.3.2). The 33kDa SDS-PAGE protein gel band shown in figure 5.2.3.2 was subsequently excised and sent to a commercial laboratory, Covalab, for antibody production.

5.2.4. Testing Anti-RGN Antibody Using Original Recombinant RGN Antigen & Human RGN Over-Expressing COS-7 Cells

In order to test the efficiency of antigen recognition by the custom-made anti-RGN antibody, and to provide a system for studying the role of RGN in mammalian cells later on, COS-7 cells were made to express human RGN by transfecting them with hSMP30-pcDNA3.1(-) plasmid DNA with the same transfection method that had previously been used to successfully transfect COS-7 cells with hSPCA1d/hSERCA2b-pMT2 plasmid DNA (chapter 4). Figure 5.2.4.1 shows the DNA fragments obtained from a NdeI and XhoI double restriction digest of minipreps for both hSMP30-pcDNA3.1(-) and control pcDNA3.1(-) plasmids, along with the restriction digest map for hSMP30-pcDNA3.1(-) indicating the expected sizes of DNA fragments from such a restriction digest reaction. From this, it was observed that restriction digests of the two plasmids were successful, based on the correctly-sized 4.79kb DNA fragment being present for both plasmids (representing the pcDNA3.1(-) vector alone), as well as an additional 1.5kb fragment for hSMP30-pcDNA3.1(-) representing the full mRNA coding sequence (including non-coding regions) for human RGN.

Figure 5.2.4.2 shows anti-RGN in a bleed taken from a rabbit 88 days after its first immunisation with recombinant rat RGN was able to allow detection of over-expressed RGN in transfected COS-7 cells, as well as strong detection of its recombinant RGN antigen at a dilution ratio as low was 1:750, thus making it very sensitive. This bleed was also able to detect an abundant 33kDa protein present in the cytosolic fraction of adult male rat liver, which is likely to indeed be RGN because this tissue has already proven to express abundant levels of this protein (section 5.2.1-2). RGN was not detected in total cell lysate samples collected from COS-7 cells that were transfected with control pcDNA3.1(-) plasmid DNA.

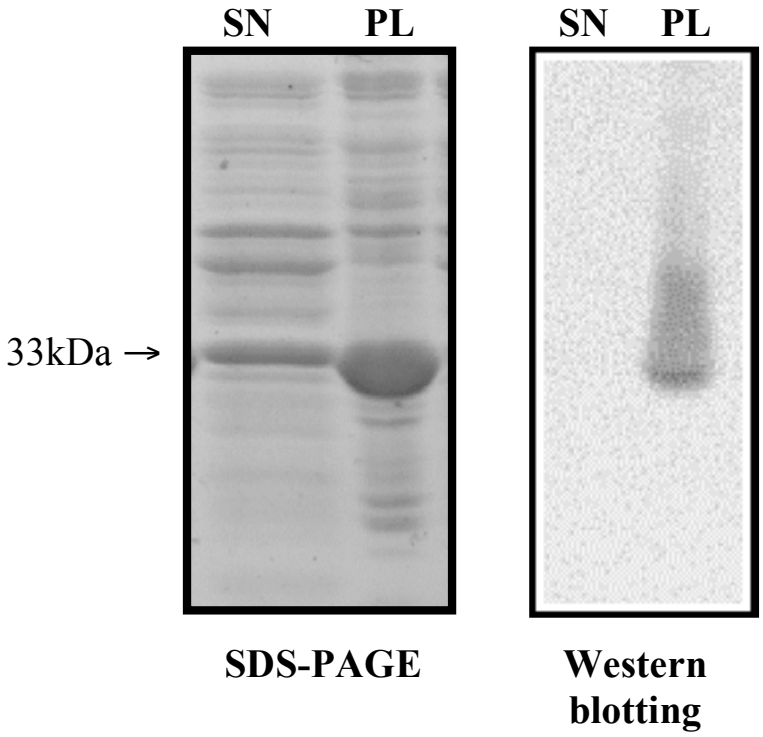

Figure 5.2.3.1. SDS-PAGE & Western Blot Analysis of 20,000g Centrifugation Spin Pellets & Supernatants for Over-Expressed 33kDa Hisx6-Tagged RGN Protein

Coomassie-stained SDS-PAGE gel (left) of 20,000g centrifugation spin supernatants ("**SN"**) and pellets ("**PL"**) of total cell lysates from sonicated pET21a-RGN-transformed BL21 cells, which were induced with 0.25mM IPTG and grown overnight at 17^{o}C. These samples were also subjected to Western blotting (right) with polyclonal anti-Hisx6 antibody. The expected position of 33kDa protein is indicated on the left and applies to both images. All protein samples were loaded at equal volumes at each lane.

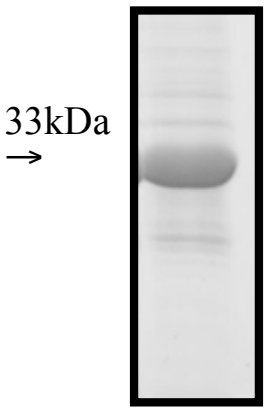

Scan(s)	Peptide	MH+
gi|408807|dbj|BAA07490.1| regucalcin [Rattus norvegicus]		
697	-.LDPETGKR.-	915.48944
716	-.LDPETGK.-	759.38831
797	K.TTSCCFGGK.D	1017.41290
844	R.FNDGKVDPAGR.Y	1175.58032
845	R.FNDGKVDPAGR.Y	1175.58032
961	R.FN@DGKVDPAGR.Y	1176.56438
968	R.FN@DGKVDPAGR.Y	1176.56438
1028	R.WDSISNR.V	877.41626
1215	R.QSGGYVATIGTK.F	1181.61609
1241	K.IECVLR.E	789.42877

Figure 5.2.3.2. SDS-PAGE & FT-ICR Identification of 33kDa Over-Expressed Recombinant Protein from Solubilised Inclusion Bodies of pET21a-RGN-Transformed BL21 Cells

Coomassie blue-stained SDS-PAGE gel (left) of 6M urea-solubilised inclusion bodies dialysed into 50mM Tris-HCl (pH 7.2) buffer with 15% glycerol. The inclusion bodies were isolated from cultures of pET21a-RGN-transformed BL21 cells induced with 0.25mM IPTG and grown overnight at 17^{o}C. The expected position of 33kDa protein is indicated.

A sample of FT-ICR mass spectroscopy data (right), which showed the first 10 most common peptide fragments identified in the 33kDa protein band (left). Rat RGN was predicted as the most abundant protein in the 33kDa protein band by having the most detected peptides associated with it.

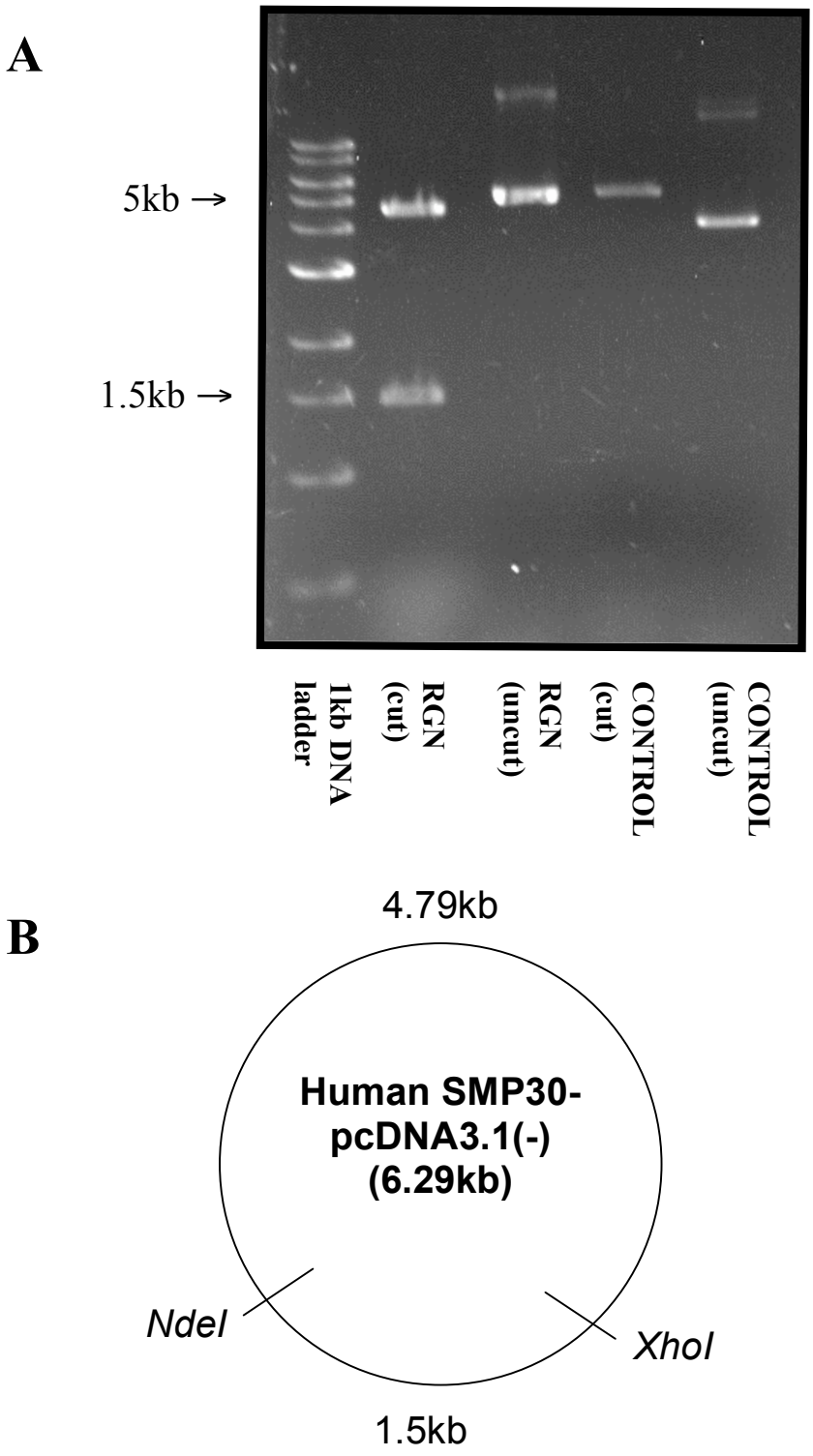

Figure 5.2.4.1. NdeI & XhoI Double Restriction Digest of human SMP30-pcDNA3.1(-)

Figure 5.2.4.1. NdeI & XhoI Double Restriction Digest of Human SMP30-pcDNA3.1(-)

(A) Agarose gel electrophoresis of DNA fragments in reaction mixtures from restriction digest ("cut") of human SMP30-pcDNA3.1 ("RGN") and empty pcDNA3.1(-) vector ("CONTROL") with NdeI and XhoI, alongside their undigested DNA ("uncut"). The expected DNA fragment sizes were 1.5kb (full RGN mRNA sequence) and 4.79kb (pcDNA3.1(-) vector). The positions of 1.5kb and 5kb DNA markers are indicated. All samples were loaded at equal volumes in each lane.

(B) The restriction digest map for NdeI and XhoI double digest of human SMP30-pcDNA3.1.

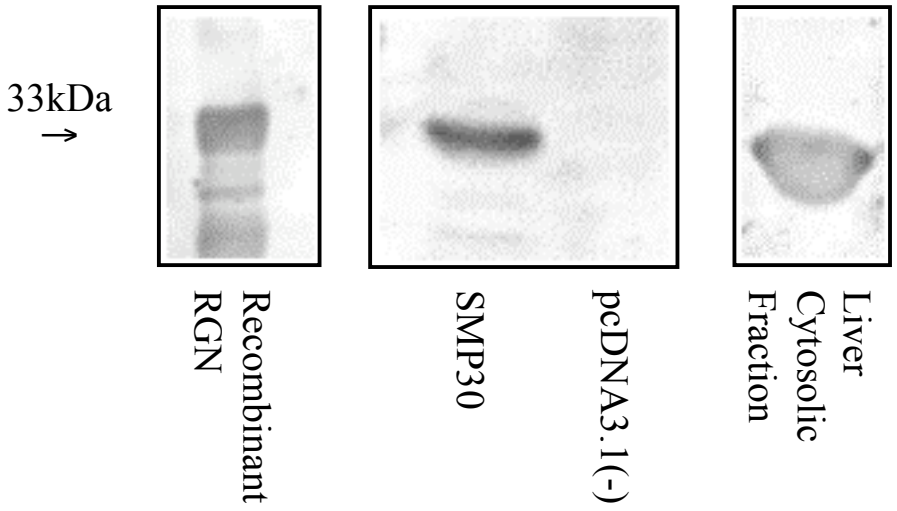

Figure 5.2.4.2. Western Blots for Identification of RGN in Recombinant Rat RGN, COS-7 Total Cell Lysates & Rat Liver Cytosolic Fraction with Final Anti-RGN Bleed

Detection of RGN in samples of recombinant rat RGN protein, total cell lysates from COS-7 cells transfected with hSMP30-pcDNA3.1(-) and control pcDNA3.1(-) plasmids, and cytosolic fraction from adult male rat liver. Total protein amounts loaded of each sample were 25µg of recombinant rat RGN and rat liver cytosolic fraction, and 20µg of COS-7 total cell lysates. The expected position of 33kDa protein on the blots is indicated at each image.

The seeding density used for transfection of COS-7 cells was $1x10^5$ cells per well in a 6-well plate and a 9:3 ratio of reagent(µl)-to-DNA(µg) was used 24 hours after seeding the cells. Total cell lysate samples were collected 48 hours after start of transfection. Dilution ratios of anti-RGN used were 1:50 for COS-7 total cell lysates, and 1:750 for recombinant RGN and rat liver cytosolic fraction.

5.2.5. Detection of RGN at the Protein Level: Cytosolic Fractions of Rat Organs, Total Cell Lysate of Boar Sperm & Total Cell Lysate of Established Cell Lines

The cytosolic fractions of seven different types of rat organs were probed by Western blotting for the presence of RGN protein using the custom-made anti-RGN antibody. These organs were liver, kidney, brain, testes, lung, heart and fat pads. All had originally been isolated from male adult rats that were over 5 weeks old. Figure 5.2.5.1 shows detection of RGN was visible in samples from liver, kidney and brain, which were expected because these are organs that have already been demonstrated to express RGN protein according to previous publications (Fujita et al., 1996, Tobisawa and Yamaguchi, 2003a). The absence of RGN protein in the cytosolic fractions of adult male rat heart and lungs was also expected because the same finding was concluded from results from another previous study (Yamaguchi et al., 2002).

However, it was unexpected that the cytosolic fraction isolated from rat adult testes did not produce a detectable 33kDa protein band in this and repeat Western blots. This latter observation conflicts with that made from the results of PCR experiments presented above (section 5.2.1). Instead, a 66kDa protein band was detected in this sample, which was not the case for the other six samples tested. Control Western blots were done to show that the 66kDa protein band did not originate from any substance that was present in the PBS that was used for the isolation of all samples of cytosolic fractions (data not shown).

Another sample that was tested by Western blotting for the presence of RGN protein was adult boar sperm. This was chosen in an attempt to build on the interesting finding that RGN mRNA sequence could be detected from tissues of the male reproductive organs according to results collected from the PCR experiments of the present study (section 5.2.1). The result, also presented in figure 5.2.5.1, was the same as that obtained from Western blotting with samples from adult rat testes. Control Western blots with the PBS and lysis buffer used to prepare total cell lysate samples of boar sperm showed the 66kDa protein did not originate from these solutions alone. An attempt to identify the localisation of this 66kDa protein in fresh intact boar sperm was made via immunofluorescence (figure 5.2.5.2), with control experiments using antibodies that recognised SPCA1 and SERCA Ca^{2+}-ATPases also

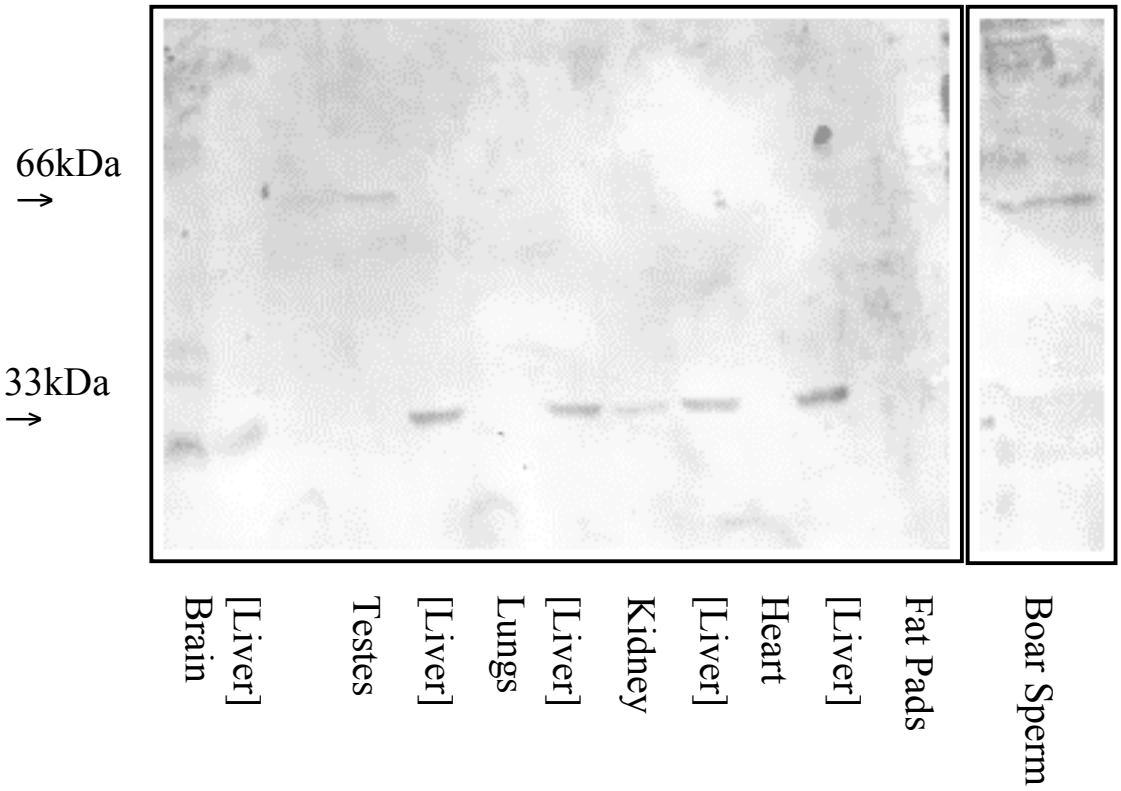

Figure 5.2.5.1. Western blots for RGN Detection in Cytosolic Fractions of Different Adult Male Rat Tissues & Adult Boar Sperm Total Cell Lysate

Lanes on the blot are labelled with the name of the tissue type from which the cytosolic fraction samples they contain were isolated. This included adult male rat liver cytosolic fraction samples ("[Liver]"), which was added as a positive control for the detection of RGN by custom-made anti-RGN antibody. Positions of 33kDa and 66kDa proteins on the blot are indicated on the left and apply to both images. All samples except liver (10μg) and brain (20μg) were loaded at 30μg of total protein per well. Anti-RGN was used at a dilution ratio of 1:100.

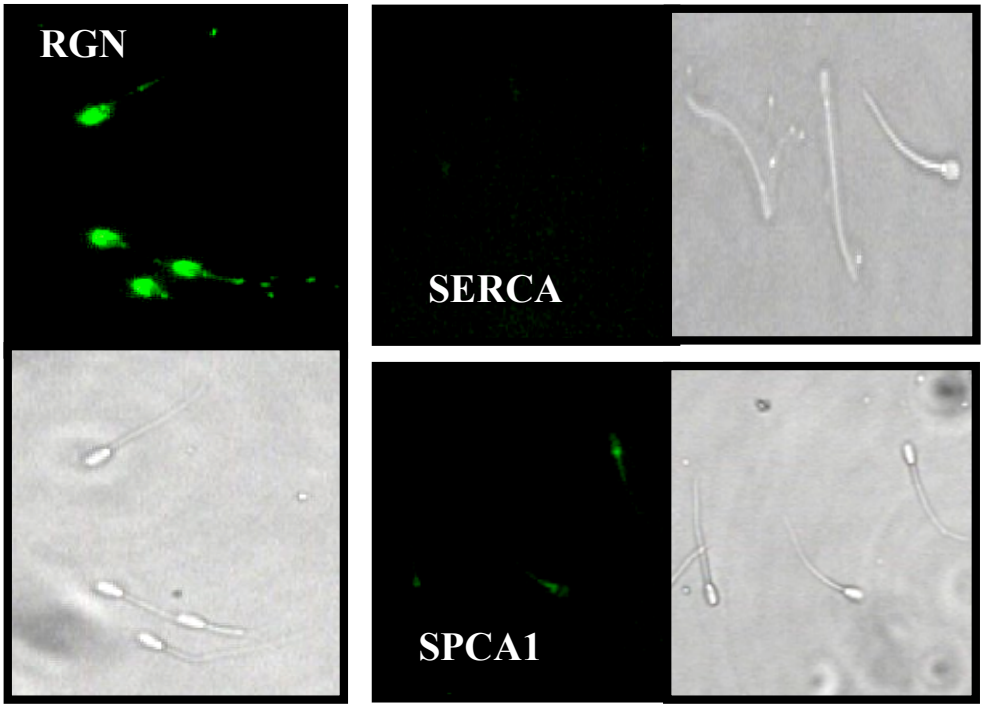

Figure 5.2.5.2. Localisation of Anti-RGN, Anti-SPCA1 & Anti-SERCA (Y1F4) Antibodies in Adult Boar Sperm

Fresh adult boar sperm cells were isolated from semen by centrifugation, fixed with formaldehye and permeabilised with Triton X100 before incubation with anti-RGN, anti-SPCA1 or anti-SERCA (Y1F4) antibody. The locations at which of these antibodies bound within the cells, and thus presumably the localisation of each antibodies intended target antigen ("RGN", "SPCA1", "SERCA") were visualised using FITC-conjugated secondary antibodies and fluorescence microscopy (green labelled images). Matching light microscopy images were also taken (grey images). Antibody dilutions used were 1: 50 (anti-SPCA1, anti-SERCA Y1F4) and 1:100 (anti-RGN, anti-rabbit/mouse FITC conjugates). Images were taken at x200 magnification.

undertaken at the same time to ensure the method used was effective on this sample. Indeed the result obtained with these control experiments matched those of a previous study (Harper et al., 2005). This suggested the method used was suitably implemented and the identification of anti-RGN localisation at the acrosomal region of boar sperm was not due to non-specific antibody binding. Control experiments with FITC-conjugated secondary antibodies alone showed there were virtually no non-specific background fluorescence (data not shown).

It has already been shown that RGN cannot be detected from total cell lysates of COS-7 cells as a notable 33kDa protein band on Western blots unless they are made to over-express this protein via transfection methods (figure 5.2.4.2). The total cell lysates of three other types of established cell lines were also probed by Western blotting for the presence of any RGN protein they may express endogenously. These three cell lines were A7r5, TM4 and SH-SY5Y, which are representative of aortic, testicular and neuronal cells, respectively. Samples from A7r5 cells were collected from cultures, whereas those from SH-SY5Y and TM4 cells was collected from cells that had been thawed from frozen stocks (in the same way as done for rejuvenating cells), but isolated by centrifugation after thawing and not grown in flasks afterwards.

In all three cases, 33kDa protein bands representative of RGN could not be detected. Instead, all total cell lysate samples from established cell lines, including those of pcDNA3.1(-)-transfected and hSMP30-pcDNA3.1(-)-transfected COS-7 cells, produced strongly detectable 66kDa protein bands on Western blots. Control experiments with samples of their culture media and BSA also gave such a band detected by anti-RGN (figure 5.2.5.3). This suggested the 66kDa bands detected on the Western blots of total cell lysates from cultures of COS-7, A7r5, TM4 and SHSY5Y cells were most likely to originate from the recognition of BSA in traces of media in these samples. The ability of polyclonal antibodies to bind to BSA protein is a common finding due to its use in the formulation of immunogenic solutions in the process of antibody production. Other bands detected on the blots in figure 5.2.5.3 and not around 33kDa in molecular mass were dismissed as also non-specific bands recognised anti-RGN.

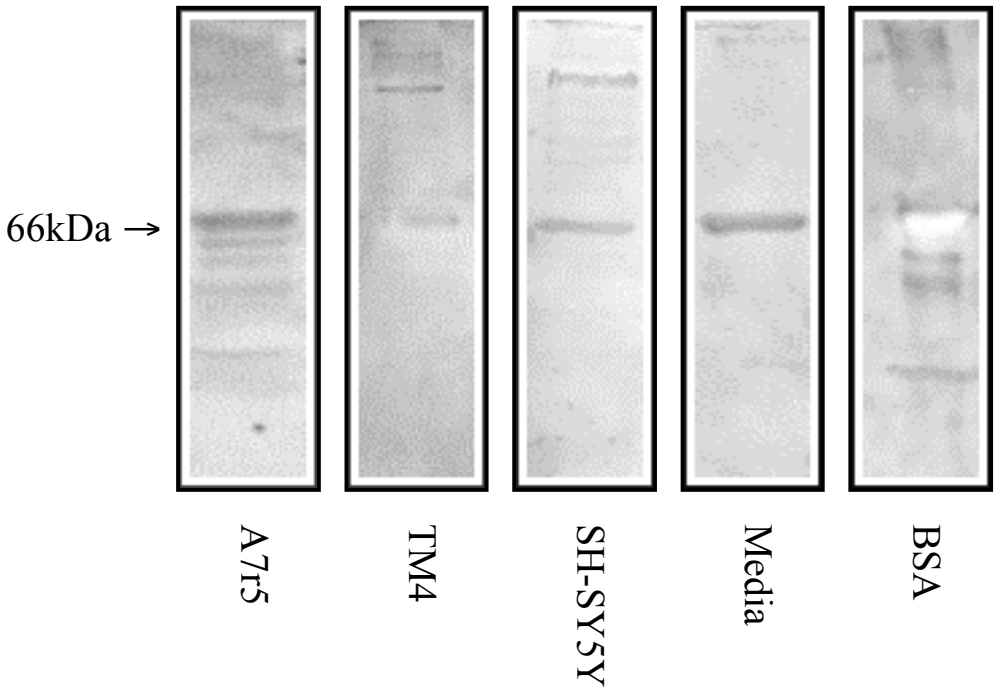

Figure 5.2.5.3. Detection of 66kDa Protein in Total Lysates of A7r5, TM4 & SH-SY5Y Cells, with Media & BSA Controls

Sample contents of each Western blot lane image are as labelled below them, with "A7r5", "TM4" and "SH-SY5Y" being the three different established cell-lines tested for their ability to express RGN endogenously. The media sample presented was that for SH-SY5Y cells and represents the same observation seen from Western blots with media for A7r5, TM4 and COS-7 cells. The expected position of 66kDa protein bands is as indicated on the left and applies to all five images. Amounts of total protein loaded in each lane were 20μg (A7r5, SH-SY5Y), 15μg (TM4), 1μg (media) and 2.5μg (BSA). The band at the 66kDa position for the BSA sample is white rather than black due to over-exposure.

5.2.6. Further Analysis of Anti-RGN Immunoreactive 66kDa Band in Adult Rat Testes Cytosolic Fractions & Adult Boar Sperm Total Cell Lysates

It was of interest to find out what protein(s) were present in the unexpected 66kDa band recognised by anti-RGN via Western blotting with samples from adult rat testes and adult boar sperm. The anti-RGN-recognised 66kDa bands from these two samples were unlikely to be explained as products of non-specific immunoreactivity by the antibody recognising albumin in the same way as done for the total cell lysates from cultures of the four established cell lines tested. This is because of a difference in the methods of sample preparation for these two sets of samples, whereby intact rat testes and boar sperm were not surrounded in media supplemented with FBS, which contains a high content of BSA, when collected for homogenisation/lysis. Rat testes were only contaminated with traces of blood, in the same way as the other six rat organs used in the present study and yet, unlike testes, those other organs did not produce 66kDa anti-RGN immunoreactive bands on their Western blots. Boar sperm cells were collected from unmodified whole ejaculate.

FT-ICR was used to identity the contents of the anti-RGN immunoreactive 66kDa protein band. Figure 5.2.6.1 shows a Coomassie-stained gel of all protein present in adult rat testes and adult boar sperm samples. These bands were expected to contain both anti-RGN immuno-reactive and non-immunoreactive proteins. The intensity of their 66kDa Coomassie-stained bands were compared to the 66kDa chemiluminescent bands on their Western blots (figure 5.2.5.1). The boar sperm sample was subsequently chosen for FT-ICR analysis because these two bands for this sample were more similar in their intensities. Whereas the Coomassie-stained band for the rat testes sample was more intense than its chemiluminescent equivalent, which suggested its FT-ICR analysis was likely to identify more proteins that were not even recognised by the anti-RGN antibody compared to the boar sperm sample.

The FT-ICR data for the 66kDa protein band from total cell lysate of adult boar sperm (figure 5.2.6.1) did not show the presence of RGN at all, which means the protein band recognised by anti-RGN in this sample was unlikely to have been a RGN isoform or splice variant, and neither was it RGN protein that had somehow aggregated even after SDS-PAGE treatment. BLAST analysis of RGN's amino acid sequence did not result in a list of sequence-similar proteins that included any of the

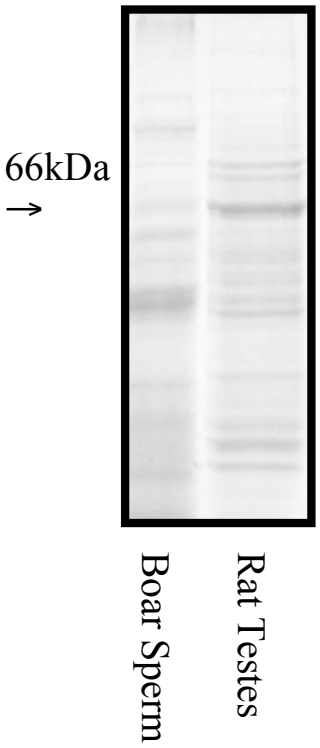

Accession #	# Peptides	MW [Da]	Description
gi178056512	127	70300	heat shock 70kDa protein 1-like [Sus scrofa]
gi47522774	79	84722	90-kDa heat shock protein [Sus scrofa]
gi112980819	41	54812	mitochondrial succinate dehydrogenase complex subunit A [Sus scrofa]
gi89574201	36	59032	succinate dehydrogenase complex subunit A [Sus scrofa]
gi194039391	45	83201	PREDICTED: heat shock 90kD protein 1, beta [Sus scrofa]
gi194042324	33	99816	PREDICTED: similar to hexokinase 1, partial [Sus scrofa]
gi194043853	23	0	PREDICTED: galactosidase, beta 1-like [Sus scrofa]
gi194033595	20	73768	PREDICTED: heat shock 70kDa protein 5, partial [Sus scrofa]
gi51592133	21	68406	ATPase, H+ transporting, lysosomal V1 subunit A [Sus scrofa]
gi833798	23	69366	albumin [Sus scrofa]

Figure 5.2.6.1. SDS-PAGE & FT-ICR Identification of 66kDa Protein Band: Adult Rat Testes Cytosolic Fraction & Adult Boar Sperm Total Cell Lysate

In the Coomassie-stained SDS-PAGE gel (left), 25μg and 30μg of total protein were loaded into each lane for the rat testes cytosolic fraction and boar sperm total cell lysate, respectively. The expected position of 66kDa protein bands is indicated. The 66kDa band for boar sperm total cell lysate was used for FT-ICR analysis (right) of its protein contents in an attempt to determine the antigen of anti-RGN in this region of a Western blot. The top ten proteins with the most protein fragments detected of them are shown (in order of descending abundance from top to bottom of the list). Note that this list does not indicate which protein was recognised by anti-RGN antibody and the most abundant was not necessarily the antigen.

proteins identified by FT-ICR analysis. Boar albumin was however detected by FT-ICR as the tenth most abundant protein in the 66kDa protein band from adult boar sperm total cell lysate. This would be the most likely antigen for anti-RGN in this sample if taking into consideration the data that has been discussed in section 5.2.5, where it appeared anti-RGN had recognised 66kDa bands that most likely had belonged to BSA in the media of A7r5, TM4 and SH-SY5Y cells (figure 5.2.5.3).

Even though cytosolic fraction samples from adult rat testes were deemed unsuitable for FT-ICR analysis, they were still subject to further additional experiments in an attempt to find out whether or not its 66kDa protein band recognised by anti-RGN did contain RGN in some unusual form. One possibility considered was that the 66kDa band detected in Western blots of this sample contained RGN that had disulphide-bonded together to form dimers, and hence produced chemiluminescent bands that were double the expected molecular mass. This would seem unlikely due to the presence of 2-β-mercaptoethanol in SDS-PAGE sample buffer that is meant to break all disulphide bonds in proteins. Though it could have been possible that the amount of 2-β-mercaptoethanol used to prepare the total cell lysate of rat testes for SDS-PAGE was insufficient to break some of the disulphide bonds present in the RGN proteins of this particular sample.

Thus Western blots were done with rat testes samples that contained different amounts of 2-β-mercaptoethanol, within the range of 5% (i.e. normal content in SDS-PAGE sample buffer) to 50%. Such Western blots, however, failed to show any difference in outcome for this cytosolic fraction sample (data not shown). Thus it was concluded that anti-RGN had recognised a non-specific 66kDa protein in adult rat testes and RGN protein had not been detected in this sample.

5.2.7. Fluo-4-Based Ca^{2+} Measurements in Single COS-7 Cells Transfected with hSMP30-pcDNA3.1(-) & Control pcDNA3.1(-) Plasmids

COS-7 cells transfected with the hSMP30-pcDNA3.1(-) plasmid to over-express human RGN, which were utilised to test anti-RGN's ability to detect RGN (section 5.2.4), were used to study the effects of RGN on Ca^{2+} mobilisation in intact single cells using Ca^{2+}-sensitive, cell-permeable fluorescent dye, Fluo-4 AM. COS-7 cells transfected with pcDNA3.1(-) plasmid DNA without the RGN mRNA coding

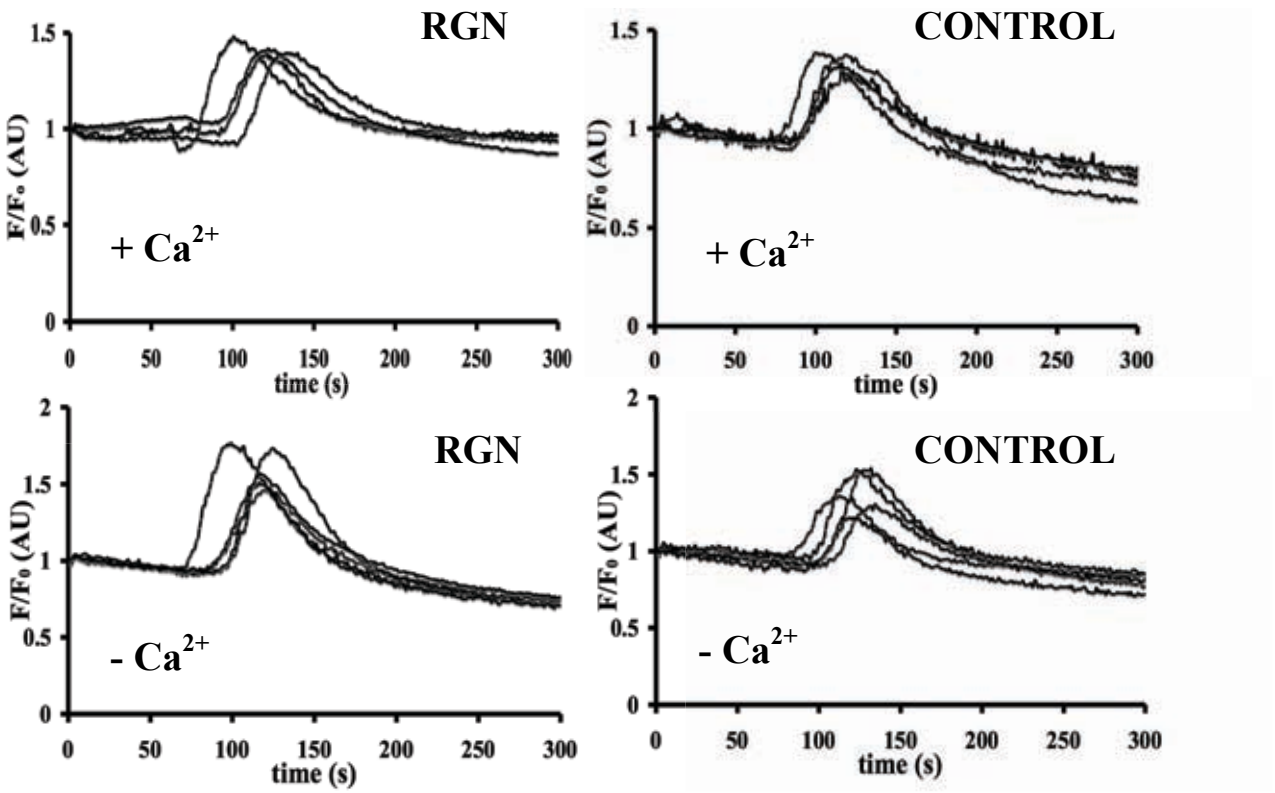

Figure 5.2.7.1. Thapsigargin-Stimulated Ca^{2+} Transients in COS-7 Cells Transfected with hSMP30-pcDNA3.1(-) & Control pcDNA3.1(-) Plasmids

Each trace represents mean data calculated from 25 cells. Data from both hSMP30-pcDNA3.1(-) ("**RGN**") and control pcDNA3.1(-) ("**CONTROL**") COS-7 transfects are shown. Cells were stimulated with 1μM thapsigargin at the 60-second time point, in either the presence ("**+ Ca^{2+}**") (n=4) or absence ("**- Ca^{2+}**") (n=5) of extracellular Ca^{2+}.

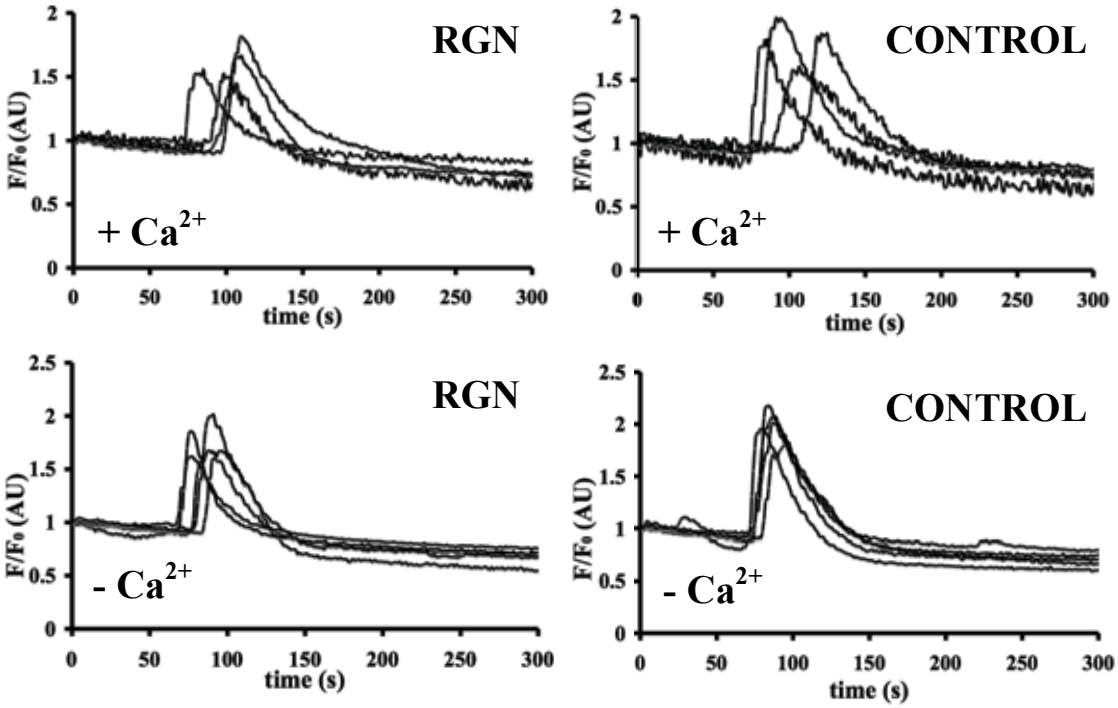

Figure 5.2.7.2. Histamine-Stimulated Ca^{2+} Transients in COS-7 Cells Transfected with hSMP30-pcDNA3.1(-) & Control pcDNA3.1(-) Plasmids

Each trace represents mean data calculated from 25 cells. Data from both hSMP30-pcDNA3.1(-) ("**RGN**") and control pcDNA3.1(-) ("**CONTROL**") COS-7 transfects are shown. Cells were stimulated with 10μM histamine at the 60-second time point, in either the presence ("**+ Ca^{2+}**") (n=4) or absence ("**- Ca^{2+}**") (n=5) of extracellular Ca^{2+}.

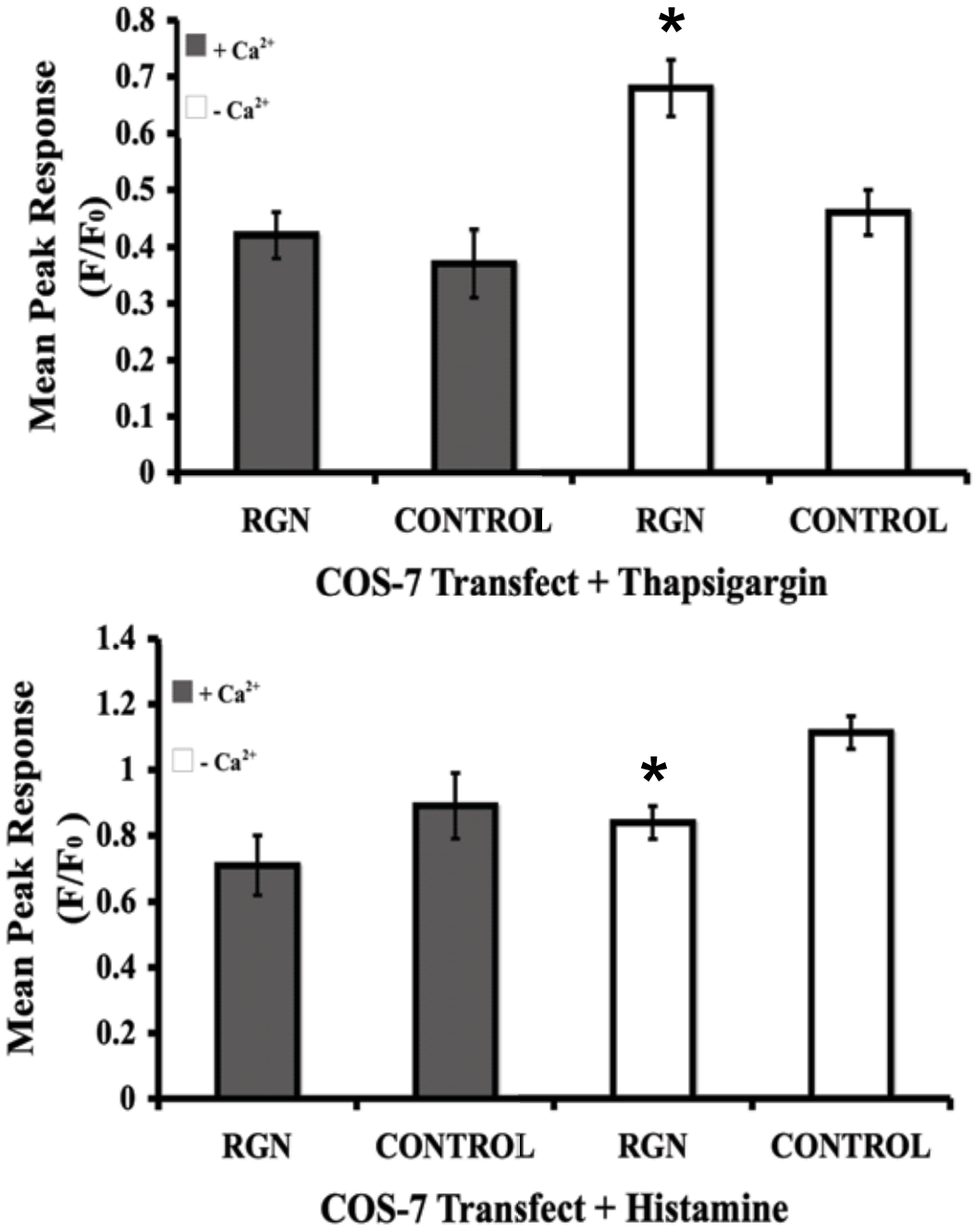

Figure 5.2.7.3. Mean Heights of Peak Ca^{2+} Response to Thapsigargin & Histamine in hSMP30-pcDNA3.1(-) & Control pcDNA3.1(-) COS-7 Transfects

Figure 5.2.7.3. Mean Heights of Peak Ca^{2+} Response to Thapsigargin & Histamine in hSMP30-pcDNA3.1(-) & Control pcDNA3.1(-) COS-7 Transfects

Each bar represents mean data calculated from experiments in either the presence ("**+ Ca^{2+}**") or absence ("**- Ca^{2+}**") of extracellular Ca^{2+} for responses to 1μM thapsigargin (top) or 10μM histamine (bottom). Values from both hSMP30-pcDNA3.1(-) ("**RGN**") and control pcDNA3.1(-) ("**CONTROL**") COS-7 transfects are shown. Error bars represent S.E.M and * indicates where $P<0.05$ compared to control pcDNA3.1(-) transfects, according to two-sample equal variance Student's T-test. Peak heights were measured from basal F/F_0 to maximum peak F/F_0 at traces of Ca^{2+} transients (figure 5.2.7.1 and 5.2.7.2).

sequence were used as controls.

Figure 5.2.7.1 shows the mean Ca^{2+} transients that were measured from hSMP30-pcDNA3.1(-) and control pcDNA3.1(-) COS-7 transfects in response to 1μM thapsigargin, in both the presence and absence of extracellular Ca^{2+}, and thus show the potential effect of RGN on SERCA-specific Ca^{2+} mobilisation. Equivalent data is given in figure 5.2.7.2 for COS-7 cell responses to 10μM histamine, which reflect the effect of RGN on hormone-induced Ca^{2+} movement via an in vivo signalling cascade. In all cases, Western blotting with anti-RGN was used to ensure all hSMP30-pcDNA3.1(-)-transfected cells used for Fluo-4 microscopy experiments did indeed over-express RGN and all control pcDNA3.1(-)-transfected cells did not (data not shown).

Analysis of the data presented here appear to show very little or no difference between RGN-over-expressing and control COS-7 cells with regards to their response timing, profile shape and duration to both thapsigargin and histamine, and both in the absence and presence of extracellular Ca^{2+}. However, there did seem to be some difference between the peak heights of response relative to basal Ca^{2+} levels, especially with both thapsigargin and histamine responses that occurred in the absence of extracellular Ca^{2+}. This observation was looked into further by measuring the mean peak heights of responses from all sets of eight graphs presented in figures 5.2.7.1 and 5.2.7.2, the values of which are given in figure 5.2.7.3 along with their S.E.Ms.

Student's T-test analysis of these mean peak heights was done to test the significance of any difference in these values between RGN-over-expressing and control COS-7 cells for all four experimental conditions tested. From this, it was found that differences in mean peak height values measured from 1μM thapsigargin and 10μM histamine response did show significant difference in the absence, but not in the presence, of extracellular Ca^{2+}. In the absence of extracellular Ca^{2+}, mean peak heights of response to 1μM thapsigargin were 0.7 ± 0.05 for RGN-over-expressing cells and 0.5 ± 0.04 for control transfects, thus RGN over-expression increased maximal amount of thapsigargin-induced Ca^{2+} release by, on average, 40%. Whereas mean peak heights of response to 10μM histamine, again in the absence of extracellular Ca^{2+}, were 0.8 ± 0.05 for RGN-over-expressing cells and 1.1 ± 0.05 for

control cells, thus RGN over-expression decreased maximal amount of histamine-induced Ca^{2+} release by, on average, 27%.

5.2.8. Immuno-detection of RGN in hSMP30-pcDNA3.1(-) & Control pcDNA3.1(-) COS-7 Transfects

Anti-RGN was used with anti-rabbit FITC-conjugated antibody to identify the localisation of over-expressed RGN in hSMP30-pcDNA3.1(-)-transfected COS-7 cells, with pcDNA3.1(-)-transfected cells as controls, using fluorescence microscopy. The images obtained (figure 5.2.8.1) showed fluorescence levels were visually higher overall for hSMP30-pcDNA3.1(-)-transfected cells than control cells, which further supported the finding from Western blots (figure 5.2.4.2) that the transfection method used gave successful RGN over-expression in COS-7 cells. The distribution pattern of fluorescence within hSMP30-pcDNA3.1(-)-transfected COS-7 cells suggested over-expressed RGN within these cells appears to concentrate in and around the nucleus, with some diffuse cytosolic localisation too, which agrees with data from previous publications (Yamaguchi et al., 1991, Fujita, 1999, Maia et al., 2009, Nakagawa and Yamaguchi, 2006). Fluorescence detected at control cells, which showed to not express RGN on Western blots, was interpreted as background labelling. This observation in control transfects was possible due to the detection of 66kDa non-specific protein in samples from the same cells (as discussed in section 5.2.5).

5.2.9. SERCA Expression Levels in COS-7 Cells Over-Expressing Human RGN

Endogenous SERCA protein levels in COS-7 cells, which were either transfected with hSMP30-pcDNA3.1- or control pcDNA3.1- plasmid, were examined using Western blotting (figure 5.2.9.1) with three samples from three pairs of human RGN-over-expressing and control cells. Analysis of their SERCA Western blot protein bands showed cells that over-expressed human RGN expressed, on average, 20.8 ± 7.3% more SERCA than control cells. Student's t-test showed this was significant with the use of three pairs of samples ($P<0.05$).

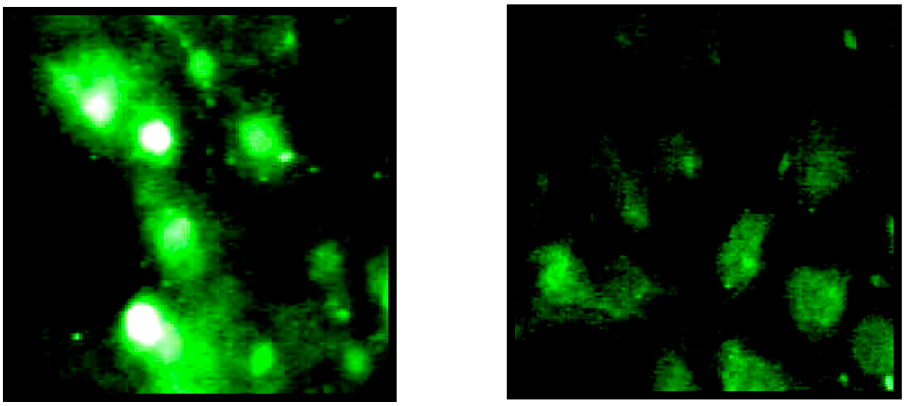

RGN CONTROL

Figure 5.2.8.1. Localisation of Anti-RGN in COS-7 Cells Transfected with hSMP30-pcDNA3.1(-) & Control pcDNA3.1(-) Plasmids

COS-7 cells transfected with hSMP30-pcDNA3.1(-) ("**RGN**") and control pcDNA3.1(-) ("**CONTROL**") plasmid DNA were fixed with formaldehyde, permeabilised with Triton X100 and incubated with antibodies at dilution ratios of 1:50 (anti-RGN) and 1:200 (anti-rabbit FITC conjugate). Anti-RGN localisation was identified by detection of FITC fluorescence in treated cells using a fluorescence microscope. Images were captured at x200 magnification. Whiter brightness represents larger amount of localisation of antibodies.

COS-7 cells were seeded and transfected in the same manner as the cells that were used for Fluo-4 microscopy experiments. Cells were seeded at density of $1x10^5$ cells per coverslip, transfected 24 hours later using a 1.5µg:4.5µl ratio of plasmid DNA-to-transfection reagent. Coverslips were used 48 hours after transfection.

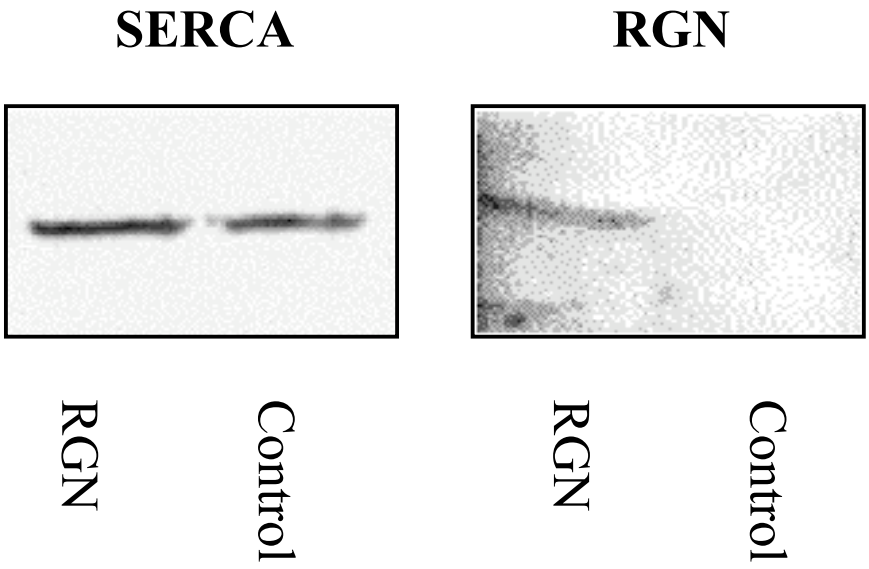

Figure 5.2.9.1. Endogenous SERCA Expression Levels in COS-7 Cells Transfected with hSMP30-pcDNA3.1(-) & Control pcDNA3.1(-) Plasmids

Total cell lysates from COS-7 cells transfected with either hSMP30-pcDNA3.1(-) ("**RGN**") or control pcDNA3.1(-) ("**Control**") plasmids were probed with anti-SERCA Y1F4 (left; "SERCA") and anti-RGN (right; "RGN") antibodies. The two images shown represent Western blot protein bands detected from the same pair of samples. In both cases, 20μg of total protein were loaded at each lane. Molecular masses of protein bands were approximately 100kDa and 33kDa, as expected for SERCA and RGN, respectively.

5.2.10. Optimisation of Rat RGN Expression: Attempt to Express Soluble Recombinant Protein in BL21 Cells

After noting the effects of human RGN in COS-7 cells on the intensity of their Ca^{2+}-mediated responses to 1μM thapsigargin and 10μM histamine, an attempt was initiated to produce correctly folded recombinant rat RGN protein using the BL21 expression system that was used to produce the custom-made anti-RGN's antigen (section 5.2.2). It was intended that purified and correctly folded recombinant rat RGN could be used in further studies to examine the details behind its role in Ca^{2+} signalling, as a follow up to the results obtained with human RGN-over-expressing COS-7 cells.

IPTG stimulates recombinant protein expression in BL21 cells transformed with pET21a plasmids, containing coding sequences inserted into their multi-cloning sites, by inducing expression of bacterial T7 RNA polymerase, which binds to the T7 promoter sequence adjacent to the inserted coding sequence, and subsequently promotes the expression of the latter (Scharff et al., 2001). An increase in IPTG concentration results in an increase in recombinant protein expression. However, too much over-expression of recombinant protein in the transformed BL21 cells can lead to the formation of inclusion bodies, which are aggregates of mis-folded protein. Thus different IPTG concentrations were tested for induction of rat RGN expression in an attempt to optimise this factor to produce soluble protein within pET21a-RGN-transformed BL21 cells.

BL21 cells induced with 0.1mM IPTG were sonicated and centrifuged at 20,000g for 20 minutes to separate inclusion bodies and cell debris from soluble proteins, which were analysed by SDS-PAGE and the resulting gels are shown in figure 5.2.10.1. Inclusion bodies were expected to be localised to the 20,000g centrifugation spin pellet and soluble proteins were found in the corresponding supernatant fraction. It was observed that over-expressed protein, which was represented by the most densely stained band in Coomassie blue stained gels, was 33kDa in molecular mass and thus likely to have been rat RGN (Yamaguchi, 2005). This identity of the heavily expressed 33kDa protein was confirmed later on using anti-Hisx6 antibody to successfully detect Hisx6-tagged RGN by Western blotting (figure 5.2.3.1). Other IPTG concentrations for induction of pET21a-RGN-transformed BL21 cells grown at 37^{o}C, within the range of 0.01-0.5mM, were tested

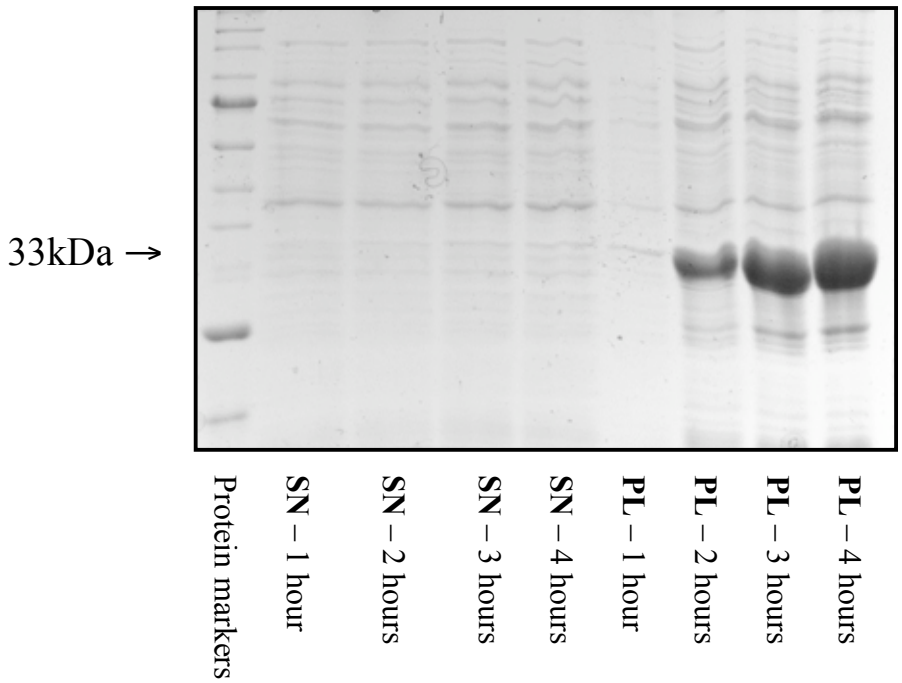

Figure 5.2.10.1. Production of Recombinant Rat RGN from pET21a-RGN-Transformed BL21 Cells After IPTG Induction

Samples shown here were collected from a culture of pET21a-RGN-transformed BL21 cells induced with 0.1mM IPTG at 0, 1, 2 and 4 hours after induction started. The culture was grown at 37^{o}C. For each sample, total cell lysates of sonicated cells (isolated from culture media by centrifugation) were centrifuged at 20,000g, and the resulting supernatant ("**SN**") and pellet ("**PL**") were subjected to SDS-PAGE.

A lane of protein molecular weight markers is shown on the left. Lanes containing samples of pellets and supernatants with their associated incubation times are labelled. The expected position of 33kDa protein bands is indicated. All samples were loaded at equal volumes in each lane.

to try and make the cells produce recombinant rat RGN that would be correctly folded and thus not form inclusion bodies. However, even at the lowest concentration of IPTG tested (0.01mM), over-expression of the 33kDa protein appeared to start approximately 1 hour after induction and most of it was detected in the 20,000g spin pellets of BL21 cell lysates, while none appeared in their counterpart supernatant (data not shown).

A lower culture temperature of 17^{o}C following IPTG addition to their media was also tried in an attempt to slow down recombinant protein production to encourage their correct folding within BL21 cells. This has been shown in the past to improve yields of soluble recombinant protein expression (Sheng et al., 2007). Although the rate of recombinant RGN expression was indeed slower at 17^{o}C compared to 37^{o}C, the protein was still being expressed in the form of inclusion bodies regardless of duration of culture time after IPTG addition and IPTG concentration used for induction, according to SDS-PAGE analysis (data not shown). Temperature shock treatments prior to the addition of IPTG to BL21 cultures were also tried, which involved heating cultures to 42^{o}C or cooling them to ice-cold temperatures to induce the expression of endogenous chaperones in the BL21 cells. This has been shown in previous studies to be possible and the chaperones can aid correct folding of recombinant proteins (Wick and Egli, 2004). However, the inclusion bodies persisted to still be produced even after these methods were tried. Thus none of the conditions tested in the process of optimising the expression of soluble recombinant protein within pET21a-RGN-transformed BL21 cells were able to promote correct folding of Hisx6-tagged rat RGN in these cells.

5.2.11. Ni^{2+} Affinity Column Chromatography with Solubilised Inclusion Bodies of Recombinant Rat RGN Protein

The purification and solubilisation of inclusion bodies, along with attempts to refold them in vitro, were tried after unsuccessful attempts to promote production of recombinant RGN protein in soluble form within BL21 cells. Figure 5.2.11.1 shows a SDS-PAGE gel of samples collected in the process of isolating inclusion bodies from IPTG-induced BL21 cells and the use of Ni^{2+} resin, which has a high binding affinity for Hisx6-tags, to purify Hisx6-tagged recombinant RGN. The inclusion bodies were

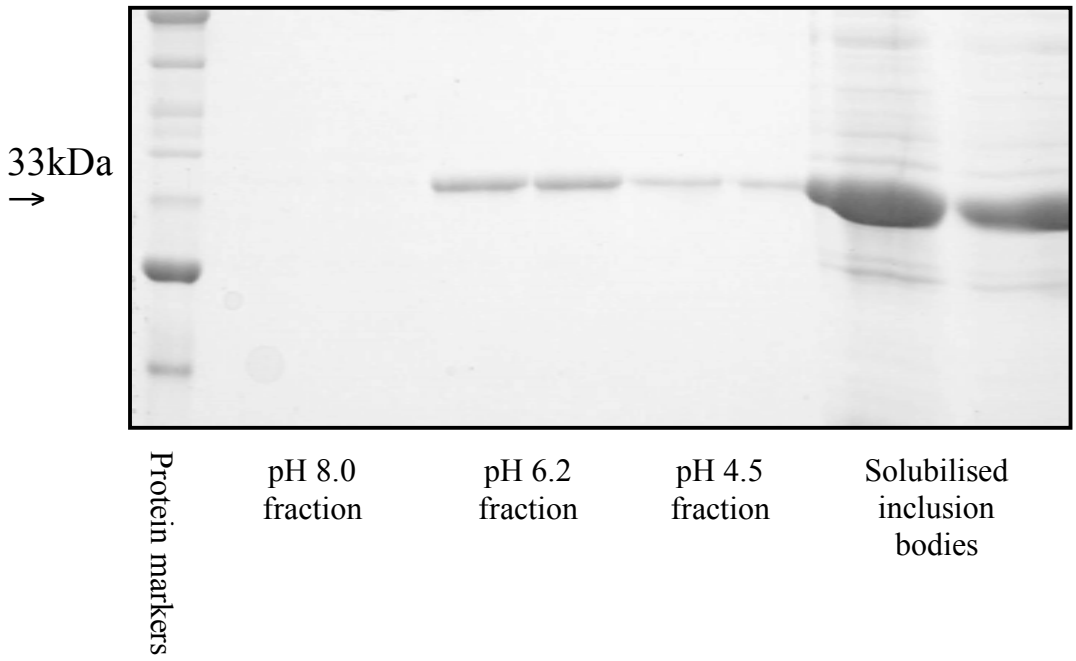

Figure 5.2.11.1. Binding of Solubilised RGN Inclusion Bodies to Ni^{2+} Resin

Binding of rat RGN solubilised inclusion bodies to Ni^{2+} resin was tested using column chromatography. The inclusion bodies were isolated from cultures of pET21a-RGN-transformed BL21 cells that were induced with 0.25mM IPTG and grown overnight at 17^{o}C.

Fractions from Ni^{2+} affinity column chromatography with 8M urea-solubilised inclusion bodies are shown, whereby the samples are labelled with the pH of buffer used to elute them off the column (two lanes are shown for each sample). A lane of protein molecular weight markers is shown on the left. The expected position of 33kDa protein bands is indicated. All samples were loaded at equal volumes in each lane.

isolated by treating 20,000g spin pellets (from centrifugation of sonicated IPTG induced BL21 cells for 20 minutes) with 8M urea, followed by centrifugation at 100,000g for 45 minutes, to solubilise and separate them from most of the contaminating proteins and cell debris also present in the 20,000g spin pellet.

Furthermore, incubation of these solubilised inclusion bodies with Ni^{2+} resin, using column chromatography, demonstrated the ability of its abundant 33kDa protein content to bind to such resin, as well as appear in the pH 6.2 and, to a smaller extent, pH 4.5 column eluants but not that of pH 8.0. This confirmed the inclusion bodies consisted of Hisx6-tagged RGN protein and demonstrated the use of Ni^{2+}-affinity column chromatography could be used to concentrate and further purify this protein after solubilisation of its mis-folded form among cell debris. Even though more recombinant RGN was expected to be found in the pH 4.5 elution fraction rather than the pH 6.2 wash fraction, the latter of which elutes weakly bound protein, the pH 6.2 wash fraction contained only 33kDa protein according to SDS-PAGE analysis and so was still used for refolding experiments due to the visible absence of contaminants.

5.2.12. Refolding of Purified Rat RGN: Use of Dialysis & Dilution to Refold Solubilised Inclusion Bodies

Following successful purification of Hisx6-tagged RGN by solubilisation of inclusion bodies and use of Ni^{2+} affinity column chromatography to remove contaminating proteins, the next step that had to be optimised was the refolding of the urea-solubilised Hisx6-tagged protein. Two methods of refolding were tested, which were one-step dialysis and crash dilution (Tsumoto et al., 2003). Both worked by dilution of urea away from the protein, thus removing the denaturing effect of the former and allowing the latter to spontaneously fold. Dialysis allows a slower process of refolding than dilution. Both methods were tried because it was unknown which method would suit Hisx6-tagged rat RGN protein best.

Use of the wrong conditions for protein folding led to the formation of precipitated protein, which was indicated by visible white precipitant or cloudiness of the protein solution. Precipitation of mis-folded protein was often observed following dialysis of samples that were high in protein concentration, which would have resulted in crowding and interaction between different peptides during the process of refolding. Thus Ni^{2+} affinity chromatography column fractions that were used for dialysis refolding of purified Hisx6-tagged protein were diluted to a concentration of

0.2mg/ml before being dialysed. Refolding by dilution method involved rapidly diluting the pH 6.2 column fraction (abundant in 33kDa protein) by adding refolding buffer to it to give a final protein concentration of 0.1mg/ml, before being dialysed to remove glycerol and DTT in the dilution buffer to further aid refolding.

Glycerol and DTT were added to refolding buffers for both dialysis and dilution methods. The use of glycerol was included to reduce the chance of protein aggregation. DTT was included because analysis of recombinant rat RGN amino acid sequence showed it contains ten cysteine residues and thus it is possible the structure of this protein requires the formation of disulphide bridges. The presence of DTT was expected to prevent disulphide bridges from forming while the protein refolded into its correct tertiary structure before DTT was diluted away to allow the correct disulphide bridges to form only when the protein was in the correct tertiary structure. DTT concentrations used were 0.5mM for dialysis refolding and 5mM for crash dilution refolding. After all refolding attempts, the protein contents of samples were concentrated with the use of Vivaspin centrifugal concentrators to allow for them to be used in further analysis, such as circular dichroism spectroscopy.

5.2.13. Circular Dichroism Analysis of Refolding Success for Recombinant Rat RGN

Two samples of recombinant rat RGN protein solutions, one for each of the refolding methods used as discussed above (section 5.2.12), were subjected to circular dichroism (CD) spectroscopy in order to give an indication of whether or not they had correctly folded. Both samples consisted of a pH 6.2 fraction from Ni^{2+} column chromatography treatment of 8M urea solubilised inclusion bodies from pET21a-RGN-transformed BL21 cells, which had been induced with 0.25mM IPTG and cultured overnight at 17^{o}C. SDS-PAGE was used to ensure the pH 6.2 fractions did indeed contain only 33kDa protein (data not shown).

CD spectroscopy was used to identity the protein secondary structures present in the two protein samples and indicate how ordered those protein structures were overall. The CD spectra that were obtained from analysis of both samples (figure 5.2.13.1-2) are given. Control CD spectra from fresh dialysis buffer (in which the protein solutions were dialysed to remove Cl^{-} in their preparation for CD spectroscopy) without protein was also collected after experiments with each protein

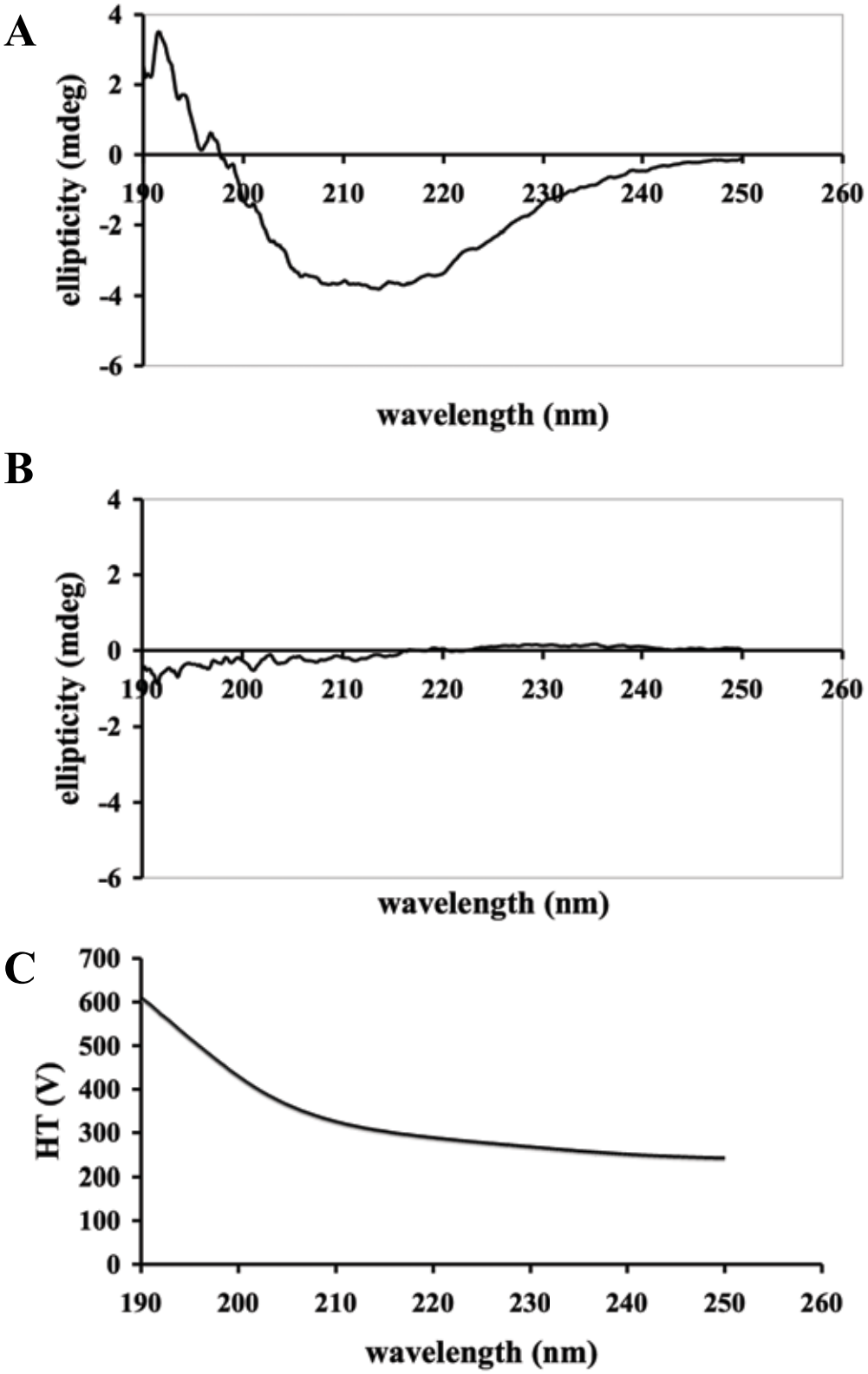

Figure 5.2.13.1. CD & Light Absorbance Spectra From CD Experiments with One-Step Dialysis-Refolded Recombinant Rat RGN

Figure 5.2.13.1. CD & Light Absorbance Spectra From CD Experiments with One-Step Dialysis-Refolded Recombinant Rat RGN

(A) CD spectrum collected for the protein sample was corrected by subtracting values from spectrum (B), which was the control CD collected from buffer alone, and all values were normalised to the baseline value at 260nm. (C) Absorbance spectrum for the protein sample, which resembles that for buffer control and values for both were all at or below 600V throughout the 260-190nm wavelength range of polarised light used.

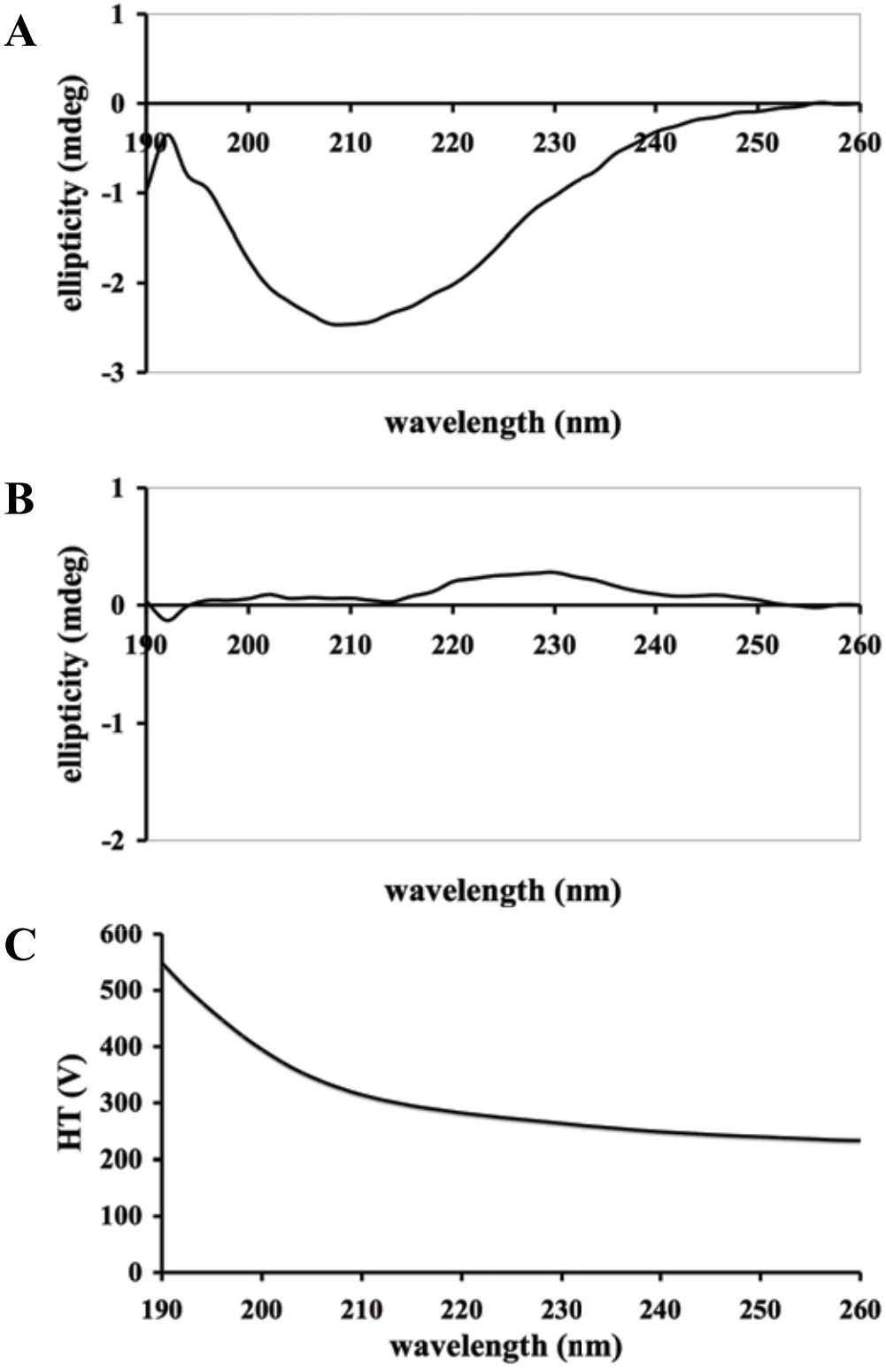

Figure 5.2.13.2. CD & Light Absorbance Spectra From CD Experiments with Crash Dilution-Refolded Recombinant Rat RGN

Figure 5.2.13.2. CD & Light Absorbance Spectra From CD Experiments with Crash Dilution-Refolded Recombinant Rat RGN

(A) CD spectrum collected for the protein sample was corrected by subtracting values from spectrum (B), which was the control CD collected from buffer alone, and all values were normalised to the baseline value at 260nm. (C) Absorbance spectrum for the protein sample, which resembles that for buffer control and values for both were all below 600V throughout the 260-190nm wavelength range of polarised light used.

solution and used to correct the spectra values of the latter to subtract any effects from the buffer solution alone. Light absorbance spectra were also recorded for each and all experiments to monitor the linearity of polarised light absorbance by the samples, whereby CD data collected at any point when absorbance values were greater than 600V was deemed unreliable due to loss of linearity in the effects of polarised light on the protein sample detected. The 600V threshold is a standard value used for all CD experiments (as advised by Dr. T. Dafforn, The University of Birmingham).

Taking into consideration the standard guidelines of how to read CD spectra based on the values and intensities of minimum/maximum peak values (Fasman, 1996), spectra for both samples can be interpreted to show the protein structures in these samples contained a mixture of β-sheets and α-helices due to the broadness of the single minimum negative peak value around 210nm in both cases. The CD spectral region between 190-200nm needed to show a maximum positive peak value that was at least the same intensity as that of the minimum negative value to suggest it was well folded. This was almost the case for dialysis-refolded protein but far less so for dilution-refolded protein. The negative maximum peak value for the latter sample suggests it contained partially unfolded protein. From qualitative analysis of the spectra, dialysis-refolded protein was likely to have contained less mis-folded protein and thus appears to be the better method of refolding.

Note that both CD spectra showed some resemblance to that first collected by Yamaguchi (Yamaguchi, 1988). However, the CD spectroscopy method that was used in this early study is questionable due to the use of 50mM Tris-HCl buffer, which was likely to have interfered with light absorbance by the sample and thus the CD spectra presented may contain invalid data. Furthermore, these early spectra of RGN that had been isolated from rat liver tissue shows maximum negative peak values, indicating the protein samples contained mis-folded protein. Thus comparisons between the spectra from the present study and that of the earliest study on RGN's structure with the use CD have to be kept to a minimum. With regards to the human RGN crystal structure (Chakraborti and Bahnson, 2010), the CD spectra of recombinant Hisx6-tagged rat RGN from the present study appears to not fit the six-β-propeller barrel fold presented by the former. Such a highly ordered fold of predominantly β-sheets would have given a CD spectrum for protein with a single minimum negative peak

value between 210-225nm and one maximum positive peak value, of at least equal intensity to the minimum peak, between 190-200nm (Fasman, 1996).

Analysis of human RGN's PDB file (reference number 3G4E) showed it contains 64% β-sheet, 1.3% α-helix and 34.7% random fold. Prediction of secondary structure proportions from the CD spectra obtained in the present study using an online analysis program, K2D2, suggested the dialysis-refolded protein contained 30.8% β-sheet, 16.0% α-helix and 53.2% random fold. Whereas K2D2 predicted the dilution-refolded protein contained 44.5% β-sheet, 3.7% α-helix and 51.8% random fold. Although the dilution-refolded protein appeared to have more predicted β-sheet than dialysis-refolded protein, the predicted fit of the CD spectra was not as good for the former as it was for the latter (figure 5.2.13.3) and thus the dialysis-refolded protein still remained the better-folded sample. Though neither protein samples had secondary structure predictions that matched the values given by the human RGN crystal structure, which again strongly suggests the recombinant rat RGN produced in the present study had not been folded correctly. Note that the crystal structure shows RGN bound to Ca^{2+}, whereas the recombinant rat RGN produced and refolded in the present study was in the absence of Ca^{2+}. It is possible that in the absence of Ca^{2+}, RGN's structure is less well ordered than when bound to Ca^{2+}.

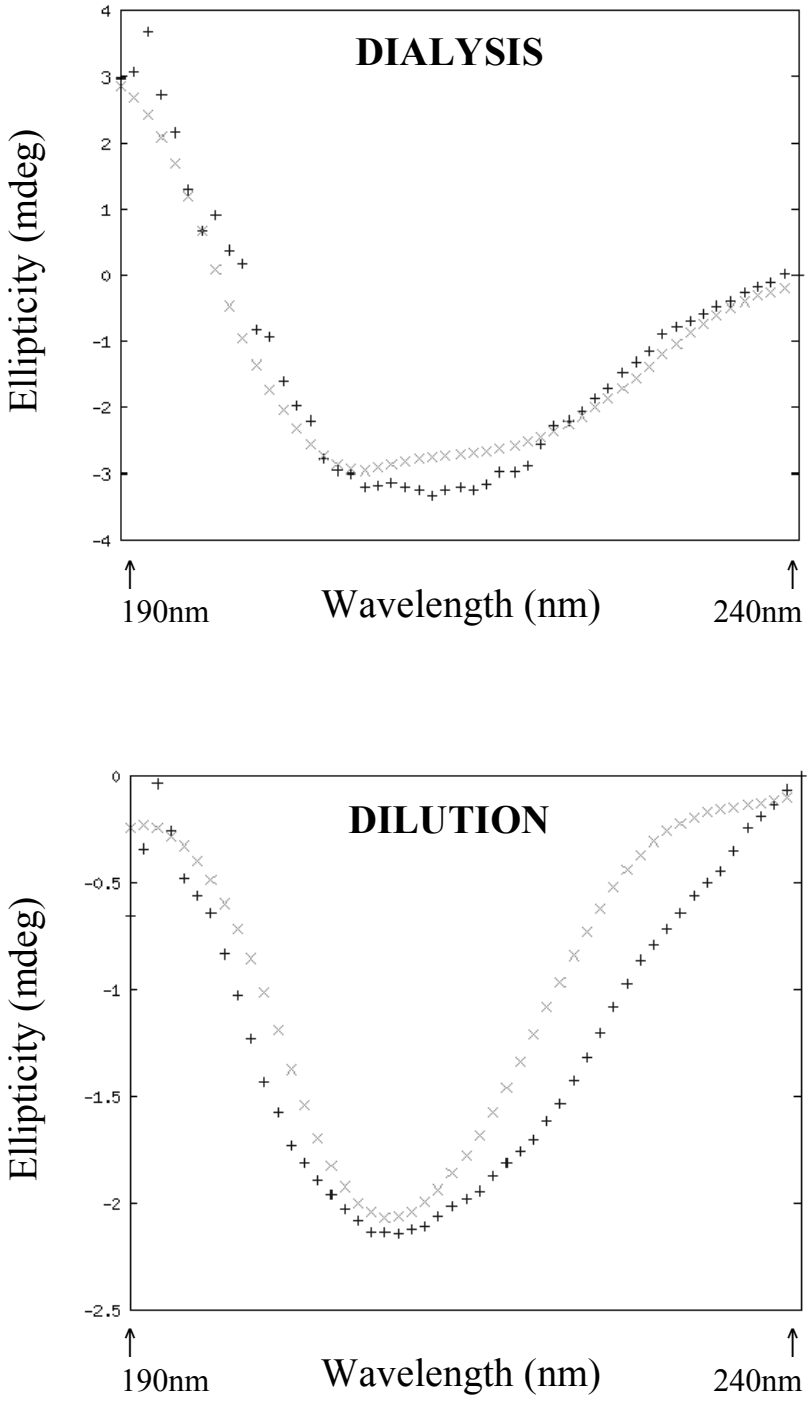

Figure 5.2.13.3. K2D2 Prediction of Secondary Structure in Samples of One-Step Dialysis & Crash Dilution Refolded Recombinant Rat RGN

Figure 5.2.13.3. K2D2 Prediction of Secondary Structure in Samples of One-Step Dialysis & Crash Dilution Refolded Recombinant Rat RGN

Fitting of CD spectra for both one-step dialysis ("**DIALYSIS**") and crash dilution ("**DILUTION**") refolded protein samples was done by the K2D2 program to predict their contents of secondary structure, which were as stated in section 5.2.13. Data for the actual CD spectra ("+") that was entered into the K2D2 program to be analysed, along with the 'predicted' spectra ("**x**") that K2D2 generated to give the closest fit to the former in order to predict contents of secondary structure are shown.

5.3. Discussion

Distribution of RGN expression has proven to not be widespread across different types of tissues and cells, both in previous and present research, at the mRNA and protein level. In agreement with previous studies, RGN was detected in samples derived from liver, kidney and brain from adult rat (Yamaguchi et al., 1991), whereby the former was notably observed as the tissue with the highest RGN abundance at both mRNA and protein levels out of all the samples that were tested. For lung, heart and skeletal muscle from adult rat, there was both agreement and disagreement with findings from past publications. Lung tissue has been shown to not express RGN in rat in both present and past (Yamaguchi et al., 2002) studies, but has been suggested to express RGN in mice (Mori et al., 2004). Heart has been shown to express RGN in some studies with rats and mice (Yamaguchi and Nakajima, 2002, Doran et al., 2006), whilst none have been detected in rats in other studies (Yamaguchi et al., 1991, Yamaguchi and Isogai, 1993, Yamaguchi et al., 2002). Though it has recently been suggested that RGN expression levels can vary with age in the heart (Akhter et al., 2007, Lim et al., 2009), which is supported by the present study because RGN mRNA was detected in a sample from juvenile, and not adult, rat heart. Skeletal muscle was shown to not express RGN in the present study, which conflicts with a previous study that did detect RGN protein in samples of mice limb muscle (Doran et al., 2006) but does agree with another study that could not detect RGN protein in rat muscle samples (Yamaguchi et al., 2002). In the case of lungs and skeletal muscle, this altogether suggests a possible difference in distribution of RGN in rats and mice, which are expected to use RGN differently because only mice is likely to use RGN for vitamin C biosynthesis (whereas rats cannot synthesise their own vitamin C).

Fat pads from adult rat have not been screened in past studies, though rat adipose tissue has been shown to be able to express RGN mRNA (Yamaguchi and Nakagawa, 2007). In the present study, it has been shown that rat fat pads do not express RGN at the protein level. Although both rat brain (Yamaguchi et al., 1999) and heart (Yamaguchi and Nakajima, 2002) have been demonstrated in past studies to express RGN, distribution of abundant RGN levels at specific regions within these two organs of rat has not been demonstrated before. For brain tissue, samples from mice have been previously used to show RGN expression can be detected specifically in the

cerebrum (Mori et al., 2004). While the cerebral cortex and hippocampus of rat brain has been tested in the past and found to express virtually no RGN protein (Yamaguchi and Isogai, 1993). In the present study, it was shown that RGN mRNA is detectable in the cerebellum of adult rat brain and aorta of adult rat heart.

After screening for RGN mRNA expression levels in a range of samples from various rat tissues, the focus of interest with regards to RGN distribution in tissues became the male reproductive organs. At the mRNA level, strong levels of RGN expression were detected in multiple samples from rat testes. However, RGN was not detected at the protein level in the present study with rat tissue samples. The amount of RGN expressed in testis has yet to be made clear due to differences in the data presented in past studies. Immunofluorescence experiments have shown RGN is not expressed in rat testis (Yamaguchi et al., 1991), ELISA experiments have shown RGN can be detected but at levels 2000-fold lower than that found in rat liver and at ng/mg of tissue concentrations (Yamaguchi and Isogai, 1993), and PCR experiments have shown RGN mRNA is detectable in mice testis at the mRNA level (Mori et al., 2004).

With regards to the discrepancy between RGN detection at the mRNA and protein levels with samples from adult rat testis in the present study only, a possible explanation could be made from the age dependence of RGN expression that has already been demonstrated for other tissues, such as the liver and kidney (Fujita et al., 1996). In the present study, RGN mRNA was detected in both juvenile and adult testis samples, which originated from rats that were 5 days and 5 weeks old, respectively. However, tissues samples (used for RGN detection at the protein level in the present study) were prepared from intact testis that had been obtained from adult rats much older than 5 weeks old. Thus the conflict between RGN detection at mRNA and protein levels observed in the present study could be a demonstration of RGN's age dependence in its expression in rat testis, whereby the RGN abundance decreases with increasing age. The possibility of RGN expression levels being affected by age in the testis of male rats, which could potentially also be the case for humans, has not been suggested in the past. On the other hand, another possible explanation could be that there is a difference in expression rate or turnover of RGN between the mRNA and protein levels. Thus RGN expression may be more stable at the mRNA level than

protein level, which would make detection of the former more successful than the latter, as demonstrated in the present study.

In addition to RGN expression levels found in rat testis, RGN mRNA had also been detected in the present study within samples from germ cells, myeloid cells and Sertoli cells, all of which are specialised cell types found in the male reproductive system. The expression of RGN in these specific cell types has never been noted in past publications. One specialised tissue type of the male reproductive system of rats that has been noted to express RGN in a past study is the prostate (Maia et al., 2009). It was the detection of RGN mRNA in the cell types tested in the present study, along with testis, of both adult and juvenile male rats that led to experiments with adult boar sperm, with the intention of seeing whether RGN is also expressed in sperm. In the end, it was concluded that RGN could not be detected in adult boar sperm, but again the factor of age dependence of RGN expression could have also applied in this case.

With regards to normal established cell-lines, RGN protein could not be detected in those representative of embryonic rat aorta-derived cells (A7r5), adult mice Sertoli cells (TM4), human brain neuroblastoma cells (SH-SY5Y) and monkey kidney cells (COS-7). Thus although RGN expression was successfully detected in their associated organs at the mRNA level (and at the protein level for brain and kidney) using samples from tissues that had been extracted from rats (and had not been established in cell culture), the same could not be said for the established cell-line equivalents, which is an observation that connects well with the age-dependence feature of RGN expression that gave this protein its alternative name, 'senescence' marker protein 30 (SMP30) (Fujita, 1999). This overall finding suggests de-differentiation (a feature of aging and formation of established cell-lines) causes loss of RGN expression, which would agree with a previous study that showed RGN expression decreased in breast and prostate tissue as they progressively de-differentiated in the process of tumorigenesis (Maia et al., 2009). However, other established cell-lines have been noted to be able to express RGN in normal cell culture, such as the human hepatoma cell-line, HepG2 (Murata et al., 1997), rat hepatoma cell-line, H4-II-E (Nakajima et al., 1999) and mouse osteoblastic cell-line, MC3T3-E1 (Yamaguchi et al., 2008a). This conflict between past and present studies may be attributed to a difference in control of RGN expression in established cell-lines from different tissue types,

whereby cell-types from certain tissues are better at retaining the ability to express RGN than others when de-differentiated.

The absence of endogenous RGN expression and their ease of use in transfections made COS-7 cells an ideal model to study the effect of human RGN expression on Ca^{2+} mobilisation in intact cells. From their use, the present study demonstrated over-expression of human RGN in COS-7 cells can influence the intensity in changes to their cytosolic Ca^{2+} levels in response to hormone stimulation and SERCA inhibition, which were noted to be especially visible in the absence of extracellular Ca^{2+}. A 40% increase in maximal amount of thapsigargin-induced Ca^{2+} release and 27% decrease in maximal amount of histamine-induced change in cytosolic Ca^{2+} levels were observed in the present study. These values suggest RGN can increase both the Ca^{2+} storage capacity and Ca^{2+} uptake efficiency of the ER. Furthermore, average SERCA protein levels in human RGN-over-expressing cells were found to be higher than those in control COS-7 cells by a mean average of 20.8 ± 7.3%, which indicated RGN over-expression had promoted an increase in SERCA expression. This change in SERCA protein levels would certainly correspond well with the idea that ER Ca^{2+} storage efficiency had improved in the event of RGN over-expression, which would explain the observations made in intact cells regards to their thapsigargin and histamine responses in the absence of extracellular Ca^{2+}. Changes in SERCA expression levels caused by RGN over-expression have not been demonstrated before. Although one past study has shown RGN over-expression in a rat kidney epithelial cell-line (NRK52E) can increase or decrease the mRNA expression levels of their endogenous L-type Ca^{2+} channel and Ca^{2+}-sensing receptor (CaR) (Nakagawa and Yamaguchi, 2006).

Two previous studies that used similar RGN over-expression experimental models have suggested RGN increases PMCA activity (Fujita et al., 1998, Son et al., 2008), which may also be the case for the present study and it is possible that increased PMCA activity would have caused a decreased peak height of Ca^{2+}-mediated response to histamine. However, increased PMCA activity would not account for an increased peak height of Ca^{2+} release from thapsigargin treatment. The absence of visible difference in intensity, shape and duration of Ca^{2+}-mediated responses between RGN-over-expressing and control COS-7 cells in the presence of

extracellular Ca^{2+}, for both response to thapsigargin and histamine, would also argue against PMCA having any significant effect in the event of RGN over-expression in COS-7 cells. However, an influx of extracellular Ca^{2+} (possibly by, for example, store-operated Ca^{2+} entry) from Ca^{2+}-supplemented media could have obscured the effects of PMCA. This would make higher than normal PMCA activity detectable, in the form of a decreased height in Ca^{2+}-mediated response to histamine, only in the absence of extracellular Ca^{2+}.

It should also be noted that one of these two past studies also showed RGN over-expression does not affect cellular response to thapsigargin (Son et al., 2008), which would conflict to observations from the present study. This discrepancy is likely to be attributed to a difference in experimental procedures, whereby the past study in question had only monitored the first 60 seconds of thapsigargin response in population-based studies, whereas the present study monitored thapsigargin-stimulated Ca^{2+}-transients from single cells for 4 minutes after thapsigargin was added to them. It should also be noted that past studies have shown RGN can increase SERCA activity in kidney (Kurota and Yamaguchi, 1997), liver (Yamaguchi and Mori, 1989) and heart (Yamaguchi and Nakajima, 2002). Observations made of over-expressed RGN's ability to weaken Ca^{2+}-mediated hormone response and strengthen Ca^{2+} uptake by up-regulating SERCA connect well with RGN's age-dependent pattern of expression. This is because SERCA expression has also been shown to be age-dependent (Periasamy and Kalyanasundaram, 2007).

In light of recent determination of human RGN's K_d value for Ca^{2+}, which has been stated to be 0.57mM, it is unlikely RGN mediates its effects at the cytosol because cytosolic Ca^{2+} levels would only reach this concentration in the event of apoptotic cell death and not when responding to hormone stimulation. However, Ca^{2+} concentrations in the ER and mitochondria can reach up to 0.5mM in stimulated cells (at least in HeLa cells) (Pinton et al., 1998, Vay et al., 2009). RGN has not been previously been shown to localise in the ER, though would exist in this organelle during its synthesis. This is in contrast to the mitochondria (Yamaguchi et al., 2008b). However, any effects that RGN over-expression may have had on mitochondrial Ca^{2+} storage is most likely to have been indirect (for example via its linkage with the ER) at least according to the present study because immunofluorescence experiments were

unable to detect specific RGN localisation at the mitochondria. It should be noted that RGN has been shown to be able to increase mitochondrial Ca^{2+} uptake (Takahashi and Yamaguchi, 2000) and that aging leads to a decrease in this activity of the mitochondria (Beal, 2005), which would correlate well with age-dependent decrease in RGN expression (Fujita et al., 1996).

According to past studies, it is possible for RGN to localise in the lumen of the nucleus (Nakagawa and Yamaguchi, 2008) and influence gene transcription levels (Yamaguchi, 2000b). This would correspond well with the observation of both RGN localisation at the nucleus and increased SERCA protein levels in RGN-over-expressing cells. However, for any effects of RGN on SERCA expression to be Ca^{2+}-related, the over-expression of RGN must have had to increase the Ca^{2+}-storage capacity of the nucleus because a past study has shown the nuclear luminal free Ca^{2+} level is 0.1μM (at least in HeLa cells) (Badminton et al., 1996), which is 5700 times lower than RGN's K_d for Ca^{2+}-binding. Otherwise, alteration of SERCA expression levels caused by RGN over-expression is unlikely to have been caused by increased Ca^{2+} storage capacity at the nucleus. An increase in Ca^{2+}-storage capacity at the nucleus could have also meant this organelle contributed to the effects of Ca^{2+}-mediated responses seen for thapsigargin and histamine.

To aid future studies, the availability of a fully functional recombinant rat RGN would be useful in, for example, studies with isolated membranes to test RGN's ability to directly interact with SERCA or PMCA. This would certainly help to further define the details associated with the observations made on RGN-over-expressing COS-7 cells discussed above. Thus the next step in the present study was to attempt to refold the inclusion bodies produced of recombinant rat RGN, which was used for anti-RGN production. To date, a Hisx6-tagged recombinant rat RGN that has been folded to contain all the same secondary structures of those shown to exist in the crystal structure of human RGN (Chakraborti and Bahnson, 2010) has yet to be obtained from the present study.

It has been shown in past studies with recombinant forms of both human RGN (Choi et al., 2010b) and a diisopropylfluorophosphatase (DFP) from squid (*Loligo vulgaris*), (the latter of which is both functionally related to rat RGN (Kondo et al., 2004) and

also has the same tertiary fold as human RGN, (Scharff et al., 2001)) that the six-β-propeller fold is difficult to achieve and these proteins often form inclusion bodies if expression in BL21 cells is not supported by either the use of protein-folding chaperones or an expression vector that promotes slow protein expression, respectively. Furthermore, it should be noted that both the crystal structure of human RGN and squid DFPase were produced with recombinant RGN protein that had Ca^{2+} bound to them, whereas the present study did not use refolding buffers that were supplemented with Ca^{2+} and thus the CD spectra presented here show the features of RGN protein not bound to Ca^{2+}.

Ca^{2+} has been noted to be able to alter the α-helical content of rat liver RGN (Yamaguchi, 1988), whereby adding Ca^{2+} to the protein reduces its α-helical content, which would support the idea that Ca^{2+} is required to promote the formation of β-sheets in RGN. Though the amount of decrease in α-helical content of rat liver RGN in this past study was calculated to only be 4.5% in the presence of 1mM $CaCl_2$, which was the same concentration of $CaCl_2$ used throughout the purification process of recombinant human RGN that was used to obtain its crystal structure. This minor Ca^{2+}-induced change of α-helical content in rat liver RGN would still not have represented a structure that was the same as that of the human RGN structure, the latter of which has an α-helical content of 1.3%. This difference between the two RGN structures may have been caused by differences in structural analysis methods used (modern X-ray crystallography vs. early CD spectroscopy).

In conclusion, the data presented here supports past studies made on RGN expression, which have shown it is widely distributed across different organs, but is not expressed in all organs with the same abundance and it is possible the pattern of RGN distribution is different between mice and rats. The present study has shown RGN mRNA is expressed in a number of specialised cell types from the male reproductive system, which have not been shown previously, and suggests RGN plays a role in male fertility. Over-expression of human RGN has been shown, for the first time, to significantly influence the maximal strength of Ca^{2+}-mediated responses to SERCA inhibition by thapsigargin and hormone stimulation in intact single cells. It is possible that this nuclear localisation of over-expressed RGN can influence SERCA

expression levels, which is an effect that would correlate well with the age-dependence of both RGN and SERCA expression. Furthermore, the integrity of RGN's structure is suggested to be dependent on the presence of Ca^{2+}, whereby the absence of Ca^{2+} potentially hinders the formation of β-sheets in RGN. Further research will be required to refine the details behind RGN's role in Ca^{2+} homeostasis, which may be assisted with the use of recombinant rat RGN and anti-RGN antibody that have been produced as part of this study.

CHAPTER 6.

FINAL DISCUSSION

CHAPTER 6.
FINAL DISCUSSION

6.1. Final Discussion – SPCA

SPCA provides Ca^{2+} to the Golgi apparatus by acting as a Ca^{2+}-ATPase specific to this organelle. The luminal Ca^{2+} supply of the Golgi apparatus is required for the modulation of activities from its contents of Ca^{2+}-dependent enzymes, which play a role in post-translational modification of proteins en-route through the secretory pathway. Secreted proteins potentially cannot function correctly without there being Ca^{2+} present and its levels precisely regulated by SPCA in the Golgi apparatus. This is demonstrated in the form of HHD in human skin pathology, which is caused by mutations in the ATP2C1 gene that encodes SPCA. Recently, changes in SPCA expression levels have also been suggested to contribute to diabetes (Mitchell et al., 2004) and neurodegenerative diseases (Sepulveda et al., 2007).

SPCA1 has now been demonstrated to be sensitive to glucose homeostasis in VSMCs, whereby experimental glucose concentrations used to resemble those in tissues in the diabetic condition were able to increase both the expression and activity levels of this Ca^{2+}-ATPase. How this occurs has not been elucidated, but one possibility is that SPCA1 expression levels can be altered by the glycosylation of its transcription factors. The observation of SPCA1 being sensitive to glucose levels in VSMCs fits well with the secretory phenotype of VSMCs in the diabetic disease state. If SPCA1 expression and activity is also affected in the same way in diabetic humans, this could provide a novel drug target for treatment of this condition.

Known inhibitors of SPCA now include TFP, TBBPA, 2-APB and BPA. Here it has been demonstrated that bis-phenol is the most potent inhibitor of human SPCA (isoform 1d) because it is effective at sub-micromolar concentrations and can inhibit 100% activity of SPCA without affecting human SERCA (isoform 2b) activity at the same concentrations. With the knowledge of how bis-phenol is believed to affect SERCA and the kinetic differences between these two Ca^{2+}-ATPases, it is possible to suggest bis-phenol inhibits SPCA better than SERCA because it binds to the E2 conformation with stronger affinity in SPCA. Studies on the binding kinetics of bis-

phenol for SPCA will be required to ascertain this. The concentration of bis-phenol effective at specifically inhibiting SPCA in intact cells needs to be optimised. It remains promising that bis-phenol can be used as a tool for future research on SPCA and possibly be used as a template for drug design for diseases associated with SPCA, such as diabetes (as suggested above).

6.2. Final Discussion – RGN

The importance of RGN in Ca^{2+} homeostasis has been debated. Past studies have demonstrated its ability to affect the activities of proteins involved in Ca^{2+} signalling, including Ca^{2+}-ATPases, at the cytosol and even in organelles that store Ca^{2+} (nucleus and mitochondria). RGN has also been suggested to have other roles, including DNA-binding (Tsurusaki and Yamaguchi, 2004) and controlling oxidative stress (Ichikawa and Yamaguchi, 2004). It was research associated with RGN's role in vitamin C biosynthesis by acting as a gluconolactonase that brought up the argument against RGN's ability to bind Ca^{2+}. However, RGN is expressed in organisms that do not synthesise their own supply of vitamin C, including humans. RGN was first demonstrated to be able to bind Ca^{2+} (using early biochemical methods) at the same time it was presented as a novel protein. The Ca^{2+}-binding role of RGN has also recently been elucidated from its crystal structure, along with its K_d for Ca^{2+}-binding (0.57mM) taking away the debate of whether or not it can bind Ca^{2+}. However, this low affinity for Ca^{2+}-binding indicates this role of RGN is not important in resting cells when in the cytosol.

It has now been further emphasised that RGN is not expressed in all tissue types. To add to this observation, it has also been suggested that RGN mRNA and protein levels in rat testis may not directly correlate with each other due to a possible difference in their turnover rates, and that RGN expression in this tissue type may be age-dependent like in liver, kidney, heart and brain. Further studies on RGN expression in testicular tissue will be required to ascertain this. As RGN expression does occur in a number of different specialised cell types of the male reproductive system (in addition to testes and prostate), it could be involved in male fertility and therefore requires further research.

To add to the support of RGN having a role in Ca^{2+} homeostasis, it has now been shown that RGN can influence Ca^{2+} mobilisation in cells and is likely to do so by acting on SERCA. RGN over-expression experiments using COS-7 cells also indicate that RGN could be increasing SERCA expression levels, by acting to enhance transcription or remove gene repressor activity. Further studies will be required to refine the details behind RGN's ability to apparently increase the capacity of ER Ca^{2+} stores and weaken Ca^{2+}-mediated responses to hormone stimulation.

6.3. Final Discussion – Future Studies on SPCA & RGN

The research that has been discussed here in detail has explored SPCA's role in Ca^{2+} homeostasis, with regards to its ability to regulate Ca^{2+}-mediated hormone response (by providing the Golgi apparatus with a thapsigargin-insensitive releaseable Ca^{2+} store) in VSMCs under experimental conditions that mimic the diabetic state. For SPCA, the work discussed here has also shown its own activity can be specifically regulated, with the use of bis-phenol, in experimental systems that include the presence of the closely related SERCA. Though there are still plenty of questions that can be asked about the regulation of SPCA activity, which is an area of research that has yet to be fully explored. How is SPCA activity controlled endogenously in the cell? NAADP and cADPR have now been shown to not have any direct effects on SPCA. Other second messengers and even proteins, such as phospholamban and calmodulin, should also be tried in the future to see whether they regulate SPCA activity in the same way that they do for SERCA and PMCA, respectively. Can SPCA be post-translationally modified by, for example, by phosphorylation or nitrosylation?

In the present study, the expression of RGN mRNA has now been shown for the first time in specialised cell types of the male reproductive system. RGN's influence of Ca^{2+}-mediated hormone response in intact cells has also now been demonstrated for the first time. Furthermore, both a recombinant rat RGN and anti-RGN antibody are now made available for future use. The former can be used to further explore the folding kinetics of RGN and, if successfully folded, can be used to demonstrate whether or not it can directly interact with proteins involved in Ca^{2+} homeostasis through direct binding experiments. The latter can be used to screen more samples from different cell and tissue types that have still yet to be tested for their ability to

express RGN in an age-dependent manner, as well as be used in experiments such as affinity chromatography and pull-down assays to purify RGN and study its ability to bind other proteins or be post-translationally modified. RGN's ability to directly interact with other proteins or be subject to post-translational modification has yet to be demonstrated in past publications.

Another point of interest with RGN is its role in humans. RGN is known to participate in vitamin C synthesis as a gluconolactonase in mice. However, humans have been shown to express RGN even though they do not synthesise their own vitamin C. So what is the role of RGN in humans? RGN has been demonstrated to have the ability to function as a gluconolactonase (Kondo et al., 2006) and thus this enzymatic activity of RGN may still be relevant in humans, though not for the purpose of vitamin C synthesis. The present study with human RGN showed it can control intracellular Ca^{2+} stores when abundantly expressed, which may make an important contributor to the age-dependent loss of control in Ca^{2+} homeostasis that has been well documented in past studies (Periasamy and Kalyanasundaram, 2007). However, this is an activity of RGN that is unlikely to require its ability to act as a gluconolactonase.

Where RGN's enzymatic activity would fit in and be of use in humans is in the pentose phosphate pathway, where there is a possibility that it is the equivalent of a 6-phosphogluconolactonase that has been described previously to be expressed in human erythrocytes (Bauer et al., 1983). Its molecular weight has been determined to be approximately 31kDa and its isoelectric point is pH 6.0, which are both features very similar to those of RGN. 6-phosphogluconolactonase hydrolyses 6-phosphoglucono-δ-lactone to 6-phosphogluconate, which is a reaction that is the second step of the hexose monophosphate shunt and part of the pentose phosphate pathway (Moir and Stokes, 1988). It is also a reaction similar to that catalysed by RGN, which is the hydrolysis of D-glucono-δ-lactone to gluconic acid. Hence RGN potentially plays a role in supporting NADPH production, which would fit well with the anti-oxidative effects of RGN that have been noted in mice. This will have to be tested in the future with enzymatic experiments using human RGN and 6-phosphoglucono-δ-lactone, although it should be noted that recombinant human RGN

has been previously shown to be able to hydrolyse D-glucono-δ-lactone (Chakraborti and Bahnson, 2010).

The effects of over-expressing human RGN on SERCA protein levels shown in the present study also indicate another possible role for RGN. It has been suggested in the past that RGN can alter the expression levels of other proteins, such as L-type Ca^{2+} channel (Nakagawa and Yamaguchi, 2006), PI3K (Nakashima and Yamaguchi, 2007), p53 (Tsurusaki and Yamaguchi, 2004) and leptin (Yamaguchi and Nakagawa, 2007). Co-incidentally, RGN's six-β-propeller structure strongly resembles that of three gene transcription repressor proteins, Tup1 (Sprague et al., 2000), UNC-37 (Pflugrad et al., 1997) and Keap1 (Padmanabhan et al., 2008). From this, it can be suggested that RGN may alter the expression of some proteins by acting as a gene transcription repressor, which may or may not be a function that would be linked to its ability to bind Ca^{2+}, and future experiments with RGN will be needed to explore this possibility further.

LIST OF REFERENCES

LIST OF REFERENCES

AKHTER, T., NAKAGAWA, T., KOBAYASHI, A. & YAMAGUCHI, M. 2007. Suppression of regucalcin mRNA expression in the hearts of rats administered with free radical compound: The administration-induced death is accelerated in regucalcin transgenic rats. *International Journal of Molecular Medicine,* 19**,** 653-658.

AL-BADER, M. D. & AL-SARRAF, H. A. 2005. Housekeeping gene expression during fetal brain development in the rat - validation by semi-quantitative RT-PCR. *Developmental Brain Research,* 156**,** 38-45.

ANDERSEN, J. P., SORENSEN, T. L. M., POVLSEN, K. & VILSEN, B. 2001. Importance of transmembrane segment M3 of the sarcoplasmic reticulum Ca2+-ATPase for control of the gateway to the Ca2+ sites. *Journal of Biological Chemistry,* 276**,** 23312-23321.

ANTEBI, A. & FINK, G. R. 1992. THE YEAST CA-2+-ATPASE HOMOLOG, PMR1, IS REQUIRED FOR NORMAL GOLGI FUNCTION AND LOCALIZES IN A NOVEL GOLGI-LIKE DISTRIBUTION. *Molecular Biology of the Cell,* 3**,** 633-654.

APELL, H. J. 2004. How do P-type ATPases transport ions? *Bioelectrochemistry,* 63**,** 149-156.

ARAI, K. Y., SATO, Y., KONDO, Y., KUDO, C., TSUCHIYA, H., NOMURA, Y., ISHIGAMI, A. & NISHIYAMA, T. 2009. Effects of vitamin C deficiency on the skin of the senescence marker protein-30 (SMP30) knockout mouse. *Biochemical and Biophysical Research Communications,* 385**,** 478-483.

ARCHER, S. L. 1996. Diversity of phenotype and function of vascular smooth muscle cells. *J Lab Clin Med,* 127**,** 524-9.

ARONSON, D. 2008. Hyperglycemia and the pathobiology of diabetic complications. *Cardiovascular Diabetology: Clinical, Metabolic and Inflammatory Facets.* Basel: Karger.

BADMINTON, M. N., CAMPBELL, A. K. & REMBOLD, C. M. 1996. Differential regulation of nuclear and cytosolic Ca2+ in HeLa cells. *Journal of Biological Chemistry,* 271**,** 31210-31214.

BAILEY, K. 1942. Myosin and adenosinetriphosphatase. *Biochemical Journal,* 36**,** 121-139.

BARBAGALLO, M., SHAN, J., PANG, P. K. T. & RESNICK, L. M. 1995. GLUCOSE-INDUCED ALTERATIONS OF CYTOSOLIC-FREE CALCIUM IN CULTURED RAT TAIL ARTERY VASCULAR SMOOTH-MUSCLE CELLS. *Journal of Clinical Investigation,* 95**,** 763-767.

BARON, S., STRUYF, S., WUYTACK, F., VAN DAMME, J., MISSIAEN, L., RAEYMAEKERS, L. & VANOEVELEN, J. 2009. Contribution of intracellular Ca(2+) stores to Ca(2+) signaling during chemokinesis of human neutrophil granulocytes. *Biochim Biophys Acta,* 1793**,** 1041-9.

BAUER, H. P., SRIHARI, T., JOCHIMS, J. C. & HOFER, H. W. 1983. 6-PHOSPHOGLUCONOLACTONASE - PURIFICATION, PROPERTIES AND ACTIVITIES IN VARIOUS TISSUES. *European Journal of Biochemistry,* 133, 163-168.

BAUMRUCKER, C. R. & KEENAN, T. W. 1975. MEMBRANES OF MAMMARY-GLAND .10. ADENOSINE-TRIPHOSPHATE DEPENDENT CALCIUM ACCUMULATION BY GOLGI APPARATUS RICH FRACTIONS FROM BOVINE MAMMARY-GLAND. *Experimental Cell Research,* 90**,** 253-260.

BEHNE, M. J., TU, C. L., ARONCHIK, I., EPSTEIN, E., BENCH, G., BIKLE, D. D., POZZAN, T. & MAURO, T. M. 2003. Human keratinocyte ATP2C1 localizes to the Golgi and controls Golgi Ca2+ stores. *Journal of Investigative Dermatology,* 121**,** 688-694.

BENEDECZ.I, SMITH, A. D. & DUBOIS, F. 1972. CYTOCHEMICAL STUDY OF CALCIUM-ACTIVATED ADENOSINE-TRIPHOSPHATASE IN HAMSTER ADRENAL-MEDULLA - ITS OCCURRENCE IN GOLGI REGION OF CHROMAFFIN CELLS. *Histochemie,* 29**,** 16-&.

BENTIVOGLIO, M. 1998. 1898: The Golgi apparatus emerges from nerve cells. *Trends in Neurosciences,* 21**,** 195-200.

BERRIDGE, M. J. 2006. Calcium microdomains: Organization and function. *Cell Calcium,* 40**,** 405-412.

BERRIDGE, M. J., BOOTMAN, M. D. & RODERICK, H. L. 2003. Calcium signalling: Dynamics, homeostasis and remodelling. *Nature Reviews Molecular Cell Biology,* 4**,** 517-529.

BILMEN, J. G., WOOTTON, L. L., GODFREY, R. E., SMART, O. S. & MICHELANGELI, F. 2002. Inhibition of SERCA Ca2+ pumps by 2-aminoethoxydiphenyl borate (2-APB) - 2-APB reduces both Ca2+ binding and phosphoryl transfer from ATP, by interfering with the pathway leading to the Ca2+-binding sites. *European Journal of Biochemistry,* 269, 3678-3687.

BOOTMAN, M. D., COLLINS, T. J., PEPPIATT, C. M., PROTHERO, L. S., MACKENZIE, L., DE SMET, P., TRAVERS, M., TOVEY, S. C., SEO, J. T., BERRIDGE, M. J., CICCOLINI, F. & LIPP, P. 2001. Calcium signalling - an overview. *Seminars in Cell & Developmental Biology,* 12**,** 3-10.

BREITBART, H. 2002. Intracellular calcium regulation in sperm capacitation and acrosomal reaction. *Molecular and Cellular Endocrinology,* 187**,** 139-144.

BRINI, M. 2009. Plasma membrane Ca2+-ATPase: from a housekeeping function to a versatile signaling role. *Pflugers Archiv-European Journal of Physiology,* 457**,** 657-664.

BROWN, G. R., BENYON, S. L., KIRK, C. J., WICTOME, M., EAST, J. M., LEE, A. G. & MICHELANGELI, F. 1994. CHARACTERIZATION OF A NOVEL CA2+ PUMP INHIBITOR (BIS-PHENOL) AND ITS EFFECTS ON INTRACELLULAR CA2+ MOBILIZATION. *Biochimica Et Biophysica Acta-Biomembranes,* 1195**,** 252-258.

BROWN, G. R., SAYERS, L. G., KIRK, C. J., MICHELL, R. H. & MICHELANGELI, F. 1992. THE OPENING OF THE INOSITOL 1,4,5-TRISPHOSPHATE-SENSITIVE CA2+ CHANNEL IN RAT CEREBELLUM IS INHIBITED BY CAFFEINE. *Biochemical Journal,* 282**,** 309-312.

BURDAKOV, D., PETERSEN, O. H. & VERKHRATSKY, A. 2005. Intraluminal calcium as a primary regulator of endoplasmic reticulum function. *Cell Calcium,* 38**,** 303-310.

BYRON, K. L. & TAYLOR, C. W. 1995. VASOPRESSIN STIMULATION OF CA2+ MOBILIZATION, 2 BIVALENT CATION ENTRY PATHWAYS AND CA2+ EFFLUX IN A7R5 RAT SMOOTH-MUSCLE CELLS. *Journal of Physiology-London,* 485**,** 455-468.

CALCRAFT, P. J., RUAS, M., PAN, Z., CHENG, X. T., ARREDOUANI, A., HAO, X. M., TANG, J. S., RIETDORF, K., TEBOUL, L., CHUANG, K. T., LIN, P. H., XIAO, R., WANG, C. B., ZHU, Y. M., LIN, Y. K., WYATT, C. N., PARRINGTON, J., MA, J. J., EVANS, A. M., GALIONE, A. & ZHU, M. X. 2009. NAADP mobilizes calcium from acidic organelles through two-pore channels. *Nature,* 459**,** 596-U130.

CALLEWAERT, G., PARYS, J. B., DE SMEDT, H., RAEYMAEKERS, L., WUYTACK, F., VANOEVELEN, J., VAN BAELEN, K., SIMONI, A., RIZZUTO, R. & MISSIAEN, L. 2003. Similar Ca2+-signaling properties in keratinocytes and in COS-1 cells overexpressing the secretory-pathway Ca2+-ATPase SPCA1. *Cell Calcium,* 34**,** 157-162.

CARAFOLI, E. 2002. Calcium signaling: A tale for all seasons. *Proceedings of the National Academy of Sciences of the United States of America,* 99**,** 1115-1122.

CHAKRABORTI, S. & BAHNSON, B. J. 2010. Crystal Structure of Human Senescence Marker Protein 30: Insights Linking Structural, Enzymatic, and Physiological Functions. *Biochemistry,* 49**,** 3436-3444.

CHO, J. H., KO, K. M., SINGARAVELU, G. & AHNN, J. 2005. Caenorhabditis elegans PMR1, a P-type calcium ATPase, is important for calcium/manganese homeostasis and oxidative stress response. *Febs Letters,* 579**,** 778-782.

CHOI, K. J., KIM, K. S., KIM, S. H., KIM, D. K. & PARK, H. S. 2010a. Caffeine and 2-Aminoethoxydiphenyl Borate (2-APB) Have Different Ability to Inhibit Intracellular Calcium Mobilization in Pancreatic Acinar Cell. *Korean Journal of Physiology & Pharmacology,* 14, 105-111.

CHOI, M. S., SAXENA, A. & CHILUKURI, N. 2010b. A strategy for the production of soluble human senescence marker protein-30 in Escherichia coli. *Biochem Biophys Res Commun,* 393**,** 509-13.

COHEN, P., KLEE, C. B., PICTON, C. & SHENOLIKAR, S. 1980. Calcium control of muscle phosphorylase kinase through the combined action of calmodulin and troponin. *Ann N Y Acad Sci,* 356**,** 151-61.

COPELLO, J. A., QI, Y., JEYAKUMAR, L. H., OGUNBUNMI, E. & FLEISCHER, S. 2001. Lack of effect of cADP-ribose and NAADP on the activity of skeletal muscle and heart ryanodine receptors. *Cell Calcium,* 30, 269-284.

CUNNINGHAM, K. W. & FINK, G. R. 1994. CA2+ TRANSPORT IN SACCHAROMYCES-CEREVISIAE. *Journal of Experimental Biology,* 196**,** 157-166.

CUNNINGHAM, K. W. & FINK, G. R. 1996. Calcineurin inhibits VCX1-dependent H+/Ca2+ exchange and induces Ca2+ ATPases in Saccharomyces cerevisiae. *Molecular and Cellular Biology,* 16**,** 2226-2237.

DARGIE, P. J., AGRE, M. C. & LEE, H. C. 1990. COMPARISON OF CA-2+ MOBILIZING ACTIVITIES OF CYCLIC ADP-RIBOSE AND INOSITOL TRISPHOSPHATE. *Cell Regulation,* 1, 279-290.

DE CRESCENZO, V., ZHUGE, R. H., VELAZQUEZ-MARRERO, C., LIFSHITZ, L. M., CUSTER, E., CARMICHAEL, J., LAI, F. A., TUFT, R. A., FOGARTY, K. E., LEMOS, J. R. & WALSH, J. V. 2004. Ca2+ syntillas, miniature Ca2+ release events in terminals of hypothalamic neurons, are increased in frequency by depolarization in the absence of Ca2+ influx. *Journal of Neuroscience,* 24**,** 1226-1235.

DE MATTEIS, M. A., DI CAMPLI, A. & GODI, A. 2005. The role of the phosphoinositides at the Golgi complex. *Biochimica Et Biophysica Acta-Molecular Cell Research,* 1744**,** 396-405.

DELUCA, H. F. & ENGSTROM, G. W. 1961. CALCIUM UPTAKE BY RAT KIDNEY MITOCHONDRIA. *Proceedings of the National Academy of Sciences of the United States of America,* 47**,** 1744-&.

DHITAVAT, J., DODE, L., LESLIE, N., SAKUNTABHAI, A., LORETTE, G. & HOVNANIAN, A. 2003. Mutations in the sarcoplasmic/endoplasmic reticulum Ca2+ ATPase isoform cause Darier's disease. *Journal of Investigative Dermatology,* 121**,** 486-489.

DI NAPOLI, P., CHIERCHIA, S., TACCARDI, A. A., GRILLI, A., FELACO, M., DE CATERINA, R. & BARSOTTI, A. 2007. Trimetazidine improves post-ischemic recovery by preserving endothelial nitric oxide synthase expression in isolated working rat hearts. *Nitric Oxide-Biology and Chemistry,* 16**,** 228-236.

DMITRIEV, R. I., PESTOV, N. B., KORNEENKO, T. V., SOROKINA, E. S., KAZMIN, A. A., KOSTINA, M. B. & SHAKHPARONOV, M. I. 2003. Liver SPCA, a secretory pathway Ca2+-ATPase, is predominantly localized in plasma membrane. *Biologicheskie Membrany,* 20**,** 480-485.

DOBSON-STONE, C., FAIRCLOUGH, R. E., DUNNE, E., BROWN, J., DISSANAYAKE, M., MUNRO, C. S., STRACHAN, T., BURGE, S., SUDBRAK, R., MONACO, A. P. & HOFNANIAN, A. 2002. Hailey-Hailey disease: Molecular and clinical characterization of novel mutations in the ATP2C1 gene. *Journal of Investigative Dermatology,* 118**,** 338-343.

DODE, L., ANDERSEN, J. P., RAEYMAEKERS, L., MISSIAEN, L., VILSEN, B. & WUYTACK, F. 2005. Functional comparison between secretory pathway Ca2+/Mn2+-ATPase (SPCA) 1 and sarcoplasmic reticulum Ca2+-ATPase (SERCA) 1 isoforms by steady-state and transient kinetic analyses. *Journal of Biological Chemistry,* 280**,** 39124-39134.

DODE, L., ANDERSEN, J. P., VANOEVELEN, J., RAEYMAEKERS, L., MISSIAEN, L., VILSEN, B. & WUYTACK, F. 2006. Dissection of the functional differences between human secretory pathway Ca2+/Mn2+-ATPase (SPCA) 1 and 2 isoenzymes by steady-state and transient kinetic analyses. *Journal of Biological Chemistry,* 281**,** 3182-3189.

DOLMAN, N. J. & TEPIKIN, A. V. 2006. Calcium gradients and the Golgi. *Cell Calcium,* 40**,** 505-512.

DONOHOE, B. S., MOGELSVANG, S. & STAEHELIN, L. A. 2006. Electron tomography of ER, Golgi and related membrane systems. *Methods,* 39**,** 154-162.

DORAN, P., DOWLING, P., DONOGHUE, P., BUFFINI, M. & OHLENDIECK, K. 2006. Reduced expression of regucalcin in young and aged mdx diaphragm indicates abnormal cytosolic calcium handling in dystrophin-deficient muscle. *Biochimica Et Biophysica Acta-Proteins and Proteomics,* 1764**,** 773-785.

DROSCHER, A. 1998. The history of the Golgi apparatus in neurones from its discovery in 1898 to electron microscopy. *Brain Research Bulletin,* 47**,** 199-203.

DUCHEN, M. R., VERKHRATSKY, A. & MUALLEM, S. 2008. Mitochondria and calcium in health and disease. *Cell Calcium,* 44**,** 1-5.

DURR, G., STRAYLE, J., PLEMPER, R., ELBS, S., KLEE, S. K., CATTY, P., WOLF, D. H. & RUDOLPH, H. K. 1998. The medial-Golgi ion pump Pmr1 supplies the yeast secretory pathway with Ca2+ and Mn2+ required for glycosylation, sorting, and endoplasmic reticulum associated protein degradation. *Molecular Biology of the Cell,* 9**,** 1149-1162.

EBASHI, S. 1961. CALCIUM BINDING ACTIVITY OF VESICULAR RELAXING FACTOR. *Journal of Biochemistry,* 50**,** 236-&.

ENGELENDER, S. & DEMEIS, L. 1996. Pharmacological differentiation between intracellular calcium pump isoforms. *Molecular Pharmacology,* 50, 1243-1252.

FAIRCLOUGH, R. J., DODE, L., VANOEVELEN, J., ANDERSEN, J. P., MISSIAEN, L., RAEYMAEKERS, L., WUYTACK, F. & HOVNANIAN, A. 2003. Effect of Hailey-Hailey disease mutations on the function of a new variant of human secretory pathway Ca2+/Mn2+-ATPase (hSPCA1). *Journal of Biological Chemistry,* 278**,** 24721-24730.

FLEISCHHACKER, E., ESENABHALU, V. E., SPITALER, M., HOLZMANN, S., SKRABAL, F., KOIDL, B., KOSTNER, G. M. & GRAIER, W. F. 1999. Human

diabetes is associated with hyperreactivity of vascular smooth muscle cells due to altered subcellular Ca2+ distribution. *Diabetes,* 48**,** 1323-1330.
FREEDMAN, R. A., WEISER, M. M. & ISSELBACHER, K. J. 1977. CALCIUM TRANSLOCATION BY GOLGI AND LATERAL-BASAL MEMBRANE-VESICLES FROM RAT INTESTINE - DECREASE IN VITAMIN D-DEFICIENT RATS. *Proceedings of the National Academy of Sciences of the United States of America,* 74**,** 3612-3616.
FUJITA, T. 1999. Senescence marker protein-30 (SMP30): Structure and biological function. *Biochemical and Biophysical Research Communications,* 254**,** 1-4.
FUJITA, T., INOUE, H., KITAMURA, T., SATO, N., SHIMOSAWA, T. & MARUYAMA, N. 1998. Senecence marker protein-30 (SMP30) rescues cell death by enhancing plasma membrane Ca2+ pumping activity in Hep G2 cells. *Hepatology,* 28**,** 636.
FUJITA, T., MANDEL, J. L., SHIRASAWA, T., HINO, O., SHIRAI, T. & MARUYAMA, N. 1995. ISOLATION OF CDNA CLONE ENCODING HUMAN HOMOLOG OF SENESCENCE MARKER PROTEIN-30 (SMP30) AND ITS LOCATION ON THE X-CHROMOSOME. *Biochimica Et Biophysica Acta-Gene Structure and Expression,* 1263**,** 249-252.
FUJITA, T., UCHIDA, K. & MARUYAMA, N. 1992. PURIFICATION OF SENESCENCE MARKER PROTEIN-30 (SMP30) AND ITS ANDROGEN-INDEPENDENT DECREASE WITH AGE IN THE RAT-LIVER. *Biochimica Et Biophysica Acta,* 1116**,** 122-128.
GALIONE, A. & CHURCHILL, G. C. 2002. Interactions between calcium release pathways: multiple messengers and multiple stores. *Cell Calcium,* 32, 343-354.
GERASIMENKO, J. V., SHERWOOD, M., TEPIKIN, A. V., PETERSEN, O. H. & GERASIMENKO, O. V. 2006. NAADP, cADPR and IP3 all release Ca2+ from the endoplasmic reticulum and an acidic store in the secretory granule area. *Journal of Cell Science,* 119, 226-238.
GOMES, D. A., LEITE, M. F., BENNETT, A. M. & NATHANSON, M. H. 2006. Calcium signaling in the nucleus. *Canadian Journal of Physiology and Pharmacology,* 84**,** 325-332.
GUNARATNE, H. J. & VACQUIER, V. D. 2006. Evidence for a secretory pathway Ca2+-ATPase in sea urchin spermatozoa. *Febs Letters,* 580**,** 3900-3904.
GUNTESKI-HAMBLIN, A. M., CLARKE, D. M. & SHULL, G. E. 1992. MOLECULAR-CLONING AND TISSUE DISTRIBUTION OF ALTERNATIVELY SPLICED MESSENGER-RNAS ENCODING POSSIBLE MAMMALIAN HOMOLOGS OF THE YEAST SECRETORY PATHWAY CALCIUM-PUMP. *Biochemistry,* 31**,** 7600-7608.
HAMANO, T. & YAMAGUCHI, M. 2001. Inhibitory role of regucalcin in the regulation of Ca2+-dependent protein kinases activity in rat brain neurons. *Journal of the Neurological Sciences,* 183**,** 33-38.
HAN, I. & KUDLOW, J. E. 1997. Reduced O glycosylation of Sp1 is associated with increased proteasome susceptibility. *Molecular and Cellular Biology,* 17**,** 2550-2558.
HANAHISA, Y. & YAMAGUCHI, M. 2001. Decrease in Ca2+-ATPase activity in the brain plasma membrane of rats with increasing age: Involvement of brain calcium accumulation. *International Journal of Molecular Medicine,* 7**,** 407-411.
HANDA, S., MARUYAMA, N. & ISHIGAMI, A. 2009. Over-expression of Senescence Marker Protein-30 Decreases Reactive Oxygen Species in Human Hepatic Carcinoma Hep G2 Cells. *Biological & Pharmaceutical Bulletin,* 32**,** 1645-1648.
HARPER, C., WOOTTON, L., MICHELANGELI, F., LEFIEVRE, L., BARRATT, C. & PUBLICOVER, S. 2005. Secretory pathway Ca2+-ATPase (SPCA1) Ca2+

pumps, not SERCAs, regulate complex [Ca2+], signals in human spermatozoa. *Journal of Cell Science,* 118**,** 1673-1685.

HASEGAWA, G., YAMASAKI, M., KADONO, M., TANAKA, M., ASANO, M., SENMARU, T., KONDO, Y., FUKUI, M., OBAYASHI, H., MARUYAMA, N., NAKAMURA, N. & ISHIGAMI, A. 2010. Senescence Marker Protein-30/Gluconolactonase Deletion Worsens Glucose Tolerance through Impairment of Acute Insulin Secretion. *Endocrinology,* 151**,** 529-536.

HICKS, S. W. & MACHAMER, C. E. 2005. Golgi structure in stress sensing and apoptosis. *Biochimica Et Biophysica Acta-Molecular Cell Research,* 1744**,** 406-414.

HIROMURA, M., CHOI, C. H., SABOURIN, N. A., JONES, H., BACHVAROV, D. & USHEVA, A. 2003. YY1 is regulated by O-linked N-acetylglucosaminylation (O-GlcNAcylation). *Journal of Biological Chemistry,* 278**,** 14046-14052.

HOKIN, L. E. 1966. EFFECTS OF CALCIUM OMISSION ON ACETYLCHOLINE-STIMULATED AMYLASE SECRETION AND PHOSPHOLIPID SYNTHESIS IN PIGEON PANCREAS SLICES. *Biochimica Et Biophysica Acta,* 115**,** 219-&.

HU, Z. L., BONIFAS, J. M., BEECH, J., BENCH, G., SHIGIHARA, T., OGAWA, H., IKEDA, S., MAURO, T. & EPSTEIN, E. H. 2000. Mutations in ATP2C1, encoding a calcium pump, cause Hailey-Hailey disease. *Nature Genetics,* 24**,** 61-65.

HUGHES, P. J., MCLELLAN, H., LOWES, D. A., KHAN, S. Z., BILMEN, J. G., TOVEY, S. C., GODFREY, R. E., MICHELL, R. H., KIRK, C. J. & MICHELANGELI, F. 2000. Estrogenic alkylphenols induce cell death by inhibiting testis endoplasmic reticulum Ca2+ pumps. *Biochemical and Biophysical Research Communications,* 277, 568-574.

ICHIKAWA, E., TSURUSAKI, Y. & YAMAGUCHI, M. 2004. Suppressive effect of regucalcin on protein phosphatase activity in the heart cytosol of normal and regucalcin transgenic rats. *International Journal of Molecular Medicine,* 13**,** 289-293.

ICHIKAWA, E. & YAMAGUCHI, M. 2004. Regucalcin increases superoxide dismutase activity in the heart cytosol of normal and regucalcin transgenic rats. *International Journal of Molecular Medicine,* 14**,** 691-695.

IIDA, H. & PAGE, E. 1989. Localization of wheat-germ agglutinin-binding sites in the Golgi complex of cultured rat atrial myocytes. *Cell Tissue Res,* 257**,** 325-31.

IKEDA, S., WELSH, E. A., PELUSO, A. M., LEYDEN, W., DUVIC, M., WOODLEY, D. T. & EPSTEIN, E. H. 1994. LOCALIZATION OF THE GENE WHOSE MUTATIONS UNDERLIE HAILEY-HAILEY DISEASE TO CHROMOSOME. *Human Molecular Genetics,* 3**,** 1147-1150.

INAGAKI, S. & YAMAGUCHI, M. 2000. Enhancement of protein tyrosine phosphatase activity in the proliferation of cloned rat hepatoma H4-II-E cells: Suppressive role of endogenous regucalcin. *International Journal of Molecular Medicine,* 6**,** 323-328.

ISHIGAMI, A., FUJITA, T., HANDA, S., SHIRASAWA, T., KOSEKI, H., KITAMURA, T., ENOMOTO, N., SATO, N., SHIMOSAWA, T. & MARUYAMA, N. 2002. Senescence marker protein-30 knockout mouse liver is highly susceptible to tumor necrosis factor-alpha- and Fas-mediated apoptosis. *American Journal of Pathology,* 161**,** 1273-1281.

ISHIGAMI, A., HANDA, S., MARUYAMA, N. & SUPAKAR, P. C. 2003. Nuclear localization of senescence marker protein-30, SMP30, in cultured mouse Hepatocytes and its similarity to RNA polymerase. *Bioscience Biotechnology and Biochemistry,* 67**,** 158-160.

ISHIGAMI, A., KONDO, Y., NANBA, R., OHSAWA, T., HANDA, S., KUBO, S., AKITA, M. & MARUYAMA, N. 2004. SMP30 deficiency in mice causes an accumulation of neutral lipids and phospholipids in the liver and shortens the life span. *Biochemical and Biophysical Research Communications,* 315**,** 575-580.

ISOGAI, M., KUROTA, H. & YAMAGUCHI, M. 1997. Hepatic calcium-binding protein regucalcin concentration is decreased by streptozotocin-diabetic state and ethanol ingestion in rats. *Molecular and Cellular Biochemistry,* 168**,** 67-72.

JAAG, H. M., POGANY, J. & NAGY, P. D. 2010. A Host Ca2+/Mn2+ Ion Pump Is a Factor in the Emergence of Viral RNA Recombinants. *Cell Host & Microbe,* 7**,** 74-81.

JEONG, D. H., GOO, M. J., HONG, I. H., YANG, H. J., KI, M. R., DO, S. H., HA, J. H., LEE, S. S., PARK, J. K. & JEONG, K. S. 2008. Inhibition of Radiation-Induced Apoptosis via Overexpression of SMP30 in Smad3-Knockout Mice Liver. *Journal of Radiation Research,* 49**,** 653-660.

KASHIO, A., AMANO, A., KONDO, Y., SAKAMOTO, T., IWAMURA, H., SUZUKI, M., ISHIGAMI, A. & YAMASOBA, T. 2009. Effect of vitamin C depletion on age-related hearing loss in SMP30/GNL knockout mice. *Biochemical and Biophysical Research Communications,* 390**,** 394-398.

KATSUMATA, T. & YAMAGUCHI, M. 1998. Inhibitory effect of calcium-binding protein regucalcin on protein kinase activity in the nuclei of regenerating rat liver. *Journal of Cellular Biochemistry,* 71**,** 569-576.

KAWADA, H., NISHIYAMA, C., TAKAGI, A., TOKURA, T., NAKANO, N., MAEDA, K., MAYUZUMI, N., IKEDA, S., OKUMURA, K. & OGAWA, H. 2005. Transcriptional regulation of ATP2C1 gene by Sp1 and YY1 and reduced function of its promoter in Hailey-Hailey disease keratinocytes. *Journal of Investigative Dermatology,* 124**,** 1206-1214.

KIRK, C. J., BOTTOMLEY, L., MINICAN, N., CARPENTER, H., SHAW, S., KOHLI, N., WINTER, M., TAYLOR, E. W., WARING, R. H., MICHELANGELI, F. & HARRIS, R. A. 2003. Environmental endocrine disrupters dysregulate estrogen metabolism and Ca2+ homeostasis in fish and mammals via receptor-independent mechanisms. *Comparative Biochemistry and Physiology a-Molecular & Integrative Physiology,* 135, 1-8.

KLEIN, R. L., THURESON.A & YEN, S. S. 1972. CRITIQUE ON K-PYROANTIMONATE METHOD FOR SEMIQUANTITATIVE ESTIMATION OF CATIONS IN CONJUNCTION WITH ELECTRON-MICROSCOPY. *Journal of Histochemistry & Cytochemistry,* 20**,** 65-&.

KOIKE, K., KONDO, Y., SEKIYA, M., SATO, Y., TOBINO, K., IWAKAMI, S., GOTO, S., TAKAHASHI, K., MARUYAMA, N., SEYAMA, K. & ISHIGAMI, A. 2010. Complete lack of vitamin C intake generates pulmonary emphysema in senescence marker protein-30 knockout mice. *American Journal of Physiology-Lung Cellular and Molecular Physiology,* 298**,** L784-L792.

KONDO, Y., INAI, Y., SATO, Y., HANDA, S., KUBO, S., SHIMOKADO, K., GOTO, S., NISHIKIMI, M., MARUYAMA, N. & ISHIGAMI, A. 2006. Senescence marker protein 30 functions as gluconolactonase in L-ascorbic acid biosynthesis, and its knockout mice are prone to scurvy. *Proceedings of the National Academy of Sciences of the United States of America,* 103**,** 5723-5728.

KONDO, Y., ISHIGAMI, A., KUBO, S., HANDA, S., GOMI, K., HIROKAWA, K., KAJIYAMA, N., CHIBA, T., SHIMOKADO, K. & MARUYAMA, N. 2004. Senescence marker protein-30 is a unique enzyme that hydrolyzes diisopropyl phosphorofluoridate in the liver. *FEBS Lett,* 570**,** 57-62.

KONDO, Y., SASAKI, T., SATO, Y., AMANO, A., AIZAWA, S., IWAMA, M., HANDA, S., SHIMADA, N., FUKUDA, M., AKITA, M., LEE, J., JEONG, K.

S., MARUYAMA, N. & ISHIGAMI, A. 2008. Vitamin C depletion increases superoxide generation in brains of SMP30/GNL knockout mice. *Biochemical and Biophysical Research Communications,* 377**,** 291-296.

KUROTA, H. & YAMAGUCHI, M. 1996. Steroid hormonal regulation of calcium-binding protein regucalcin mRNA expression in the kidney cortex of rats. *Molecular and Cellular Biochemistry,* 155**,** 105-111.

KUROTA, H. & YAMAGUCHI, M. 1997. Regucalcin increases Ca2+-ATPase activity and ATP-dependent calcium uptake in the microsomes of rat kidney cortex. *Molecular and Cellular Biochemistry,* 177**,** 201-207.

LANINI, L., BACHS, O. & CARAFOLI, E. 1992. THE CALCIUM-PUMP OF THE LIVER NUCLEAR-MEMBRANE IS IDENTICAL TO THAT OF ENDOPLASMIC-RETICULUM. *Journal of Biological Chemistry,* 267**,** 11548-11552.

LAPINSKAS, P. J., CUNNINGHAM, K. W., LIU, X. F., FINK, G. R. & CULOTTA, C. 1995. MUTATIONS IN PMR1 SUPPRESS OXIDATIVE DAMAGE IN YEAST-CELLS LACKING SUPEROXIDE-DISMUTASE. *Molecular and Cellular Biology,* 15**,** 1382-1388.

LEE, A. G. 1998. How lipids interact with an intrinsic membrane protein: The case of the calcium pump. *In Search of a New Biomembrane Model,* 49**,** 115-120.

LEE, H. C. & AARHUS, R. 1995. A DERIVATIVE OF NADP MOBILIZES CALCIUM STORES INSENSITIVE TO INOSITOL TRISPHOSPHATE AND CYCLIC ADP-RIBOSE. *Journal of Biological Chemistry,* 270, 2152-2157.

LEV, S. Year. Lipid homoeostasis and Golgi secretory function. *In:* Biochemical-Society Focused Meeting, Dec 15-16 2005 London, ENGLAND. Portland Press Ltd, 363-366.

LEVY, J. 1999. Abnormal cell calcium homeostasis in type 2 diabetes mellitus - A new look on old disease. *Endocrine,* 10**,** 1-6.

LIM, S., SONG, B. W., CHA, M. J., CHOI, E. J., HAM, O., LEE, C. Y., CHOI, S. Y., LEE, S. Y., JANG, Y. & HWANG, K. C. 2009. Differential Expression of Regucalcin (SMP30) and Its Function in Hypoxic Cardiomyocytes. *Tissue Engineering and Regenerative Medicine,* 6**,** 1273-1281.

LISSANDRON, V., PODINI, P., PIZZO, P. & POZZAN, T. 2010. Unique characteristics of Ca2+ homeostasis of the trans-Golgi compartment. *Proceedings of the National Academy of Sciences of the United States of America,* 107**,** 9198-9203.

LUKYANENKO, V., GYORKE, I., WIESNER, T. F. & GYORKE, S. 2001. Potentiation of Ca2+ release by cADP-ribose in the heart is mediated by enhanced SR Ca2+ uptake into the sarcoplasmic reticulum. *Circulation Research,* 89, 614-622

MA, Z. J. & YAMAGUCHI, M. 2002. Suppressive role of endogenous regucalcin in the regulation of nitric oxide synthase activity in heart muscle cytosol of normal and regucalcin transgenic rats. *International Journal of Molecular Medicine,* 10**,** 761-766.

MACGREGOR, A., YAMASAKI, M., RAKOVIC, S., SANDERS, L., PARKESH, R., CHURCHILL, G. C., GALIONE, A. & TERRAR, D. A. 2007. NAADP controls cross-talk between distinct Ca2+ stores in the heart. *Journal of Biological Chemistry,* 282, 15302-15311.

MAIA, C., SANTOS, C., SCHMITT, F. & SOCORRO, S. 2009. Regucalcin is under-expressed in human breast and prostate cancers: Effect of sex steroid hormones. *J Cell Biochem*.

MAIA, C. J. B., SANTOS, C. R., SCHMITT, F. & SOCORRO, S. 2008. Regucalcin is expressed in rat mammary gland and prostate and down-regulated by 17 beta-estradiol. *Molecular and Cellular Biochemistry,* 311**,** 81-86.

MANDAL, D., WOOLF, T. B. & RAO, R. 2000. Manganese selectivity of Pmr1, the yeast secretory pathway ion pump, is defined by residue Gln(783) in transmembrane segment 6 - Residue Asp(778) is essential for cation transport. *Journal of Biological Chemistry,* 275**,** 23933-23938.

MARSH, B. J. & HOWELL, K. E. 2002. The mammalian Golgi - complex debates. *Nature Reviews Molecular Cell Biology,* 3**,** 789-795.

MATHEOS, D. P., KINGSBURY, T. J., AHSAN, U. S. & CUNNINGHAM, K. W. 1997. Tcn1p/Crz1p a calcineurin-dependent transcription factor that differentially regulates gene expression in Saccharomyces cerevisiae. *Genes & Development,* 11**,** 3445-3458.

MAZZONE, T., CHAIT, A. & PLUTZKY, J. 2008. Cardiovascular disease risk in type 2 diabetes mellitus: insights from mechanistic studies. *Lancet,* 371**,** 1800-1809.

MCINTOSH, D. B., WOOLLEY, D. G., VILSEN, B. & ANDERSEN, J. P. 1996. Mutagenesis of segment (487)Phe-Ser-Arg-Asp-Arg-Lys(492) of sarcoplasmic reticulum Ca2+-ATPase produces pumps defective in ATP binding. *Journal of Biological Chemistry,* 271**,** 25778-25789.

MICHELANGELI, F., COLYER, J., EAST, J. M. & LEE, A. G. 1990. EFFECT OF PH ON THE ACTIVITY OF THE CA-2++MG-2+-ACTIVATED ATPASE OF SARCOPLASMIC-RETICULUM. *Biochemical Journal,* 267**,** 423-429.

MICHELANGELI, F., DIVIRGILIO, F., VILLA, A., PODINI, P., MELDOLESI, J. & POZZAN, T. 1991. IDENTIFICATION, KINETIC-PROPERTIES AND INTRACELLULAR-LOCALIZATION OF THE (CA2+-MG2+)-ATPASE FROM THE INTRACELLULAR STORES OF CHICKEN CEREBELLUM. *Biochemical Journal,* 275**,** 555-561.

MICHELANGELI, F., OGUNBAYO, O. A. & WOOTTON, L. L. 2005. A plethora of interacting organellar Ca2+ stores. *Current Opinion in Cell Biology,* 17**,** 135-140.

MISAWA, H., INAGAKI, S. & YAMAGUCHI, M. 2001. Suppression of cell proliferation and deoxyribonucleic acid synthesis in cloned rat hepatoma H4-II-E cells overexpressing regucalcin. *Journal of Cellular Biochemistry,* 84**,** 143-149.

MISAWA, H. & YAMAGUCHI, M. 2000a. The gene of Ca2+-binding protein regucalcin is highly conserved in vertebrate species. *International Journal of Molecular Medicine,* 6**,** 191-196.

MISAWA, H. & YAMAGUCHI, M. 2000b. Transcript heterogeneity of the human gene for Ca2+-binding protein regucalcin. *International Journal of Molecular Medicine,* 5**,** 283-287.

MISAWA, H. & YAMAGUCHI, M. 2001. Molecular cloning and sequencing of the cDNA coding for a novel regucalcin gene promoter region-related protein in rat, mouse and human liver. *International Journal of Molecular Medicine,* 8**,** 513-520.

MISAWA, H. & YAMAGUCHI, M. 2002. Gene expression for a novel protein RGPR-p117 in various species: The stimulation by intracellular signaling factors. *Journal of Cellular Biochemistry,* 87**,** 188-193.

MISSIAEN, L., VAN ACKER, K., PARYS, J. B., DE SMEDT, H., VAN BAELEN, K., WEIDEMA, A. F., VANOEVELEN, J., RAEYMAEKERS, L., RENDERS, J., CALLEWAERT, G., RIZZUTO, R. & WUYTACK, F. 2001. Baseline cytosolic Ca2+ oscillations derived from a non-endoplasmic reticulum Ca2+ store. *Journal of Biological Chemistry,* 276**,** 39161-39170.

MISSIAEN, L., VANOEVELEN, J., PARYS, J. B., RAEYMAEKERS, L., DE SMEDT, H., CALLEWAERT, G., ERNEUX, C. & WUYTACK, F. 2002. Ca2+ uptake and release properties of a thapsigargin-insensitive nonmitochondrial Ca2+ store in A7r5 and 16HBE14o-cells. *Journal of Biological Chemistry,* 277**,** 6898-6902.

MITCHELL, K. J., TSUBOI, T. & RUTTER, G. A. 2004. Role for plasma membrane-related Ca2+-ATPase-1 (ATP2C1) in pancreatic beta-cell Ca2+ homeostasis revealed by RNA silencing. *Diabetes,* 53**,** 393-400.

MOGELSVANG, S., MARSH, B. J., LADINSKY, M. S. & HOWELL, K. E. 2004. Predicting function from structure: 3D structure studies of the mammalian Golgi complex. *Traffic,* 5**,** 338-345.

MOIR, R. D. & STOKES, G. B. 1988. A SPECTROPHOTOMETRIC ASSAY FOR 6-PHOSPHOGLUCONOLACTONASE INVOLVING THE USE OF IMMOBILIZED ENZYMES TO PREPARE THE LABILE 6-PHOSPHOGLUCONO-DELTA-LACTONE SUBSTRATE. *Biochemical Journal,* 256, 69-73.

MOLLER, J. V., JUUL, B. & LEMAIRE, M. 1996. Structural organization, ion transport, and energy transduction of P-type ATPases. *Biochimica Et Biophysica Acta-Reviews on Biomembranes,* 1286**,** 1-51.

MOLLER, J. V., NISSEN, P., SORENSEN, T. L. M. & LE MAIRE, M. 2005. Transport mechanism of the sarcoplasmic reticulum Ca2+-ATPase pump. *Current Opinion in Structural Biology,* 15**,** 387-393.

MORI, T., ISHIGAMI, A., SEYAMA, K., ONAI, R., KUBO, S., SHIMIZU, K., MARUYAMA, N. & FUKUCHI, Y. 2004. Senescence marker protein-30 knockout mouse as a novel murine model of senile lung. *Pathology International,* 54**,** 167-173.

MOROOKA, Y. & YAMAGUCHI, M. 2002. Suppressive effect of endogenous regucalcin on deoxyribonuclic acid synthesis in the nuclei of rat renal cortex. *Molecular and Cellular Biochemistry,* 229**,** 157-162.

MULLER-TAUBENBERGER, A. & ANDERSON, K. I. 2007. Recent advances using green and red fluorescent protein variants. *Appl Microbiol Biotechnol,* 77, 1-12.

MURATA, T. & YAMAGUCHI, M. 1998. Ca2+ administration stimulates the binding of AP-1 factor to the 5 '-flanking region of the rat gene for the Ca2+-binding protein regucalcin. *Biochemical Journal,* 329**,** 157-163.

MURATA, T. & YAMAGUCHI, M. 1999. Promoter characterization of the rat gene for Ca2+-binding protein regucalcin - Transcriptional regulation by signaling factors. *Journal of Biological Chemistry,* 274**,** 1277-1285.

NAKAGAWA, T. & YAMAGUCHI, M. 2006. Overexpression of regucalcin enhances its nuclear localization and suppresses L-type Ca2+ channel and calcium-sensing receptor mRNA expressions in cloned normal rat kidney proximal tubular epithelial NRK52E cells. *Journal of Cellular Biochemistry,* 99**,** 1064-1077.

NAKAGAWA, T. & YAMAGUCHI, M. 2008. Nuclear localization of regucalcin is enhanced in culture with protein kinase C activation in cloned normal rat kidney proximal tubular epithelial NRK52E cells. *International Journal of Molecular Medicine,* 21**,** 605-610.

NAKASHIMA, C. & YAMAGUCHI, M. 2007. Overexpression of regucalcin suppresses gene expression of insulin signaling-related proteins in cloned rat hepatoma H4-II-E cells: Involvement of insulin resistance. *International Journal of Molecular Medicine,* 20**,** 709-716.

NAORA, H., MIRSKY, A. E. & ALLFREY, V. G. 1961. MAGNESIUM AND CALCIUM IN ISOLATED CELL NUCLEI. *Journal of General Physiology,* 44**,** 713-&.

NICOTERA, P., MCCONKEY, D. J., JONES, D. P. & ORRENIUS, S. 1989. ATP STIMULATES CA-2+ UPTAKE AND INCREASES THE FREE CA-2+ CONCENTRATION IN ISOLATED RAT-LIVER NUCLEI. *Proceedings of the National Academy of Sciences of the United States of America,* 86**,** 453-457.

OGUNBAYO, O. A., LAI, P. F., CONNOLLY, T. J. & MICHELANGELI, F. 2008. Tetrabromobisphenol A (TBBPA), induces cell death in TM4 Sertoli cells by modulating Ca2+ transport proteins and causing dysregulation of Ca2+ homeostasis. *Toxicology in Vitro,* 22**,** 943-952.

OGUNBAYO, O. A. & MICHELANGELI, F. 2007. The widely utilized brominated flame retardant tetrabromobisphenol A (TBBPA) is a potent inhibitor of the SERCA Ca2+ pump. *Biochemical Journal,* 408, 407-415.

OKUNADE, G. W., MILLER, M. L., AZHAR, M., ANDRINGA, A., SANFORD, L. P., DOETSCHMAN, T., PRASAD, V. & SHULL, G. E. 2007. Loss of the Atp2c1 secretory pathway Ca2+-ATPase (SPCA1) in mice causes golgi stress, apoptosis, and midgestational death in homozygous embryos and squamous cell tumors in adult Heterozygotes. *Journal of Biological Chemistry,* 282, 26517-26527.

OMURA, M. & YAMAGUCHI, M. 1998. Inhibition of Ca2+/calmodulin-dependent phosphatase activity by regucalcin in rat liver cytosol: Involvement of calmodulin binding. *Journal of Cellular Biochemistry,* 71**,** 140-148.

OMURA, M. & YAMAGUCHI, M. 1999. Regulation of protein phosphatase activity by regucalcin localization in rat liver nuclei. *Journal of Cellular Biochemistry,* 75**,** 437-445.

ORRENIUS, S., ZHIVOTOVSKY, B. & NICOTERA, P. 2003. Regulation of cell death: The calcium-apoptosis link. *Nature Reviews Molecular Cell Biology,* 4**,** 552-565.

OWENS, G. K., LOEB, A., GORDON, D. & THOMPSON, M. M. 1986. EXPRESSION OF SMOOTH-MUSCLE SPECIFIC ALPHA-ISOACTIN IN CULTURED VASCULAR SMOOTH-MUSCLE CELLS - RELATIONSHIP BETWEEN GROWTH AND CYTODIFFERENTIATION. *Journal of Cell Biology,* 102**,** 343-352.

PADMANABHAN, B., TONG, K. I., KOBAYASHI, A., YAMAMOTO, M. & YOKOYAMA, S. 2008. Structural insights into the similar modes of Nrf2 transcription factor recognition by the cytoplasmic repressor Keap1. *Journal of Synchrotron Radiation,* 15**,** 273-276.

PARK, J. K., KI, M. R., LEE, H. R., HONG, I. H., JI, A. R., ISHIGAMI, A., PARK, S. I., KIM, J. M., CHUNG, H. Y., YOO, S. E. & JEONG, K. S. 2010. Vitamin C Deficiency Attenuates Liver Fibrosis by Way of Up-regulated Peroxisome Proliferator-Activated Receptor-gamma Expression in Senescence Marker Protein 30 Knockout Mice. *Hepatology,* 51**,** 1766-1777.

PAVLIKOVA, M., TATARKOVA, Z., SIVONOVA, M., KAPLAN, P., KRIZANOVA, O. & LEHOTSKY, J. 2009. Alterations Induced by Ischemic Preconditioning on Secretory Pathways Ca(2+)-ATPase (SPCA) Gene Expression and Oxidative Damage After Global Cerebral Ischemia/Reperfusion in Rats. *Cell Mol Neurobiol*.

PEPPIATT, C. M., COLLINS, T. J., MACKENZIE, L., CONWAY, S. J., HOLMES, A. B., BOOTMAN, M. D., BERRIDGE, M. J., SEO, J. T. & RODERICK, H. L. 2003. 2-Aminoethoxydiphenyl borate (2-APB) antagonises inositol 1,4,5-trisphosphate-induced calcium release, inhibits calcium pumps and has a use-dependent and slowly reversible action on store-operated calcium entry channels. *Cell Calcium,* 34, 97-108.

PERIASAMY, M. & KALYANASUNDARAM, A. 2007. SERCA pump isoforms: Their role in calcium transport and disease. *Muscle & Nerve,* 35**,** 430-442.

PETERSEN, O. H., SUTTON, R. & CRIDDLE, D. N. 2006. Failure of calcium microdomain generation and pathological consequences. *Cell Calcium,* 40**,** 593-600.

PFLUGRAD, A., MEIR, J. Y. J., BARNES, T. M. & MILLER, D. M. 1997. The Groucho-like transcription factor UNC-37 functions with the neural specificity

gene unc-4 to govern motor neuron identity in C-elegans. *Development,* 124**,** 1699-1709.
PINTON, P., POZZAN, T. & RIZZUTO, R. 1998. The Golgi apparatus is an inositol 1,4,5-trisphosphate-sensitive Ca2+ store, with functional properties distinct from those of the endoplasmic reticulum. *Embo Journal,* 17**,** 5298-5308.
RADER, D. J. & DAUGHERTY, A. 2008. Translating molecular discoveries into new therapies for atherosclerosis. *Nature,* 451**,** 904-13.
RAMOS-CASTANEDA, J., PARK, Y. N., LIU, M., HAUSER, K., RUDOLPH, H., SHULL, G. E., JONKMAN, M. F., MORI, K., IKEDA, S., OGAWA, H. & ARVAN, P. 2005. Deficiency of ATP2C1, a golgi ion pump, induces secretory pathway defects in endoplasmic reticulum (ER)-associated degradation and sensitivity to ER stress. *Journal of Biological Chemistry,* 280**,** 9467-9473.
RANDALL, R. D. & THAYER, S. A. 1992. GLUTAMATE-INDUCED CALCIUM TRANSIENT TRIGGERS DELAYED CALCIUM OVERLOAD AND NEUROTOXICITY IN RAT HIPPOCAMPAL-NEURONS. *Journal of Neuroscience,* 12**,** 1882-1895.
RATH, B., PANDEY, R. S., DEBATA, P. R., MARUYAMA, N. & SUPAKAR, P. C. 2008. Molecular characterization of senescence marker protein-30 gene promoter: Identification of repressor elements and functional nuclear factor binding sites. *Bmc Molecular Biology,* 9.
RAYCHAUDHURY, B., GUPTA, S., BANERJEE, S. & DATTA, S. C. 2006. Peroxisome is a reservoir of intracellular calcium. *Biochimica Et Biophysica Acta-General Subjects,* 1760**,** 989-992.
REINHARDT, T. A., FILOTEO, A. G., PENNISTON, J. T. & HORST, R. L. 2000. Ca2+-ATPase protein expression in mammary tissue. *American Journal of Physiology-Cell Physiology,* 279**,** C1595-C1602.
REINHARDT, T. A., HORST, R. L. & WATERS, W. R. 2004. Characterization of Cos-7 cells overexpressing the rat secretory pathway Ca2+-ATPase. *American Journal of Physiology-Cell Physiology,* 286**,** C164-C169.
REINHARDT, T. A. & HORST, R. L. 1999. Ca2+-ATPases and their expression in the mammary gland of pregnant and lactating rats. *American Journal of Physiology-Cell Physiology,* 276, C796-C802.
REINHARDT, T. A. & LIPPOLIS, J. D. 2009. Mammary gland involution is associated with rapid down regulation of major mammary Ca2+-ATPases. *Biochemical and Biophysical Research Communications,* 378**,** 99-102.
RENSEN, S. S., DOEVENDANS, P. A. & VAN EYS, G. J. 2007. Regulation and characteristics of vascular smooth muscle cell phenotypic diversity. *Neth Heart J,* 15**,** 100-8.
RIZZUTO, R. & POZZAN, T. 2006. Microdomains of intracellular Ca2+: Molecular determinants and functional consequences. *Physiological Reviews,* 86**,** 369-408.
ROTH, S. I. & RAISZ, L. G. 1964. EFFECT OF CALCIUM CONCENTRATION ON ULTRASTRUCTURE OF RAT PARATHYROID IN ORGAN CULTURE. *Laboratory Investigation,* 13**,** 331-&.
RUDOLPH, H. K., ANTEBI, A., FINK, G. R., BUCKLEY, C. M., DORMAN, T. E., LEVITRE, J., DAVIDOW, L. S., MAO, J. & MOIR, D. T. 1989. THE YEAST SECRETORY PATHWAY IS PERTURBED BY MUTATIONS IN PMR1, A MEMBER OF A CA-2+ ATPASE FAMILY. *Cell,* 58**,** 133-145.
SAKUNTABHAI, A., BURGE, S., MONK, S. & HOVNANIAN, A. 1999. Spectrum of novel ATP2A2 mutations in patients with Darier's disease. *Human Molecular Genetics,* 8**,** 1611-1619.

SAR, P., RATH, B., SUBUDHI, U., CHAINY, G. B. N. & SUPAKAR, P. C. 2007. Alterations in expression of senescence marker protein-30 gene by 3,3 ',5-triiodo-L-thyronine (T-3). *Molecular and Cellular Biochemistry,* 303**,** 239-242.

SATO, T., SEYAMA, K., SATO, Y., MORI, H., SOUMA, S., AKIYOSHI, T., KODAMA, Y., MORI, T., GOTO, S., TAKAHASHI, K., FUKUCHI, Y., MANUYAMA, N. & ISHIGAMI, A. 2006. Senescence marker protein-30 protects mice lungs from oxidative stress, aging, and smoking. *American Journal of Respiratory and Critical Care Medicine,* 174**,** 530-537.

SAWADA, N. & YAMAGUCHI, M. 2005. A novel regucalcin gene promoter region-related protein: Comparison of nucleotide and amino acid sequences in vertebrate species. *International Journal of Molecular Medicine,* 15**,** 97-104.

SCHATZMA.HJ 1973. DEPENDENCE ON CALCIUM CONCENTRATION AND STOICHIOMETRY OF CALCIUM-PUMP IN HUMAN RED-CELLS. *Journal of Physiology-London,* 235**,** 551-569.

SELINGER, Z., NAIM, E. & LASSER, M. 1970. ATP-DEPENDENT CALCIUM UPTAKE BY MICROSOMAL PREPARATIONS FROM RAT PAROTID AND SUBMAXILLARY GLANDS. *Biochimica Et Biophysica Acta,* 203**,** 326-&.

SEPULVEDA, M. R., BERROCAL, M., MARCOS, D., WUYTACK, F. & MATA, A. M. 2007. Functional and immunocytochemical evidence for the expression and localization of the secretory pathway Ca2+-ATPase isoform 1 (SPCA1) in cerebellum relative to other Ca2+ pumps. *Journal of Neurochemistry,* 103**,** 1009-1018.

SEPULVEDA, M. R., MARCOS, D., BERROCAL, M., RAEYMAEKERS, L., MATA, A. M. & WUYTACK, F. 2008. Activity and localization of the Secretory Pathway Ca2+-ATPase isoform 1 (SPCA1) in different areas of the mouse brain during postnatal development. *Molecular and Cellular Neuroscience,* 38**,** 461-473.

SEPULVEDA, M. R., VANOEVELEN, J., RAEYMAEKERS, L., MATA, A. M. & WUYTACK, F. 2009. Silencing the SPCA1 (Secretory Pathway Ca2+-ATPase Isoform 1) Impairs Ca2+ Homeostasis in the Golgi and Disturbs Neural Polarity. *Journal of Neuroscience,* 29**,** 12174-12182.

SERRANO, R., KIELLANDBRANDT, M. C. & FINK, G. R. 1986. YEAST PLASMA-MEMBRANE ATPASE IS ESSENTIAL FOR GROWTH AND HAS HOMOLOGY WITH (NA++K+), K+- AND CA-2+-ATPASES. *Nature,* 319**,** 689-693.

SHAHBAZI, S., LENTING, P. J., FRIBOURG, C., TERRAUBE, V., DENIS, C. V. & CHRISTOPHE, O. D. 2007. Characterization of the interaction between von Willebrand factor and osteoprotegerin. *Journal of Thrombosis and Haemostasis,* 5**,** 1956-1962.

SHIGEKAWA, M., DOUGHERTY, J. P. & KATZ, A. M. 1978. REACTION MECHANISM OF CALCIUM ION DEPENDENT ATP HYDROLYSIS BY SKELETAL MUSCLE SARCOPLASMIC RETICULUM IN THE ABSENCE OF ADDED ALKALI METAL SALTS PART 1 CHARACTERIZATION OF STEADY-STATE ATP HYDROLYSIS AND COMPARISON WITH THAT IN THE PRESENCE OF POTASSIUM CHLORIDE. *Journal of Biological Chemistry,* 253**,** 1442-1450.

SHIMOKAWA, N., ISOGAI, M. & YAMAGUCHI, M. 1995. SPECIFIC SPECIES AND TISSUE DIFFERENCES FOR THE GENE-EXPRESSION OF CALCIUM-BINDING PROTEIN REGUCALCIN. *Molecular and Cellular Biochemistry,* 143**,** 67-71.

SINGARAVELU, K. & DEITMER, J. W. 2006. Calcium mobilization by nicotinic acid adenine dinucleotide phosphate (NAADP) in rat astrocytes. *Cell Calcium,* 39, 143-153.

SLOMIANY, A., GRABSKA, M., SLOMIANY, B. A., GRZELINSKA, E., MORITA, M. & SLOMIANY, B. L. 1993. INTRACELLULAR-TRANSPORT, ORGANELLE BIOGENESIS AND ESTABLISHMENT OF GOLGI IDENTITY - IMPACT OF BREFELDIN-A ON THE ACTIVITY OF LIPID SYNTHESIZING ENZYMES. *International Journal of Biochemistry,* 25**,** 891-901.

SOKOLOVE, P. M., ALBUQUERQUE, E. X., KAUFFMAN, F. C., SPANDE, T. F. & DALY, J. W. 1986. PHENOLIC ANTIOXIDANTS - POTENT INHIBITORS OF THE (CA-2++MG-2+)-ATPASE OF SARCOPLASMIC-RETICULUM. *Febs Letters,* 203, 121-126.

SON, T. G., KIM, S. J., KIM, K., KIM, M. S., CHUNG, H. Y. & LEE, J. 2008. Cytoprotective roles of senescence marker protein 30 against intracellular calcium elevation and oxidative stress. *Archives of Pharmacal Research,* 31**,** 872-877.

SON, T. G., PARK, H. R., KIM, S. J., KIM, K., KIM, M. S., ISHIGAMI, A., HANDA, S., MARUYAMA, N., CHUNG, H. Y. & LEE, J. 2009. Senescence Marker Protein 30 Is Up-Regulated in Kainate-Induced Hippocampal Damage Through ERK-Mediated Astrocytosis. *Journal of Neuroscience Research,* 87**,** 2890-2897.

SON, T. G., ZOU, Y. N., JUNG, K. J., YU, B. P., ISHIGAMI, A., MARUYAMA, N. & LEE, J. 2006. SMP30 deficiency causes increased oxidative stress in brain. *Mechanisms of Ageing and Development,* 127**,** 451-457.

SORIN, A., ROSAS, G. & RAO, R. 1997. PMR1, a Ca2+-ATPase in yeast Golgi, has properties distinct from sarco/endoplasmic reticulum and plasma membrane calcium pumps. *Journal of Biological Chemistry,* 272**,** 9895-9901.

SOUTHALL, T. D., TERHZAZ, S., CABRERO, P., CHINTAPALLI, V. R., EVANS, J. M., DOW, J. A. T. & DAVIES, S. A. 2006. Novel subcellular locations and functions for secretory pathway Ca2+/Mn2+-ATPases. *Physiological Genomics,* 26**,** 35-45.

SPRAGUE, E. R., REDD, M. J., JOHNSON, A. D. & WOLBERGER, C. 2000. Structure of the C-terminal domain of Tup1, a corepressor of transcription in yeast. *Embo Journal,* 19**,** 3016-3027.

STALKER, T. J., GONG, Y. L. & SCALIA, R. 2005. The calcium-dependent protease calpain causes endothelial dysfunction in type 2 diabetes. *Diabetes,* 54**,** 1132-1140.

STEEN, M., KIRCHBERGER, T. & GUSE, A. H. 2007. NAADP mobilizes calcium from the endoplasmic reticular Ca2+ store in T-lymphocytes. *Journal of Biological Chemistry,* 282, 18864-18871.

STOKES, D. L. & GREEN, N. M. 2003. Structure and function of the calcium pump. *Annual Review of Biophysics and Biomolecular Structure,* 32**,** 445-468.

SUDBRAK, R., BROWN, J., DOBSON-STONE, C., CARTER, S., RAMSER, J., WHITE, J., HEALY, E., DISSANAYAKE, M., LARREGUE, M., PERRUSSEL, M., LEHRACH, H., MUNRO, C. S., STRACHAN, T., BURGE, S., HOVNANIAN, A. & MONACO, A. P. 2000. Hailey-Hailey disease is caused by mutations in ATP2C1 encoding a novel Ca2+ pump. *Human Molecular Genetics,* 9**,** 1131-1140.

SUN, L. W., WANG, L., SUN, Y., TANG, S. W. & HU, Y. H. 2006. Protective effects of EUK4010 on beta-amyloid(1-42) induced degeneration of neuronal cells. *European Journal of Neuroscience,* 24**,** 1011-1019.

SWULIUS, M. T. & WAXHAM, M. N. 2008. Ca2+/calmodulin-dependent protein kinases. *Cellular and Molecular Life Sciences,* 65**,** 2637-2657.

SZIGETI, R., MISETA, A. & KELLERMAYER, R. 2005. Calcium and magnesium competitively influence the growth of a PMR1 deficient Saccharomyces cerevisiae strain. *Fems Microbiology Letters,* 251**,** 333-339.
SZYMANSKI, E. S. & FARRELL, H. M. 1982. ISOLATION AND SOLUBILIZATION OF CASEIN KINASE FROM GOLGI-APPARATUS OF BOVINE MAMMARY-GLAND AND PHOSPHORYLATION OF PEPTIDES. *Biochimica Et Biophysica Acta,* 702**,** 163-172.
TAKAHASHI, H. & YAMAGUCHI, M. 1994. ACTIVATING EFFECT OF REGUCALCIN ON (CA2+-MG2+)- ATPASE IN RAT-LIVER PLASMA-MEMBRANES - RELATION TO SULFHYDRYL-GROUP. *Molecular and Cellular Biochemistry,* 136**,** 71-76.
TAKAHASHI, H. & YAMAGUCHI, M. 1999. Role of regucalcin as an activator of Ca2+-ATPase activity in rat liver microsomes. *Journal of Cellular Biochemistry,* 74**,** 663-669.
TAKAHASHI, H. & YAMAGUCHI, M. 2000. Stimulatory effect of regucalcin on ATP-dependent Ca2+ uptake activity in rat liver mitochondria. *Journal of Cellular Biochemistry,* 78**,** 121-130.
TAKAHASHI, H. & YAMAGUCHI, M. 2001. Activatory effect of regucalcin on GTPase activity in rat liver plasma membranes. *Molecular and Cellular Biochemistry,* 224**,** 117-122.
TAKAKUWA, Y. & KANAZAWA, T. 1981a. REACTION-MECHANISM OF (CA2+,MG2+)-ATPASE OF SARCOPLASMIC-RETICULUM VESICLES .1. PHOSPHOENZYME WITH BOUND CA2+ WHICH IS EXPOSED TO THE EXTERNAL MEDIUM. *Journal of Biological Chemistry,* 256**,** 2691-2695.
TAKAKUWA, Y. & KANAZAWA, T. 1981b. REACTION-MECHANISM OF (CA2+,MG2+)-ATPASE OF SARCOPLASMIC-RETICULUM VESICLES .2. (ATP,ADP)-DEPENDENT CA2+-CA2+ EXCHANGE ACROSS THE MEMBRANES. *Journal of Biological Chemistry,* 256**,** 2696-2700.
TAYLOR, R. S., JONES, S. M., DAHL, R. H., NORDEEN, M. H. & HOWELL, K. E. 1997. Characterization of the Golgi complex cleared of proteins in transit and examination of calcium uptake activities. *Molecular Biology of the Cell,* 8**,** 1911-1931.
TESHIMA, Y., TAKAHASHI, N., SAIKAWA, T., HARA, M., YASUNAGA, S., HIDAKA, S. & SAKATA, T. 2000. Diminished expression of sarcoplasmic reticulum Ca2+-ATPase and ryanodine sensitive Ca2+ channel mRNA in streptozotocin-induced diabetic rat heart. *Journal of Molecular and Cellular Cardiology,* 32**,** 655-664.
TEUNISSEN, B. E. J., JANSEN, A. T., VAN AMERSFOORTH, S. C. M., O'BRIEN, T. X., JONGSMA, H. J. & BIERHUIZEN, M. F. A. 2003. Analysis of the rat connexin 43 proximal promoter in neonatal cardiomyocytes. *Gene,* 322**,** 123-136.
THYBERG, J. 1998. Tyrphostin A9 and wortmannin perturb the Golgi complex and block proliferation of vascular smooth muscle cells. *European Journal of Cell Biology,* 76**,** 33-42.
THYBERG, J., HEDIN, U., SJOLUND, M., PALMBERG, L. & BOTTGER, B. A. 1990. Regulation of differentiated properties and proliferation of arterial smooth muscle cells. *Arteriosclerosis,* 10**,** 966-90.
TOBISAWA, M. & YAMAGUCHI, M. 2003. Role of endogenous regucalcin in brain function: Suppression of cytosolic nitric oxide synthase and nuclear protein tyrosine phosphatase activities in brain tissue of transgenic rats. *International Journal of Molecular Medicine,* 12**,** 581-585.
TOMONO, S., SAWADA, N. & YAMAGUCHI, M. 2007. Overexpression of RGPR-p117 induces the decrease in protein and DNA contents in cloned normal rat

kidney proximal tubular epithelial NRK52E cells. *International Journal of Molecular Medicine,* 20**,** 79-83.
TON, V. K., MANDAL, D., VAHADJI, C. & RAO, R. 2002. Functional expression in yeast of the human secretory pathway Ca2+, Mn2+-ATPase defective in Hailey-Hailey disease. *Journal of Biological Chemistry,* 277**,** 6422-6427.
TONG, X., YING, J., PIMENTEL, D. R., TRUCILLO, M., ADACHI, T. & COHEN, R. A. 2008. High glucose oxidizes SERCA cysteine-674 and prevents inhibition by nitric oxide of smooth muscle cell migration. *Journal of Molecular and Cellular Cardiology,* 44**,** 361-369.
TOVEY, S. C., LONGLAND, C. L., MEZNA, M. & MICHELANGELI, F. 1998. 2-Hydroxycarbazole induces Ca2+ release from sarcoplasmic reticulum by activating the ryanodine receptor. *European Journal of Pharmacology,* 354**,** 245-251.
TOYOSHIMA, C. 2008. Structural aspects of ion pumping by Ca2+-ATPase of sarcoplasmic reticulum. *Archives of Biochemistry and Biophysics,* 476**,** 3-11.
TOYOSHIMA, C., NAKASAKO, M., NOMURA, H. & OGAWA, H. 2000. Crystal structure of the calcium pump of sarcoplasmic reticulum at 2.6 angstrom resolution. *Nature,* 405**,** 647-655.
TRAASETH, N., ELFERING, S., SOLIEN, J., HAYNES, V. & GIULIVI, C. 2004. Role of calcium signaling in the activation of mitochondrial nitric oxide synthase and citric acid cycle. *Biochimica Et Biophysica Acta-Bioenergetics,* 1658**,** 64-71.
TSURUSAKI, Y. & YAMAGUCHI, M. 2000a. Role of endogenous regucalcin in the regualtion of Ca2+-ATPase activity in rat liver nuclei. *Journal of Cellular Biochemistry,* 78**,** 541-549.
TSURUSAKI, Y. & YAMAGUCHI, M. 2000b. Suppressive effect of endogenous regucalcin on the enhancement of protein synthesis and aminoacyl-tRNA synthetase activity in regenerating rat liver. *International Journal of Molecular Medicine,* 6**,** 295-299.
TSURUSAKI, Y. & YAMAGUCHI, M. 2004. Role of regucalcin in liver nuclear function: Binding of regucalcin to nuclear protein or DNA and modulation of tumor-related gene expression. *International Journal of Molecular Medicine,* 14**,** 277-281.
UCHIYAMA, S. & YAMAGUCHI, M. 2004. Bone loss in regucalcin transgenic rats: Enhancement of osteoclastic cell formation from bone marrow of rats with increasing age. *International Journal of Molecular Medicine,* 14**,** 451-455.
UEOKA, S. & YAMAGUCHI, M. 1998. Sexual difference of hepatic calcium-binding protein regucalcin mRNA expression in rats with different ages: Effect of ovarian hormone. *Biological & Pharmaceutical Bulletin,* 21**,** 405-407.
VAN BAELEN, K., VANOEVELEN, J., CALLEWAERT, G., PARYS, J. B., DE SMEDT, H., RAEYMAEKERS, L., RIZZUTO, R., MISSIAEN, L. & WUYTACK, F. 2003. The contribution of the SPCA1 Ca2+ pump to the Ca2+ accumulation in the Golgi apparatus of HeLa cells assessed via RNA-mediated interference. *Biochemical and Biophysical Research Communications,* 306, 430-436.
VAN BAELEN, K., VANOEVELEN, J., MISSIAEN, L., RAEYMAEKERS, L. & WUYTACK, F. 2001. The Golgi PMR1 P-type ATPase of Caenorhabditis elegans - Identification of the gene and demonstration of calcium and manganese transport. *Journal of Biological Chemistry,* 276**,** 10683-10691.
VANOEVELEN, J., DODE, L., VAN BAELEN, K., FAIRCLOUGH, R., MISSIAEN, L., WUYTACK, F. & RAEYMAEKERS, L. 2005a. ATP2C2 encodes a novel isoform of secretory pathway Ca2+-transport ATPase. *Febs Journal,* 272**,** 204-204.

VANOEVELEN, J., DODE, L., VAN BAELEN, K., FAIRCLOUGH, R. J., MISSIAEN, L., RAEYMAEKERS, L. & WUYTACK, F. 2005b. The secretory pathway Ca2+/Mn2+-ATPase 2 is a Golgi-localized pump with high affinity for Ca2+ ions. *Journal of Biological Chemistry,* 280**,** 22800-22808.

VANOEVELEN, J., RAEYMAEKERS, L., PARYS, J. B., DE SMEDT, H., VAN BAELEN, K., CALLEWAERT, G., WUYTACK, E. & MISSIAEN, L. 2004. Inositol trisphosphate producing agonists do not mobilize the thapsigargin-insensitive part of the endoplasmic-reticulum and Golgi Ca2+ store. *Cell Calcium,* 35**,** 115-121.

VARADI, A., MOLNAR, E., OSTENSON, C. G. & ASHCROFT, S. J. H. 1996. Isoforms of endoplasmic reticulum Ca2+-ATPase are differentially expressed in normal and diabetic islets of Langerhans. *Biochemical Journal,* 319**,** 521-527.

VAY, L., HERNANDEZ-SANMIGUEL, E., LOBATON, C. D., MORENO, A., MONTERO, M. & ALVAREZ, J. 2009. Mitochondrial free Ca2+ levels and the permeability transition. *Cell Calcium,* 45**,** 243-250.

VERMA, A. K., FILOTEO, A. G., STANFORD, D. R., WIEBEN, E. D., PENNISTON, J. T., STREHLER, E. E., FISCHER, R., HEIM, R., VOGEL, G., MATHEWS, S., STREHLERPAGE, M. A., JAMES, P., VORHERR, T., KREBS, J. & CARAFOLI, E. 1988. COMPLETE PRIMARY STRUCTURE OF A HUMAN-PLASMA MEMBRANE CA-2+ PUMP. *Journal of Biological Chemistry,* 263**,** 14152-14159.

VIRK, S. S., KIRK, C. J. & SHEARS, S. B. 1985. CA-2+ TRANSPORT AND CA-2+-DEPENDENT ATP HYDROLYSIS BY GOLGI VESICLES FROM LACTATING RAT MAMMARY-GLANDS. *Biochemical Journal,* 226**,** 741-748.

WAJIH, N., BORRAS, T., XUE, W., HUTSON, S. M. & WALLIN, R. 2004. Processing and transport of matrix gamma-carboxyglutamic acid protein and bone morphogenetic protein-2 in cultured human vascular smooth muscle cells - Evidence for an uptake mechanism for serum fetuin. *Journal of Biological Chemistry,* 279**,** 43052-43060.

WARIZAYA, M., KINOSHITA, T., YAMAOKA, M., SHIBATA, T., SAITO, N., NAKAJIMA, H. & FUJII, T. 2004. Expression, purification, crystallization and preliminary X-ray diffraction studies of human liver regucalcin. *Acta Crystallographica Section D-Biological Crystallography,* 60**,** 2019-2021.

WATTERS, C. D. 1984. A CA-2+-STIMULATED ADENOSINE-TRIPHOSPHATASE IN GOLGI-ENRICHED MEMBRANES OF LACTATING MURINE MAMMARY TISSUE. *Biochemical Journal,* 224**,** 39-45.

WATTERS, C. D. & NEVILLE, M. C. 1981. THE CALCIUM-STIMULATED HYDROLYSIS OF ATP BY A GOLGI-ENRICHED MEMBRANE-FRACTION FROM MURINE MAMMARY TISSUE. *Biophysical Journal,* 33**,** A299-A299.

WEBER, A., HERZ, R. & REISS, I. 1963. ON MECHANISM OF RELAXING EFFECT OF FRAGMENTED SARCOPLASMIC RETICULUM. *Journal of General Physiology,* 46**,** 679-&.

WEI, Y., CHEN, J., ROSAS, G., TOMPKINS, D. A., HOLT, P. A. & RAO, R. 2000. Phenotypic screening of mutations in Pmr1, the yeast secretory pathway Ca2+/Mn2+-ATPase, reveals residues critical for ion selectivity and transport. *Journal of Biological Chemistry,* 275**,** 23927-23932.

WEST, D. W. 1981. ENERGY-DEPENDENT CALCIUM SEQUESTRATION ACTIVITY IN A GOLGI-APPARATUS FRACTION DERIVED FROM LACTATING RAT MAMMARY-GLANDS. *Biochimica Et Biophysica Acta,* 673**,** 374-386.

WILLIAMS, R. J. P. 2006. The evolution of calcium biochemistry. *Biochimica Et Biophysica Acta-Molecular Cell Research,* 1763**,** 1139-1146.
WOOTTON, L. L., ARGENT, C. C. H., WHEATLEY, M. & MICHELANGELI, F. 2004. The expression, activity and localisation of the secretory pathway Ca2+-ATPase (SPCA1) in different mammalian tissues. *Biochimica Et Biophysica Acta-Biomembranes,* 1664**,** 189-197.
WOOTTON, L. L. & MICHELANGELI, F. 2006. The effects of the phenylalanine 256 to valine mutation on the sensitivity of sarcoplasmic/endoplasmic reticulum Ca2+ ATPase (SERCA) Ca2+ pump isoforms 1, 2, and 3 to thapsigargin and other inhibitors. *Journal of Biological Chemistry,* 281**,** 6970-6976.
WRIGHT, C. S. 1984. STRUCTURAL COMPARISON OF THE 2 DISTINCT SUGAR BINDING-SITES IN WHEAT-GERM-AGGLUTININ ISOLECTIN-II. *Journal of Molecular Biology,* 178**,** 91-104.
WUYTACK, F., RAEYMAEKERS, L. & MISSIAEN, L. 2003. PMR1/SPCA Ca2+ pumps and the role of the Golgi apparatus as a Ca2+ store. *Pflugers Archiv-European Journal of Physiology,* 446**,** 148-153.
WUYTACK, F., RAEYMAEKERS, L. & MISSIAEN, L. 2002. Molecular physiology of the SERCA and SPCA pumps. *Cell Calcium,* 32**,** 279-305.
XIANG, M. H., MOHAMALAWARI, D. & RAO, R. 2005. A novel isoform of the secretory pathway Ca2+, Mn2+-ATPase, hSPCA2, has unusual properties and is expressed in the brain. *Journal of Biological Chemistry,* 280**,** 11608-11614.
YAMAGUCHI, M. 1988. PHYSICOCHEMICAL PROPERTIES OF CALCIUM-BINDING PROTEIN ISOLATED FROM RAT-LIVER CYTOSOL - CA-2+-INDUCED CONFORMATIONAL-CHANGES. *Chemical & Pharmaceutical Bulletin,* 36**,** 286-290.
YAMAGUCHI, M. 2000a. Minireview - Role of regucalcin in calcium signaling. *Life Sciences,* 66**,** 1769-1780.
YAMAGUCHI, M. 2000b. The role of regucalcin in nuclear regulation of regenerating liver. *Biochemical and Biophysical Research Communications,* 276**,** 1-6.
YAMAGUCHI, M. 2005. Role of regucalcin in maintaining cell homeostasis and function (Review). *International Journal of Molecular Medicine,* 15**,** 371-389.
YAMAGUCHI, M. 2009. Novel protein RGPR-p117: its role as the regucalcin gene transcription factor. *Mol Cell Biochem,* 327**,** 53-63.
YAMAGUCHI, M., HANAHISA, Y. & MURATA, T. 1999. Expression of calcium-binding protein regucalcin and microsomal Ca2+-ATPase regulation in rat brain: Attenuation with increasing age. *Molecular and Cellular Biochemistry,* 200**,** 43-49.
YAMAGUCHI, M., IGARASHI, A., UCHIYAMA, S. & SAWADA, N. 2004a. Hyperlipidemia is induced in regucalcin transgenic rats with increasing age. *International Journal of Molecular Medicine,* 14**,** 647-651.
YAMAGUCHI, M. & ISOGAI, M. 1993. TISSUE CONCENTRATION OF CALCIUM-BINDING PROTEIN REGUCALCIN IN RATS BY ENZYME-LINKED IMMUNOADSORBENT ASSAY. *Molecular and Cellular Biochemistry,* 122**,** 65-68.
YAMAGUCHI, M., ISOGAI, M., KATO, S. & MORI, S. 1991. IMMUNOHISTOCHEMICAL DEMONSTRATION OF CALCIUM-BINDING PROTEIN REGUCALCIN IN THE TISSUES OF RATS - THE PROTEIN LOCALIZES IN LIVER AND BRAIN. *Chemical & Pharmaceutical Bulletin,* 39**,** 1601-1603.
YAMAGUCHI, M. & KANAYAMA, Y. 1995. ENHANCED EXPRESSION OF CALCIUM-BINDING PROTEIN REGUCALCIN MESSENGER-RNA IN REGENERATING RAT-LIVER. *Journal of Cellular Biochemistry,* 57**,** 185-190.

YAMAGUCHI, M. & KANAYAMA, Y. 1996. Calcium-binding protein regucalcin inhibits deoxyribonucleic acid synthesis in the nuclei of regenerating rat liver. *Molecular and Cellular Biochemistry,* 162**,** 121-126.

YAMAGUCHI, M., KOBAYASHI, M. & UCHIYAMA, S. 2005. Suppressive effect of regucalcin on cell differentiation and mineralization in osteoblastic MC3T3-E1 cells. *Journal of Cellular Biochemistry,* 96**,** 543-554.

YAMAGUCHI, M., MISAWA, H. & MA, Z. L. 2003a. Novel protein RGPR-p117: The gene expression in physiologic state and the binding activity to regucalcin gene promoter region in rat liver. *Journal of Cellular Biochemistry,* 88**,** 1092-1100.

YAMAGUCHI, M., MISAWA, H., UCHIYAMA, S., MOROOKA, Y. & TSURUSAKI, Y. 2002a. Role of endogenous regucalcin in bone metabolism: Bone loss is induced in regucalcin transgenic rats. *International Journal of Molecular Medicine,* 10**,** 377-383.

YAMAGUCHI, M. & MORI, S. 1989. ACTIVATION OF HEPATIC-MICROSOMAL CA-2+-ADENOSINE TRIPHOSPHATASE BY CALCIUM-BINDING PROTEIN REGUCALCIN. *Chemical & Pharmaceutical Bulletin,* 37**,** 1031-1034.

YAMAGUCHI, M. & MORI, S. 1990. INHIBITORY EFFECT OF CALCIUM-BINDING PROTEIN REGUCALCIN ON PROTEIN KINASE-C ACTIVITY IN RAT-LIVER CYTOSOL. *Biochemical Medicine and Metabolic Biology,* 43**,** 140-146.

YAMAGUCHI, M., MORI, S. & KATO, S. 1988. CALCIUM-BINDING PROTEIN REGUCALCIN IS AN ACTIVATOR OF (CA-2+-MG-2+)-ADENOSINE TRIPHOSPHATASE IN THE PLASMA-MEMBRANES OF RAT-LIVER. *Chemical & Pharmaceutical Bulletin,* 36**,** 3532-3539.

YAMAGUCHI, M., MORI, S. & SUKETA, Y. 1989. EFFECTS OF CA-2+ AND V-5+ ON GLUCOSE-6-PHOSPHATASE ACTIVITY IN RAT-LIVER MICROSOMES - THE CA-2+ EFFECT IS REVERSED BY REGUCALCIN. *Chemical & Pharmaceutical Bulletin,* 37**,** 388-390.

YAMAGUCHI, M., MOROOKA, Y., MISAWA, H., TSURUSAKI, Y. & NAKAJIMA, R. 2002b. Role of endogenous regucalcin in transgenic rats: Suppression of kidney cortex cytosolic protein phosphatase activity and enhancement of heart muscle microsomal Ca2+-ATPase activity. *Journal of Cellular Biochemistry,* 86**,** 520-529.

YAMAGUCHI, M. & NAKAGAWA, T. 2007. Change in lipid components in the adipose and liver tissues of regucalcin transgenic rats with increasing age: Suppression of leptin and adiponectin gene expression. *International Journal of Molecular Medicine,* 20**,** 323-328.

YAMAGUCHI, M. & NAKAJIMA, R. 2002. Role of regucalcin as an activator of sarcoplasmic reticulum Ca2+-ATPase activity in rat heart muscle. *Journal of Cellular Biochemistry,* 86**,** 184-193.

YAMAGUCHI, M. & NISHINA, N. 1995. CHARACTERIZATION OF REGUCALCIN EFFECT ON PROTEOLYTIC ACTIVITY IN RAT-LIVER CYTOSOL - RELATION TO CYSTEINYL-PROTEASES. *Molecular and Cellular Biochemistry,* 148**,** 67-72.

YAMAGUCHI, M. & OISHI, K. 1995. 17-BETA-ESTRADIOL STIMULATES THE EXPRESSION OF HEPATIC CALCIUM-BINDING PROTEIN REGUCALCIN MESSENGER-RNA IN RATS. *Molecular and Cellular Biochemistry,* 143**,** 137-141.

YAMAGUCHI, M., OISHI, K. & ISOGAI, M. 1995. EXPRESSION OF HEPATIC CALCIUM-BINDING PROTEIN REGUCALCIN MESSENGER-RNA IS ELEVATED BY REFEEDING OF FASTED RATS - INVOLVEMENT OF

GLUCOSE, INSULIN AND CALCIUM AS STIMULATING FACTORS. *Molecular and Cellular Biochemistry,* 142**,** 35-41.

YAMAGUCHI, M., OTOMO, Y., UCHIYAMA, S. & NAKAGAWA, T. 2008a. Hormonal regulation of regucalcin mRNA expression in osteoblastic MC3T3-E1 cells. *International Journal of Molecular Medicine,* 21**,** 771-775.

YAMAGUCHI, M. & SAKURAI, T. 1991. INHIBITORY EFFECT OF CALCIUM-BINDING PROTEIN REGUCALCIN ON CA-2+ -ACTIVATED DNA FRAGMENTATION IN RAT-LIVER NUCLEI. *Febs Letters,* 279**,** 281-284.

YAMAGUCHI, M., SAWADA, N., UCHIYAMA, S., MISAWA, H. & MA, Z. J. 2004b. Expression of regucalcin in rat bone marrow cells: Involvement of osteoclastic bone resorption in regucalcin transgenic rats. *International Journal of Molecular Medicine,* 13**,** 437-443.

YAMAGUCHI, M. & TAI, H. 1991. INHIBITORY EFFECT OF CALCIUM-BINDING PROTEIN REGUCALCIN ON CA2+ CALMODULIN-DEPENDENT CYCLIC-NUCLEOTIDE PHOSPHODIESTERASE ACTIVITY IN RAT-LIVER CYTOSOL. *Molecular and Cellular Biochemistry,* 106**,** 25-30.

YAMAGUCHI, M., TAKAHASHI, H. & TSURUSAKI, Y. 2003b. Suppressive role of endogenous regucalcin in the enhancement of nitric oxide synthase activity in liver cytosol of normal and regucalcin transgenic rats. *Journal of Cellular Biochemistry,* 88**,** 1226-1234.

YAMAGUCHI, M., TAKAKURA, Y. & NAKAGAWA, T. 2008b. Regucalcin increases Ca2+-ATPase activity in the mitochondria of brain tissues of normal and transgenic rats. *Journal of Cellular Biochemistry,* 104**,** 795-804.

YAMAGUCHI, M., TOMONO, S. & NAKAGAWA, T. 2007. Overexpression of RGPR-p117 suppresses apoptotic cell death and its related gene expression in cloned normal rat kidney proximal tubular epithelial NRK52E cells. *International Journal of Molecular Medicine,* 20**,** 565-571.

YAMAGUCHI, M. & YAMAMOTO, T. 1978. PURIFICATION OF CALCIUM-BINDING SUBSTANCE FROM SOLUBLE FRACTION OF NORMAL RAT-LIVER. *Chemical & Pharmaceutical Bulletin,* 26**,** 1915-1918.

YAMASAKI-MANN, M., DEMURO, A. & PARKER, I. 2009. cADPR stimulates SERCA activity in Xenopus oocytes. *Cell Calcium,* 45, 293-9.

YANAGIMACHI, R. & USUI, N. 1974. CALCIUM DEPENDENCE OF ACROSOME REACTION AND ACTIVATION OF GUINEA-PIG SPERMATOZOA. *Experimental Cell Research,* 89**,** 161-174.

YU, M. H., ZHANG, L. L., RISHI, A. K., KHADEER, M., INESI, G. & HUSSAIN, A. 1998. Specific substitutions at amino acid 256 of the sarcoplasmic/endoplasmic reticulum Ca2+ transport ATPase mediate resistance to thapsigargin in thapsigargin-resistant hamster cells. *Journal of Biological Chemistry,* 273**,** 3542-3546.

ZHANG, Z. S., LEWIS, D., SUMBILLA, C., INESI, G. & TOYOSHIMA, C. 2001. The role of the M6-M7 loop (L67) in stabilization of the phosphorylation and Ca2+ binding domains of the sarcoplasmic reticulum Ca2+-ATPase (SERCA). *Journal of Biological Chemistry,* 276**,** 15232-15239.

ZHANG, F. & LI, P. L. 2007. Reconstitution and characterization of a nicotinic acid adenine dinucleotide phosphate (NAADP)-sensitive Ca2+ release channel from liver Lysosomes of rats. *Journal of Biological Chemistry,* 282, 25259-25269.

APPENDIX

Michelangeli, F and Lai, P (2009) *Changes in expression and activity of the secretory pathway Ca2+ ATPase 1 (SPCA1) in A7r5 vascular smooth muscle cells, cultured at different glucose concentrations.* Bioscience Reports, 29 . pp. 397-404. ISSN 0144-8463

URL of Published Version: http://dx.doi.org/10.1042/BSR20090058

Identification Number/DOI: 10.1042/BSR20090058

Abstract

Diabetes mellitus-related vascular disease is often associated with both a dysregulation of Ca2+ homoeostasis and enhanced secretory activity in VSMCs (vascular smooth muscle cells). Here, we employ a commonly used rat cell line for VSMCs (A7r5 cells) to investigate the effects of glucose on the expression and activity of the SPCA1 (secretory pathway Ca2+-ATPase 1; also known as ATP2C1), which is a P-type Ca2+ pump located in the Golgi apparatus that plays a key role in the secretory pathway. Our results show that mRNA expression levels of SPCA1 are significantly increased in A7r5 cells cultured in high glucose (25.0 mM)-supplemented medium compared with normal glucose (5.55 mM)-supplemented medium. SPCA1 protein expression levels and thapsigargin-insensitive Ca2+-dependent ATPase activity were also consistent with a higher than normal expression level of SPCA1 in high-glucose-cultured A7r5 cells. Analysis of AVP (arginine-vasopressin)-induced cytosolic Ca2+ transients in A7r5 cells (after pre-treatment with thapsigargin) showed faster rise and decay phases in cells grown in high glucose medium compared with cells grown in normal glucose medium, supporting the observation of increased SPCA expression/activity. The significant levels of both Ca2+-ATPase activity and AVP-induced Ca2+ transients, in the presence of thapsigargin, indicate that SPCA must play a significant role in Ca2+ uptake within VSMCs. We therefore propose that, if such increases in SPCA expression and activity also occur in primary VSMCs, this may play a substantial role in the aetiology of diabetes mellitus-associated vascular disease, due to alterations in Ca2+ homoeostasis within the Golgi apparatus.

www.bioscirep.org